

Synthetic Firefly Luciferins  
for Bioluminescence Imaging

February 2020

IKEDA, Yuma

A Thesis for the Degree of Ph.D. in Engineering

Synthetic Firefly Luciferins  
for Bioluminescence Imaging

February 2020

Graduate School of Science and Technology  
Keio University

IKEDA, Yuma

# Table of Contents

<b>Chapter 1 General Introduction</b>	1
1.1. Molecular Imaging	2
1.2. Bioluminescence	5
1.2.1. Short history of bioluminescence	5
1.2.2. Comparison of fluorescent and bioluminescence probes	6
1.2.2.1. Autofluorescence from mice	6
1.2.2.2. Autoluminescence from mice	7
1.2.2.3. Comparison of bioluminescent and fluorescent results	7
1.2.2.4. Imaging of bone marrow-derived cells in brain inflammation	7
1.2.3. Trans-scale imaging	8
1.3. Firefly Bioluminescence as Imaging Probes	9
1.3.1. Light emitting reaction on firefly bioluminescence	9
1.3.2. D-luciferin as shared substrate	10
1.3.3. Limitations of “native” firefly bioluminescence	13
1.3.3.1. Non-orthogonal emission	13
1.3.3.2. Wavelength	14
1.3.3.3. Diffusion	16
1.3.4. Synthetic firefly luciferins	17
1.3.4.1. Thiazoline analogues	17
1.3.4.2. Benzothiazole analogues	18
1.4. Scope of This Thesis	24
References	25
<b>Chapter 2 An Allylated Firefly Luciferin Analogue with Luciferase Specific Response In Living Cells</b>	29
2.1. Introduction	30
2.2. Results and Discussion	32
2.2.1. Design and synthesis of 7'-AllylLuc	32
2.2.2. Light-emitting potential of 7'-AllylLuc	33
2.2.3. Kinetic evaluation	39
2.2.4. Orthogonal bioluminescence emission in living cells	41
2.3. Conclusions	44

2.4. Experimental Section	45
2.4.1. Material and methods	45
2.4.1.1. General	45
2.4.1.2. Chemiluminescence spectra	45
2.4.1.3. Absorbance and fluorescence spectra	45
2.4.1.4. Bioluminescence emission spectra	46
2.4.1.5. Bioluminescence intensities and kinetic reaction analysis	46
2.4.1.6. Determination of quantum yields	46
2.4.1.7. Plasmid construction	47
2.4.1.8. Cell culture and plasmid transfection	47
2.4.1.9. Live cell bioluminescence assays	47
2.4.1.10. Cytotoxicity assay	48
2.4.2. Synthetic procedures	48
2.4.3. NMR spectra	50
References	54

### **Chapter 3 Demonstration of an Azetidine-Substituent Effect on Firefly Luciferin Analogues**

	56
3.1. Introduction	57
3.2. Results and Discussion	59
3.2.1. Design and synthesis of luciferin analogues with an azetidine donor	59
3.2.2. Bioluminescence assays with recombinant firefly luciferase	61
3.2.3. Verification of an azetidine-replacement effect	64
3.2.4. Cellular bioluminescence applications	68
3.3. Conclusions	71
3.4. Experimental Section	72
3.4.1. Material and methods	72
3.4.1.1. General	72
3.4.1.2. Bioluminescence spectra	72
3.4.1.3. Bioluminescence intensities and kinetic measurements	72
3.4.1.4. Fluorescence measurements	73
3.4.1.5. Computational quantum chemical calculations	73
3.4.1.6. Cellular bioluminescence assays	73
3.4.2. Synthetic procedures	74
3.4.3. NMR spectra	81
References	103

<b>Chapter 4 Ring-Fused Firefly Luciferins: Expanded Palette of Near-Infrared Emitting Bioluminescent Substrates</b>	105
4.1. Introduction	106
4.2. Results and Discussion	109
4.2.1. Design and synthesis of NIRLucs	109
4.2.2. Evaluation of light emitting potential of NIRLucs	110
4.2.3. Bioluminescence activity <i>in vitro</i>	113
4.2.4. Theoretical calculation of oxy-NIRLucs	117
4.2.5. Light emission in luciferase-expressing live cells	120
4.2.6. <i>In vivo</i> applications of NIRLuc2 to mice bearing subcutaneous tumors	122
4.3. Conclusions	126
4.4. Experimental Section	127
4.4.1. Material and methods	127
4.4.1.1. General	127
4.4.1.2. Chemiluminescence spectra	127
4.4.1.3. Fluorescence spectroscopy	128
4.4.1.4. Bioluminescence spectra	128
4.4.1.5. Bioluminescence kinetic measurements	128
4.4.1.6. Quantum chemical calculations	129
4.4.1.7. Cellular bioluminescence assays	129
4.4.1.8. Mice	129
4.4.1.9. Measurements of blood retention	129
4.4.1.10. <i>In vivo</i> subcutaneous tumor imaging	130
4.4.2. Synthetic procedures	130
4.4.3. NMR spectra	138
References	168
<b>Chapter 5 General Conclusions</b>	171
5.1. Summary of the results	172
5.2. Future outlook	174
Achievement list	177
Acknowledgement	

# List of Figures

<b>Figure 1.1.</b> A summary of modalities used for molecular imaging.	4
<b>Figure 1.2.</b> Chemical structures of luciferins.	6
<b>Figure 1.3.</b> In vivo imaging of bone marrow-derived cells.	8
<b>Figure 1.4.</b> Light emitting reaction pathway of D-luciferin catalyzed by firefly luciferase.	9
<b>Figure 1.5.</b> (A) Chemical structures of oxyluciferin analogue, 1-OCH <sub>3</sub> and 1-O <sup>-</sup> . (B) Emission color modulation mechanism of firefly (beetle) bioluminescence.	12
<b>Figure 1.6.</b> Schematic illustration of color modulation in the active site of a luciferase.	13
<b>Figure 1.7.</b> Triple <i>in vivo</i> bioluminescence imaging.	14
<b>Figure 1.8.</b> Interaction of light with tissue.	15
<b>Figure 1.9.</b> Biodistribution of [ <sup>125</sup> I]iodo-D-luciferin in ICR mice.	16
<b>Figure 1.10.</b> Structure activity relationship of D-luciferin.	17
<b>Figure 1.11.</b> Structures of thiazoline analogues.	18
<b>Figure 1.12.</b> Structures of altered push-pull analogues.	19
<b>Figure 1.13.</b> Structures of steric modified analogues.	19
<b>Figure 1.14.</b> Rapid BLI <i>in vitro</i> and <i>in vivo</i> .	20
<b>Figure 1.15.</b> Structures of benzothiazole core replaced analogues.	21
<b>Figure 1.16.</b> Performance of engineered AkaLumine/Akaluc versus natural D-luciferin/Fluc for <i>in vitro</i> and <i>in vivo</i> bioluminescence imaging.	22
<b>Figure 1.17.</b> Chronic video-rate AkaBLI of brain striatal neurons in a common marmoset.	23
<b>Figure 2.1.</b> Chemical structures of luciferins.	31
<b>Figure 2.2.</b> Chemiluminescence spectra of D-luciferin methyl ester and 7'-AllylLuc methyl ester with <i>t</i> -BuOK in DMSO.	33
<b>Figure 2.3.</b> Normalized bioluminescence emission spectra obtained with various luciferases for D-luciferin and 7'-AllylLuc at pH 8.0.	34
<b>Figure 2.4.</b> Fluc-catalyzed bioluminescence emission of D-luciferin and 7'-AllylLuc.	35
<b>Figure 2.5.</b> Absorbance and fluorescence spectra of D-luciferin and 7'-AllylLuc recorded at pH 8.0 in 0.1M GTA buffer.	35
<b>Figure 2.6.</b> Bioluminescence spectra of D-luciferin and 7'-AllylLuc with Fluc at various pH values.	36
<b>Figure 2.7.</b> Consideration of color modulation mechanism.	37
<b>Figure 2.8.</b> Light emission time courses obtained with various luciferases.	38
<b>Figure 2.9.</b> Initial bioluminescence intensity from 7'-AllylLuc with purified luciferases (1 µg/mL) at various luciferin concentrations (1-20 µM).	39
<b>Figure 2.10.</b> Quantum yield measurements.	40
<b>Figure 2.11.</b> Light emission from luciferase-expressing COS-7 cells treated with 7'-AllylLuc.	41

<b>Figure 2.12.</b> Light emission from luciferase-expressing COS-7 cells treated with D-luciferin.	42
<b>Figure 2.13.</b> Comparison of Light emission intensities from luciferase-expressing COS-7 cells treated with D-luciferin and 7'-AllylLuc at 500 $\mu$ M substrate.	42
<b>Figure 2.14.</b> Cell viability evaluated by MTT assay.	43
<b>Figure 3.1.</b> Azetidine-substituent approach on firefly bioluminescence.	58
<b>Figure 3.2.</b> Bioluminescence intensities for dimethylamino and azetidinyl analogues.	62
<b>Figure 3.3.</b> Michaelis-Menten plots.	63
<b>Figure 3.4.</b> Comparison of the photon flux from azetidinyl and dimethylamino analogues for each luciferin core structures at 5 $\mu$ M luciferin.	64
<b>Figure 3.5.</b> Absolute fluorescence quantum yields of D-1 and A-1 in various solvent (DMSO, acetonitrile, 2-propanol, methanol and water).	66
<b>Figure 3.6.</b> Calculated potential energy surfaces of benzothiazole core analogues in water.	66
<b>Figure 3.7.</b> Bioluminescence spectra of azetidinyl and dimethylamino analogues with Fluc.	67
<b>Figure 3.8.</b> Comparison of the fluorescence and bioluminescence spectra for benzothiazole core analogues (D-1, A-1).	67
<b>Figure 3.9.</b> Photon flux from the Fluc-expressing cells.	68
<b>Figure 3.10.</b> Quantitative analysis of the photon flux from Fluc-expressing cells.	69
<b>Figure 3.11.</b> Time courses of photon outputs from Fluc expressing B16F10 cells.	70
<b>Figure 4.1.</b> Reaction of firefly luciferin and chemical structures of NIR emitting luciferins.	108
<b>Figure 4.2.</b> Chemiluminescence of NIRLucs.	111
<b>Figure 4.3.</b> Normalized fluorescence emission spectra of AkaLumine and NIRLucs in 50 mM GTA buffer (pH 8.0).	112
<b>Figure 4.4.</b> Bioluminescence emission spectra of AkaLumine and the NIRLucs with native Fluc.	113
<b>Figure 4.5.</b> Dose-dependent bioluminescent emission intensities.	114
<b>Figure 4.6.</b> Burst kinetic profiles of 10 $\mu$ M of each luciferin with 5.0 $\mu$ g/mL native Fluc in 50 mM GTA buffer (pH 8.0).	114
<b>Figure 4.7.</b> Luciferin saturation assay with increasing concentration of luciferins (0.05-10 $\mu$ M).	115
<b>Figure 4.8.</b> pH-Dependence of bioluminescence spectra of D-luciferin (a), AkaLumine (b) and NIRLucs (c-h) with Fluc in 50 mM GTA buffer (pH 5.5-8.5).	116
<b>Figure 4.9.</b> pH-Dependence of bioluminescence emission intensities.	116
<b>Figure 4.10.</b> Chemical structures of oxidized forms of AkaLumine (5) and NIRLucs.	118
<b>Figure 4.11.</b> Comparison of HOMO (bottom) and LUMO (top) energy levels for the oxidized form of AkaLumine (5) and NIRLucs.	118
<b>Figure 4.12.</b> Correlation between calculated wavelengths and experimentally obtained wavelengths.	119
<b>Figure 4.13.</b> Cell number-dependent bioluminescence of stably luciferase-expressing B16F10 cells with 25 $\mu$ M luciferins.	120
<b>Figure 4.14.</b> Dose-response photon flux from luciferase-expressing cells.	121

<b>Figure 4.15.</b> Time-dependent photon output from stably Fluc-expressing B16F10 cells treated with 0.25 $\mu$ M luciferins.	122
<b>Figure 4.16.</b> Blood retention of NIRLuc2, D-luciferin (1) and AkaLumine (5) in ICR mice ( $n = 4$ ).	123
<b>Figure 4.17.</b> Bioluminescence spectra from subcutaneous tumors of B16-F10-Fluc cells.	124
<b>Figure 4.18.</b> Time course of bioluminescent photon flux from subcutaneous tumors <i>in vivo</i> with open filter (A) or NIR ( $680 \pm 10$ nm) filter (B).	124
<b>Figure 4.19.</b> Tumor bioluminescence imaging with NIRLuc2 <i>in vivo</i> .	125
<b>Figure 5.1.</b> Summary of the synthetic luciferins developed in thesis.	172
<b>Figure 5.2.</b> Chemical structure of luciferyl adenylate and research strategy.	174
<b>Figure 5.3.</b> Cyanine fusion luciferins.	175
<b>Figure 5.2.</b> Key technologies for future bioluminescence imaging.	176

# List of Schemes

<b>Scheme 2.1.</b> Synthesis of 7'-AllylLuc.	33
<b>Scheme 3.1.</b> Synthesis of the azetidine-substituent benzothiazole core analogue (A-1).	59
<b>Scheme 3.2.</b> Synthesis of the azetidine-substituent styrenyl core analogues (A-2, 3-OMe).	60
<b>Scheme 3.3.</b> Synthesis of the azetidine-substituent naphthyl core analogues (A) A-4-OMe, (B) A-5-OMe.	60
<b>Scheme 3.4.</b> Synthesis of the azetidine-substituent analogues (A-2, A-3, A-4 and A-5) through lipase-promoted ester hydrolysis.	61
<b>Scheme 4.1.</b> Synthesis of NIRLuc.	110

# List of Tables

<b>Table 1.1.</b> Currently available imaging modalities.	2
<b>Table 1.2.</b> Molecular properties of beetle luciferases.	11
<b>Table 2.1.</b> Kinetic properties of allyl luciferin in combination with various luciferases.	40
<b>Table 2.2.</b> Bioluminescence quantum yields ( $n = 3$ ).	40
<b>Table 3.1.</b> Characteristics of dimethylamino and azetidinylluciferins.	63
<b>Table 3.2.</b> Comparison of the fluorescence quantum yields in buffer (pH 8.0).	65
<b>Table 4.1.</b> Characteristics of AkaLumine (5) and NIRLucs.	117
<b>Table 4.2.</b> Calculated Frontier orbitals and oscillator strengths of AkaLumine (5) and NIRLucs at the basis of B3LYP/6-31+G(d).	119

# Chapter 1

## General Introduction

# 1.1. Molecular Imaging

Molecular imaging provides opportunities for better “seeing” and “understanding” the complex and interesting living subject. Recent progress in imaging technologies have made it possible to image the actual amount / function of genes and specific molecules such as target proteins in cells and *in vivo*. In addition, visualizing the amount/ function of “molecules” can promote the treatment and diagnosis of various diseases. The essential requirements for imaging technologies, especially *in vivo* imaging, are as follows; 1) Safety (non-toxicity and non-invasiveness), 2) High spatial and temporal resolution, 3) Deep penetration depth, 4) Sensitivity, 5) Selectivity, 6) Low cost. The typically available imaging modalities for *in vivo* are magnetic resonance imaging (MRI), positron electron tomography (PET), single photon emission computed tomography (SPECT), computed tomography (CT), ultrasound and optical imaging (fluorescence and bioluminescence) (summarized in **Table 1.1, Figure 1.1**).<sup>1-2</sup> However, no imaging modalities are available that meets all these requirements.

**Table 1.1. Currently available imaging modalities.** (based on Gambhir, S. S. *et al.*, *Chem. Rev.*, **2017**, *117*, 901-986.)

modality	signal type	resolution		penetration depth	sensitivity	cost
		spatial	temporal			
Magnetic resonance imaging (MRI)	Radio frequency	25-100 $\mu\text{m}$ (preclinical) ~1 mm (clinical)	min-h	Unlimited	$10^{-3}$ - $10^{-5}$ M	\$\$\$
Positron electron tomography (PET)	Radionuclide (positron)	<1 mm (preclinical) ~5 mm (clinical)	s-min	Unlimited	$10^{-11}$ - $10^{-12}$ M	\$\$\$
Single photon emission computed tomography (SPECT)	Radionuclide ( $\gamma$ -rays detected)	0.5-2 mm (preclinical) 8-10 mm (clinical)	min	Unlimited	$10^{-10}$ - $10^{-11}$ M	\$\$\$
Computed tomography (CT)	X-rays	25-200 $\mu\text{m}$ (preclinical) 0.5-1 mm (clinical)	s-min	Unlimited	$\sim 10^{-3}$ M	\$\$
Ultra sound	Sound waves	10-100 $\mu\text{m}$ (at ~mm depth) 1-2 cm (at ~cm depth)	s-min	10 ms	$10^{-6}$ - $10^{-9}$ M	\$
Optical imaging (fluorescence / bioluminescence)	UV-NIR light	2-3 mm	s-min	< 2cm	$10^{-9}$ - $10^{-12}$ M	\$

Abbreviations: \$, Inexpensive; \$\$, Moderately Priced; \$\$\$, Expensive.

MRI is a clinically applied technology that uses strong magnetic fields and radio waves to detect nuclei of water molecules in the tissue by nuclear magnetic resonance. Sometimes a small molecular tracer such as gadolinium chelates are utilized to improve image contrast specifically. Although MRI afford high spatial resolution and soft-tissue contrast, it takes long time (20-60 min) and is high costs.

PET/SPECT are also clinical imaging methods using radioactive tracers. The PET system detects positrons and a pair of  $\gamma$ -rays emitted from drugs labeled with radionuclides such as  $^{11}\text{C}$ ,  $^{13}\text{N}$ ,  $^{15}\text{O}$  and  $^{18}\text{F}$ . The advantage of PET imaging is high sensitivity with unlimited depth penetration. However, since the lifetimes of radionuclides for PET are short ( $^{11}\text{C}$ : ~20 min,  $^{13}\text{N}$ : ~10 min,  $^{15}\text{O}$ : ~2 min,  $^{18}\text{F}$ : ~110 min), a cyclotron for producing them must be required.<sup>3</sup> Furthermore, the synthesis and quality control of labeled drugs must be carried out, except for them labeled with a relatively long half-life radionuclides. On the other hand, SPECT system requires a drug labeled with a  $\gamma$ -emitting radioisotope, directly detects  $\gamma$ -rays. The synthesis labeled drugs can be easily performed with a commercially available kit. The radioisotopes used in SPECT ( $^{99m}\text{Tc}$ : ~6 h,  $^{201}\text{Tl}$ : =73 h,  $^{111}\text{In}$ : ~2.8 d,  $^{123}\text{I}$ : =~13 h,  $^{130}\text{Xe}$ : 5.24 d) have a longer half-life than those in PET.<sup>4</sup>

CT utilizes X-rays to image the difference in polarization and absorption in tissue without any small molecular tracers. The advantages of CT are a high spatial resolution and easily obtained tomographic images specializing in bone/lung imaging. In contrast, CT suffers from lack of target specificity and poor soft-tissue contrast.<sup>5</sup>

Ultra sound imaging is an imaging method that detects the echoes of ultrasonic waves. This imaging modality is an extremely non-invasive technique with high spatial and temporal resolution.

Optical imaging technologies are currently playing an important role in the biomedical research fields, although they are limited clinical translation. In this modality, fluorescence and bioluminescence probes are adopted to see inside a cell or tissue. For fluorescence imaging, various fluorescent tracers such as genetically encodable fluorescent proteins, organic fluorescent dyes and metal complexes etc. are mainly used depending on the applications. In fluorescence imaging, fluorescent probes are excited by light-irradiation, then the excited molecules release a photon. The fluorescence method can be observed with relatively high spatial and temporal resolution. In addition, multichannel imaging is possible by combining probes with different fluorescence wavelengths. However, fluorescence method sometimes suffers from an inherent "barrier" caused by an excitation light source. Nowadays, bioluminescence imaging has become a standard non-invasive modality for tracking biological functions because it does not require any excitation light sources. The photon productions on bioluminescence relies on a light emitting molecule "luciferin" and a genetically encodable enzyme "luciferase". Recent numerous efforts have successfully imaged even single cell in an animal. Therefore, bioluminescence imaging potentially has the possibility to realize "trans-scale imaging" from a cell to whole body.

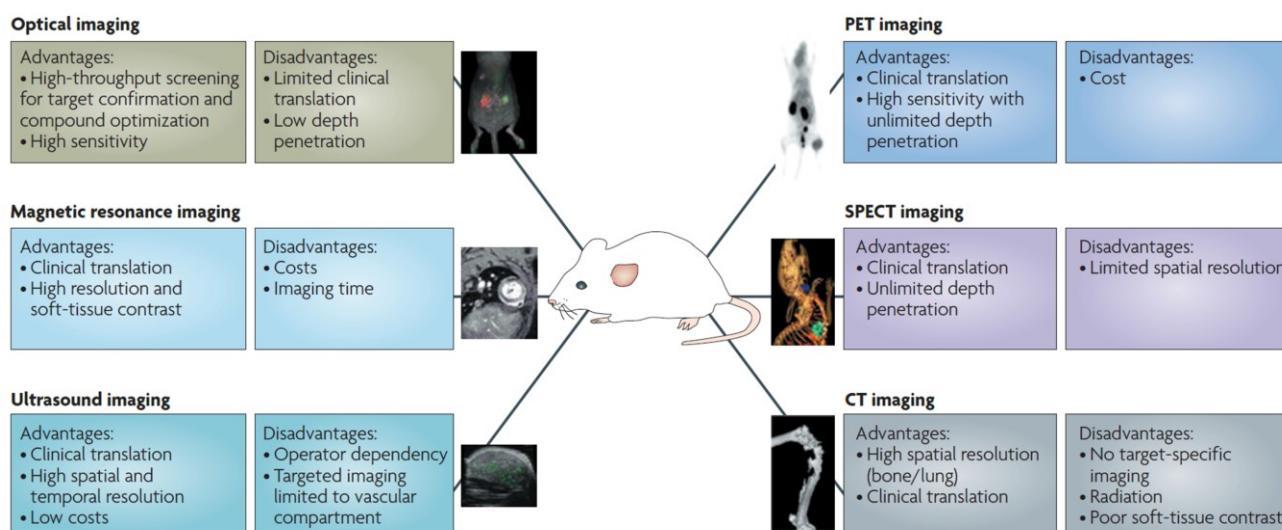


**Figure 1.1. A summary of modalities used for molecular imaging.** Each modality has particular characteristics, advantages and limitations, which are highlighted here. Most imaging modalities are used clinically and can be translated from animals to humans in the drug development process. The different imaging modalities are generally considered complementary rather than competitive. CT, computed tomography; PET, positron-electron tomography; SPECT, single-photon-emission computed tomography. Adapted by permission from Ref 5, Springer Nature, Nature Reviews Drug Discovery, Copyright 2008.

## 1.2. Bioluminescence

### 1.2.1. Short history of bioluminescence<sup>6</sup>

The history of bioluminescence research dates back to 1667. Robert Boyle, a scientist from Irish Lismore, has discovered a glowing decayed tree. He confirmed that the light emitted from the tree was extinguished when it was put into a self-made experimental glass box and the air was evacuated by a vacuum pump. This luminescence was actually due to the luminescent mycelium, and his experiment is the first example to probe that air (e.g. oxygen) is required for bioluminescence reaction. Later, Lazzaro Spallanzani, an Italian naturalist, has revealed that bioluminescence is caused by chemical reactions, regardless of "life". In 1885, a major turning point on bioluminescence research, Raphael Dubois has discovered that the bioluminescence reaction requires two kinds of "substances". The experiment conducted by Dubois were as follows; "The bioluminescent organs of *pyrophorus* were collected and extracted with cold water. Then, it became clear that the extract emitted for a while, but gradually decayed. On the other hand, no luminescence was observed from extracts with hot water. Once mixed these two extracts, strong luminescence was recovered". From this experiment, he has identified two kinds of chemicals, a heat-stable organic compound and an enzyme catalyzing oxidation, named the former compound as luciferin, and the latter as luciferase.

The principle chemical reaction in bioluminescence is the oxidation of luciferin catalyzed by luciferase. During the oxidative process, an excited molecule, oxyluciferin, is produced, and then the relaxation of this molecule to ground state release a photon. Nowadays, several types of luciferins and corresponding several types of luciferases have been identified in nature (**Figure 1.2**). Moreover, some of them have already been utilized as an imaging probe to track cellular functions and protein-protein interactions and so on.

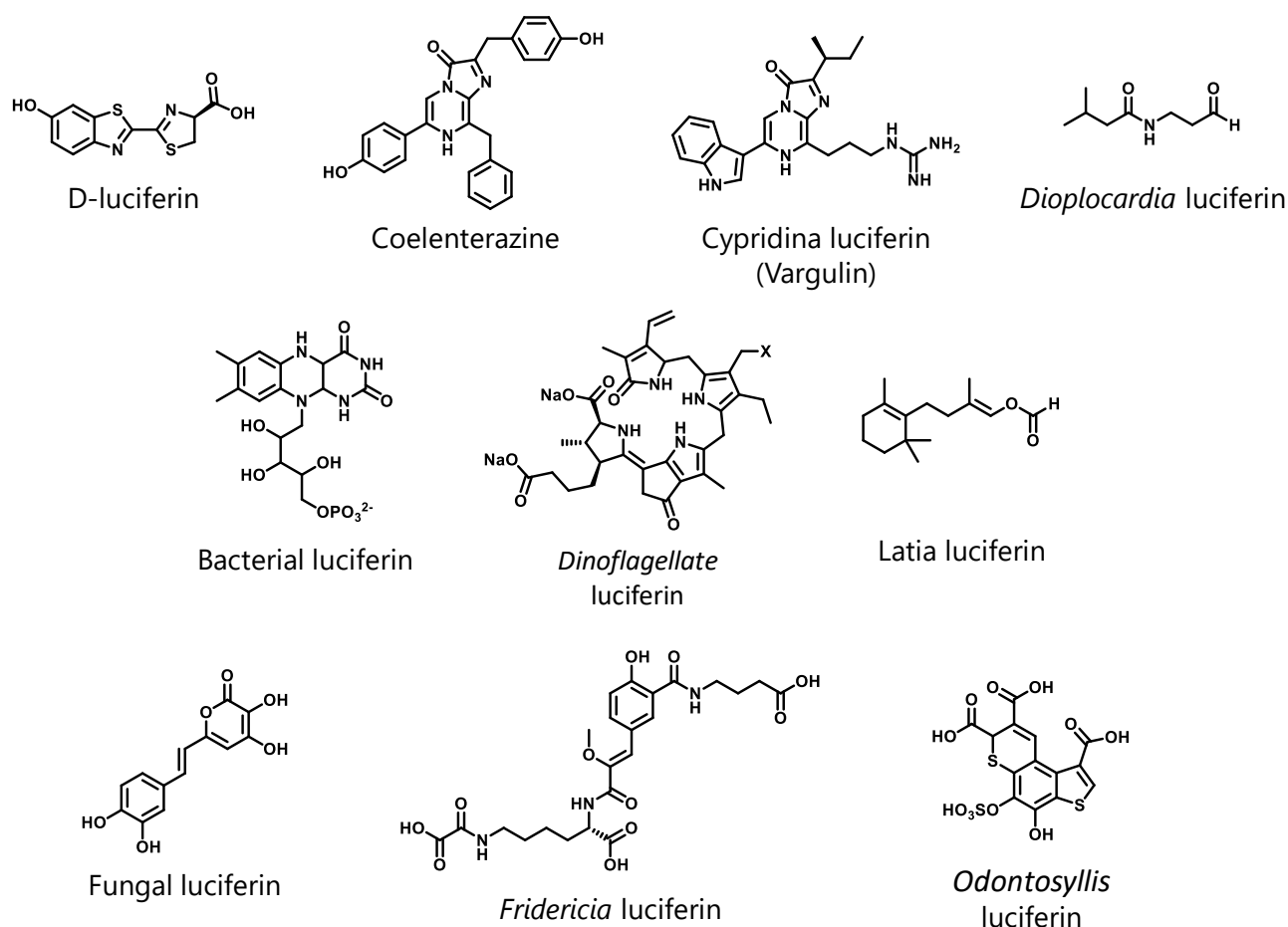


**Figure 1.2. Chemical structures of luciferins.**

## 1.2.2. Comparison of fluorescent and bioluminescent probes<sup>7</sup>

Among the many of luciferin-luciferase pairs, the most commonly adopted luciferin-luciferase pairs in bioluminescence imaging originate from insects, such as fireflies and click beetles. These bioluminescence systems consist of D-luciferin and the corresponding insect luciferases, for example Fluc from *photinus pylalis*, and emit yellow-green to orange light (530-640 nm) (*for further details, please see the section 1.3*).<sup>8-10</sup> In 2004, Troy and colleagues quantitatively compared the sensitivity of fluorescent and bioluminescent reporters (e.g. D-luciferin/Fluc pair) in mice model, including various factors such as autoluminescence, autofluorescence and so on.<sup>7</sup> A brief results of their work are described follows.

### 1.2.2.1. Autofluorescence from mice

For highly contrasted *in vivo* imaging, the background signal from a mouse (or an animal) should be as low as possible. However, many endogenous chromophores such as elastin, collagen, tryptophan, NADH, porphyrins, and flavins often causes serious autofluorescence, making difficult to

obtain high signal to noise ratio. Generally, the autofluorescence spectra are higher at short wavelengths (359-550 nm) than near-infrared (NIR) wavelengths (650-900 nm, *see the section 1.3.3.2*). In addition, the alfalfa containing in the regular mouse food has significant fluorescent signature over the entire wavelengths from visible to NIR. The concentrated photon outputs in around liver are often found due to the chlorophyll. Therefore, the food that do not contain alfalfa must be selected for optical imaging, especially for fluorescence imaging.

### 1.2.2.2. Autoluminescence from mice

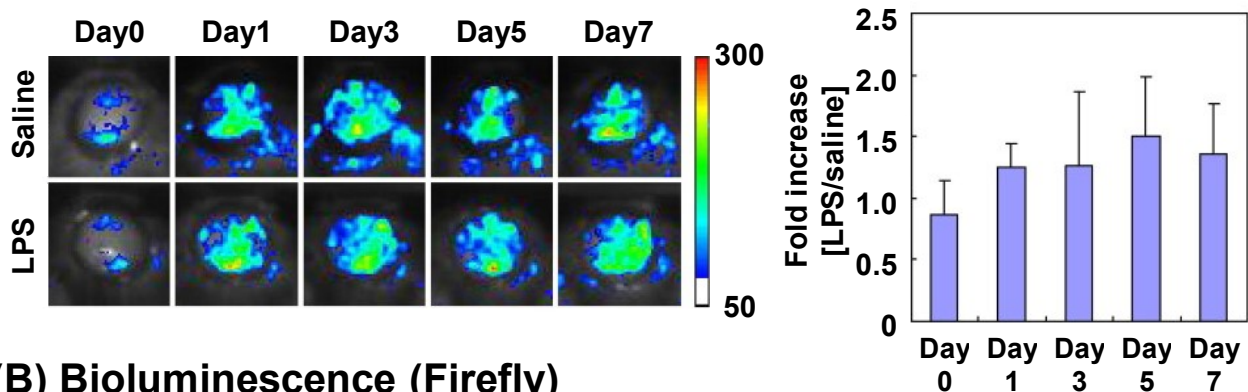
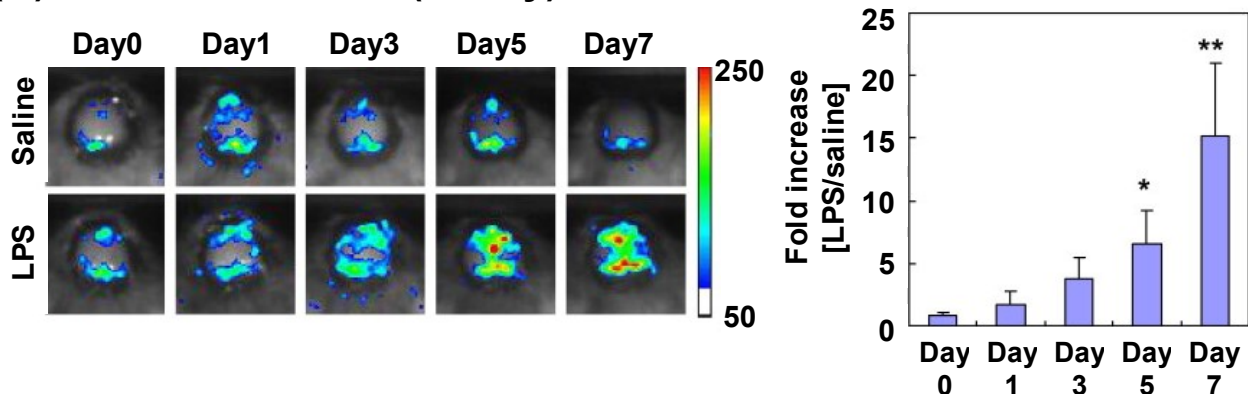
Troy and colleagues have also evaluated autoluminescence from a mouse body due to the internal chemiluminescence. As a result, averaged photon flux was confirmed to be about 1000~1600 photons/sec/cm<sup>2</sup>/sr by an IVIS imaging system, which are above the detection limit of photon flux of IVIS imaging systems (100 photons/sec/cm<sup>2</sup>/sr). For information, the autoluminescence spectrum is located in around 590-740 nm, which roughly agree with tissue transmission curve.

### 1.2.2.3. Comparison of bioluminescent and fluorescent results

Quantitative comparison of bioluminescence and fluorescence imaging *in vivo* have been performed in a Nu/nu mouse subcutaneously implanted with PC-3M-luc/DsRed cells. Direct comparison of fluorescence signal from DsRed and bioluminescence revealed the significance of bioluminescence imaging. Although fluorescence signal was 110-times higher than that of bioluminescence, fluorescence methods resulted in terrible signal to background ratio; 7.8 for fluorescence, 7500 for bioluminescence. Troy and colleagues have concluded that fluorescence imaging requires at least  $3.8 \times 10^5$  cells to afford signal above autofluorescence whereas bioluminescence imaging only requires 400 cells to detect photon outputs above autoluminescence. These investigations clearly demonstrated the potential of bioluminescence imaging as a “trans-scale imaging” modality.

### 1.2.2.4. Imaging of bone marrow-derived cells in brain inflammation

As an example showing the significance of bioluminescence imaging, the results of monitoring the infiltration of bone marrow cells into the brain are introduced here. Akimoto and colleagues have demonstrated monitoring the infiltration of cells into brain during brain inflammation by fluorescence (GFP) and bioluminescence (Firefly luciferin/luciferase) imaging. As a result, only bioluminescence imaging successfully reflected the increase in signal, proving that cells infiltrate into the brain from bone marrow cells and regenerate cells in the brain (**Figure 1.3**).<sup>11</sup>

**(A) Fluorescence (GFP)****(B) Bioluminescence (Firefly)**

**Figure 1.3. *In vivo* imaging of bone marrow-derived cells.** (A) Fluorescence (B) Bioluminescence. Right graphs show quantitative analysis of bone marrow-derived cells related photon emissions. Robust signals were detected in both saline- and LPS-injected mice and observed no significant differences over time in saline vs LPS (means  $\pm$  SD,  $n = 3$  (Fluorescence), 6 (bioluminescence)). For statistical evaluation, ANOVA with Dunnett's test was applied, symbol \* and \*\* denote  $P < 0.05$  and  $P < 0.01$  vs Day 0, respectively. Adapted by permission from Ref 11, Elsevier, *Biochemical and Biophysical Research Communications*, Copyright 2009.

### 1.2.3. Trans-scale imaging

A major limitation of imaging technology is that there is no translation between targets. In order to truly understand complex biological phenomena, it is necessary to measure, analyze, and verify a huge system in "all space" and "all time". For this purpose, an imaging system that can visualize "molecules-cells-organs" across scales is required. This is achieved by compensating for the shortcomings of each imaging modality.<sup>12</sup> In particular, bioluminescence has a minimal background signal, so it may contribute to imaging of a minority of cells or targets.

# 1.3. Firefly Bioluminescence as Imaging Probes

## 1.3.1. Light emitting reaction on firefly bioluminescence

Light emitting reaction on firefly bioluminescence proceeds in two stages; A) adenylation, B) oxidation, and reaction process is currently proposed as follows (**Figure 1.4**);<sup>13</sup>

- D-luciferin reacts with ATP catalysed by a luciferase in the presence of  $Mg^{2+}$  to form a chemically activated luciferyl adenylate.
- Luciferyl adenylate is chemically converted to an unstable dioxetanone intermediate through oxidative reaction. Subsequently, excited oxyluciferin is generated in the process of decomposition of dioxetanone structure, this molecule emits light when it transitions to the ground state.

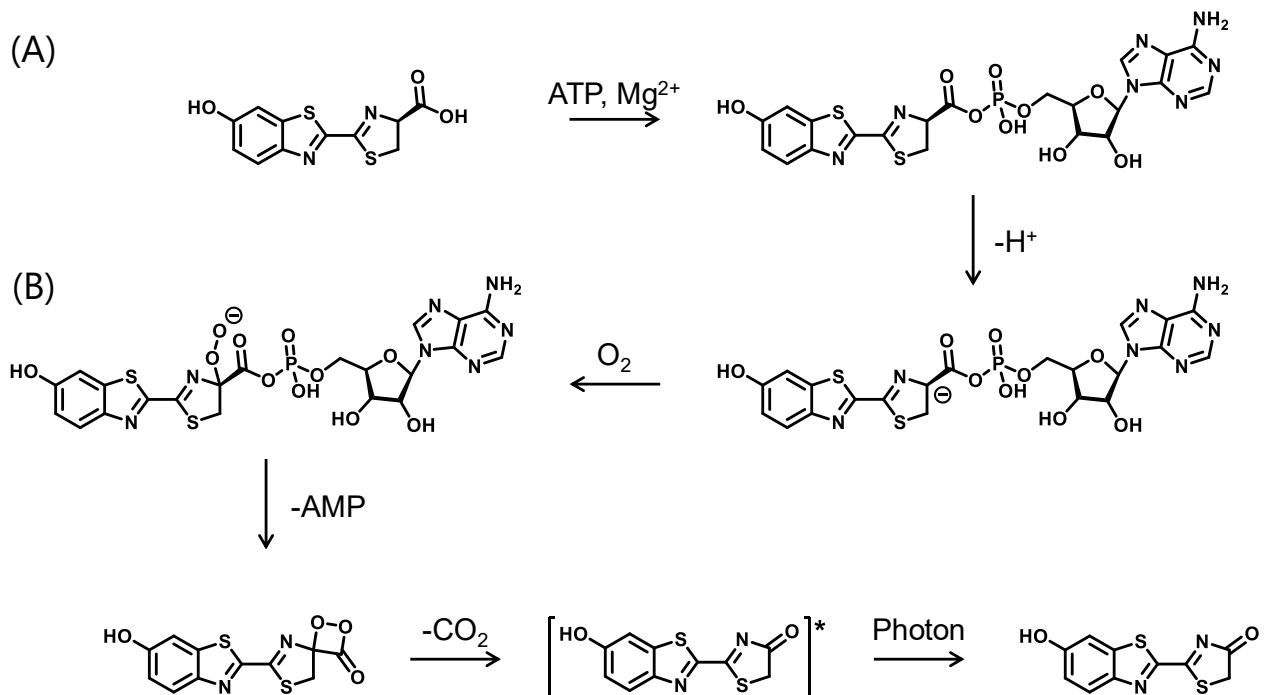


**Figure 1.4. Light emitting reaction pathway of D-luciferin catalysed by firefly luciferase.**<sup>13</sup>

Theoretically, one excited oxyluciferin is generated from a D-luciferin, thus the one photon is emitted from a D-luciferin. The bioluminescence quantum yield is defined as the ratio of the number of photons emitted from bioluminescence reaction to the number of luciferins, and is expressed by the following equation (**eq. 1**).

$$\varphi_{\text{BL}} = \varphi_{\text{FI}}\varphi_{\text{R}}\varphi_{\text{ES}} \quad (1)$$

where  $\varphi_{\text{FI}}$  is the fluorescence quantum yield of the oxyluciferin,  $\varphi_{\text{R}}$  is the reaction yield of the oxyluciferin formation from the corresponding luciferin, and  $\varphi_{\text{ES}}$  is the production yield of oxyluciferin in the excited state.<sup>14-15</sup> The quantum yields of firefly bioluminescence have been reported as 0.15-0.61 depending the luciferases.<sup>16-18</sup>

### 1.3.2. D-luciferin as shared substrate

Many kinds of beetle luciferases have been identified and cloned, but all luciferases from insects share the D-luciferin as a light emitting substrate. Interestingly, beetle bioluminescence reactions exhibit different emission colors from green to red (530-640 nm) depending on luciferases even though D-luciferin is the only substrate (**Table 1.2**).<sup>8-10</sup> Multicolor light emission results from environmental responsive chromic effect of oxyluciferin, the oxidized form of D-luciferin. However, this mysterious chromic mechanism still remains unclear. As an example, this section describes the emission color control mechanism focusing on the solvatochromism of oxyluciferin. Firefly luciferin has a carboxyl group as an electron withdrawing group (EWG) and a hydroxyl group as an electron donating group (EDG). Oxyluciferin also has a pair of EWG and EDG. This internal charge transfer (ICT) molecular structure causes a solvatochromism, a property that changes its absorption and/or fluorescence wavelengths depending on the environment polarity surrounding the substrate. In 2009, Hirano and colleagues have worked to elucidate the color control mechanism on firefly bioluminescence by focusing on the solvatochromic effect of luciferin.<sup>19</sup> For this purpose, they have synthesized two types of oxyluciferin analogues (**Figure 1.5A**), and examined the fluorescence properties under several solvents in combination with some bases. Finally, they proposed a following color modulation model as follows (**Figure 1.5B, 1.6**);

- 1) The actual light emitter is the excited state of the oxyluciferin phenolate anion.
- 2) Emission color is modulated by following two factors: 1) the polarity of the active site of a luciferase, 2) covalent strength of the hydrogen bond between the phenolate anion of (oxy)luciferin and the protonated amino acid residues at the active site.

**Table 1.2. Molecular properties of beetle luciferases.**(based on Gambhir, V. R. Viviani, *Cell. Mol. Life Sci*, **2002**, 59, 1833-1850.)

Luciferase	Residues	Identity with <i>Photinus pyralis</i> luciferase [%]	pI	$\lambda_{\max}$ [nm]	Genebank assignment
<b>pH-sensitive</b>					
<b>Lampyridae (fireflies)</b>					
<i>Photinus pyralis</i>	550	1	6.4	562	M15077
<i>Pyrocoelia miyako</i>	548	82	6.1	550	L39928
<i>Hotaria parvula</i>	548	68	6.3	568	L39929
<i>Luciola mingrelica</i>	548	67	6.2	570	S61961
<i>Luciola cruciate</i>	548	67	7.1	562	M26194
<i>Luciola lateralis</i>	548	67	6.5	552	X66919
<i>Lampyrus noctiluca</i>	547	83	6.1	550	X89479
<i>Photuris pennsilvanica</i>	545	58	8.4	538	U31240
<b>pH-insensitive</b>					
<b>Phengodidae (railroad worms)</b>					
<i>Phenogodes</i>	546	54	-	546	
<i>Phrixothrix Viviani</i>	545	55	6.3	548	AF139644
<i>P. hirtus</i>	546	47	7.0	623	AF139645
<i>Ragophthalmus ohbai</i>	543	53	-	555	-
<b>Elateridae (click beetles)</b>					
<i>Pyrophorus plagiophthalmus</i>					
GR	543	47	6.5	546	-
YG	543	46	6.5	560	-
YE	543	47	6.5	578	-
OR	542	46	6.4	593	-
<i>Pyrearinus termitilluminans</i>	543	46	6.75	536	AF116843

The pI was calculated from protein sequences.

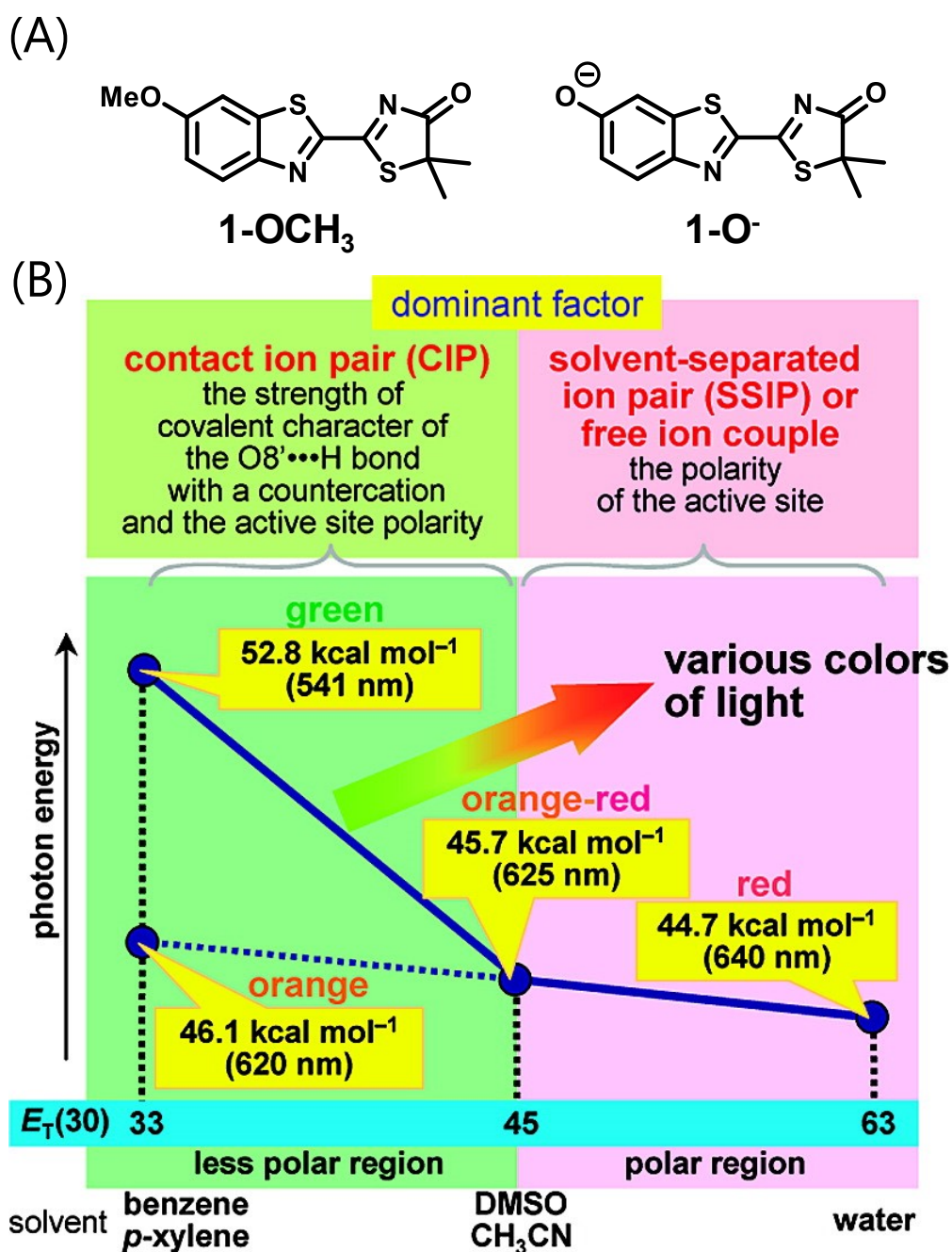


**Figure 1.5. (A) Chemical structures of oxyluciferin analogue, 1-OCH<sub>3</sub> and 1-O<sup>-</sup>. (B) Emission color modulation mechanism of firefly (beetle) bioluminescence.** "The solid line of the correlation between photon energy (PE) and  $E_T(30)$  was made by combining the  $E_F$ -versus-  $E_T(30)$  plots for 1-O<sup>-</sup> in polar solvents with those for 1-O<sup>-</sup>/H-TBA<sup>+</sup> in less polar solvents". "Yellow-green colors cannot be reproduced in polar media".<sup>19</sup> Adapted with permission from Ref. 19. Copyright 2009 American Chemical Society.

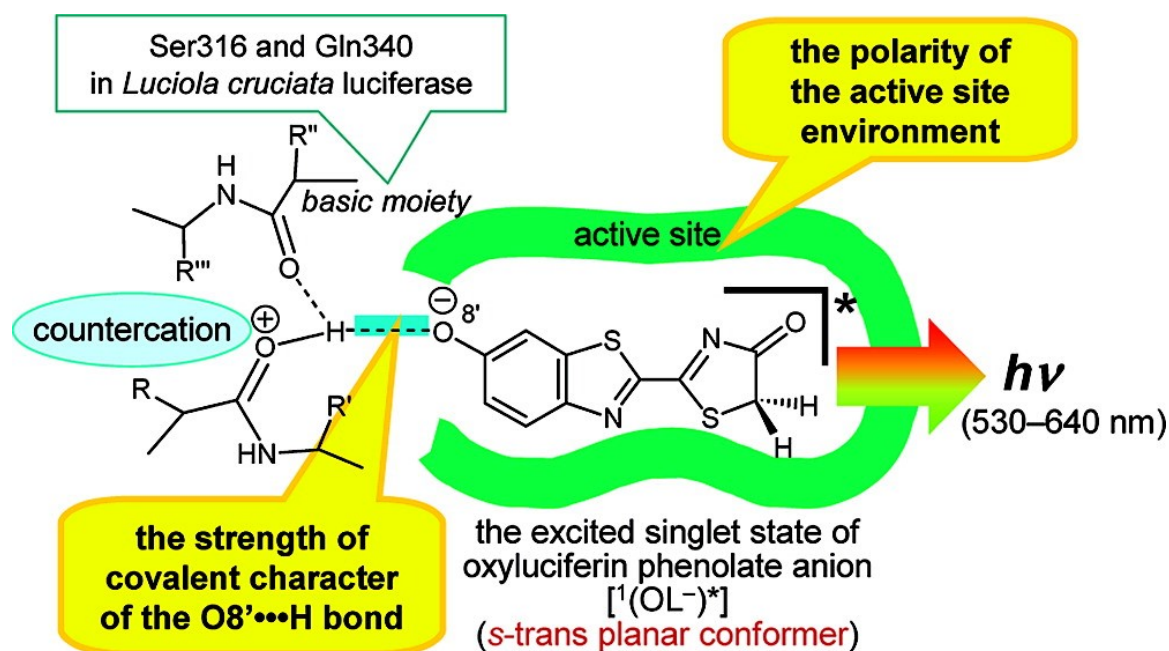


**Figure 1.6. Schematic illustration of color modulation in the active site of a luciferase.** Adapted with permission from Ref. 19. Copyright 2009 American Chemical Society.

### 1.3.3. Limitations of “native” firefly bioluminescence

Although D-luciferin, the native substrate of firefly (beetle) bioluminescence, has been widely applied to imaging applications, it is sometimes not the ideal substrate for *in vivo* applications. Herein, I described the three points to be improved for future progress of firefly bioluminescence imaging.

#### 1.3.3.1. Non-orthogonal emission

As already described above, all firefly (beetle) luciferases share the D-luciferin as their luminescent substrate to produce unique light emissions. This fact can be applied to multicolour bioluminescence imaging in combination with appropriate emission filter.<sup>20-22</sup> However, if want to “see” the different cell types or functions, sometimes it hard to distinguish in a single subject.<sup>23-24</sup> Some approaches combining the other bioluminescent reporters, especially coelenterazine/Renilla luciferase pairs, have been proposed as a distinguishable bioluminescent reporter system (**Figure 1.7**),<sup>25</sup> but coelenterazine is less ideal substrate because of instable properties *in vivo*.<sup>24, 26</sup>

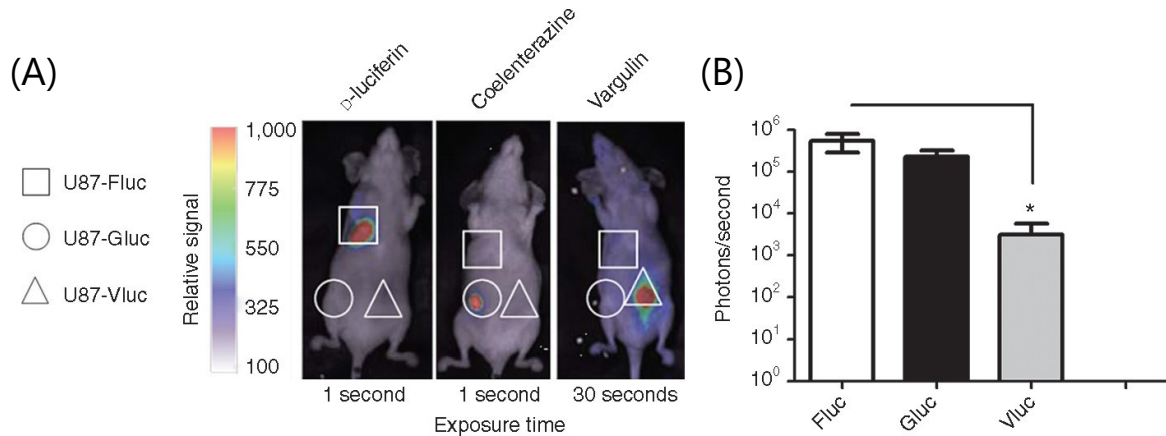


**Figure 1.7. Triple *in vivo* bioluminescence imaging.** (A) U87 glioma cells stably expressing Gluc, Vluc or Fluc were injected subcutaneously in nude mice at different sites. Ten days later, sequential imaging Fluc, Gluc and Vluc was performed (1 day apart) after injection of D-luciferin, coelenterazine, and vargulin. A representative mouse from each imaging session is shown ( $n = 3$ ). (B) A region of interest (ROI) was drawn around each tumor location and photons/second were calculated.  $*P = 0.016$ . Reprinted from ref. 25 by permission from Macmillan Publishers, Lt: *Molecular Therapy – Nucleic Acids*.

### 1.3.3.2. Wavelength

The various emission colors from firefly bioluminescence reaction have undoubtedly pushed firefly bioluminescence into the gold standard as a bioluminescence imaging tool. However, especially for *in vivo* applications, the emissions from firefly bioluminescence suffer from strong absorption of light by biological components such as water and haemoglobin.<sup>27</sup> This means that a great portion of light from firefly luciferase catalysed reaction is easily absorbed by the surrounding tissue and almost no light could be detected *in vivo* applications. Near-infrared (NIR) light ranging from 650-900 nm is effective for *in vivo* because this range has less absorption by endogenous biochemicals described above. In fact, Weissleder, a specialist for molecular optical imaging, stated as follows in an important review on optical imaging;<sup>28</sup>

*“One of the key strategies for imaging deeper tissues (that is, more than a few millimetres inside the sample) has been the use of NIR light. This is because hemoglobin (the principal absorber of visible light) and water and lipids (the principal absorbers of infrared light) have their lowest absorption coefficient in the NIR region of around 650–900 nm”.* (Figure 1.8)

Another advantage in NIR range is less autofluorescence from tissue, making it higher contrasted imaging (high signal to noise ratio) (Figure 1.8). For these reasons, bioluminescence emission in NIR range is prefer characteristics for *in vivo* applications, especially for deep tissue.

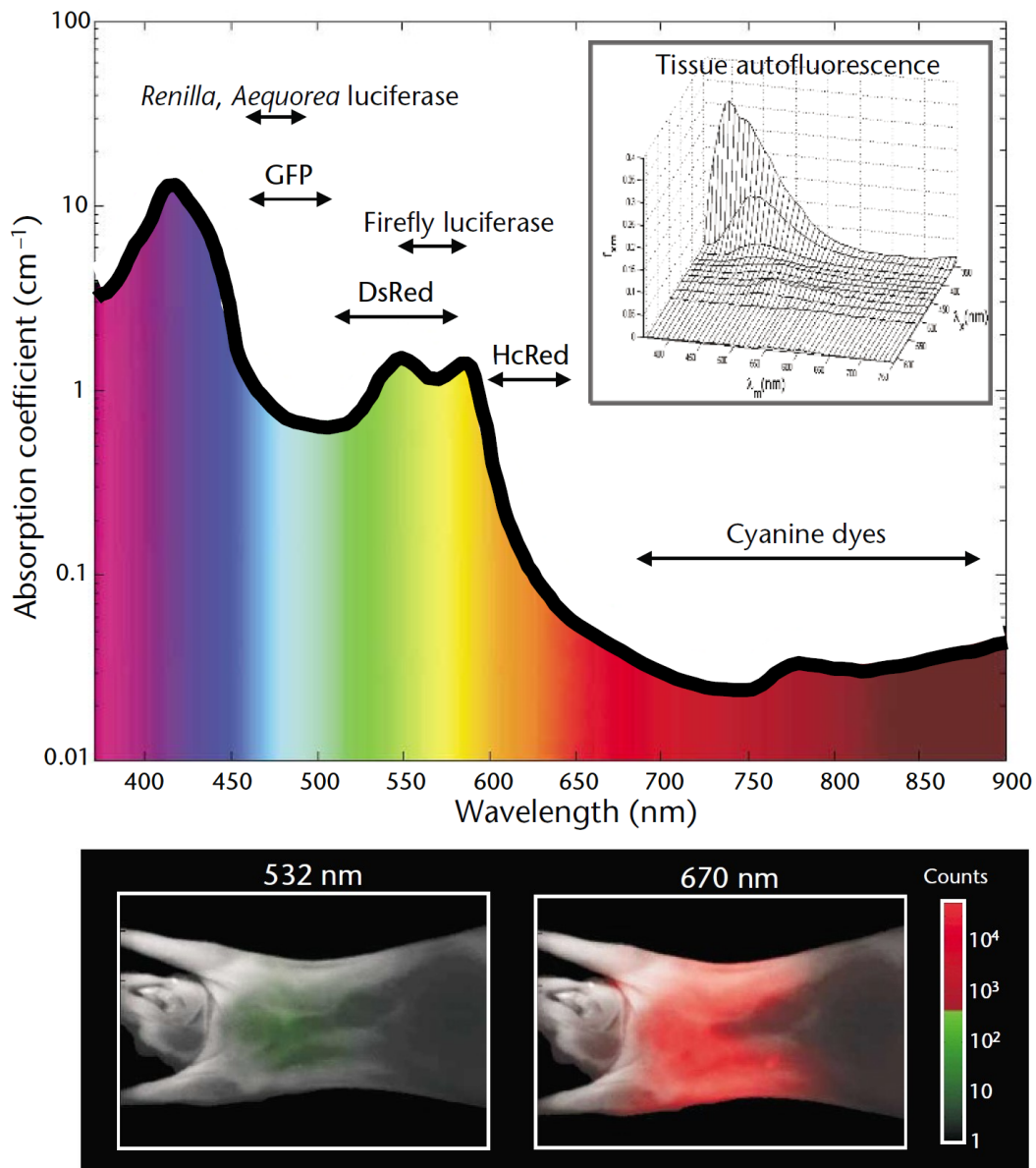


**Figure 1.8. Interaction of light with tissue.** The absorption coefficient of light in tissue is dependent on wavelength and results from absorbers such as hemoglobins, lipids and water. The graph is calculated assuming normally oxygenated tissue (saturation of 70%), a hemoglobin concentration of 50 mM, and a composition of 50% water and 15% lipids. The graph also lists the emission range of several common fluorochromes and luciferases used for imaging. The insert shows autofluorescence spectra obtained *in vivo* at different excitation wavelengths. The excitation range, denoted as  $\lambda_x$ , is from 337 to 610 nm, and the emission range ( $\lambda_m$ ) is from 360 to 750 nm. Note the much lower tissue autofluorescence at longer wavelengths. The mouse images at the bottom show experimentally measured photon counts through the body of a nude mouse at 532 nm (left) and 670 nm (right). The excitation source was a point illumination placed on the posterior chest wall. Signal in the NIR range is ~4 orders of magnitude stronger for illumination in the NIR compared with illumination with green light under otherwise identical conditions, illustrating the advantages for imaging with NIR photons. Adapted by permission from Ref 28, Springer Nature, *Nature Medicine*, Copyright 2003.

### 1.3.3.3. Diffusion

The behavior of D-luciferin as a “drug” *in vivo* should be mentioned here. Generally, D-luciferin is injected to an animal through an intravenous or intraperitoneal administration. B. T. Kim and colleagues have investigated the cellular uptake and *in vivo* biodistribution by synthesizing radiolabeled D-luciferin analogue, [<sup>125</sup>I]iodo-D-luciferin. Their results indicated a low level of cellular uptake and rapid washout of luciferin. Biodistribution study in ICR mice revealed that early uptakes especially in liver, myocardium and muscle were lower with intraperitoneal than intravenous administration. In addition, uptake in brain was extremely low level, therefore, luciferin concentration might be a limiting factor for luminescence reaction (**Figure 1.9**).<sup>29</sup>

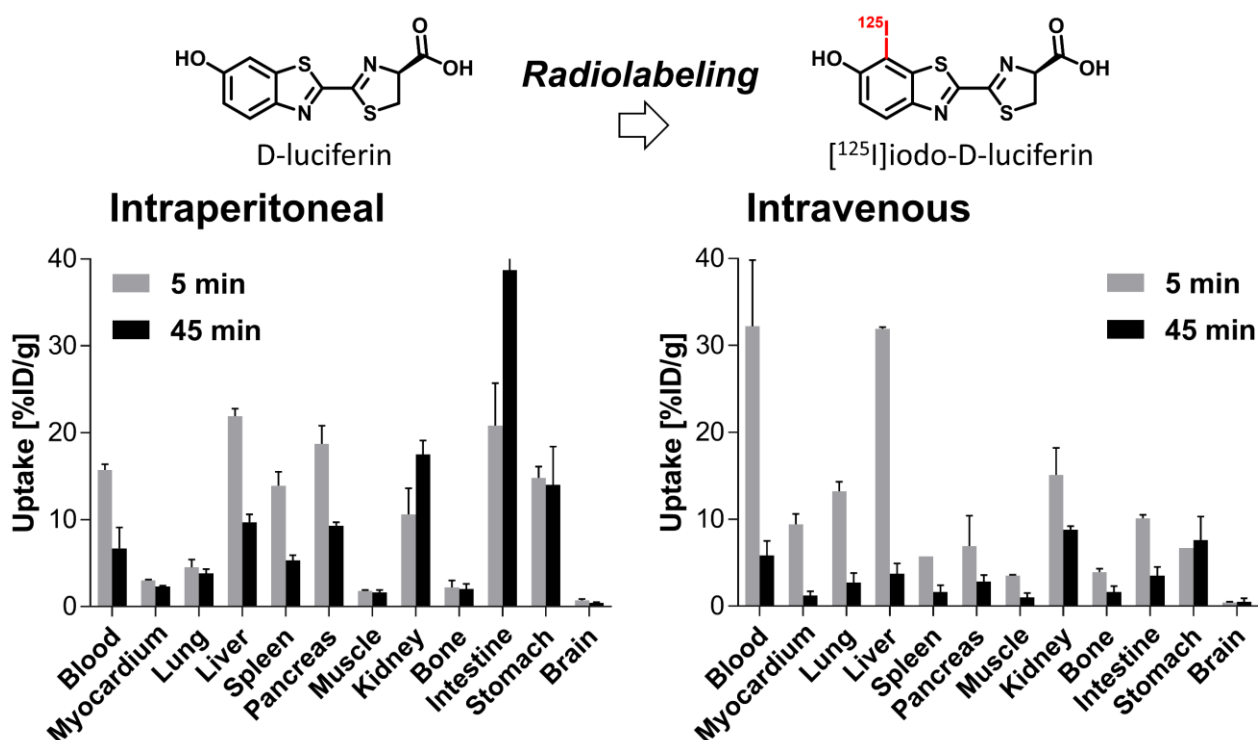


**Figure 1.9. Biodistribution of [<sup>125</sup>I]iodo-D-luciferin in ICR mice.** Adapted by permission from Ref 29, Copyright © 2003, © 2003 Lippincott Williams.

The corresponding luciferases are expressed inside cells. Therefore, D-luciferin must be delivered through cell membrane to emit light. However, cell membrane permeability of D-luciferin is moderate due to its anionic property. In addition, D-luciferin has a relatively modest affinity to luciferase (ca. 28  $\mu$ M for Fluc),<sup>15</sup> making it difficult to achieve saturate conditions.

### 1.3.4. Synthetic firefly luciferins

Synthetic luciferins are a solution to overcome the limitations of “native” firefly bioluminescence.<sup>30-</sup>  
<sup>31</sup> Fortunately, firefly (beetle) luciferases, commonly Fluc is often adopted, tolerate synthetic luciferins as light emitting substrates. The chemical structure of D-luciferin is divided into two main fragments: 1) thiazoline ring and 2) benzothiazole ring including an electron donor at C-6 position (**Figure 1.10**).

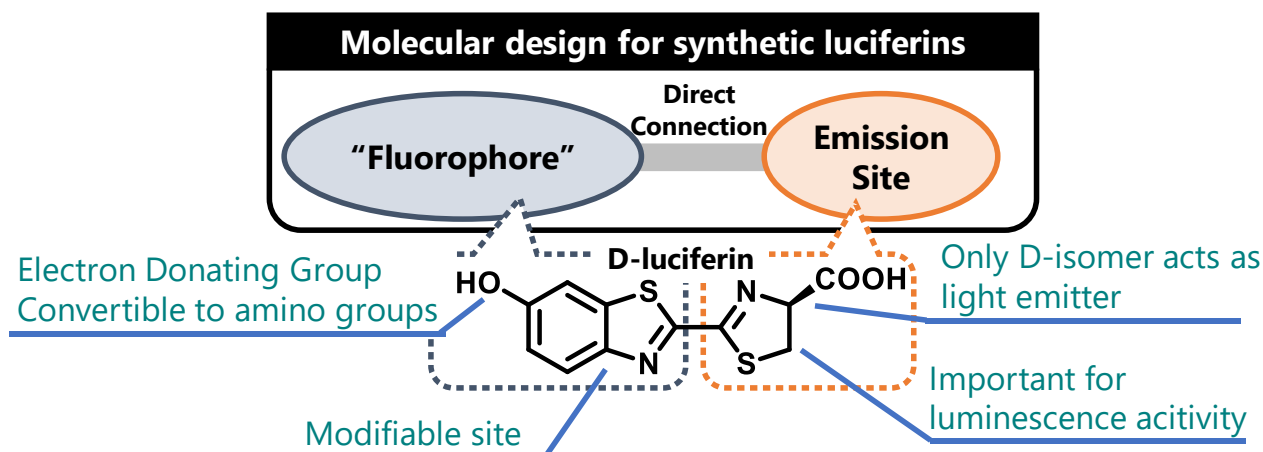


**Figure 1.10. Structure activity relationship of D-luciferin.** The chemical structure of D-luciferin is divided into two fragments: 1) thiazoline ring and 2) benzothiazole ring.

#### 1.3.4.1. Thiazoline analogues

During the light emitting reaction, firefly luciferin has to react with ATP to produce an activated luciferin-AMP intermediate (**Figure 1.4**). Therefore, carboxyl group on the thiazoline ring plays an important role in enzyme recognition and luminescence. Representative thiazoline analogues are summarized in **Figure 1.11**. L-luciferin (**1**), the optical isomer of D-luciferin, does not act as a light emitting substrate.<sup>32</sup> On the contrary, L-luciferin is known to be a strong inhibitor for firefly (beetle) luciferases. Non-carboxylated analogue (**2**) and esterified analogue (**3**) were also non luminogenic substrate for luciferase.<sup>33-34</sup>

Some analogues modified or converted to different (hetero)cyclics have also been reported. One methylated analogue (**4**) at C-5 position was luminogenic, but demethylated analogue (**5**) was not. Interestingly, adenylated analogue (**6**) of **5** displayed relatively strong emission catalyzed by a luciferase.<sup>35</sup> These results suggested that the sterically hindered substituent causes inhibition of adenylation. In 2011, Moerner and colleagues have developed a selenium analogue (**7**) in which sulfur atom was replaced. This selenium analogue (**7**) was successfully recognized by a native luciferase, resulting red-shifted bioluminescence emission ( $\lambda_{\max} = 600 \text{ nm}$ ) due to an increased electron density on the heterocycle.<sup>36</sup> The analogue (**8**) converted thiazoline to imidazoline was also non-luminogenic.<sup>37</sup> The carboluciferin (**9**) which was replaced sulfur atom to carbon afforded slightly blue-

shifted emission ( $\lambda_{\max} = 547 \text{ nm}$ ). Moreover, all non-cyclic analogues (**10-12**) were completely non-luminogenic.<sup>38</sup>

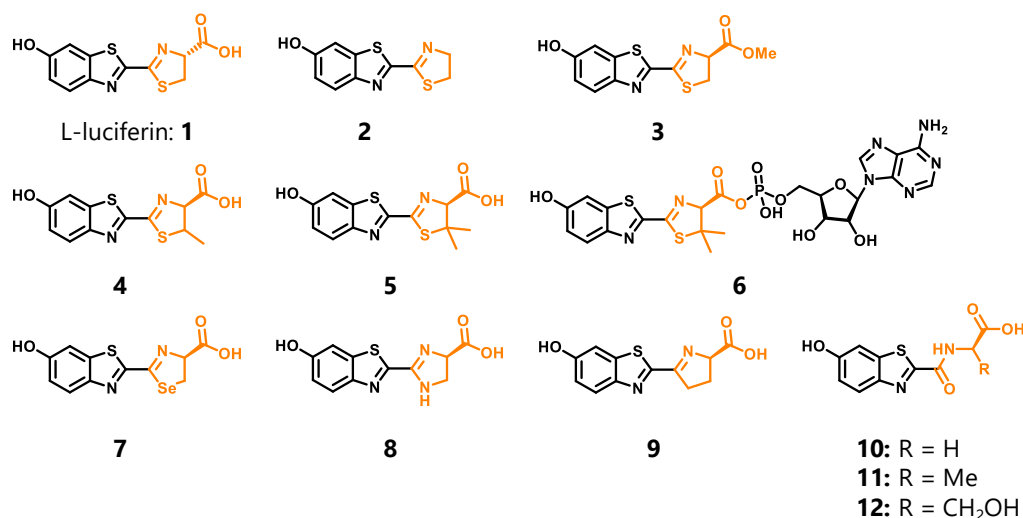


**Figure 1.11. Structures of thiazoline analogues.**

### 1.3.4.2. Benzothiazole analogues

In contrast to severity of thiazoline modifications, synthetic approaches on the benzothiazole moiety usually bring better results. Herein, the synthetic analogues are summarized by three classifications: i) Altered push-pull, ii) Steric appendages and iii) Core replacements.

#### **i) Altered push-pull (Figure 1.12)**

From 1965 to 1966, White and colleagues have reported non luminogenic analogues lacking the hydroxyl group (**13**) and methylated (**14**).<sup>33-34</sup> However, It is well-known that the aminoluciferin (**15**), in which hydroxyl group is replaced into an amino group is a highly bright analogue. Moreover, the emission wavelength of aminoluciferin was 610 nm, which are more red-shifted the D-luciferin. This bathochromic effect is due to more strongly electron donation from an amino group. In fact, dimethylated aminoluciferin (**16**) resulted in further red-shifted emission.<sup>39</sup> In 2010, Miller and colleagues have developed a series of conformationally restricted alkylaminoluciferins, **CycLucs**. Overall light emission from **CycLuc1 (17)** with Ultra-Glo™, a modified luciferase, was greatly higher than that of D-luciferin and acyclic alkylaminoluciferins.<sup>40</sup> **CycLuc1 (17)** has been applied to *in vivo* imaging and afforded much better signals than that of D-luciferin.<sup>41</sup> They have also extended this strategy to develop deep red-shifted emitting luciferins (**18-26**) and successfully achieved 642 nm emission.<sup>42</sup> The amino donor can be replaced to cyclic amino derivatives (**29, 30**).

## i) Altered push-pull

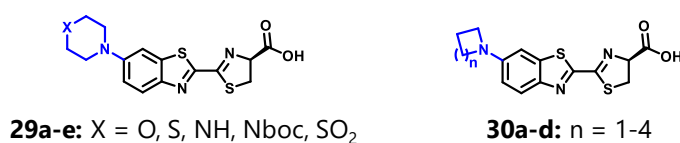
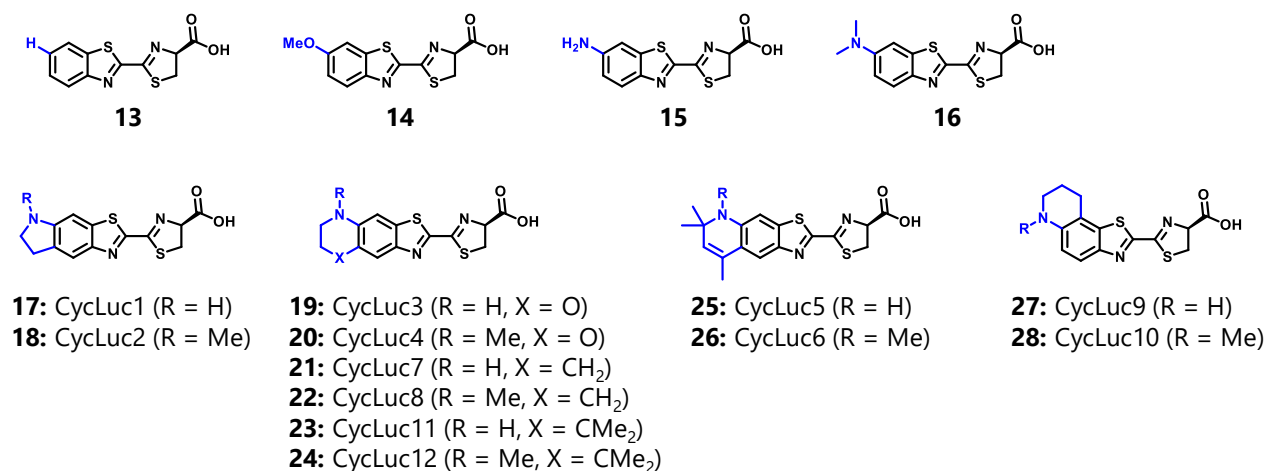


Figure 1.12. Structures of altered push-pull analogues.

## ii) Steric appendages (Figure 1.13)

In recent years, Prescher and colleagues have focused on the creation of orthogonal luciferin/luciferase pairs by introducing steric appendages to D-luciferin.<sup>43</sup> Especially, they have focused on the C-4' and C-7' position on the benzothiazole ring, and attached some steric modifications (**31-38**).

## ii) Steric appendages

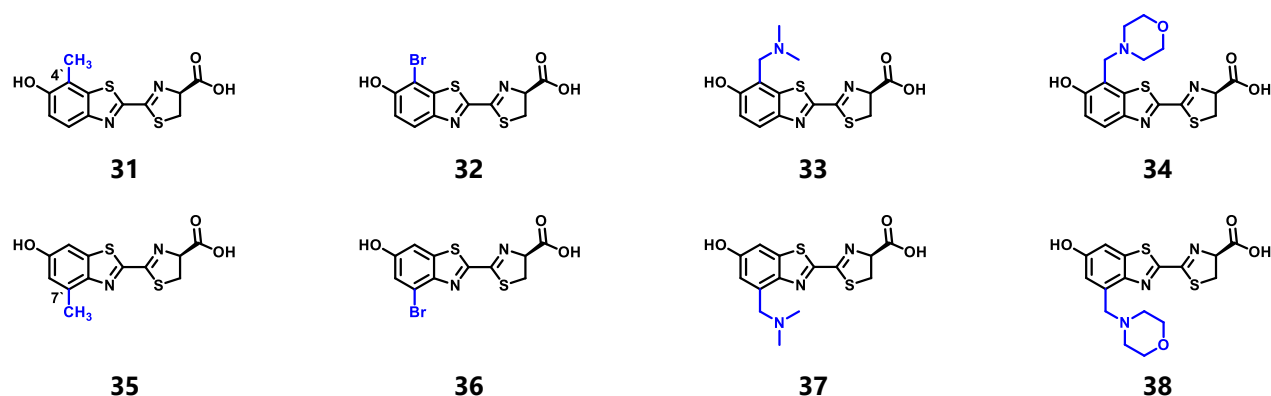
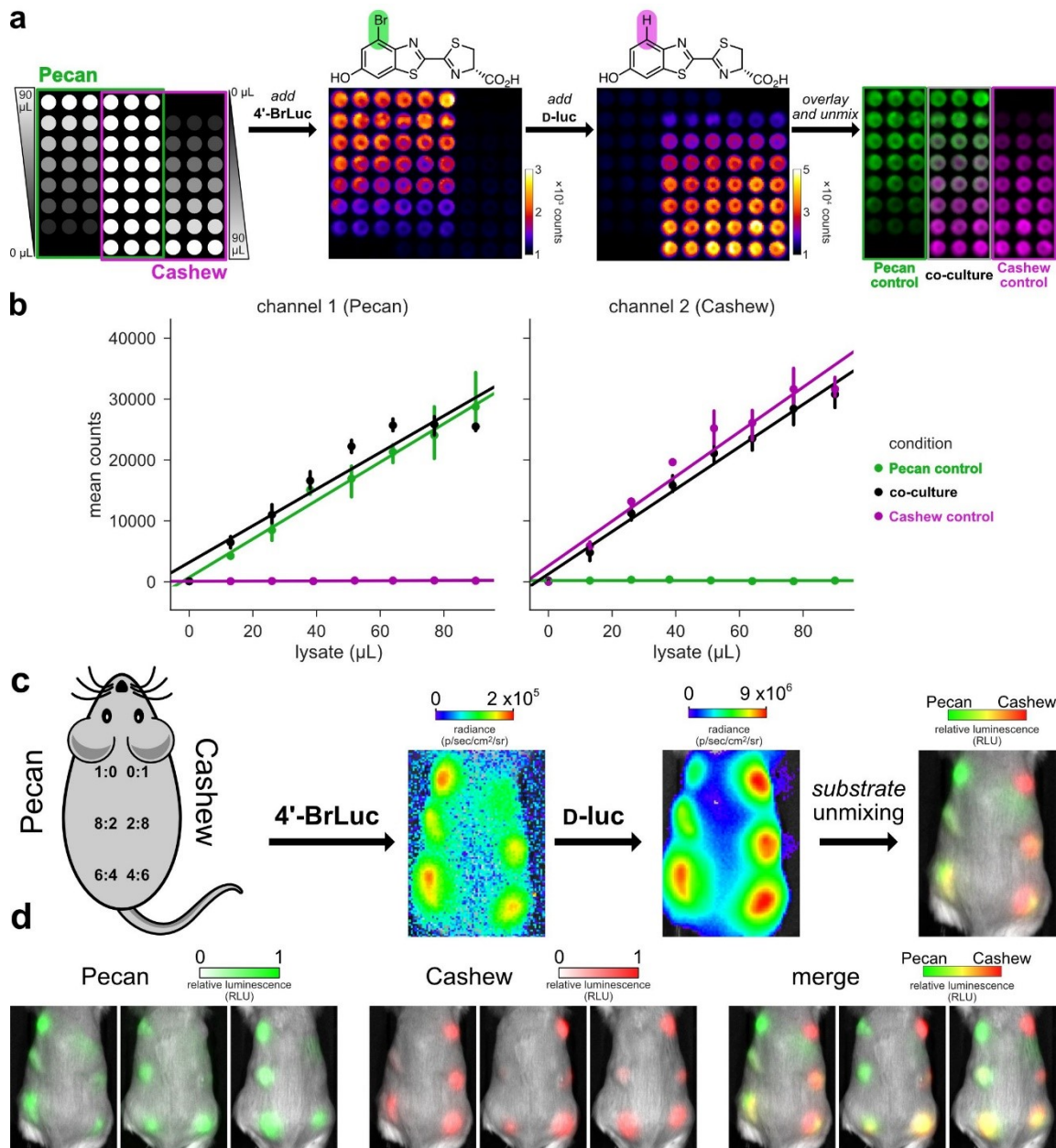


Figure 1.13. Structures of steric modified analogues.

More recently, they have successfully established multicomponent bioluminescence imaging with orthogonal luciferins through parallel evolution of luciferases (**Figure 1.14**).<sup>44</sup>



**Figure 1.14. Rapid BLI *in vitro* and *in vivo*.** (a) Pecan and Cashew were plated in a gradient fashion (as shown). The samples were treated with 4'-BrLuc (100  $\mu$ M), followed by D-luc (100  $\mu$ M). Raw images were acquired after each substrate addition. The substrate-specific signals were unmixed, assigned false colors and overlaid. (b) Quantification of the images from (a), fit via linear regression. Error bars represent the standard error of the mean for  $n = 3$  experiments. (c-d) Orthogonal bioluminescent probes can be distinguished in mice. (c) Ratios of Cashew- and Pecan expressing cells implanted in mice. Orthogonal substrates (65 mM) were administered sequentially via i.p. injection (100  $\mu$ L). Images were acquired 35 min after each injection. (d) Unmixed channels for each mouse replicate are shown. Color bars indicate normalized luminescence values. Reproduced from "C. M. Rathbun, J. A. Prescher *et al.*, "Rapid multicomponent bioluminescence imaging via substrate unmixing", *bioRxiv*, 2019 (DOI: <https://doi.org/10.1101/811026>), Ref 44.

### iii) Core replacements (Figure 1.15)

Fortunately, luciferases can accept benzothiazole core replaced analogues as a luminogenic substrate. Branchini have replaced a benzothiazole core to naphthyl (**39**) quinoyl (**40**) core.<sup>45</sup> In 2013, Maki and colleagues have introduced a styrenyl scaffold.<sup>46</sup> A series of styrenyl luciferins (**41-46**) were well tolerated by Fluc. Worthy of attention is a modulation of emission wavelengths in styrenyl analogues. Extension of olefin or replacement of a hydroxyl group with a dimethylamino group results in a larger (ca. 100 nm) or smaller bathochromic shifts (ca. 30 nm), respectively.<sup>47</sup> Importantly, the luciferin (**46**), **AkaLumine**, is one of the landmark for NIR emission ( $\lambda_{\max} = 675 \text{ nm/Fluc}$ ).<sup>48</sup> Starting with the discovery of AkaLumine, various types of NIR emitting luciferins (**47-53**) have been developed so far.<sup>46, 49-53</sup> Nowadays, parallel design of luciferases optimized for synthetic luciferins is enabling single-cell bioluminescence imaging in freely moving animals (Figure 1.16, 17).<sup>54</sup>

#### iii) Core replacements

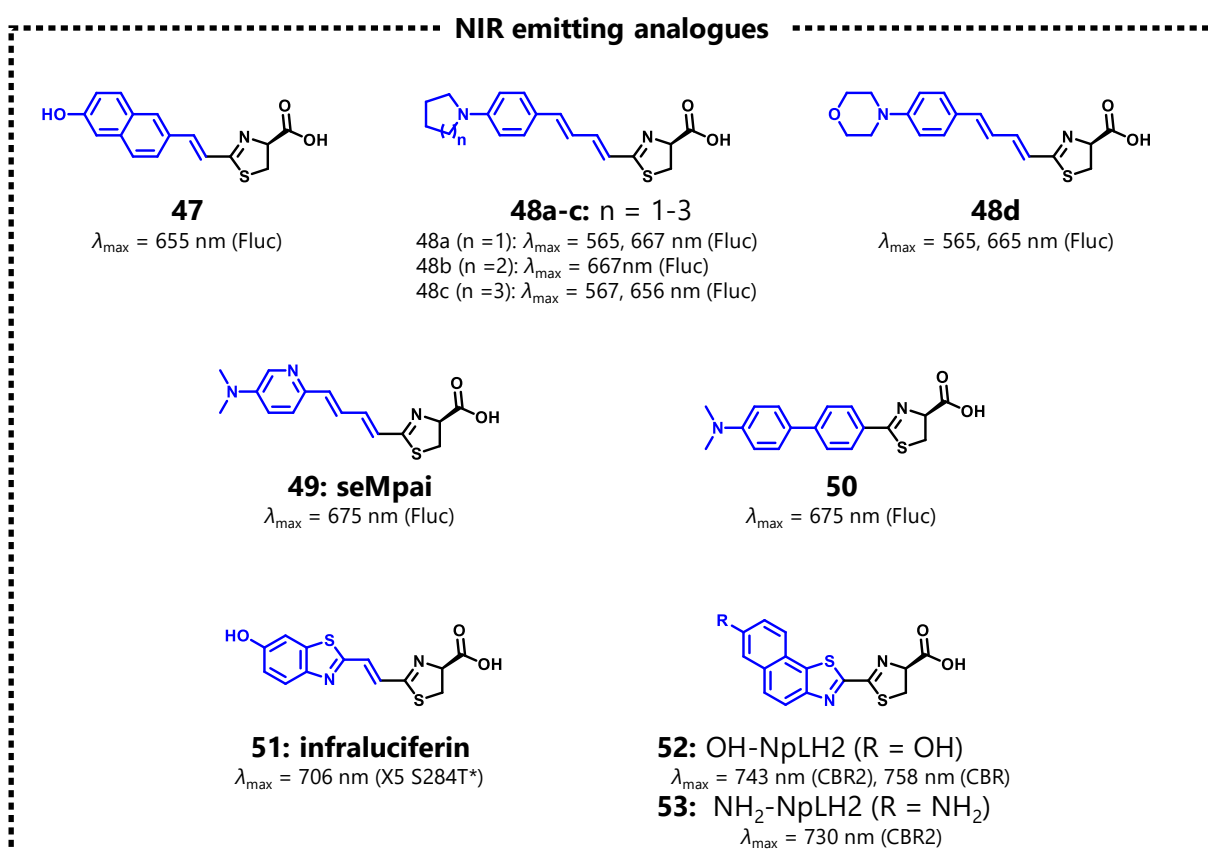
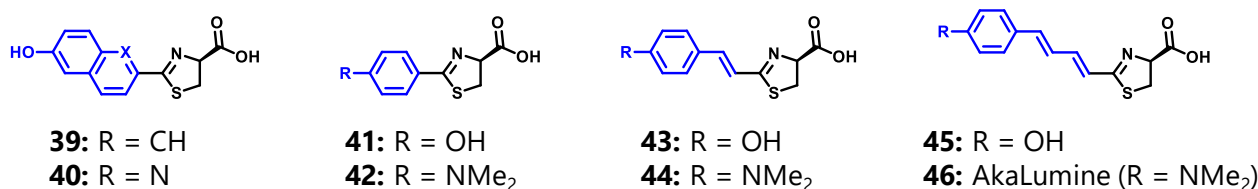
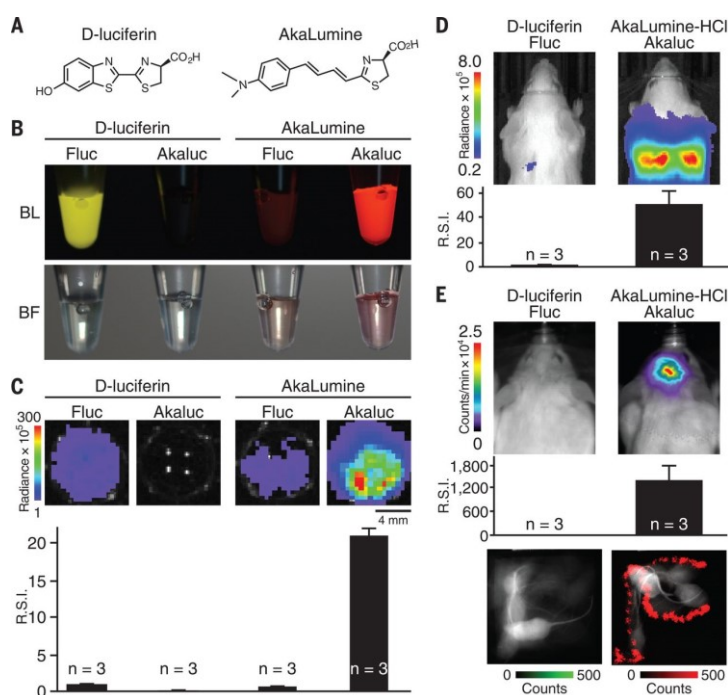


Figure 1.15. Structures of benzothiazole core replaced analogues.



**Figure 1.16. Performance of engineered AkaLumine/Akaluc versus natural D-luciferin/Fluc for *in vitro* and *in vivo* bioluminescence imaging.** (A) Chemical structures of D-luciferin (left) and AkaLumine (right). (B) BLI of four mixtures of the substrate (100  $\mu$ M) and enzyme (2 mg/ml). Color images of solutions containing (from left to right) D-luciferin/Fluc,

D-luciferin/Akaluc, AkaLumine/Fluc, and AkaLumine/Akaluc. BL, bioluminescence (top). BF, bright-field (bottom). (C) Comparative BLI of cultured cells with the four substrate/enzyme combinations described in (B). HeLa cells

expressing Fluc or Akaluc were treated with 250  $\mu$ M D-luciferin (left) or 250  $\mu$ M AkaLumine (right) and imaged using a cooled charge-coupled device (CCD) camera (1-min exposure time). Similar results were obtained from two other experiments. Bioluminescence signals were quantified and normalized to that of the D-luciferin/Fluc system. Data are presented as mean  $\pm$  SEM of three independent experiments. (D) Bioluminescence images of mice intravenously injected with  $10^3$  HeLa cells expressing Fluc (left) or Akaluc (right). Substrate administration was performed intraperitoneally. Images were acquired using a cooled CCD camera (1-min exposure time). The AkaLumine-HCl/Akaluc signals were statistically compared to D-luciferin/Fluc signals. Data are presented as mean  $\pm$  SEM of  $n = 3$  mice. (E) Bioluminescence images of mice 2 weeks after viral infection for expression of Fluc (left) and Akaluc (right) in the right striatum. Immediately after substrate administration (intraperitoneal), anesthetized mice were imaged using a cooled CCD camera (top). The AkaLumine-HCl/Akaluc signals were statistically compared to D-luciferin/Fluc signals (middle). Data are presented as mean  $\pm$  SEM of  $n = 3$  mice. After intravenous injection with their respective substrates, mice were allowed to behave naturally in the arena (bottom). Bioluminescence and bright-field images (30-msec exposure time for each) were alternately acquired using an electron-multiplying CCD (EM-CCD) camera. An integrated image spanning 5 s is shown. Bioluminescence signals are shown in green (D-luciferin/Fluc) and red (AkaLumine-HCl/Akaluc). Bright-field signals are shown in black and white. Mice were injected with 100 to 200  $\mu$ l of D-luciferin (100 mM) or AkaLumine-HCl (30 mM) [(D) and (E)]. The color bars indicate the total bioluminescence radiance (photons/sec/cm<sup>2</sup>/sr) [(C) and (D)] and counts/min (E). R.S.I., relative signal intensity [(C) to (E)]. "Single-cell bioluminescence imaging of deep tissue in freely moving animals", By Satoshi Iwano, Mayu Sugiyama, Hiroshi Hama, Akiya Watakabe, Naomi Hasegawa, Takahiro Kuchimaru, Kazumasa Z. Tanaka, Megumu Takahashi, Yoko Ishida, Junichi Hata, Satoshi Shimozono, Kana Namiki, Takashi Fukano, Masahiro Kiyama, Hideyuki Okano, Shinae Kizaka-Kondoh, Thomas J. McHugh, Tetsuo Yamamori, Hiroyuki Hioki, Shojiro Maki, Atsushi Miyawaki, *Science*, 23 Feb 2018 : 935-939, Reprinted from Ref 54 with permission from AAAS.

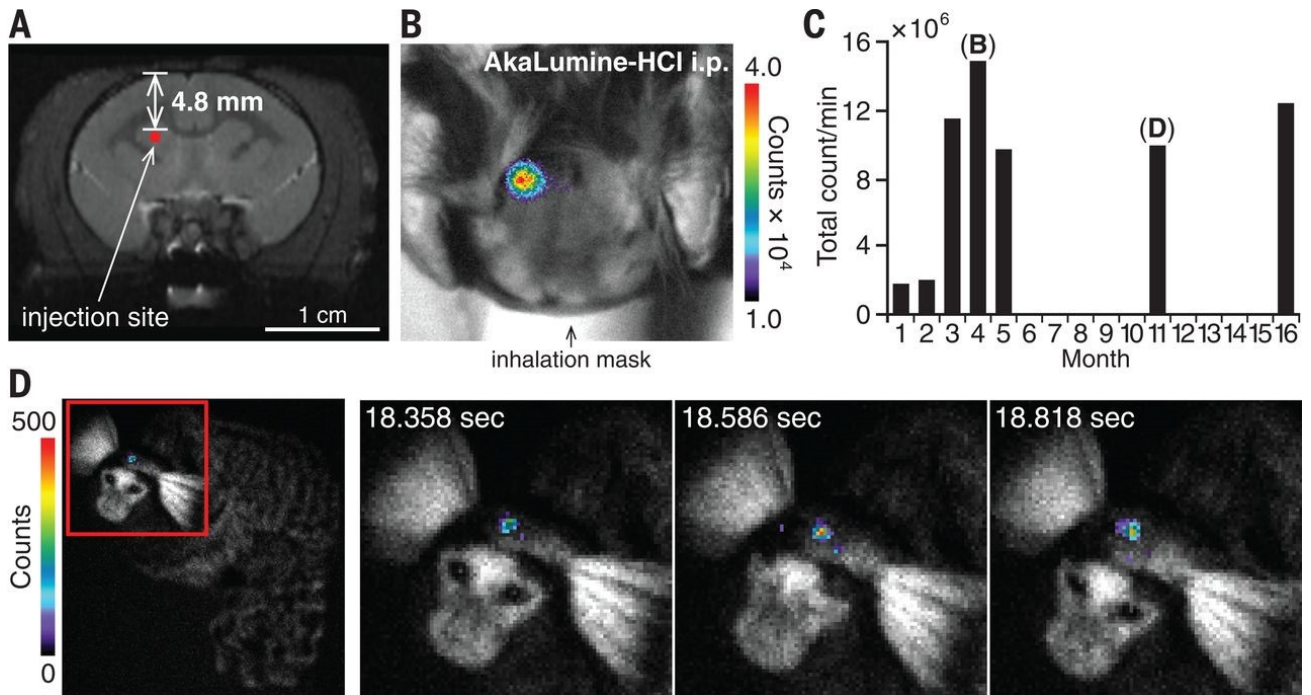


**Figure 1.17. Chronic video-rate AkaBLI of brain striatal neurons in a common marmoset.** (A) Brain MRI picture (T2 weighted image) showing guided AAV injection into the right striatum of a 4-year-old female marmoset for expression of Venus-Akaluc. (B) A bioluminescence image 4 months after injection. After the AkaLumine-HCl (75 nmol/g body weight) administration (intraperitoneal), the head of the anesthetized marmoset was imaged using an EM-CCD camera (30-s exposure time). (C) Bioluminescence signals were quantified and plotted against time after injection. Due to growth with various degrees of depilation during the long time period, the efficiency of bioluminescence collection varied, and the data are displayed by a bar graph. (D) Bioluminescence images 12 months after injection. After AkaLumine-HCl administration (intraperitoneal), the entire marmoset (naturally behaving) was imaged using an EM-CCD camera (100-msec exposure time). An eye blink was recorded in three consecutives, expanded images. The color bars indicate the total bioluminescence counts/30 s (B) and counts/100 msec (D). "Single-cell bioluminescence imaging of deep tissue in freely moving animals", By Satoshi Iwano, Mayu Sugiyama, Hiroshi Hama, Akiya Watakabe, Naomi Hasegawa, Takahiro Kuchimaru, Kazumasa Z. Tanaka, Megumu Takahashi, Yoko Ishida, Junichi Hata, Satoshi Shimozono, Kana Namiki, Takashi Fukano, Masahiro Kiyama, Hideyuki Okano, Shinae Kizaka-Kondoh, Thomas J. McHugh, Tetsuo Yamamori, Hiroyuki Hioki, Shojiro Maki, Atsushi Miyawaki, *Science*, 23 Feb 2018 : 935-939, Reprinted from Ref 54 with permission from AAAS.

## 1.4. Scope of This Thesis

Firefly bioluminescence is a promising imaging tool to track biological functions inside cells or a whole body. However, in contrast to the numerous efforts to develop fluorescent indicators or probes, few varieties of luciferins are still currently available. In order to evolve firefly bioluminescence imaging as a next generation imaging tool, expanded palettes of firefly luciferins are indispensable. In particular, 1) orthogonality 2) brightness and 3) NIR emission have the potential to expand the applications of firefly bioluminescence. For this purpose, several synthetic luciferins have been developed through each unique approach.

### **This thesis includes three parts as outlined below:**

**Chapter 2** describes an orthogonal responsive firefly luciferin analogue, **7'-AllylLuc**, substituted an allyl group. **7'-AllylLuc** can be easily accessed from commercially available starting materials in 4 steps with 68% overall yield. This analogue displayed luciferase orthogonal emission in combination with living cells expressing luciferase Eluc from *Pyrearinus termitilluminans*. In addition, the photon production from **7'-AllylLuc**/Eluc pairs lasted over 100 minutes, which is a desirable property for bioluminescence applications.

**Chapter 3** describes an approach to improve photon production on firefly luciferin analogues through an azetidine-substituent strategy. Replacing the *N, N*-dimethylamino group in classical fluorophores with a four membered azetidine ring provides improved luminescence quantum yields. This strategy was extended to bioluminescent firefly luciferin analogues and its general applicability was demonstrated. For this purpose, five-types of luciferin cores were employed, and a total of 10 analogues were evaluated. Among them, only the benzothiazole core analogue benefited from azetidine substitution and improved the fluorescence and bioluminescence emission.

**Chapter 4** describes a series of near-infrared emitting luciferin analogues, **NIRLucs**, designed through a ring fusion strategy. One limitation in firefly bioluminescence imaging is the limited variety of luciferins emitting in the near-infrared (NIR) region (650-900 nm), where tissue penetration is high. **NIRLucs** resulted in pH-independent structure-inherent NIR emission with a native firefly luciferase. When applied to cells, **NIRLucs** displayed dose-independent improved NIR emission even at low substrate concentrations where the native D-luciferin does not emit. Additionally, excellent blood retention and brighter photon flux (7-fold overall, 16-fold in the NIR spectral range) than in the case of D-luciferin have been observed with one of the **NIRLucs** in mice bearing subcutaneous tumors.

Finally, I concluded this thesis with the significance of my studies and future outlook of firefly bioluminescence imaging platform as **Chapter 5**.

# References

1. Weissleder, R. and Pittet, M. J., "Imaging in the era of molecular oncology", *Nature*, **2008**, *452*, 580-589.
2. Smith, B. R. and Gambhir, S. S., "Nanomaterials for In Vivo Imaging", *Chem. Rev.*, **2017**, *117*, 901-986.
3. Bailey, D.; Townsend, D. and Valk, P., "Positron emission tomography. Basic sciences", *Journal of Neuroradiology - J NEURORADIOL*, **2006**, *33*, 265-265.
4. Mariani, G.; Bruselli, L.; Kuwert, T.; Kim, E. E.; Flotats, A.; Israel, O.; Dondi, M. and Watanabe, N., "A review on the clinical uses of SPECT/CT", *Eur. J. Nucl. Med. Mol. Imaging*, **2010**, *37*, 1959-1985.
5. Willmann, J. K.; van Bruggen, N.; Dinkelborg, L. M. and Gambhir, S. S., "Molecular imaging in drug development", *Nat. Rev. Drug Discov.*, **2008**, *7*, 591-607.
6. Shimomura, O., "Bioluminescence: chemical principles and methods", World Scientific: **2012**.
7. Troy, T.; Jekic-McMullen, D.; Sambucetti, L. and Rice, B., "Quantitative Comparison of the Sensitivity of Detection of Fluorescent and Bioluminescent Reporters in Animal Models", *Molecular Imaging* **2004**, *3*, 9-23.
8. Seliger, H. and McElroy, W., "The colors of firefly bioluminescence: enzyme configuration and species specificity", *Proc. Natl. Acad. Sci. U.S.A.*, **1964**, *52*, 75-81.
9. Wood, K. V.; Lam, Y. A.; Seliger, H. H. and McElroy, W. D., "Complementary DNA coding click beetle luciferases can elicit bioluminescence of different colors", *Science*, **1989**, *244*, 700-702.
10. Viviani, V. R., "The origin, diversity, and structure function relationships of insect luciferases", *Cell. Mol. Life Sci.*, **2002**, *59*, 1833-1850.
11. Akimoto, H.; Kwon, H. J.; Ozaki, M.; Yasuda, K. and Ohmiya, Y. "In vivo bioluminescence imaging of bone marrow-derived cells in brain inflammation", *Biochem. Biophys. Res. Commun.*, **2009**, *380*, 844-849.
12. Farhana, I.; Hossain, M. N.; Suzuki, K.; Matsuda, T. and Nagai, T. "Genetically Encoded Fluorescence/Bioluminescence Bimodal Indicators for Ca<sup>2+</sup> Imaging", *ACS Sensors*, **2019**, *4*, 1825-1834.
13. Fraga, H., "Firefly luminescence: a historical perspective and recent developments", *Photochem. Photobiol. Sci.*, **2008**, *7*, 146-158.
14. White, E. H.; Rapaport, E.; Seliger, H. H. and Hopkins, T. A., "The chemi- and bioluminescence of firefly luciferin: an efficient chemical production of electronically excited states", *Bioorg. Chem.*, **1971**, *1*, 92-122.

15. Woodrooffe, C. C.; Meisenheimer, P. L.; Klaubert, D. H.; Kovic, Y.; Rosenberg, J. C.; Behney, C. E.; Southworth, T. L. and Branchini, B. R., "Novel heterocyclic analogues of firefly luciferin", *Biochemistry*, **2012**, *51*, 9807-9813.
16. Ando, Y.; Niwa, K.; Yamada, N.; Enomoto, T.; Irie, T.; Kubota, H.; Ohmiya, Y. and Akiyama, H., "Firefly bioluminescence quantum yield and colour change by pH-sensitive green emission", *Nat. Photonics*, **2007**, *2*, 44-47.
17. Niwa, K.; Ichino, Y.; Kumata, S.; Nakajima, Y.; Hiraishi, Y.; Kato, D. i.; Viviani, V. R. and Ohmiya, Y., "Quantum yields and kinetics of the firefly bioluminescence reaction of beetle luciferases", *Photochem. Photobiol.*, **2010**, *86*, 1046-1049.
18. Niwa, K.; Ichino, Y. and Ohmiya, Y., "Quantum Yield Measurements of Firefly Bioluminescence Reactions Using a Commercial Luminometer", *Chem. Lett.*, **2010**, *39*, 291-293.
19. Hirano, T.; Hasumi, Y.; Ohtsuka, K.; Maki, S.; Niwa, H.; Yamaji, M. and Hashizume, D., "Spectroscopic Studies of the Light-Color Modulation Mechanism of Firefly (Beetle) Bioluminescence", *J. Am. Chem. Soc.*, **2009**, *131*, 2385-2396.
20. Noguchi, T.; Michihata, T.; Nakamura, W.; Takumi, T.; Shimizu, R.; Yamamoto, M.; Ikeda, M.; Ohmiya, Y. and Nakajima, Y., "Dual-Color Luciferase Mouse Directly Demonstrates Coupled Expression of Two Clock Genes", *Biochemistry*, **2010**, *49*, 8053-8061.
21. Kitayama, Y.; Kondo, T.; Nakahira, Y.; Nishimura, H.; Ohmiya, Y. and Oyama, T., "An In vivo Dual-Reporter System of Cyanobacteria Using Two Railroad-Worm Luciferases with Different Color Emissions", *Plant Cell Physiol.*, **2004**, *45*, 109-113.
22. Branchini, B. R.; Southworth, T. L.; Khattak, N. F.; Michelini, E. and Roda, A., "Red- and green-emitting firefly luciferase mutants for bioluminescent reporter applications", *Anal. Biochem.*, **2005**, *345*, 140-148.
23. Jones, K. A.; Porterfield, W. B.; Rathbun, C. M.; McCutcheon, D. C.; Paley, M. A. and Prescher, J. A., "Orthogonal Luciferase-Luciferin Pairs for Bioluminescence Imaging", *J. Am. Chem. Soc.*, **2017**, *139*, 2351-2358.
24. Paley, M. A. and Prescher, J. A., "Bioluminescence: a versatile technique for imaging cellular and molecular features", *Med. Chem. Commun.*, **2014**, *5*, 255-267.
25. Maguire, C. A.; Bovenberg, M. S.; Crommentuijn, M. H. W.; Niers, J. M.; Kerami, M.; Teng, J.; Sena-Esteves, M.; Badr, C. E. and Tannous, B. A., "Triple Bioluminescence Imaging for In Vivo Monitoring of Cellular Processes", *Mol. Ther. - Nucleic Acids*, **2013**, *2*, e99.
26. Pichler, A.; Prior, J. L. and Piwnica-Worms, D., "Imaging reversal of multidrug resistance in living mice with bioluminescence: *MDR1* P-glycoprotein transports coelenterazine", *Proc. Natl. Acad. Sci. U.S.A.*, **2004**, *101*, 1702-1707.
27. Weissleder, R., "A clearer vision for in vivo imaging", *Nat. Biotech.*, **2001**, *19*, 316-317.
28. Weissleder, R. and Ntziachristos, V., "Shedding light onto live molecular targets", *Nat. Med.*, **2003**, *9*, 123-128.

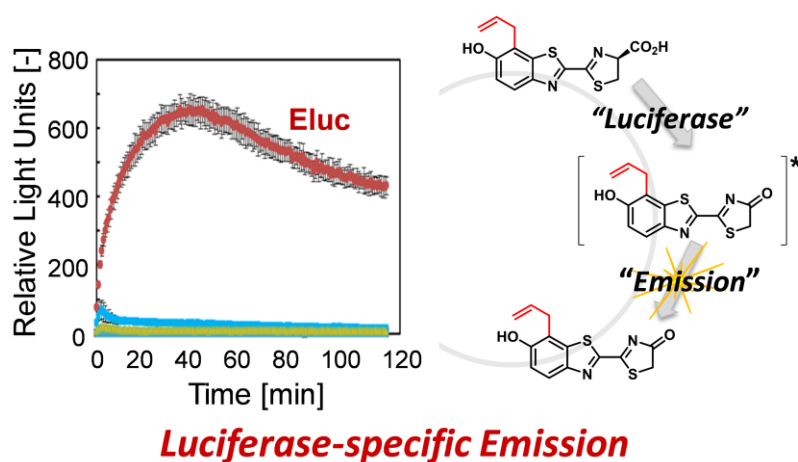
29. Lee, K.; Byun, S.; Paik, J.; Lee, S.; Song, S.; Choe, Y. and Kim, B., "Cell uptake and tissue distribution of radioiodine labelled D-luciferin: implications for luciferase based gene imaging", *Nucl. Med. Commun.*, **2003**, *24*, 1003-1009.
30. Miller, S. C.; Mofford, D. M. and Adams, S. T., Jr., "Lessons Learned from Luminous Luciferins and Latent Luciferases", *ACS Chem. Biol.*, **2018**, *13*, 1734-1740.
31. Podsiadły, R.; Grzelakowska, A.; Modrzejewska, J.; Siarkiewicz, P.; Słowiński, D.; Szala, M. and Świerczyńska, M., "Recent progress in the synthesis of firefly luciferin derivatives", *Dyes Pigments* **2019**, *170*, 107627-107653.
32. Lambert, N., "Firefly luciferase can use L-luciferin to produce light", *Biochem. J.*, **1996**, *317*, 273-277.
33. White, E. H.; Wörther, H.; Field, G. F. and McElroy, W. D., "Analogues of firefly luciferin", *J. Org. Chem.*, **1965**, *30*, 2344-2348.
34. White, E. H. and Wörther, H., "Analogues of Firefly Luciferin. III", *J. Org. Chem.* **1966**, *31*, 1484-1488.
35. Branchini, B. R.; Murtiashaw, M. H.; Magyar, R. A.; Portier, N. C.; Ruggiero, M. C. and Stroh, J. G., "Yellow-green and red firefly bioluminescence from 5, 5-dimethyloxyluciferin", *J. Am. Chem. Soc.* **2002**, *124*, 2112-2113.
36. Conley, N. R.; Dragulescu-Andrasi, A.; Rao, J. and Moerner, W. E., "A selenium analogue of firefly D-luciferin with red-shifted bioluminescence emission", *Angew. Chem. Int. Ed.*, **2012**, *51*, 3350-3353.
37. McCutcheon, D. C.; Paley, M. A.; Steinhardt, R. C. and Prescher, J. A., "Expedient synthesis of electronically modified luciferins for bioluminescence imaging", *J. Am. Chem. Soc.*, **2012**, *134*, 7604-7607.
38. Ioka, S.; Saitoh, T.; Iwano, S.; Suzuki, K.; Maki, S. A.; Miyawaki, A.; Imoto, M. and Nishiyama, S., "Synthesis of Firefly Luciferin Analogues and Evaluation of the Luminescent Properties", *Chem. Eur. J.*, **2016**, *22*, 9330-9337.
39. Hirano, T.; Nagai, H.; Matsushashi, T.; Hasumi, Y.; Iwano, S.; Ito, K.; Maki, S.; Niwa, H. and Viviani, V. R., "Spectroscopic studies of the color modulation mechanism of firefly (beetle) bioluminescence with amino-analogs of luciferin and oxyluciferin", *Photochem. Photobiol. Sci.*, **2012**, *11*, 1281-1284.
40. Reddy, G. R.; Thompson, W. C. and Miller, S. C., "Robust light emission from cyclic alkylaminoluciferin substrates for firefly luciferase", *J. Am. Chem. Soc.*, **2010**, *132*, 13586-13587.
41. Evans, M. S.; Charette, J. P.; Adams, S. T., Jr.; Reddy, G. R.; Paley, M. A.; Aronin, N.; Prescher, J. A. and Miller, S. C., "A synthetic luciferin improves bioluminescence imaging in live mice", *Nat. Methods*, **2014**, *11*, 393-395.
42. Mofford, D. M.; Reddy, G. R. and Miller, S. C., "Aminoluciferins extend firefly luciferase bioluminescence into the near-infrared and can be preferred substrates over D-luciferin", *J. Am. Chem. Soc.*, **2014**, *136*, 13277-13282.
43. Williams, S. J. and Prescher, J. A., "Building Biological Flashlights: Orthogonal Luciferases and Luciferins for *in Vivo* Imaging", *Acc. Chem. Res.* **2019**, *52*, 3039-3050.

44. Rathbun, C. M.; Ionkina, A. A.; Yao, Z.; Jones, K. A.; Porterfield, W. B. and Prescher, J. A., "Rapid multicomponent bioluminescence imaging via substrate unmixing", *bioRxiv* **2019**,. (DOI: <https://doi.org/10.1101/811026>).
45. Branchini, B. R.; Hayward, M. M.; Bamford, S.; M Brennan, P. and Lajiness, E. J., "NAPHTHYL-AND QUINOLYLLUCIFERIN: GREEN AND RED LIGHT EMITTING FIREFLY LUCIFERIN ANALOGUES", *Photochem. Photobiol.*, **1989**, *49*, 689-695.
46. Iwano, S.; Obata, R.; Miura, C.; Kiyama, M.; Hama, K.; Nakamura, M.; Amano, Y.; Kojima, S.; Hirano, T.; Maki, S. and Niwa, H., "Development of simple firefly luciferin analogs emitting blue, green, red, and near-infrared biological window light", *Tetrahedron*, **2013**, *69*, 3847-3856.
47. Kitada, N.; Saitoh, T.; Ikeda, Y.; Iwano, S.; Obata, R.; Niwa, H.; Hirano, T.; Miyawaki, A.; Suzuki, K.; Nishiyama, S. and Maki, S. A., "Toward bioluminescence in the near-infrared region: Tuning the emission wavelength of firefly luciferin analogues by allyl substitution", *Tetrahedron Lett.*, **2018**, *59*, 1087-1090.
48. Kuchimaru, T.; Iwano, S.; Kiyama, M.; Mitsumata, S.; Kadonosono, T.; Niwa, H.; Maki, S. and Kizaka-Kondoh, S., "A luciferin analogue generating near-infrared bioluminescence achieves highly sensitive deep-tissue imaging", *Nat. Commun.*, **2016**, *7*, 11856-11863.
49. Miura, C.; Kiyama, M.; Iwano, S.; Ito, K.; Obata, R.; Hirano, T.; Maki, S. and Niwa, H., "Synthesis and luminescence properties of biphenyl-type firefly luciferin analogs with a new, near-infrared light-emitting bioluminophore", *Tetrahedron*, **2013**, *69*, 9726-9734.
50. Kiyama, M.; Iwano, S.; Otsuka, S.; Lu, S. W.; Obata, R.; Miyawaki, A.; Hirano, T. and Maki, S. A., "Quantum yield improvement of red-light-emitting firefly luciferin analogues for *in vivo* bioluminescence imaging", *Tetrahedron*, **2018**, *74*, 652-660.
51. Jathoul, A. P.; Grounds, H.; Anderson, J. C. and Pule, M. A., "A dual-color far-red to near-infrared firefly luciferin analogue designed for multiparametric bioluminescence imaging", *Angew. Chem. Int. Ed.*, **2014**, *53*, 13059-13063.
52. Hall, M. P.; Woodroffe, C. C.; Wood, M. G.; Que, I.; Van't Root, M.; Ridwan, Y.; Shi, C.; Kirkland, T. A.; Encell, L. P.; Wood, K. V.; Lowik, C. and Mezzanotte, L., "Click beetle luciferase mutant and near infrared naphthyl-luciferins for improved bioluminescence imaging", *Nat. Commun.*, **2018**, *9*, 132-143.
53. Saito, R.; Kuchimaru, T.; Higashi, S.; Lu, S. W.; Kiyama, M.; Iwano, S.; Obata, R.; Hirano, T.; Kizaka-Kondoh, S. and Maki, S. A., "Synthesis and Luminescence Properties of Near-Infrared N-Heterocyclic Luciferin Analogues for *In Vivo* Optical Imaging", *Bull. Chem. Soc. Jpn*, **2019**, *92*, 608-618.
54. Iwano, S.; Sugiyama, M.; Hama, H.; Watakabe, A.; Hasegawa, N.; Kuchimaru, T.; Tanaka, K. Z.; Takahashi, M.; Ishida, Y.; Hata, J.; Shimozono, S.; Namiki, K.; Fukano, T.; Kiyama, M.; Okano, H.; Kizaka-Kondoh, S.; McHugh, T. J.; Yamamori, T.; Hioki, H.; Maki, S. and Miyawaki, A., "Single-cell bioluminescence imaging of deep tissue in freely moving animals", *Science*, **2018**, *359*, 935-939

## Chapter 2

# An Allylated Firefly Luciferin Analogue with Luciferase Specific Response in Living Cells

This chapter is based on "An Allylated Firefly Luciferin Analogue with Luciferase Specific Response in Living Cells, Yuma Ikeda, Tsuyoshi Saitoh, Kazuki Niwa, Takahiro Nakajima, Nobuo Kitada, Shojiro A. Maki, Moritoshi Sato, Daniel Citterio, Shigeru Nishiyama and Koji Suzuki, *Chem. Commun.*, **2018**, 54, 1774-1777".



## Summary

An allylated firefly luciferin was successfully synthesized and its bioluminescence properties were evaluated. When applied to cellular imaging in combination with Eluc, which is one of the commercially available luciferases, this analogue displayed a luciferase-specific bioluminescence signal with prolonged emission (>100 min).

## 2.1 Introduction

Bioluminescence-based assays with luciferin–luciferase pairs are widely used as *in vitro* and *in vivo* reporters of biologically relevant substances, gene expression, and tumor progression, among others.<sup>1-2</sup> Since bioluminescence-based assays do not require excitation light, they exhibit much lower background signals than fluorescence-based assays and are applicable to highly sensitive bioimaging.<sup>3</sup> Among the available systems, the firefly luciferin–luciferase reaction is one of the most well-studied emission systems, due to its high quantum yield ( $\phi_{\text{BL}} = 0.23\text{--}0.61$ ) and relatively long emission wavelength ( $\lambda_{\text{em}} 530\text{--}620\text{ nm}$ ).<sup>4</sup> In the firefly bioluminescence reaction, the luciferase catalyzes the oxidation of D-luciferin in the presence of adenosine triphosphate (ATP) and  $\text{Mg}^{2+}$  acting as co-factors to release a light photon (**Figure 2.1a**). A variety of luciferases has been discovered and cloned<sup>5-6</sup>, and many of them have been adapted to “spy” on cells in whole animals utilizing their different bioluminescence colors and superior properties, such as prolonged light emission and high luminescence efficiency, among others.<sup>7-8</sup> However, it is widely known that D-luciferin is the only substrate that results in light emission in combination with these luciferases. Although different luciferases can be selectively expressed to a specific target, they all result in bioluminescence emission upon introduction of D-luciferin. For this reason, it is basically not possible to distinguish between multiple targets within a single cell. Although the development of luciferases has been a very active field of research, there are unfortunately only few reports of successful development of synthetic luciferins, presumably due to the difficulty in designing and synthesizing bioluminescence active luciferins.

This chapter describes a firefly luciferin analogue modified with an allyl group at the C-7' position of its benzothiazole core (**Figure 2.1b**), exhibiting bioluminescence emission with various luciferases in analogy to D-luciferin. In mammalian cells transiently expressing luciferase, I have confirmed its utility for bioluminescence imaging as a luciferase-specific synthetic substrate.

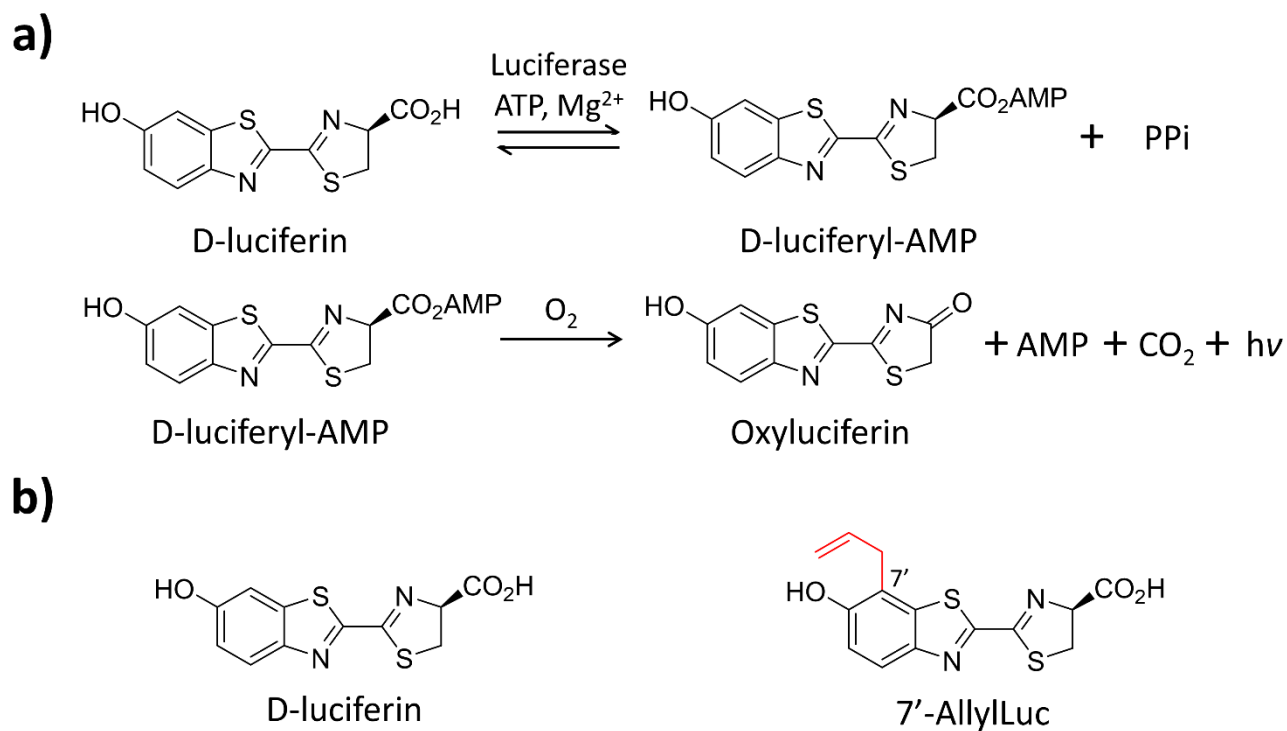


**Figure 2.1. Chemical structures of luciferins.** a) Firefly bioluminescence reaction: luciferase catalyzes the adenylation and oxidation of its substrate D-luciferin to release a photon. b) Chemical structures of D-luciferin and 7'-AllylLuc. Reproduced from "Y. Ikeda *et al.*, *Chem. Commun.*, **2018**, 54, 1774-1777 (DOI: 10.1039/C7CC09720D) with permission from The Royal Society of Chemistry.

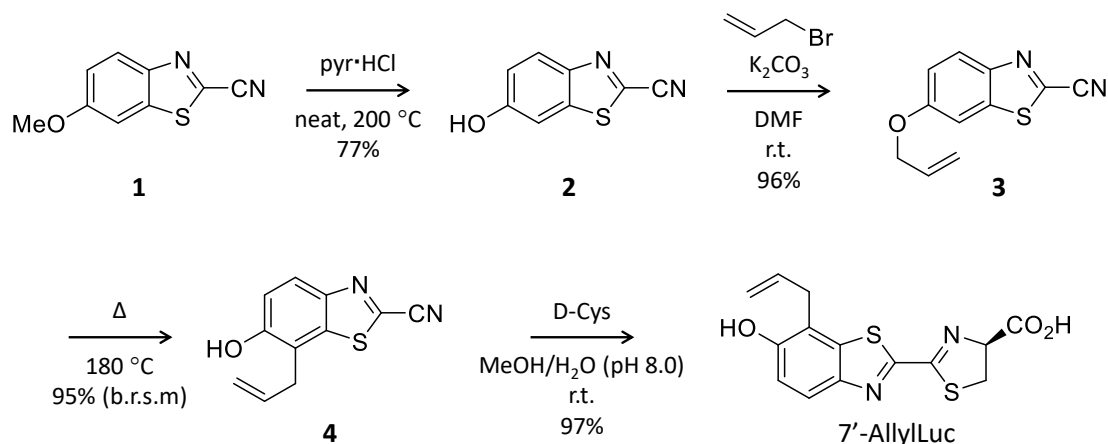
## 2.2 Results and Discussion

### 2.2.1. Design and synthesis of 7'-AllylLuc

Many details regarding bioluminescence of the firefly system still remain unknown, and random modifications of the luciferin structure may lead to the loss of the luminescence activity. Therefore, I referred to previously performed studies on the structure–activity relationship of firefly luciferin to more efficiently design analogues. The molecular structure of D-luciferin is mainly composed of two subunits, the thiazoline and the benzothiazole substructures. The position and the stereochemistry of the carboxyl group on the thiazoline ring is a crucial factor for the luminescence activity.<sup>9-11</sup> In contrast to the luminescence activity of the D-form, it is widely known that the optical isomer L-luciferin works as a potential luminescence inhibitor.<sup>12</sup> Additionally, many of the heteroatom variants and substituent modifications of this thiazoline ring have resulted in a dramatic reduction or loss of luminescence activity,<sup>13-14</sup> and thus, the thiazoline ring subunit is regarded as an essential site for substrate recognition by the luciferase enzyme and the luminescence activity. On the other hand, it has been reported that most analogues with modification at the benzothiazole ring subunit retain their luminescent activities. Actually, analogues with heteroatom substitution in the benzothiazole ring<sup>14-15</sup> and modification of its chemical structure<sup>16-18</sup> maintained the luminescence activity with shifts in the emission wavelength. Therefore, it can be said that the benzothiazole ring is the modifiable site of D-luciferin. A recent study revealed that modifications of the benzothiazole ring at the C-7' position with sterically demanding residues potentially lead to bolstered bioluminescence properties.<sup>19</sup> Furthermore, it was also shown that mutant luciferases can effectively result in substrate specific luminescent properties with structurally modified luciferin analogues.<sup>20-21</sup>

In order to expand the applications of bioluminescent systems, I have designed a firefly luciferin analogue modified with an allyl group at the C-7' position of its benzothiazole core (**Figure 2.1b**), exhibiting bioluminescence emission with various luciferases in analogy to D-luciferin, and confirmed its utility for bioluminescence imaging. To access the desired allyl-modified luciferin structure, focus was set on the Claisen rearrangement for introduction of an allyl-group (**Scheme 2.1**). The synthesis of allyl luciferin begins with pyridine hydrochloride promoted thermal deprotection of commercially available 2-cyano-6-methoxybenzothiazole (1), which is transformed to its phenol form, 2-cyano-6-hydroxybenzothiazole (2). It is then converted to the allyloxy-benzothiazole (3) by treatment with allyl bromide/ $K_2CO_3$ , which on regioselective Claisen rearrangement of the allyl group results in compound (4). The coupling reaction of 2-cyano-benzothiazole derivative (4) with D-cysteine generated 7'-

AllylLuc via the standard procedure. Thus, 7'-AllylLuc can be prepared in 4 steps from commercially available starting materials in 68% overall yield.



**Scheme 2.1. Synthesis of 7'-AllylLuc.** Reproduced from "Y. Ikeda *et al.*, *Chem. Commun.*, **2018**, 54, 1774-1777 (DOI: 10.1039/C7CC09720D) with permission from The Royal Society of Chemistry.

## 2.2.2. Light-emitting potential of 7'-AllylLuc

To explore the potential emission ability of 7'-AllylLuc, a conventional chemiluminescence assay was first conducted. This non-enzymatic emission process is a useful method for verifying the luminescence ability of the substrate itself. For this purpose, luciferin methyl esters were synthesized.<sup>13</sup> When 7'-AllylLuc methyl ester was subjected to chemiluminescence assay conditions, luminescence was observed (**Figure 2.2**). This suggested that 7'-AllylLuc is a potential emitter for luciferases.

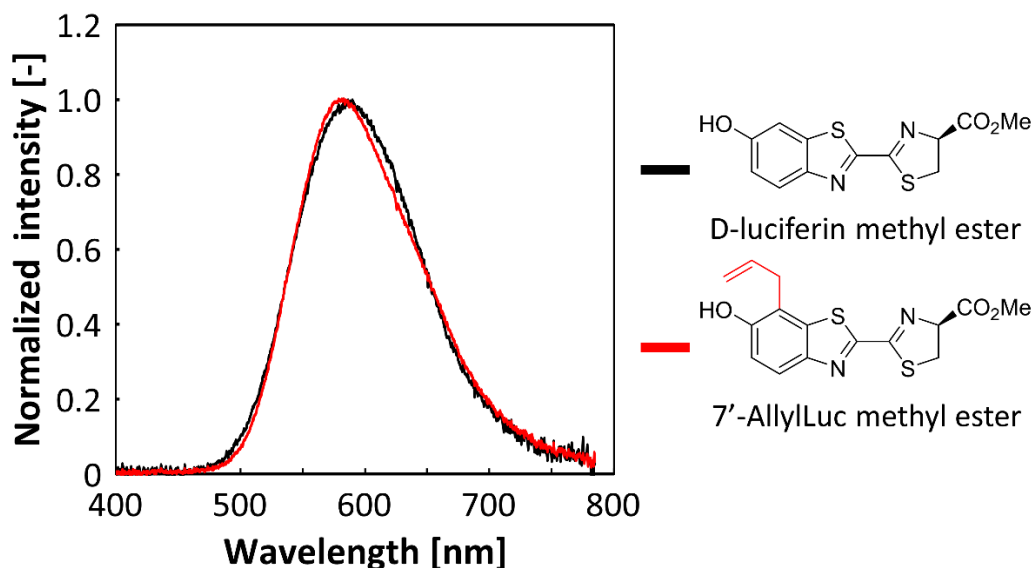


**Figure 2.2. Chemiluminescence spectra of D-luciferin methyl ester (black) and 7'-AllylLuc methyl ester (red) with *t*-BuOK in DMSO.** Reproduced from "Y. Ikeda *et al.*, *Chem. Commun.*, **2018**, 54, 1774-1777 (DOI: 10.1039/C7CC09720D) with permission from The Royal Society of Chemistry.

Next, it was investigated, whether firefly or beetle luciferases are able to recognize 7'-AllylLuc as their substrate to release a photon of light. Bioluminescence measurements with commonly used luciferases were carried out using commercially available enzymes, including firefly luciferase (Fluc) from *Photinus pyralis*, Emerald Luc (Eluc) from *Pyrearinus termitilluminans*, Stable Luciferase Green (SLG) from *Rhagophthalmus ohbai*, as well as Stable Luciferase Orange (SLO) and Stable Luciferase Red (SLR) from *Phrixothrix hirtus*. 7'-AllylLuc exhibited bioluminescence catalysed by all of these luciferases similar to that of the native luminescent substrate D-luciferin (**Figure 2.3**). Upon using Fluc as the luciferase, the bioluminescence spectra of 7'-AllylLuc showed a significant red-shift (maximum emission wavelength at 605 nm) compared with that of D-luciferin (**Figure 2.3** and **2.4**), despite having almost identical fluorescence spectra (**Figure 2.5**), whereas such a shift was not observed when using the other luciferases (Eluc, SLG, SLO and SLR). Moreover, the bioluminescence spectra obtained under several pH conditions with Fluc, known to be a pH sensitive luciferase, were completely identical like previously reported C-7' modified analogues (**Figure 2.6**).<sup>16</sup>

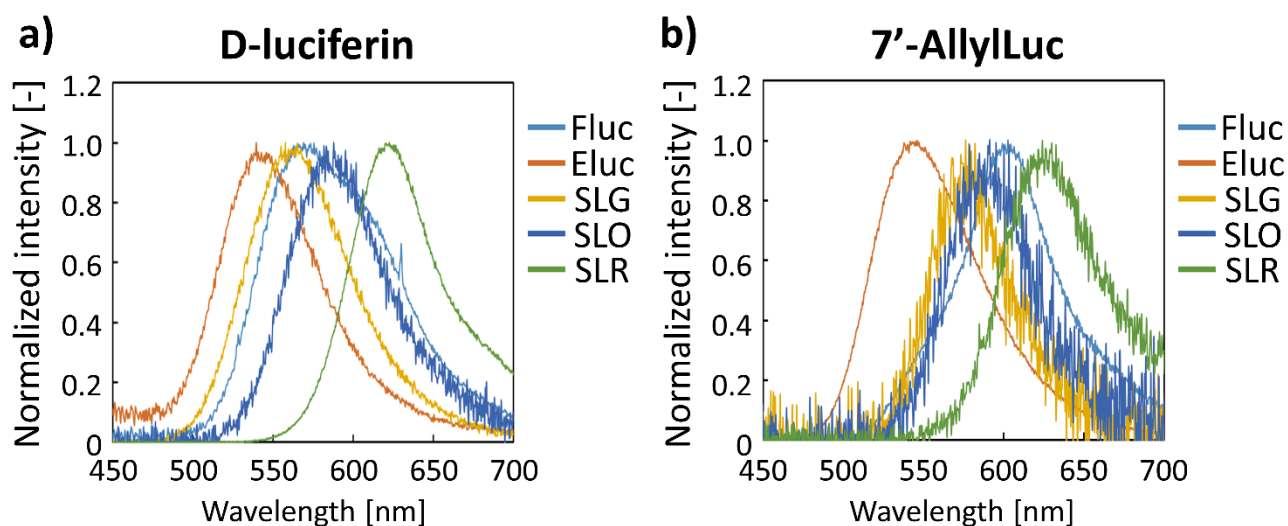


**Figure 2.3. Normalized bioluminescence emission spectra obtained with various luciferases for (a) D-luciferin and (b) 7'-AllylLuc at pH 8.0.** Adapted from "Y. Ikeda *et al.*, *Chem. Commun.*, **2018**, 54, 1774-1777 (DOI: 10.1039/C7CC09720D) with permission from The Royal Society of Chemistry.

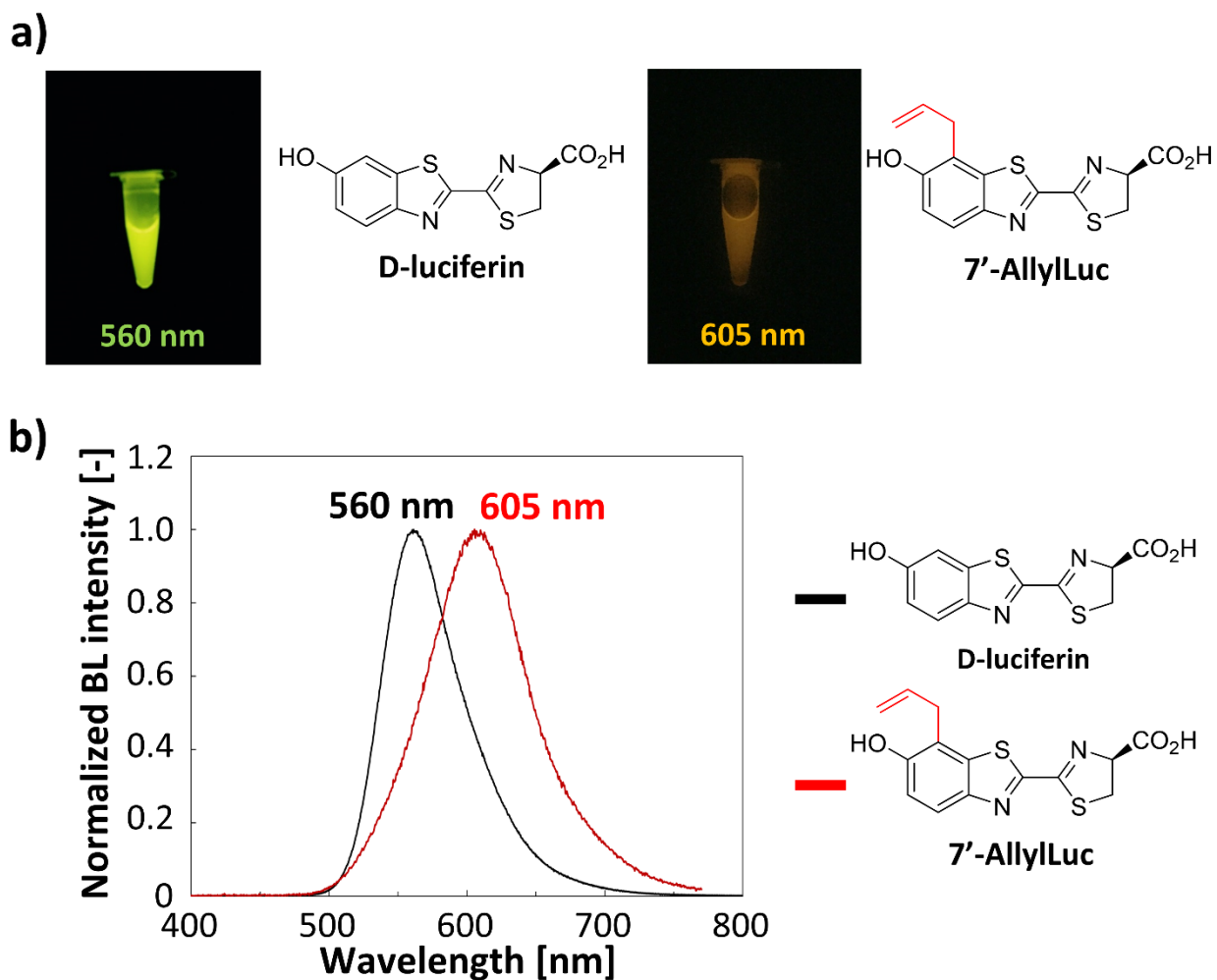


**Figure 2.4. Fluc-catalyzed bioluminescence emission of D-luciferin and 7'-AllylLuc:** a) bioluminescence images of D-luciferin and 7'-AllylLuc incubated with high concentrations of Fluc (1.0  $\mu\text{g}/\text{mL}$ ), b) bioluminescence emission spectra for D-luciferin and 7'-AllylLuc.

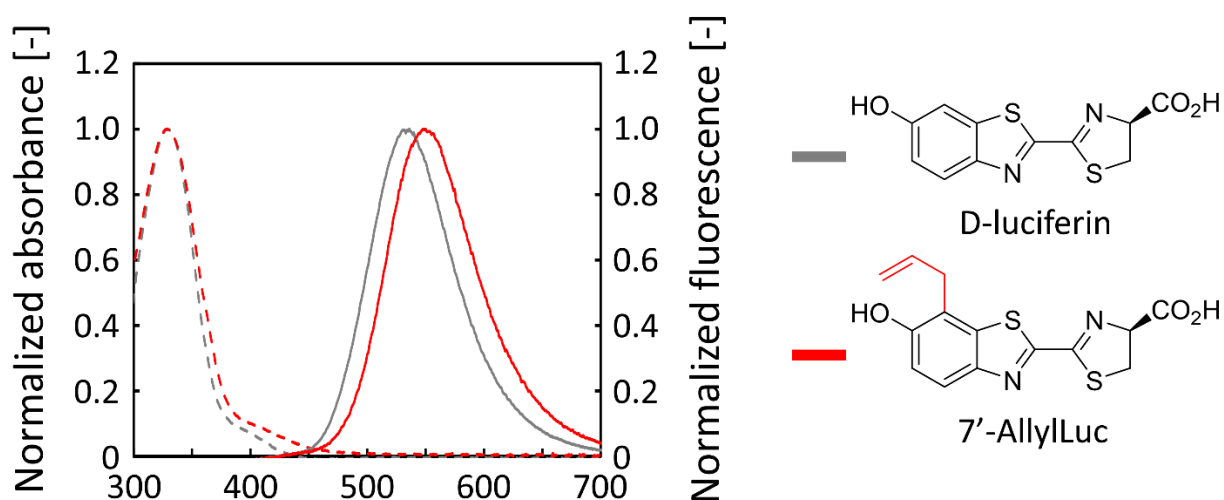


**Figure 2.5. Absorbance (dotted line) and fluorescence (solid line) spectra of D-luciferin (black) and 7'-AllylLuc (red) recorded at pH 8.0 in 0.1M GTA buffer; excited at 330 nm.**

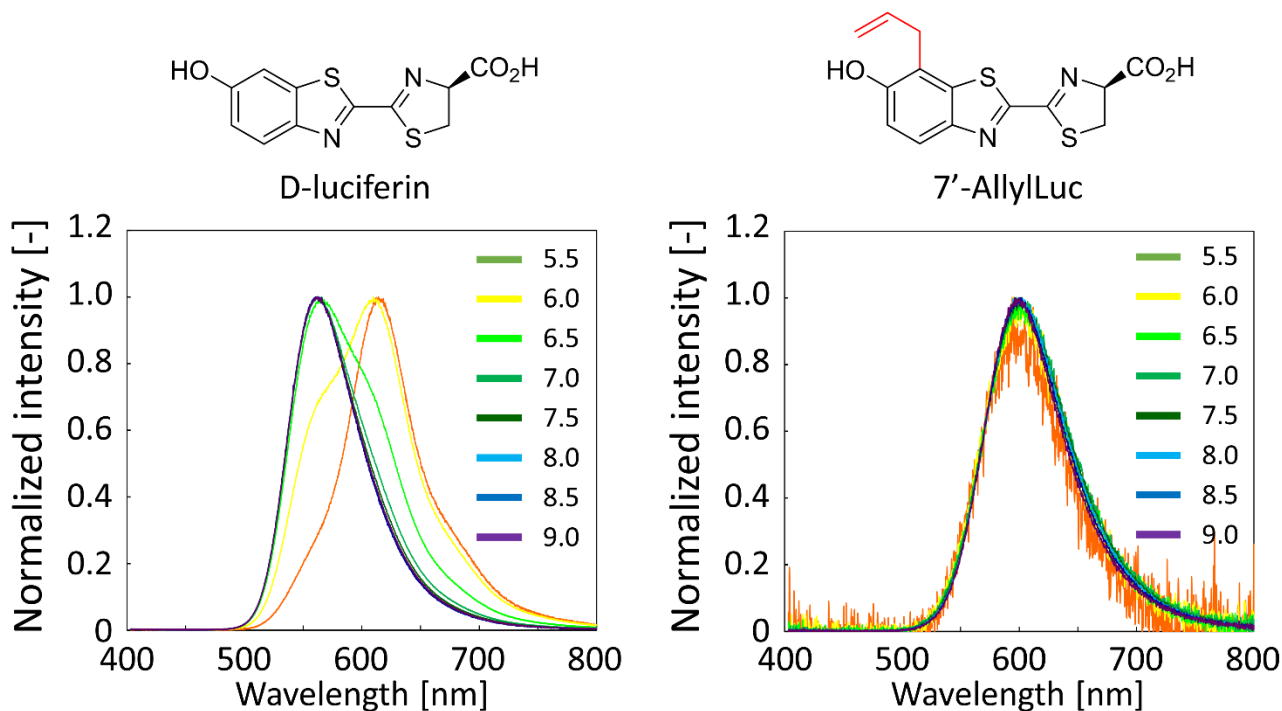


**Figure 2.6. Bioluminescence spectra of D-luciferin and 7'-AllylLuc with Fluc at various pH values.** It is widely known that the luminescence color of D-luciferin in combination with Fluc changes from green to red with increasing pH values.<sup>22</sup> In contrast, the luminescence color of 7'-AllylLuc remains unaffected by pH changes.

In the crystalline structure of *Luciola cruciate* luciferase, which is a type of luciferase with an amino acid sequence resembling that of Fluc, complexed with an inhibitor (5'-O-[*N*-(dehydrolyciferyl)-sulfamoyl]adenosine; DLSA) structurally similar to D-luciferyl-AMP, it has been clarified that luciferin is tightly sandwiched in the extremely hydrophobic microenvironment of the enzyme.<sup>23</sup> However, collapse of the planar structure of luciferin by structural modification causes a disruption of the hydrogen-bonding network around the luciferin,<sup>16</sup> which may result in a more polar microenvironment (**Figure 2.7**). Finally, the energy level of the excited state oxyluciferin is stabilized, and red-shifted bioluminescence emission is observed. Actually, previous studies have described similar red-shifted behaviour for sterically hindered luciferins (e.g. alkyn- or halogen-substituted) with Fluc.<sup>24-25</sup> The results obtained in this study suggested that allyl modification at the C-7' position influences the hydrophobic environment of the active site of Fluc, only. While continuous emission was observed for D-luciferin in all luciferases, the emission of 7'-AllylLuc with Fluc gradually decreased with time, with the emission intensity reaching half of its original value 12 seconds after the start of the reaction (**Figure 2.8a**). This decrease in bioluminescence intensity with Fluc may be due to inhibition by the reaction product. Surprisingly, the emission intensity with ELuc was the highest among all the luciferases, and the maximum emission intensity was sustained (**Figure 2.8b**). Since bioluminescence imaging generally requires long-term exposure, prolonged luminescence is a very important characteristic for both *in vitro* and *in vivo* imaging.

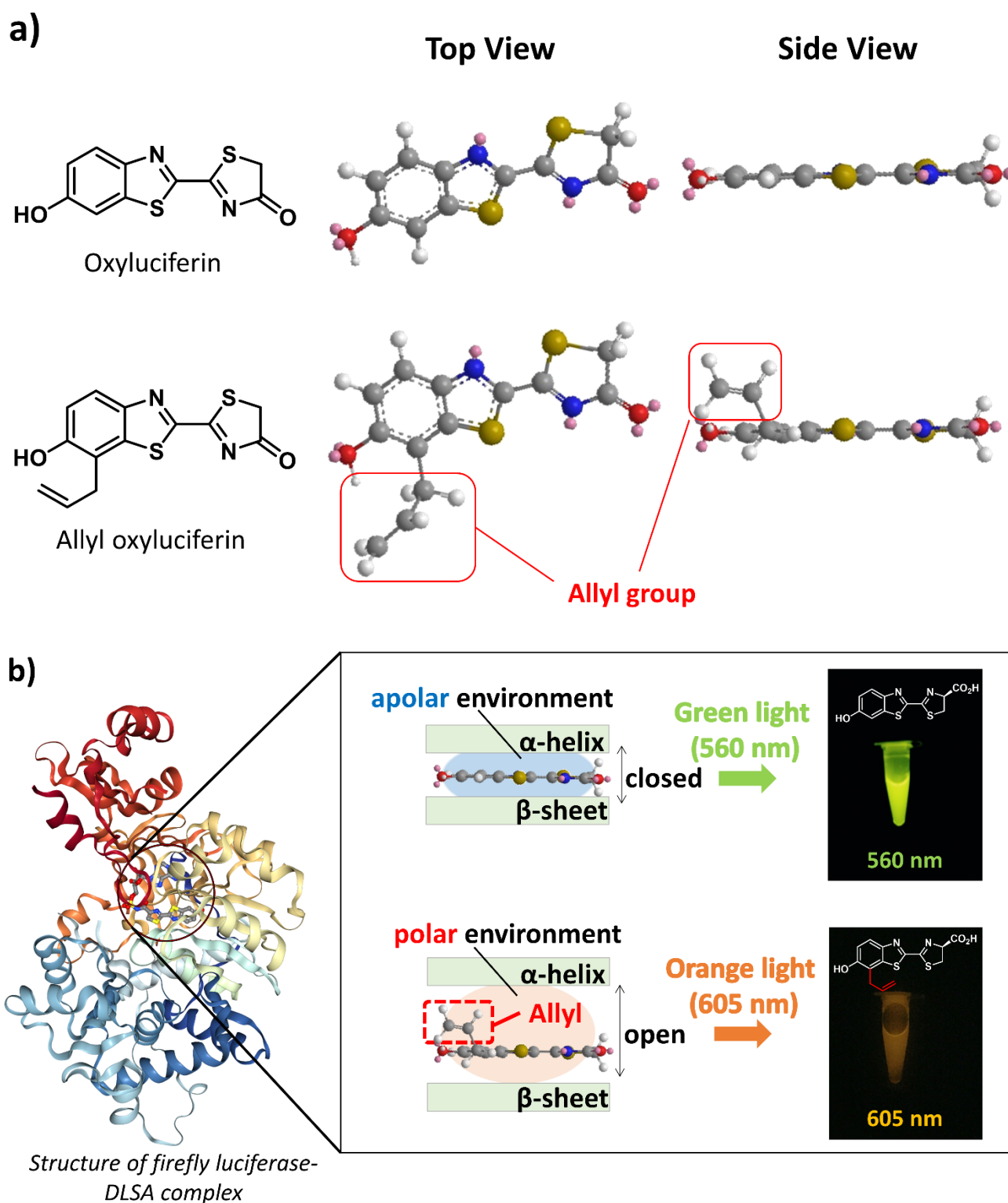


**Figure 2.7. Consideration of color modulation mechanism.** a) Molecular structures of oxyluciferin and allyl-oxyluciferin calculated by MM2. The allyl group is not part of the planar luciferin structure. Color scheme: grey = carbon; white = hydrogen; red = oxygen; blue = nitrogen; yellow = sulfur; pink = lone pair. b) Schematic diagram of luciferase active site with 7'-AllylLuc.

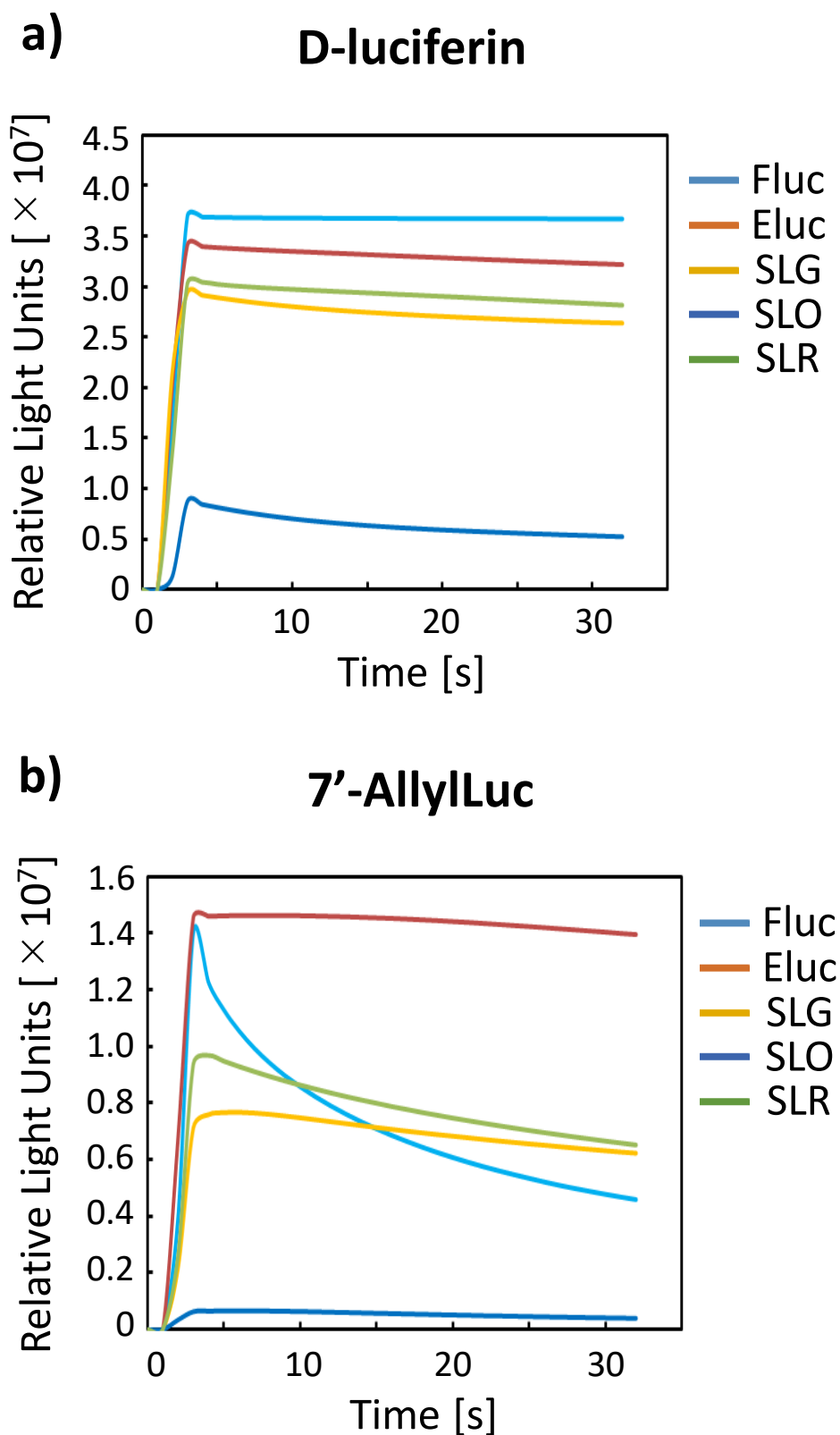


**Figure 2.8. Light emission time courses obtained with various luciferases** for a) D-luciferin and b) 7'-AllylLuc at pH 8.0. Adapted from "Y. Ikeda *et al.*, *Chem. Commun.*, **2018**, 54, 1774-1777 (DOI: 10.1039/C7CC09720D) with permission from The Royal Society of Chemistry.

### 2.2.3. Kinetic evaluation

To further understand the enzymatic reaction, the apparent Michaelis constants  $K_m$  (defined as the concentration at half of the maximum reaction rate) and the maximum velocities  $V_{max}$  for 7'-AllylLuc with each luciferase were evaluated. The initial luminescence intensity was measured as a function of luciferin concentration (**Figure 2.9**). All 7'-AllylLuc - luciferase pairs showed typical Michaelis-Menten plots. The  $K_m$  and  $V_{max}$  values were calculated from the Lineweaver-Burk plots. Little variation among  $K_m$  values was observed for allyl luciferin (**Table 2.1**). On the other hand, there were notable differences in the  $V_{max}$  values, which displayed a strong correlation with the emission intensity shown in **Figure 2.8**. Moreover, the  $V_{max}$  values were 3~100-fold lower compared with that of the D-luciferin - Fluc pair, the most commonly used luciferin-luciferase pair (data not shown). In order to further discuss the difference in luminescence efficiency between D-luciferin and 7'-AllylLuc, bioluminescence quantum yield measurements with Fluc and Eluc were performed (**Figure 2.10**). They revealed that 7'-AllylLuc has about 10% of the luminous efficiency with both luciferases (Fluc and Eluc) compared to the natural substrate D-luciferin (**Table 2.2**). These results suggest that while allyl modification at the C-7' position enables enzyme recognition; it may interfere with the catalysis necessary to emit light. Steric hindrance by modification with an allyl group may prevent effective luminescence processing of allyl luciferin, like it has been previously reported in the case of brominated luciferins.<sup>25</sup>

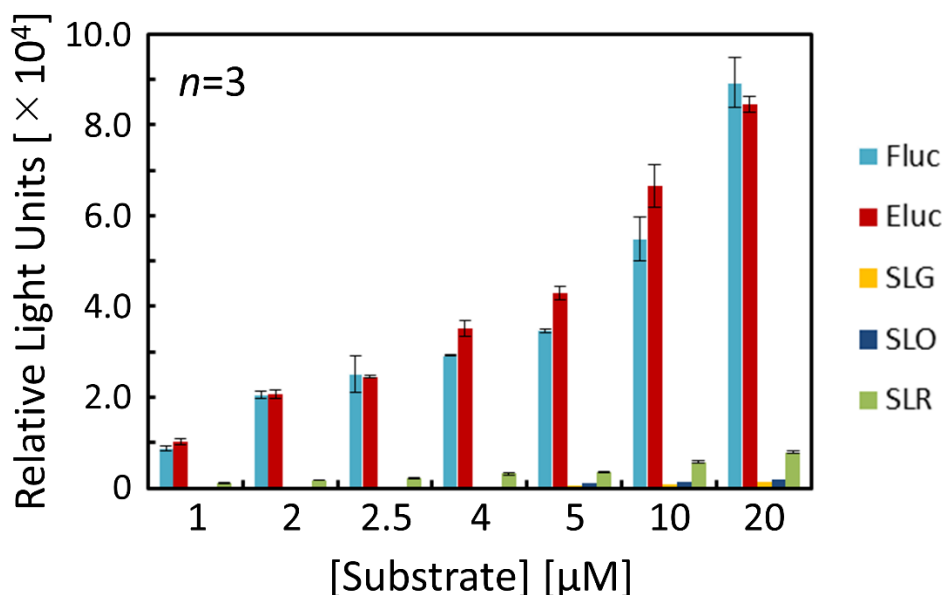


**Figure 2.9. Initial bioluminescence intensity from 7'-AllylLuc with purified luciferases (1  $\mu\text{g}/\text{mL}$ ) at various luciferin concentrations (1-20  $\mu\text{M}$ ).** Data were recorded immediately after addition of ATP- $\text{Mg}^{2+}$  solution. The initial luminescence intensity is defined as the peak intensity within the first 10 s of ATP- $\text{Mg}^{2+}$  solution addition. Error bars represent the standard deviation of 3 experiments.

**Table 2.1. Kinetic properties of allyl luciferin in combination with various luciferases.**

Luciferase	Apparent $K_m$ [ $\mu\text{M}$ ]	Apparent $V_{\max}$ <sup>a</sup> [ $\times 10^8$ photons $\text{s}^{-1}$ ]
Fluc	$23.8 \pm 6.9$	7.69
Eluc	$18.8 \pm 6.4$	6.93
SLG	$40.6 \pm 8.4$	0.0725
SLO	$10.2 \pm 4.8$	0.0292
SLR	$12.5 \pm 7.2$	0.0751

<sup>a</sup>  $V_{\max}$  values are within 5% error.

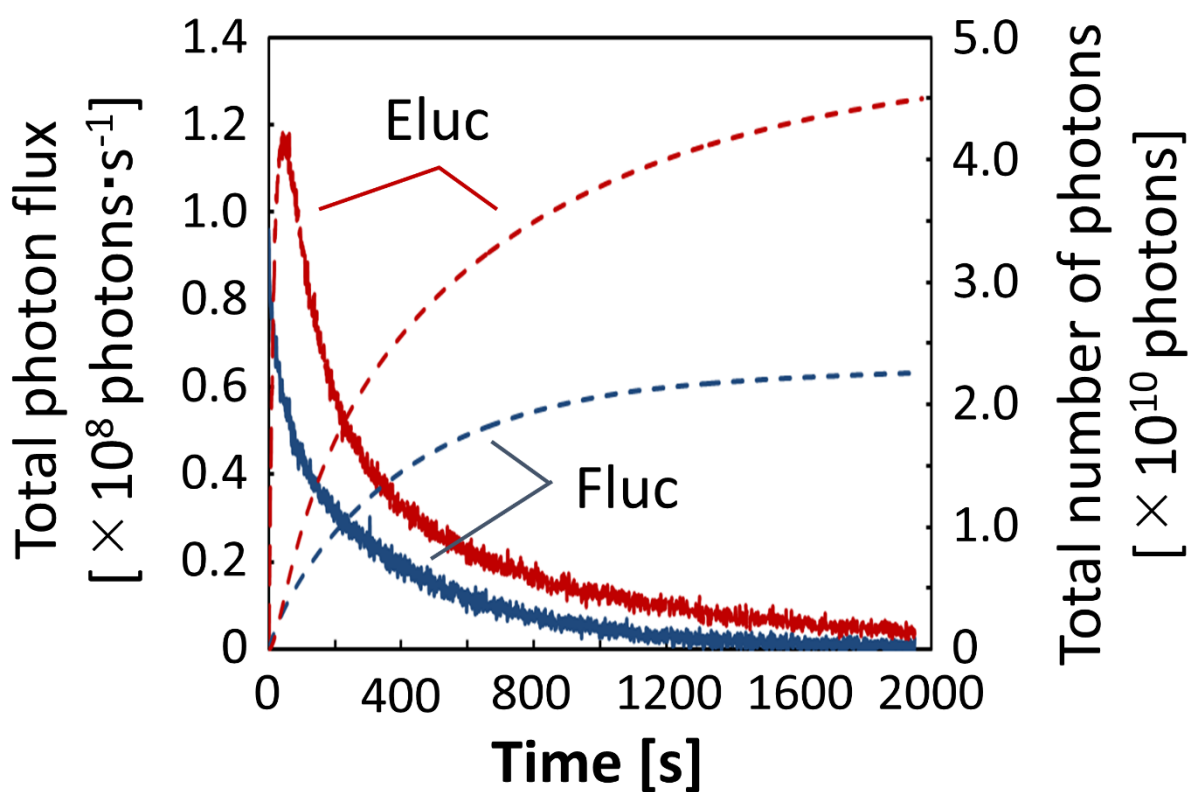


**Figure 2.10. Quantum yield measurements.** Temporal behavior of total photon flux (solid line, left-hand axis) and time-integrated total number of photons (dotted line, right-hand axis) for 7'-AllylLuc with Fluc or Eluc.

**Table 2.2. Bioluminescence quantum yields ( $n = 3$ ).**

Luciferase	Bioluminescence quantum yield $\varphi_{\text{BL}}$ [-]	
	Fluc	Eluc
D-luciferin	$0.41 \pm 0.07$	$0.61 \pm 0.08$
7'-AllylLuc	$0.043 \pm 0.007$	0.56 0.013

## 2.2.4. Orthogonal bioluminescence emission in living cells

Encouraged by these results *in vitro*, the bioluminescent properties of 7'-AllylLuc were further evaluated in live luciferase-expressing COS-7 monkey kidney tissue cells. The cells were cultured in 96-well microplates and monitored with a luminometer over 100 minutes with various substrate concentrations. While the light output from 7'-AllylLuc was weaker compared to D-luciferin (**Figure 2.11, 2.12 and 2.13**), a dose-dependent response was observed (**Figure 2.11a**). No detectable signal could be obtained at low concentrations (5  $\mu\text{M}$ ) of luciferin, presumably due to the low cell membrane permeability of the luciferins. Surprisingly, specific light emission was observed with Eluc-expressing cells, only (**Figure 2.11**). Furthermore, the 7'-AllylLuc-based light emission from Eluc-expressing cells was sustained like in the case of the native D-luciferin emitting system and lasted over 100 minutes, which is a desirable property for bioluminescence applications, as already noted before.

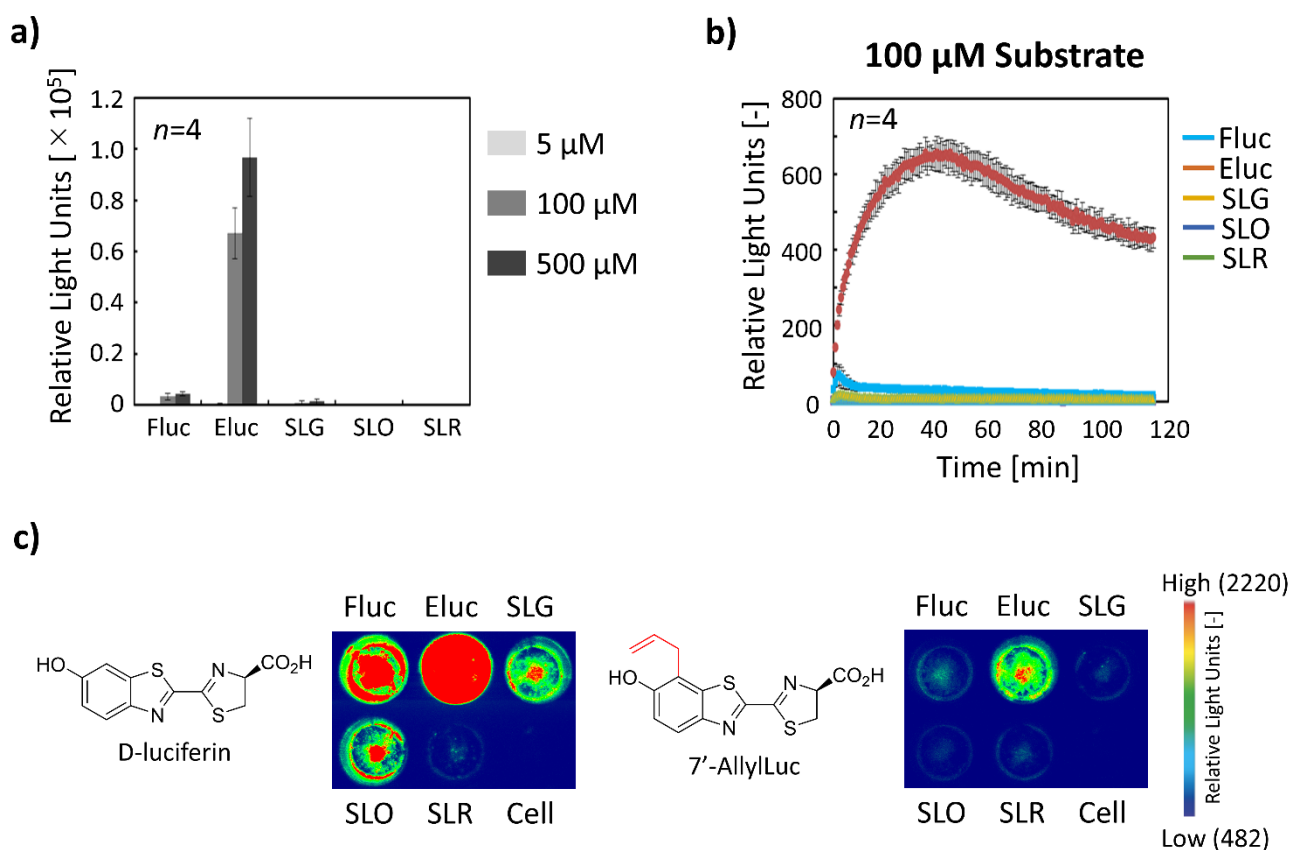


**Figure 2.11. Light emission from luciferase-expressing COS-7 cells treated with 7'-AllylLuc:** (a) total intensities of dose–response emission; (b) time courses at 100  $\mu\text{M}$  substrate; error bars represent the standard deviation of 4 experiments; (c) imaging of luciferase-expressing COS-7 cells treated with D-luciferin or 7'-AllylLuc. Adapted from “Y. Ikeda *et al.*, *Chem. Commun.*, **2018**, 54, 1774-1777 (DOI: 10.1039/C7CC09720D) with permission from The Royal Society of Chemistry.

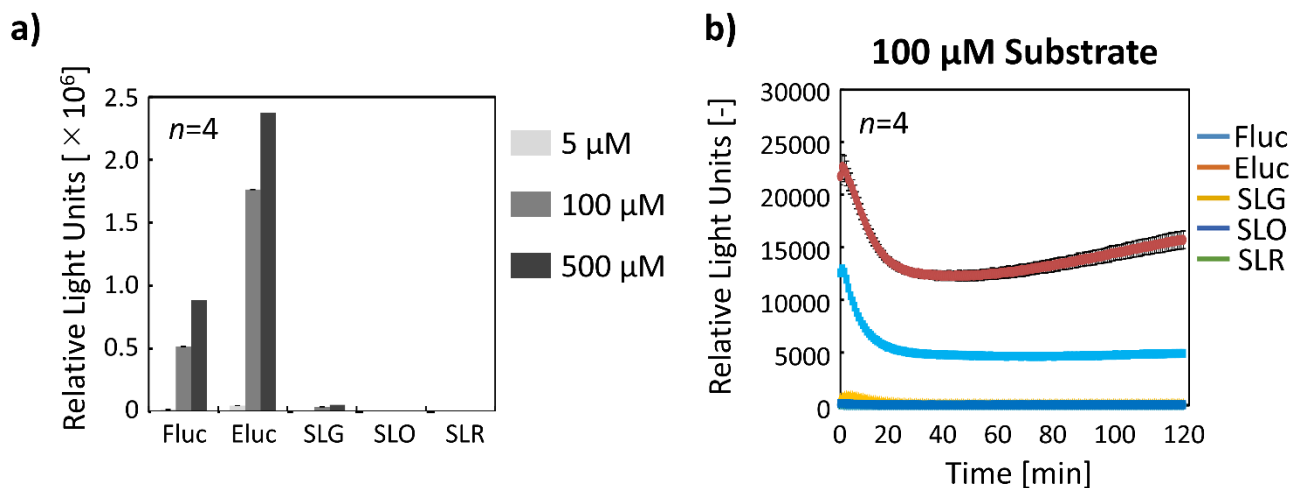


**Figure 2.12.** Light emission from luciferase-expressing COS-7 cells treated with D-luciferin: a) total intensities of dose-response emission, b) time courses at 100  $\mu\text{M}$  substrate. Error bars represent the standard deviation of 4 experiments.

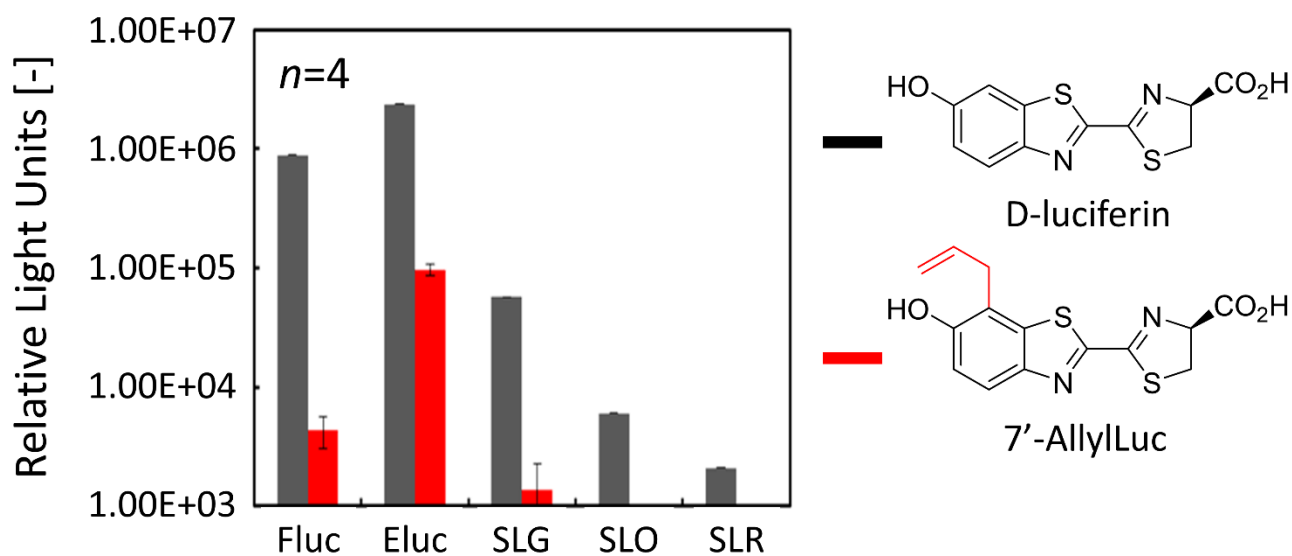


**Figure 2.13.** Comparison of Light emission intensities from luciferase-expressing COS-7 cells treated with D-luciferin and 7'-AllylLuc at 500  $\mu\text{M}$  substrate. Error bars represent the standard deviation of 4 experiments.

Cell viability evaluation by a standard MTT assay revealed that there was no significant cytotoxicity of 7'-AllylLuc even after treatment with a high dosage of 7'-AllylLuc (500  $\mu$ M) for 24 h (**Figure 2.14**). Despite 7'-AllylLuc having weaker emission intensity, a significant benefit of this analogue is its high luciferase specificity for Eluc, making it a potentially promising tool for multi-target imaging.

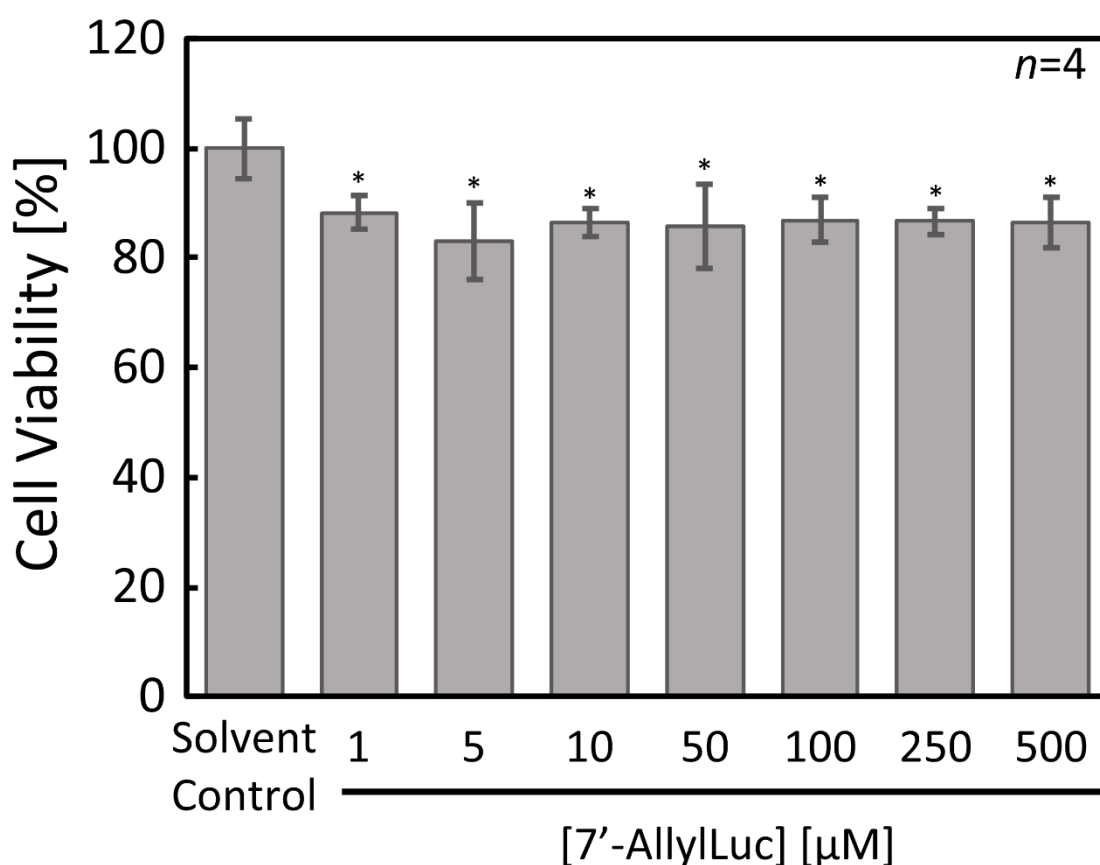


**Figure 2.14. Cell viability evaluated by MTT assay.** Cell viabilities were measured after 24 h treatment with 7'-AllylLuc at the indicated concentration. Error bars represent means  $\pm$  SEM ( $n = 4$ ). \*Not Significant ( $t$ -test).

## 2.3. Conclusions

In conclusion, a novel luciferin analogue modified with an allyl group at the C-7' position was successfully synthesized. In cellular imaging, this 7'-AllylLuc displayed a luciferase-selective bioluminescence signal in combination with Eluc, which is one of the commercially available beetle luciferases from *Pyrearinus termitilluminans*. Studies are now in progress to develop artificial beetle luciferases that display stronger bioluminescence emission with 7'-AllylLuc compared to that of D-luciferin, and to apply its selective response to bioluminescence-based reporter assays.

In addition, besides of being a promising luciferase substrate by itself, the terminal olefin function of the allyl group is available as a linker for further covalent modifications. It is convertible to aldehyde groups by Lemieux–Johnson oxidation, which can then easily react with various functional groups.<sup>17</sup> Therefore, allyl group introduction into firefly luciferin enables further useful possibilities, such as the development of various analogues and labelling applications. It is believed that this new synthetic luciferin will contribute to the expansion of bioluminescence imaging applications both *in vitro* and *in vivo*.

## 2.4. Experimental Section

### 2.4.1. Material and methods

#### 2.4.1.1 General

Reagents were purchased from Wako Pure Chemical, Tokyo Chemical Industries and Aldrich Chemical Company and were used without further purification.  $^1\text{H-NMR}$  and  $^{13}\text{C-NMR}$  spectra were obtained on JEOL JNM AL-400, JEOL JNM ECX-400, and JEOL JNM- $\alpha$ 400 spectrometers in  $\text{CD}_3\text{OD}$  solution using tetramethyl silane as an internal standard. Reference values for residual solvents were taken as  $\delta = 3.30$  ( $\text{CD}_3\text{OD}$ ) ppm for  $^1\text{H-NMR}$  and  $\delta = 49.00$  ( $\text{CD}_3\text{OD}$ ) ppm for  $^{13}\text{C-NMR}$ . Coupling constants ( $J$ ) are given in Hz and are uncorrected. High-resolution mass spectra were obtained on a Waters LCT Premier XE (ESI) instrument. For preparative and analytical TLC, silica gel plates (Kieselgel 60 F254, E. Merck AG, Germany) were used, with UV light (254 nm) and ninhydrin visualization of spots. For column chromatography, Kanto Chemical Silica 60N (spherical, neutral, 63-210  $\mu\text{m}$ ) was used. All reactions were carried out under an inert ( $\text{Ar}$  or  $\text{N}_2$ ) atmosphere unless stated otherwise.

#### 2.4.1.2 Chemiluminescence spectra

The chemiluminescence emission from the luciferin methyl esters with  $t\text{-BuOK}$  in DMSO was measured on an AB-2270 luminometer. A solution of the luciferin methyl ester (2.5 mM) in DMSO (200  $\mu\text{L}$ ) was placed in a polystyrene tube. This solution was treated with  $t\text{-BuOK}$  (250 mM) in DMSO (40  $\mu\text{L}$ ), which was injected with a syringe, to initiate the chemiluminescence reaction. The emission spectra were measured on an AB-1850 spectrophotometer for 180 s (slit width: 1.0 mm; exposure time: 180 s) with final concentrations of 1.25 mM (substrate) and 125 mM ( $t\text{-BuOK}$ ).

#### 2.4.1.3 Absorbance and fluorescence spectra

Luciferins (5  $\mu\text{M}$ ) were dissolved in 0.1 M GTA buffer (pH 8.0) and absorbance and fluorescence spectra were obtained using a VARIOSKAN FLASH (Thermo Scientific, USA) microplate reader with the excitation light and excitation/emission slit widths set to 330 nm and 1 nm, respectively. Spectral data were recorded at 25  $^\circ\text{C}$  in a 96-well microplate over the wavelength range of 300-800 nm. The composition of GTA buffer is 3,3-dimethylglutaric acid, tris(hydroxymethyl)aminomethane, 2-amino-2-methyl-1,3-propanediol, and pH was adjusted with 1M HCl or 1M NaOH solution.

### 2.4.1.4 Bioluminescence emission spectra

All bioluminescence emission spectra with luciferases were recorded on an integrating sphere based multichannel spectrometer equipped with a liquid N<sub>2</sub>-cooled CCD detector as described previously.<sup>2</sup> The absolute spectral sensitivity was calibrated with a spectral irradiance standard lamp. Bioluminescence reactions were carried out at ambient temperature in 10  $\mu$ L of reaction cocktail containing substrates and luciferase. Reactions were initiated by injection of 90  $\mu$ L of ATP-Mg<sup>2+</sup> solution (3 mM ATP-2Na, 8 mM MgSO<sub>4</sub> 7H<sub>2</sub>O in 0.1 M GTA buffer).

### 2.4.1.5 Bioluminescence intensities and kinetic reaction analysis

Kinetic reaction analysis was performed with a custom-built luminometer equipped with a Hamamatsu H11890-01 photomultiplier tube (PMT). Bioluminescence reactions were carried out at ambient temperature in reaction cocktails containing 10  $\mu$ L of 10-200  $\mu$ M luciferin and 10  $\mu$ L of 10  $\mu$ g/mL luciferase. The reaction was initiated by injection of 80  $\mu$ L of ATP-Mg<sup>2+</sup> solution (3 mM ATP-2Na, 8 mM MgSO<sub>4</sub> 7H<sub>2</sub>O in 0.1 M GTA buffer, pH 8.0). The relative light intensity was collected immediately and integrated over 10 s. The values of Michaelis-Menten constants  $K_m$  and maximum velocities  $V_{max}$  were determined by Lineweaver-Burk plots.

### 2.4.1.6 Determination of quantum yields<sup>4, 26</sup>

The custom-built luminometer equipped with the Hamamatsu H11890-01 PMT was used to determine the bioluminescence quantum yield values. The absolute responsivity of the luminometer was calibrated with an integrating sphere-based multichannel spectrometer equipped with a liquid N<sub>2</sub>-cooled CCD detector and was determined from linear fittings of the plots of the relative count value measured by the luminometer and the absolute value measure by the integrating sphere. The time-integrated total number of photons emitted in the bioluminescence reaction was measured using the calibrated luminometer. The reaction was initiated by injection of 200  $\mu$ L of ATP-Mg<sup>2+</sup> solution (3 mM ATP-2Na, 8 mM MgSO<sub>4</sub> 7H<sub>2</sub>O in 0.1 M GTA buffer, pH 8.0) to the mixed solution of 10  $\mu$ L of 10 nM luciferin solution and 10  $\mu$ L of 1.0 mg/mL luciferase solution in a test tube, which was placed in advance into the luminometer. The reaction was monitored until the light-emitting reaction was complete. The quantum yield values were calculated from the obtained total number of photons and that of the luciferin molecules.

### 2.4.1.7 Plasmid construction

For expression in mammalian cells, the genes of Fluc, Eluc, SLG, SLO, and SLR were cloned into pcDNA 3.1/V5-His A vector (Invitrogen, USA) using standard molecular biology techniques as follows. The gene of Fluc was amplified by polymerase chain reaction (PCR) from pGL4.13 (Promega, USA) using primers 5'- ATGCAAGCTTGCCACCATGGAAGATGCCAAAAC-3' and 5'- GCATCTCGAGCACGGCGATCTTGCC-3'. The gene of Eluc was amplified by PCR from pEluc-test (Toyobo, Japan) using primers 5'- ATGCAAGCTTGCCACCATGGAGAGAGAGAAG-3' and 5'- GCATCTCGAGCAGCTTAGAAGCCTT-3'. The gene of SLG was amplified by PCR from pSLG-SV40 (Toyobo, Japan) using primers 5'- ATGCAAGCTTGCCACCATGGCTAACGAGATCATC-3' and 5'- GCATCTCGAGCAGCTTGACTTCTT-3'. The gene of SLO was amplified by PCR from pSLO-SV40 (Toyobo, Japan) using primers 5'- ATGCAAGCTTGCCACCATGGCTAACGAGATCATC-3' and 5'- GCATCTCGAGCAGCTTGACTTCTT-3'. The gene of SLR was amplified by PCR from pSLR-SV40 (Toyobo, Japan) using primers 5'- ATGCAAGCTTGCCACCATGGAAGAAGAGAACATC-3' and 5'- GCATCTCGAGCAGCTTGACTTGGC-3'. All the PCR-amplified fragments were digested with Hind III and Xho I and subsequently ligated into pcDNA 3.1/V5-His A. The sequences of the amplified regions were confirmed by DNA sequencing (Eurofins Genomics, Japan). All the expression plasmids were purified using a QIAGEN plasmid kit (Qiagen, USA).

### 2.4.1.8 Cell culture and plasmid transfection

COS-7 cells, fibroblast-like cell line derived from monkey kidney tissues, were selected for live cell bioluminescence assays because artificial genes introduced from outside of the cells often function very efficiently. COS-7 cells were cultured in Dulbecco's modified Eagle's medium (Sigma, USA) supplemented with 10% fetal bovine serum (Gibco, USA), 100 U/mL penicillin and 100 µg/mL streptomycin (Gibco, USA) at 37°C in 5% CO<sub>2</sub>. The day before plasmid transfection, cells were plated onto black 96-well plates (Greiner, Austria) at a density of 10,000 cells per well. Plasmid transfection was performed using Lipofectamine 3000 (Life Technologies, USA) according to the manufacturer's instructions. Forty-eight hours after plasmid transfection, live cell bioluminescence assays were performed.

### 2.4.1.9 Live cell bioluminescence assays

Transfected COS-7 cells were washed with HBSS once. For live cell assays, the cells in 96-well plates were incubated with 100 µL of luciferin in HBSS. Live cell bioluminescence assays were performed using a microplate luminometer (Centro XS3 LB960; Berthold Technologies, Germany) without filter. Imaging of cells was performed by using an in vivo imaging system (Lumazone FA, SHOSIN EM CORPORATION, Japan) equipped with EM-CCD (Electron Multiplying Charge Coupled Device, Nippon Roper) as a detector without emission filter. For this purpose, the cells were plated in 24-well plates.

The light emission 5 min after incubation of luciferin (500  $\mu\text{M}$ ) was integrated. Exposure time = 10 s.

### 2.4.1.10 Cytotoxicity assays

The cytotoxicity of 7'-AllylLuc on COS-7 cells was evaluated by the MTT assay. The cells were seeded in 96-well plates at a density of 10,000 cells per well and cultured for 48 h in Dulbecco's modified Eagle's medium (Sigma, USA) supplemented with 10% fetal bovine serum (Gibco, USA), 100 U/mL penicillin and 100  $\mu\text{g/mL}$  streptomycin (Gibco, USA) at 37°C in 5%  $\text{CO}_2$ . The cultured cells were then exposed to 7'-AllylLuc in DMEM with 10% FBS at 37°C for 24 h in a 5%  $\text{CO}_2$  incubator. Subsequently, MTT in PBS (-) was added to each well (finally diluted to 500  $\mu\text{g/mL}$ ). After an additional 4 h incubation, the medium was removed and washed with 200  $\mu\text{L}$  of PBS (-). Then, 200  $\mu\text{L}$  of acidified isopropanol (0.04 mol/L HCl) was added to each well. The culture plates were shaken for 10 min on an oscillator. The absorbance at 570 nm was measured with a hybrid multi-mode microplate reader. The relative percentage of cell survival was calculated based on the 100% arbitrary absorbance obtained for the blank control. Reported values represent the mean s.e.m. of 4 replicates on the same plate.

## 2.4.2. Synthetic procedures

**2-Cyano-6-hydroxybenzothiazole (2):** Pyridine hydrochloride (excess) and **1** (1.18 g, 6.22 mmol) were combined in a flask and stirred at 180 °C for 2 h. The resulting brown residue was suspended in ethyl acetate and washed with saturated  $\text{NaHCO}_3$  *aq.*,  $\text{H}_2\text{O}$ , and brine. The organic layers were combined, dried over  $\text{Na}_2\text{SO}_4$ , filtered and concentrated *in vacuo*. The crude product was purified by silica gel column chromatography (ethyl acetate/*n*-hexane = 1/3) to give **2** (839.3 mg, 77%) as a pale yellow solid.  $^1\text{H-NMR}$  (400 MHz,  $\text{CD}_3\text{OD}$ ):  $\delta$  7.98 (d,  $J$  = 8.8 Hz, 1H), 7.39 (d,  $J$  = 2.4 Hz, 1H), 7.16 (dd,  $J$  = 2.4, 8.8 Hz, 1H) ppm;  $^{13}\text{C-NMR}$  (100 MHz,  $\text{CD}_3\text{OD}$ ):  $\delta$  160.3, 147.3, 139.0, 133.9, 126.6, 119.6, 114.3, 107.0 ppm; HRMS (ESI-) Calcd for  $\text{C}_8\text{H}_3\text{N}_2\text{OS}$   $[\text{M}+\text{H}]^+$ : 174.9966, Found: 174.9971.

**6-Allyloxy-2-cyanobenzothiazole (3):** A solution of **2** (429.3 mg, 2.44 mmol) and allyl bromide (0.60 mL, 7.09 mmol) in DMF (5 mL) was treated with  $\text{K}_2\text{CO}_3$  (368.1 mg, 2.66 mmol) and stirred at r.t. for 20 h. The reaction mixture was then added into water and extracted with ethyl acetate. The organic layers were combined, dried over  $\text{Na}_2\text{SO}_4$ , filtered and concentrated *in vacuo*. The crude product was purified by silica gel column chromatography (ethyl acetate/*n*-hexane = 1/5) to give **3** (504.9 mg, 96%) as a white solid.  $^1\text{H-NMR}$  (400 MHz,  $\text{CD}_3\text{OD}$ ):  $\delta$  8.05 (d,  $J$  = 9.3 Hz, 1H), 7.63 (d,  $J$  = 2.4 Hz, 1H), 7.30 (dd,  $J$  = 2.4, 9.3 Hz, 1H), 6.10 (tdd, 1H), 5.45 (ddd,  $J$  = 9.3 Hz, 1H), 5.31 (ddd,  $J$  = 9.3 Hz, 1H), 4.67 (td,  $J$  = 9.3 Hz, 2H) ppm;  $^{13}\text{C-NMR}$  (100 MHz,  $\text{CD}_3\text{OD}$ ):  $\delta$  160.9, 148.1, 138.9, 135.0, 134.0, 126.4, 120.1, 118.3, 114.2, 105.6, 70.5 ppm; HRMS (ESI+) Calcd for  $\text{C}_{11}\text{H}_9\text{N}_2\text{OS}$   $[\text{M}+\text{H}]^+$ : 217.0436, Found: 217.0458.

**7-Allyl-2-cyano-6-hydroxybenzothiazole (4): 3** (504.9 mg, 2.34 mmol) was heated at 180 °C under an Ar atmosphere for 1 h. The residue was dissolved and extracted with ethyl acetate. The organic layers were combined, dried over Na<sub>2</sub>SO<sub>4</sub>, filtered and concentrated *in vacuo*. The crude product was purified by silica gel column chromatography (ethyl acetate/*n*-hexane = 1/10) to give **4** (304.0 mg, 95% (b.r.s.m.)) as a white solid. The remaining starting material (**3**) (184.0 mg, 36%) was recovered as a white solid. <sup>1</sup>H-NMR (400 MHz, CD<sub>3</sub>OD): δ 8.05 (d, *J* = 9.3 Hz, 1H), 7.63 (d, *J* = 2.4 Hz, 1H), 7.30 (dd, *J* = 2.4, 9.3 Hz, 1H), 6.10 (tdd, 1H), 5.45 (ddd, *J* = 9.3 Hz, 1H), 5.31 (ddd, *J* = 9.3 Hz, 1H), 4.67 (td, *J* = 9.3 Hz, 2H) ppm; <sup>13</sup>C-NMR (100 MHz, CD<sub>3</sub>OD): δ 156.9, 147.2, 139.2, 134.7, 133.8, 124.6, 119.2, 119.0, 117.2, 114.3, 34.7 ppm; HRMS (ESI-) Calcd for C<sub>11</sub>H<sub>7</sub>N<sub>2</sub>OS [M-H]<sup>-</sup>: 215.0279, Found: 215.0266.

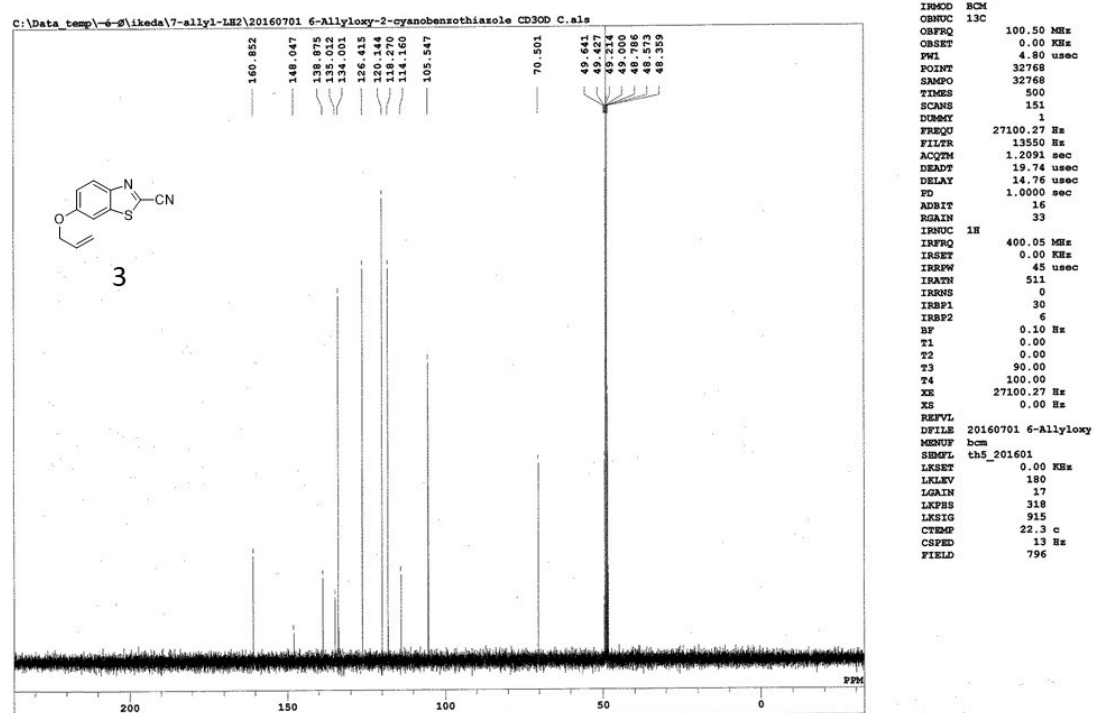
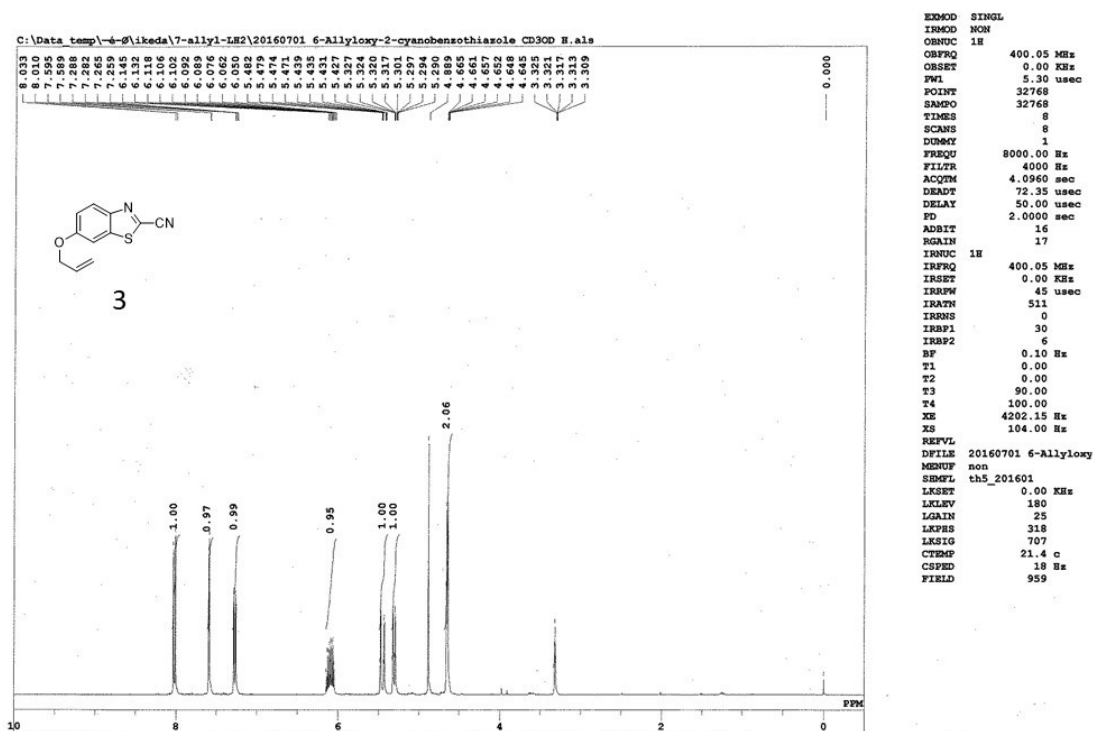
**(S)-2-(7-Allyl-6-hydroxybenzo[d]thiazol-2-yl)-4,5-dihydrothiazole-4-carboxylic acid**

**(7'-AllylLuc): 4** (66.2 mg, 0.307 mmol) was dissolved in methanol (2 mL), and then D-cysteine hydrochloride monohydrate (56.6 mg, 0.322 mmol) in aqueous K<sub>2</sub>CO<sub>3</sub> solution (1.5 mL, pH 7.8) was added and stirred at r.t. for 1 h. After complete reaction, the mixture was diluted with saturated NaHCO<sub>3</sub> solution and washed with ethyl acetate. Then, the aqueous layer was acidified with 1 M HCl *aq.* and extracted with ethyl acetate. The combined organic layers were dried over Na<sub>2</sub>SO<sub>4</sub>, filtered and concentrated *in vacuo* to give **7'-AllylLuc** (95.6 mg, 97%) as a yellow solid. <sup>1</sup>H-NMR (400 MHz, CD<sub>3</sub>OD): δ 7.78 (d, *J* = 8.8 Hz, 1H), 7.09 (d, *J* = 8.8 Hz, 1H), 5.92 (m, 1H), 5.39 (t, *J* = 9.2 Hz, 1H), 5.08 (ddd, *J* = 2.0, 10.4, 17.2 Hz, 2H), 3.75 (ddd, *J* = 9.3 Hz, 2H), 3.59 (m, 2H) ppm; <sup>13</sup>C-NMR (100 MHz, CD<sub>3</sub>OD): δ 173.4, 167.7, 158.5, 155.7, 148.1, 139.5, 123.9, 119.5, 117.7, 116.7, 79.5, 79.4, 35.9, 34.8 ppm; HRMS (ESI+) Calcd for C<sub>14</sub>H<sub>13</sub>N<sub>2</sub>O<sub>3</sub>S<sub>2</sub> [M+H]<sup>+</sup>: 321.0368, Found: 321.0378. The optical purity was determined by CSP HPLC analysis (Chiracel OZ-RH, eluent: 10-90% H<sub>2</sub>O/CH<sub>3</sub>CN, flow 0.3 mL/min) > 99 % ee [*t*<sub>R</sub> (minor) = 16.4 min, *t*<sub>R</sub> (major) = 19.1 min].

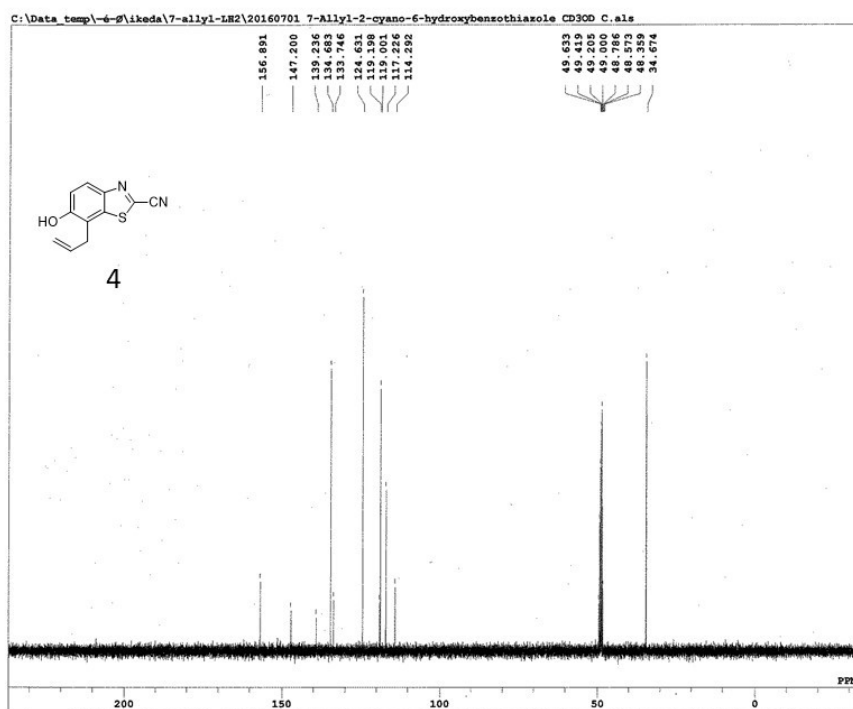
**Methyl (S)-2-(7-allyl-6-hydroxybenzo[d]thiazol-2-yl)-4,5-dihydrothiazole-4-carboxylate (7'-AllylLuc methyl ester):** To a solution of 7'-AllylLuc (22.8 mg, 71.1 μmol) in Toluene/MeOH (7.0 mL, *v/v*=1:7) was added TMSCH<sub>2</sub>N<sub>2</sub> (130 μL, ca. 0.6 M solution in hexane) at r.t., and the reaction mixture was stirred for 2 h. After concentration *in vacuo*, the crude product was purified by silica gel column chromatography (methanol/chloroform = 1/9) to give **7'-AllylLuc methyl ester** (23.4 mg, 99%) as a pale yellow solid. <sup>1</sup>H-NMR (400 MHz, CD<sub>3</sub>OD): δ 7.77 (d, *J* = 8.8 Hz, 1H), 7.09 (d, *J* = 8.8 Hz, 1H), 5.97-5.87 (m, 1H), 5.41 (t, *J* = 9.2 Hz, 1H), 5.08 (ddd, *J* = 2.0, 10.4, 17.2 Hz, 2H), 3.96 (s, 3H), 3.78 (dd, *J* = 1.6, 6.4 Hz, 2H), 3.31 (m, 2H) ppm; <sup>13</sup>C-NMR (100 MHz, CD<sub>3</sub>OD): δ 172.2, 168.0, 158.3, 155.7, 148.1, 139.5, 135.1, 123.9, 119.5, 117.7, 116.7, 79.3, 53.2, 35.7, 34.8 ppm; HRMS (ESI+) Calcd for C<sub>15</sub>H<sub>15</sub>N<sub>2</sub>O<sub>3</sub>S<sub>2</sub> [M+H]<sup>+</sup>: 335.0519, Found: 335.0524. The optical purity was not determined.

## 2.4.3. NMR spectra

## 6-Allyloxy-2-cyanobenzothiazole (3)

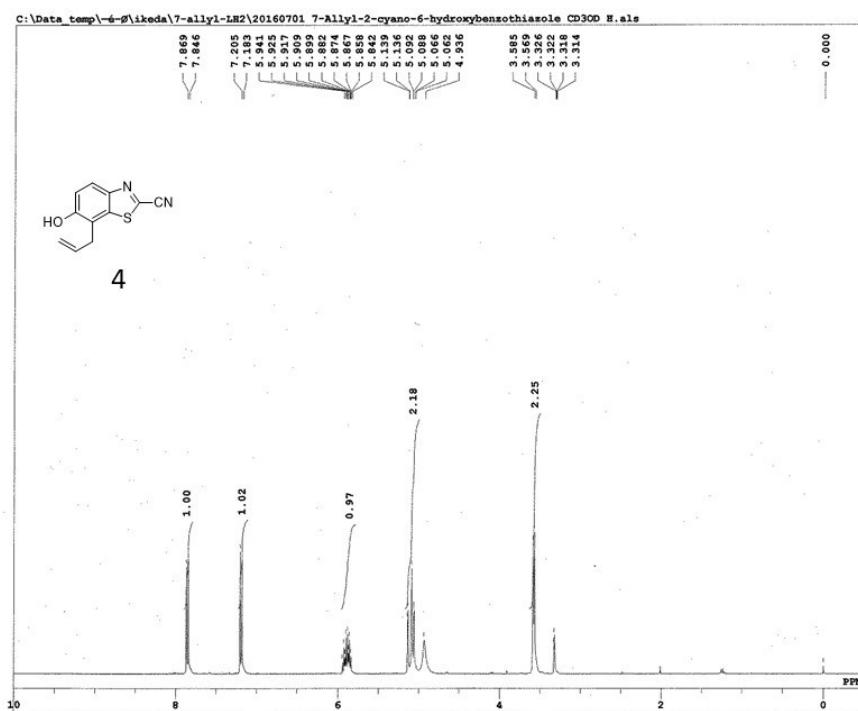


### 7-Allyl-2-cyano-6-hydroxybenzothiazole (4)



```

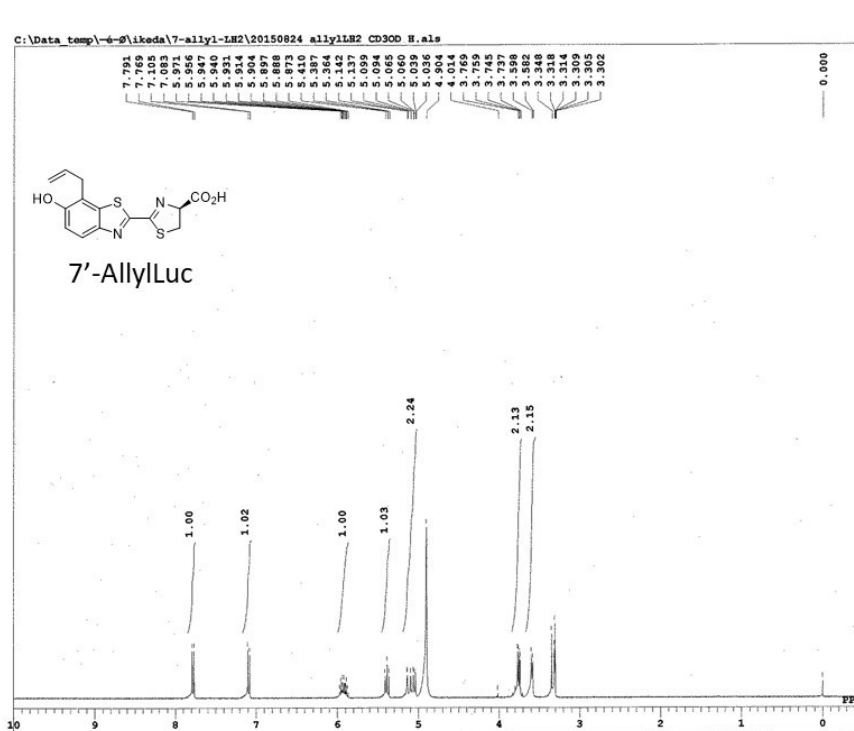
EXMOD SINGL
IRMOD BCM
OBNUC 13C
OBFRQ 100.50 MHz
ORSET 0.00 KHz
PWL 4.80 usec
POINT 32768
SAMPO 32768
TIMES 150
SCANS 150
DUMMY 1
FREQU 27100.27 Hz
FILTR 13550 Hz
ACQTM 1.2091 sec
DEADT 19.74 usec
DELAY 14.76 usec
PD 1.0000 sec
ADBIT 16
RGAIN 33
IRNUC 1H
IRFRQ 400.05 MHz
IRSEP 0.00 KHz
IRFPW 45 usec
IRATN 511
IRRSN 0
IRBPI 30
IRBPP 6
BF 0.12 Hz
T1 0.00
T2 0.00
T3 90.00
T4 100.00
XE 27100.27 Hz
XS 0.00 Hz
REFVL
DFILE 20160701 7-Allyl-2-
MENUP bcm
SIMP1 th5_201601
LKSET 0.00 KHz
LKEV 180
LGIN 17
LKPS 318
LKSIG 792
CTEMP 22.5 c
CSPE 13 Hz
FIELD 800
    
```



```

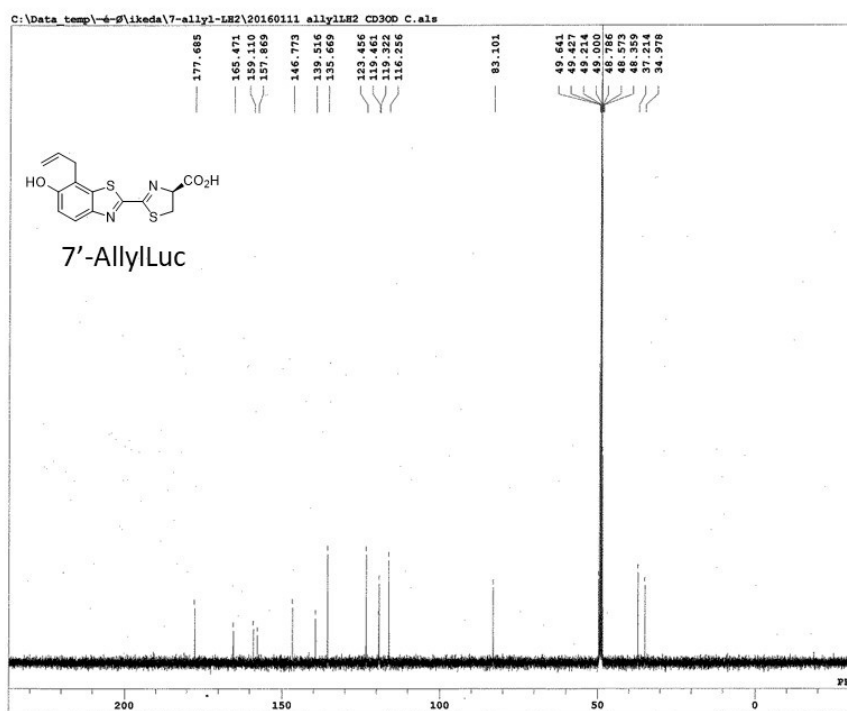
EXMOD SINGL
IRMOD NON
OBNUC 1H
OBFRQ 400.05 MHz
ORSET 0.00 KHz
PWL 5.30 usec
POINT 16384
SAMPO 16384
TIMES 8
SCANS 8
DUMMY 1
FREQU 8000.00 Hz
FILTR 4000 Hz
ACQTM 2.0480 sec
DEADT 72.35 usec
DELAY 50.00 usec
PD 2.0000 sec
ADBIT 16
RGAIN 18
IRNUC 1H
IRFRQ 400.05 MHz
IRSEP 0.00 KHz
IRFPW 45 usec
IRATN 511
IRRSN 0
IRBPI 30
IRBPP 6
BF 0.10 Hz
T1 0.00
T2 0.00
T3 90.00
T4 100.00
XE 4202.64 Hz
XS 105.96 Hz
REFVL
DFILE 20160701 7-Allyl-2-
MENUP non
SIMP1 th5_201601
LKSET 0.00 KHz
LKEV 180
LGIN 17
LKPS 318
LKSIG 451
CTEMP 22.1 c
CSPE 21 Hz
FIELD 795
    
```

**(S)-2-(7-Allyl-6-hydroxybenzo[d]thiazol-2-yl)-4,5-dihydrothiazole-4-carboxylic acid**  
**(7'-AllylLuc)**



```

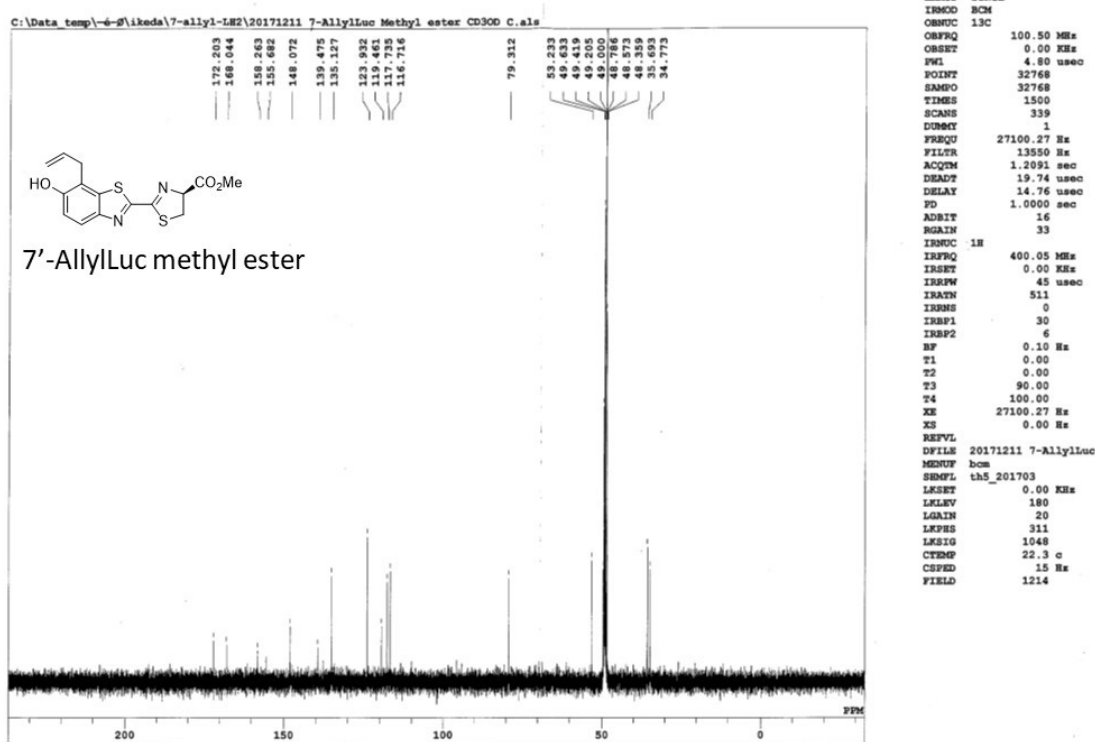
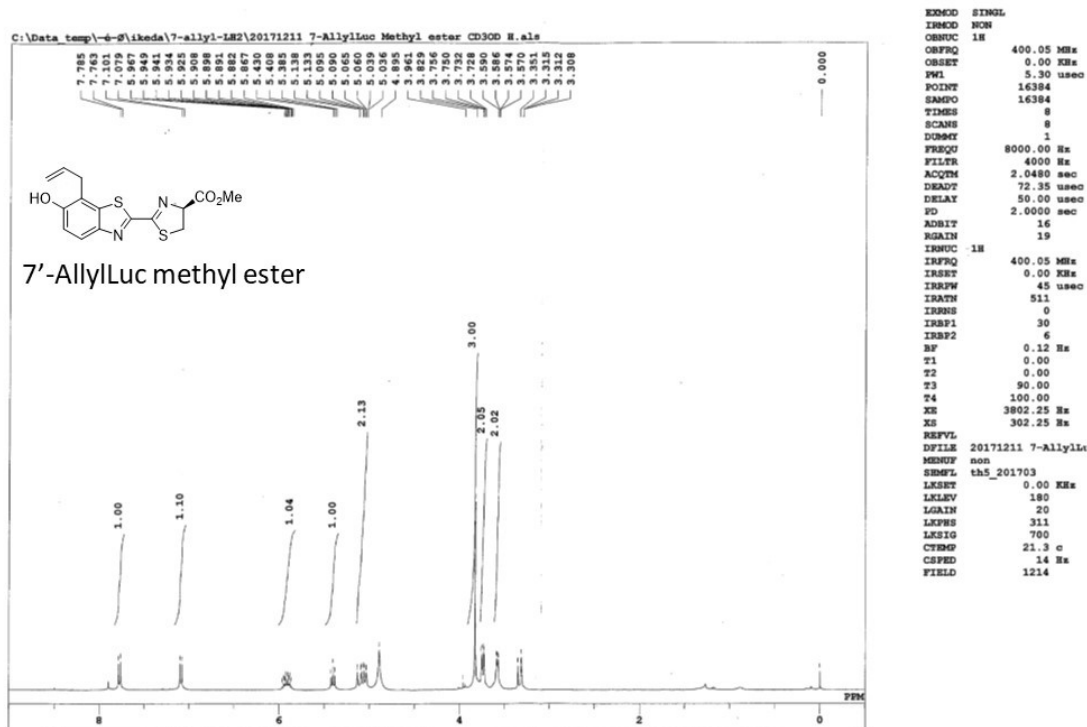
EXMOD SINGL
IRMOD NON
OBNUC 1H
OBSFQ 400.05 MHz
OBSST 0.00 KHz
PWI 5.30 usec
POINT 16384
SAMP0 16384
TIMES 8
SCANS 8
DUMY 1
FREQU 8000.00 Hz
FILTR 4000 Hz
ACQTM 2.0480 sec
DEADT 72.35 usec
DELAY 50.00 usec
PD 2.0000 sec
ADBIT 16
RGAIN 25
IRMOD 1H
IRFQ 400.05 MHz
IRSET 0.00 KHz
IRRFW 45 usec
IRATN 511
IRSN 0
IRBP1 30
IRBP2 6
BF 0.12 Hz
T1 0.00
T2 0.00
T3 90.00
T4 100.00
XE 4202.64 Hz
XS 101.07 Hz
REFVL
DFILE 20150824 allylLB2 C
MENUF non
SMBL TH5
LKSET 0.00 KHz
LKLEV 180
LGAIN 18
LRFPS 318
LRSIG 972
CTEMP 21.6 c
CSPED 14 Hz
FIELD 516
    
```



```

EXMOD SINGL
IRMOD BCM
OBNUC 13C
OBSFQ 100.50 MHz
OBSST 0.00 KHz
PWI 4.90 usec
POINT 32768
SAMP0 32768
TIMES 1200
SCANS 1200
DUMY 1
FREQU 27100.27 Hz
FILTR 13550 Hz
ACQTM 1.2091 sec
DEADT 19.74 usec
DELAY 14.76 usec
PD 1.0000 sec
ADBIT 16
RGAIN 33
IRMOD 1H
IRFQ 400.05 MHz
IRSET 0.00 KHz
IRRFW 45 usec
IRATN 511
IRSN 0
IRBP1 30
IRBP2 6
BF 0.10 Hz
T1 0.00
T2 0.00
T3 90.00
T4 100.00
XE 27100.27 Hz
XS 0.00 Hz
REFVL
DFILE 20160111 allylLB2 C
MENUF bcm
SMBL th5_201601
LKSET 0.00 KHz
LKLEV 180
LGAIN 23
LRFPS 318
LRSIG 2438
CTEMP 21.8 c
CSPED 11 Hz
FIELD 971
    
```

### Methyl (S)-2-(7-allyl-6-hydroxybenzo[d]thiazol-2-yl)-4,5-dihydrothiazole-4-carboxylate (7'-AllylLuc methyl ester)



## References

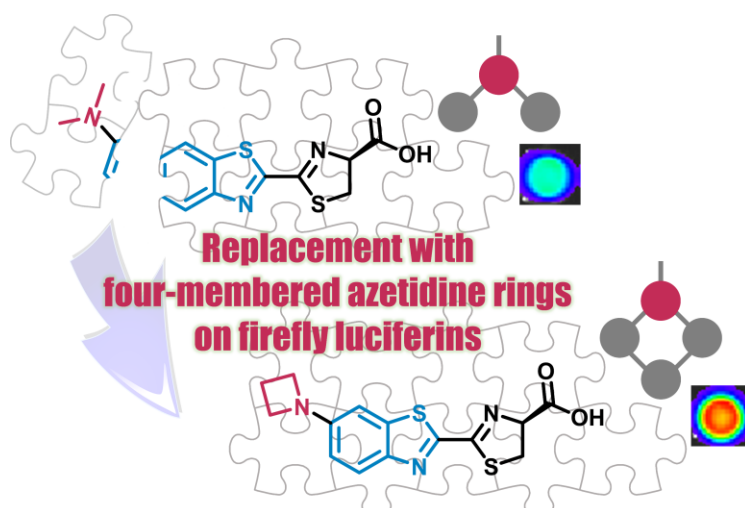
1. Prescher, J. A. and Contag, C. H., "Guided by the light: visualizing biomolecular processes in living animals with bioluminescence", *Curr. Opin. Chem. Biol.*, **2010**, *14*, 80-89.
2. Adams, S. T., Jr. and Miller, S. C., "Beyond D-luciferin: expanding the scope of bioluminescence imaging *in vivo*". *Curr. Opin. Chem. Biol.*, **2014**, *21*, 112-120.
3. Paley, M. A. and Prescher, J. A., "Bioluminescence: a versatile technique for imaging cellular and molecular features". *Med. Chem. Commun.*, **2014**, *5*, 255-267.
4. Niwa, K., Ichino, Y., Kumata, S., Nakajima, Y., Hiraishi, Y., Kato, D., Viviani, V. R. and Ohmiya, Y., "Quantum yields and kinetics of the firefly bioluminescence reaction of beetle luciferases." *Photochem. Photobiol.*, **2010**, *86*, 1046-1049.
5. Viviani, V. R., Bechara, E. J. and Ohmiya, Y., "Cloning, sequence analysis, and expression of active Phrixothrix railroad-worms luciferases: relationship between bioluminescence spectra and primary structures". *Biochemistry*, **1999**, *38*, 8271-8279.
6. Viviani, V., Silva, A., Perez, G., Santelli, R., Bechara, E. and Reinach, F., "Cloning and molecular characterization of the cDNA for the Brazilian larval click-beetle *Pyrearinus termitilluminans* luciferase". *Photochem. Photobiol.*, **1999**, *70*, 254-260.
7. Branchini, B. R., Southworth, T. L., Khattak, N. F., Michelini, E. and Roda, A., "Red-and green-emitting firefly luciferase mutants for bioluminescent reporter applications". *Anal. Biochem.*, **2005**, *345*, 140-148.
8. Nakajima, Y., Yamazaki, T., Nishii, S., Noguchi, T., Hoshino, H., Niwa, K., Viviani, V. R. and Ohmiya, Y., "Enhanced beetle luciferase for high-resolution bioluminescence imaging". *PLoS One*, **2010**, *5*, e10011.
9. White, E. H., Wörther, H., Field, G. F. and McElroy, W. D., "Analogues of firefly luciferin". *J. Org. Chem.*, **1965**, *30*, 2344-2348.
10. White, E. H., F. McCapra and Field G. F., "The structure and synthesis of firefly luciferin". *J. Am. Chem. Soc.*, **1963**, *85*, 337-343.
11. White, E. H. and Roswell, D. F., "Analogues and derivatives of firefly oxyluciferin, the light emitter in firefly bioluminescence". *Photochem. Photobiol.*, **1991**, *53*, 131-136.
12. Lambert, N., "Firefly luciferase can use L-luciferin to produce light". *Biochem. J.*, **1996**, *317*, 273-277.
13. Ioka, S., Saitoh, T., Iwano, S., Suzuki, K., Maki, S. A., Miyawaki, A., Imoto, M. and Nishiyama, S., "Synthesis of Firefly Luciferin Analogues and Evaluation of the Luminescent Properties". *Chem. - Eur. J.*, **2016**, *22*, 9330-9337.
14. McCutcheon, D. C., Paley, M. A., Steinhardt, R. C. and Prescher, J. A., "Expedient synthesis of electronically modified luciferins for bioluminescence imaging". *J. Am. Chem. Soc.*, **2012**, *134*, 7604-7607.

15. Woodroffe, C. C., Meisenheimer, P. L., Klaubert, D. H., Kovic, Y., Rosenberg, J. C., Behney, C. E., Southworth, T. L. and Branchini, B. R., "Novel heterocyclic analogues of firefly luciferin". *Biochemistry* **2012**, *51*, 9807-13.
16. Takakura, H., Kojima, R., Ozawa, T., Nagano, T. and Urano, Y., "Development of 5'- and 7'-substituted luciferin analogues as acid-tolerant substrates of firefly luciferase". *ChemBioChem*, **2012**, *13*, 1424-1427.
17. Iwano, S., Obata, R., Miura, C., Kiyama, M., Hama, K., Nakamura, M., Amano, Y., Kojima, S., Hirano, T., Maki, S. and Niwa, H., "Development of simple firefly luciferin analogs emitting blue, green, red, and near-infrared biological window light". *Tetrahedron*, **2013**, *69*, 3847-3856.
18. Miura, C., Kiyama, M., Iwano, S., Ito, K., Obata, R., Hirano, T., Maki, S. and Niwa, H., "Synthesis and luminescence properties of biphenyl-type firefly luciferin analogs with a new, near-infrared light-emitting bioluminophore". *Tetrahedron*, **2013**, *69*, 9726-9734.
19. Jones, K. A., Porterfield, W. B., Rathbun, C. M., McCutcheon, D. C., Paley, M. A. and Prescher, J. A., "Orthogonal Luciferase-Luciferin Pairs for Bioluminescence Imaging". *J. Am. Chem. Soc.*, **2017**, *139*, 2351-2358.
20. Harwood, K. R., Mofford, D. M., Reddy, G. R. and Miller, S. C., "Identification of mutant firefly luciferases that efficiently utilize aminoluciferins". *Chem. Biol.*, **2011**, *18*, 1649-1657.
21. Adams, S. T., Jr., Mofford, D. M., Reddy, G. S. and Miller, S. C., "Firefly Luciferase Mutants Allow Substrate-Selective Bioluminescence Imaging in the Mouse Brain". *Angew. Chem. Int. Ed.*, **2016**, *55*, 4943-4946.
22. Ando, Y., Niwa, K., Yamada, N., Enomoto, T., Irie, T., Kubota, H., Ohmiya, Y. and Akiyama, H., "Firefly bioluminescence quantum yield and colour change by pH-sensitive green emission". *Nat. Photonics*, **2007**, *2*, 44-47.
23. Nakatsu, T., Ichiyama, S., Hiratake, J., Saldanha, A., Kobashi, N., Sakata, K. and Kato, H., "Structural basis for the spectral difference in luciferase bioluminescence". *Nature*, **2006**, *440*, 372-376.
24. Steinhardt, R. C., O'Neill, J. M., Rathbun, C. M., McCutcheon, D. C., Paley, M. A. and Prescher, J. A., "Design and Synthesis of an Alkynyl Luciferin Analogue for Bioluminescence Imaging". *Chem. - Eur. J.*, **2016**, *22*, 3671-3675.
25. Steinhardt, R. C., Rathbun, C. M., Krull, B. T.; Yu, J. M., Yang, Y., Nguyen, B. D., Kwon, J.; McCutcheon, D. C., Jones, K. A., Furche, F. and Prescher, J. A., "Brominated Luciferins Are Versatile Bioluminescent Probes". *ChemBioChem*, **2017**, *18*, 96-100.
26. Niwa, K., Ichino, Y., Ohmiya, Y., "Quantum Yield Measurements of Firefly Bioluminescence Reactions Using a Commercial Luminometer". *Chem. Lett.*, **2010**, *39*, 291-293.

## Chapter 3

# Demonstration of an Azetidine-Substituent Effect on Firefly Luciferin Analogues

This chapter is based on "Demonstration of an Azetidine-Substituent Effect on Firefly Luciferin Analogues, Yuma Ikeda, Takahiro Nomoto, Yuki Hiruta, Nobuhiro Nishiyama and Daniel Citterio, *unpublished*".



## Summary

Replacing a *N,N*-dimethylamino group in a classical fluorophore with a four membered azetidine ring provides the improved luminescence quantum yield. Herein, I extended this strategy to firefly bioluminescent luciferin analogues, and demonstrated its generalizability. For this purpose, the five-types of luciferin core were employed, and totally 10 analogues were evaluated. Among these analogues, unexpectedly, only the benzothiazole core analogue benefited from an azetidine substitution and improved the bioluminescence. In addition, the fluorescence measurement revealed that an azetidine substitution improved 2.3-times the fluorescence quantum yield compared to a *N,N*-dimethylamino group. My findings clarified that the azetidine-substituent effect was not general for luciferins, but presented one strategy for enhancing photon outputs in bioluminescence through a synthetic approach.

## 3.1. Introduction

Recent progress in bioluminescence imaging with luciferin-luciferase pairs has enabled imaging from the level of single cell to brain tissue of freely moving marmosets.<sup>1-2</sup> A typical example of bioluminescent luciferin-luciferase pairs is the firefly luciferin, D-luciferin, and firefly luciferase (Fluc) from *photinus pyralis*. During the firefly bioluminescence reaction, D-luciferin reacts with adenosine triphosphate (ATP) and oxygen to generate electronically excited state of oxyluciferin (**Figure 3.1A**).

Researchers have great interest in this light emitting reaction, and are working on the discovery of synthetic firefly luciferins to enhance their performance as a biological reporter.<sup>3-7</sup> The chemical structure of D-luciferin can be categorized as a donor-acceptor type dipolar fluorophore. Especially, the amino luciferins, in which the hydroxyl group at C-6` position of D-luciferin was replaced by an amino-substituent, has been extensively studied because of their bioluminescence activity and applicability.<sup>4, 8-10</sup> The electron-donating substituents at the C-6` position of D-luciferin strongly affect the  $\pi$ -electronic system and spectroscopic properties. In 2010, Millar and co-workers have developed several alkylamino analogues and demonstrated that rigid and strong C-6` electron-donation enables robust and red-shifted emission similar to the trend of other donor-acceptor fluorophores.<sup>11-12</sup> Thus, the modification strategies for D-luciferin appear to be similar to those for fluorophores.

In 2015, Lavis and co-workers demonstrated a general structural modification improving the brightness of a classical family of fluorophores, such as rhodamines, coumarins and naphthalimides. One landmark discovery is that a minor alteration of an *N,N*-dimethylamino substituent in a classical dye with a cyclic amine, especially azetidine, greatly improved the fluorescence quantum yield by suppressing twisted internal charge transfer (**Figure 3.1B**).<sup>13</sup> In addition, this simple structural modification preserved spectral properties and cell membrane permeability. Also, in the design of luciferin, Hirano and co-workers developed firefly luciferin analogues which have a cyclic amine substituent (pyrrolidinyl, piperidino, azepanyl and morpholino), and compared their bioluminescent activities with an acyclic dimethylamino luciferin.<sup>14</sup> Their photochemical evaluation suggested that a minor structural change might improve the luminescent activity, as reported by Lavis. In parallel, Miller and co-workers synthesized azetidine-substituted analogues (**A-1**) through Buchwald-Hartwig amination.<sup>15</sup> The azetidine-substituted analogue (**A-1**) displayed a brighter bioluminescent signal in live cells expressing Fluc than that of dimethylamino luciferin (**D-1**). This result may also suggest

an azetidine-substituent effect like rhodamines. However, they did not mention the detailed characteristics of the analogue (**A-1**), and effect of an azetidine-substituent on the firefly luciferin analogues remain to be elucidated.

This chapter describes investigation of an azetidine-substituent effect on firefly bioluminescence. For this purpose, 10 types luciferin analogues were selected and synthesized based on the five different luciferin core structures with dimethylamino- or azetidine-substituent as an electron donating group (**Figure 3.1C**). With these analogues in hand, I have characterized the bioluminescent properties in combination with Fluc. Furthermore, I have performed a cellular application to confirm that the analogues were sufficiently cell-membrane permeable and photon emitter even in cells for an imaging application.

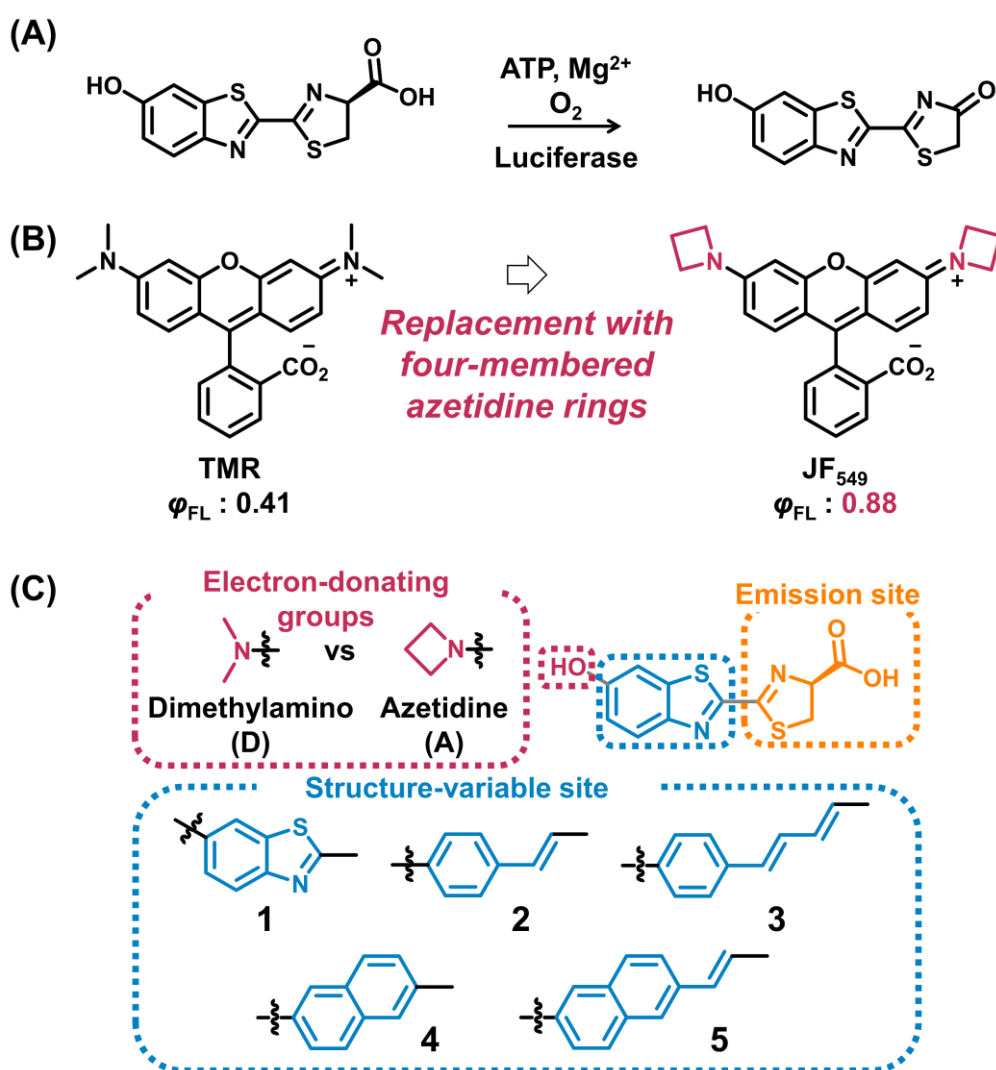
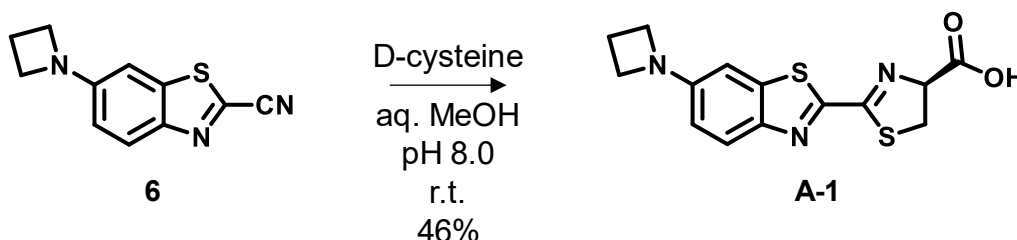


**Figure 3.1. Azetidine-substituent approach on firefly bioluminescence.** (A) Firefly bioluminescence reaction. (B) The chemical structures and the fluorescence quantum yields of tetramethyl rhodamine (TMR) and azetidine substituted rhodamine dye, JF<sub>549</sub>. (C) Molecular structures of analogues investigated in this work.

## 3.2. Results and Discussion

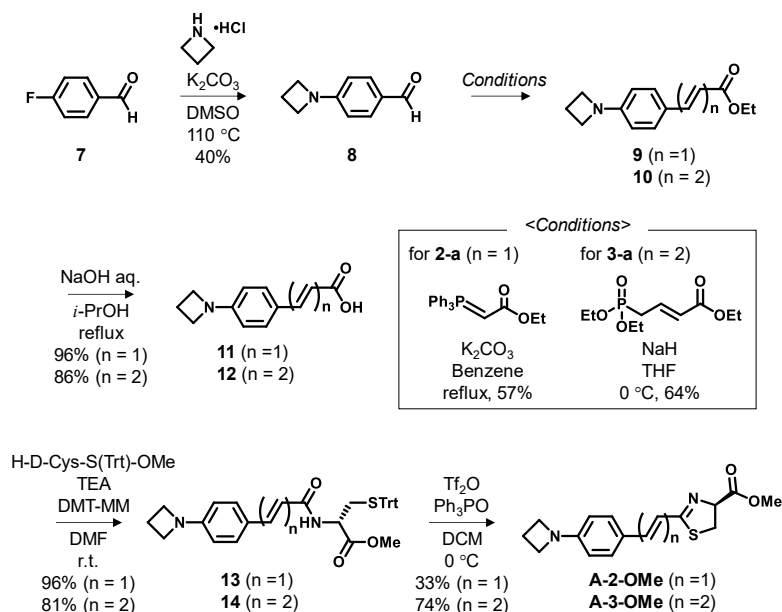
### 3.2.1. Design and synthesis of luciferin analogues with an azetidine donor

The 5 types of luciferin core structures were employed to probe the scope of azetidine-substituent effect on firefly bioluminescence (**Figure 3.1C**). Their chemical structures are roughly classified into three types; benzothiazole, naphthyl and styrenyl scaffold. All azetidine-substituted analogues were prepared according to the reported synthetic routes. The corresponding azetidine-substituted precursors were prepared via nucleophilic aromatic substitution (for styrenyl analogues) or Pd-catalyzed Buchwald-Hartwig amination (for benzothiazole and naphthyl analogues). The benzothiazole analogue (**A-1**) was readily accessed through D-cysteine condensation reaction with the nitrile precursor (**Scheme 3.1**).

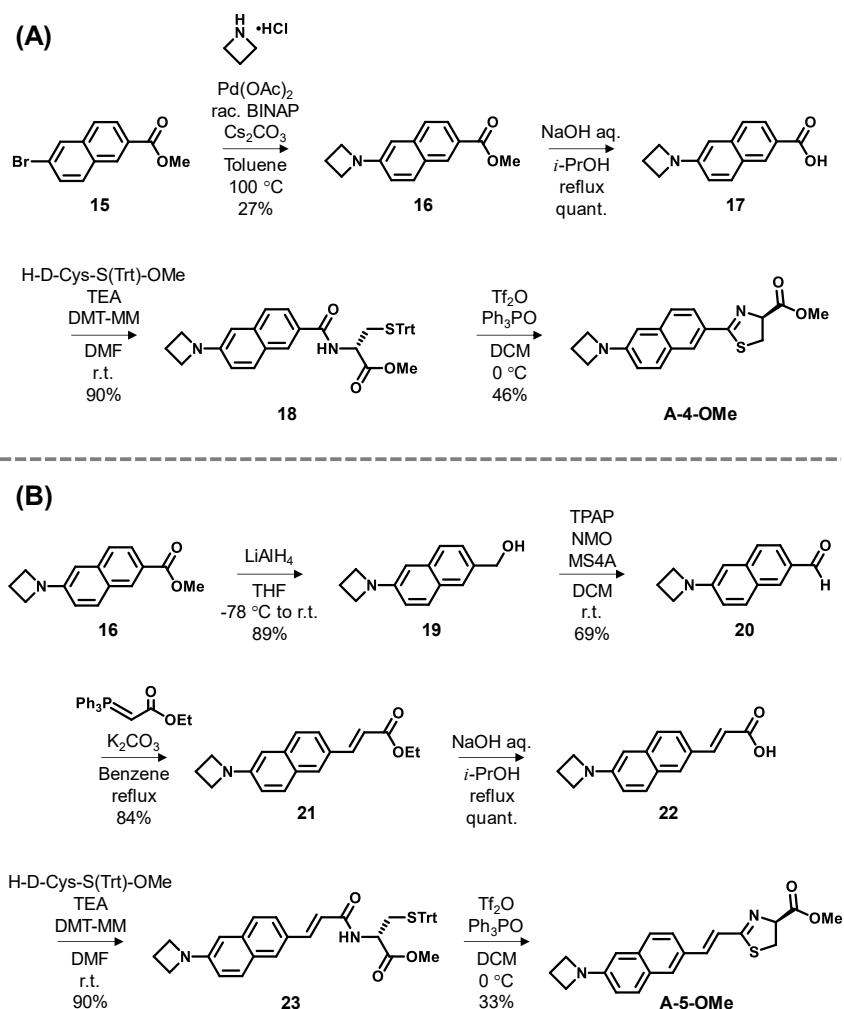


**Scheme 3.1.** Synthesis of the azetidine-substituent benzothiazole core analogue (**A-1**).

The synthesis of styrenyl analogues (**A-2**, **A-3**) was based on the previously reported synthetic route (**Scheme 3.2**).<sup>16</sup> Olefination of azetidinyl benzaldehyde (**8**) via Wittig reaction or Horner-Wadsworth-Emmons reaction, followed by condensation with protected cysteine gave the amide precursors (**13**, **14**). Intramolecular cyclization to the thiazoline (**A-2-OMe**, **A-3-OMe**) was achieved by treatment with  $\text{Tf}_2\text{O}$ -TPPO complex at 0 °C. The synthesis of naphthyl analogues (**A-4**, **A-5**) was carried out in the similar manner as described above (**Scheme 3.3**).

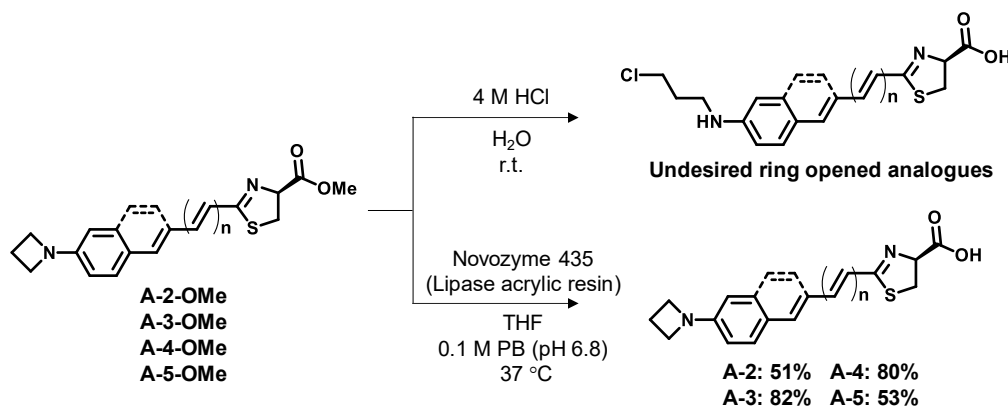


Scheme 3.2. Synthesis of the azetidine-substituent styrenyl core analogues (A-2, 3-OMe).



Scheme 3.3. Synthesis of the azetidine-substituent naphthyl core analogues (A) A-4-OMe, (B) A-5-OMe.

Finally, the deprotection of methyl esters was performed (**Scheme 3.4**). Attempted acid-catalyzed deprotection of luciferin esters afforded the undesired ring opened analogues. I therefore switched the synthetic route to enzymatic hydrolysis using lipase, and luciferin analogues (**A-2, 3, 4, 5**) were successfully synthesized. All dimethylamino analogues except for **D-5**, and azetidinyl analogues (**A-1** and **A-2**) have been reported previously.<sup>3, 15, 17-19</sup> The synthesis of **D-5** was achieved from the methyl 6-Amino-2-naphthoate by the same manner as described for the preparation of naphthyl analogues (**A-5**).



**Scheme 3.4.** Synthesis of the azetidine-substituent analogues (**A-2, A-3, A-4** and **A-5**) through lipase-promoted ester hydrolysis. Acid-catalyzed hydrolysis gave the undesired corresponding ring opened products.

### 3.2.2. Bioluminescence assays with recombinant firefly luciferase

Firstly, the bioluminescence photon production from azetidinyl analogues were evaluated in combination with the recombinant Fluc (**Figure 3.2A, B**). Dose-response photon production was observed for both azetidinyl and dimethylamino analogues as seen in previously reported luciferin analogues. For each luciferin analogue, the kinds of saturations of emitted photons at around 0.5  $\mu\text{M}$  for each luciferin were confirmed (**Figure 3.2C, D**). These results mean that all synthetic luciferins have high affinity for luciferase. The Michaelis-Menten analysis was conducted to estimate the Michaelis constant  $K_m$  and  $V_{\text{max}}$  for each luciferin (**Figure 3.3**). The bioluminescence apparent  $K_m$  values of synthetic luciferins fall within the range of 0.015-0.5  $\mu\text{M}$ , which are lower than that of native D-luciferin substrate ( $K_m$ : 19  $\mu\text{M}$ , data not shown) (**Table 3.1**).

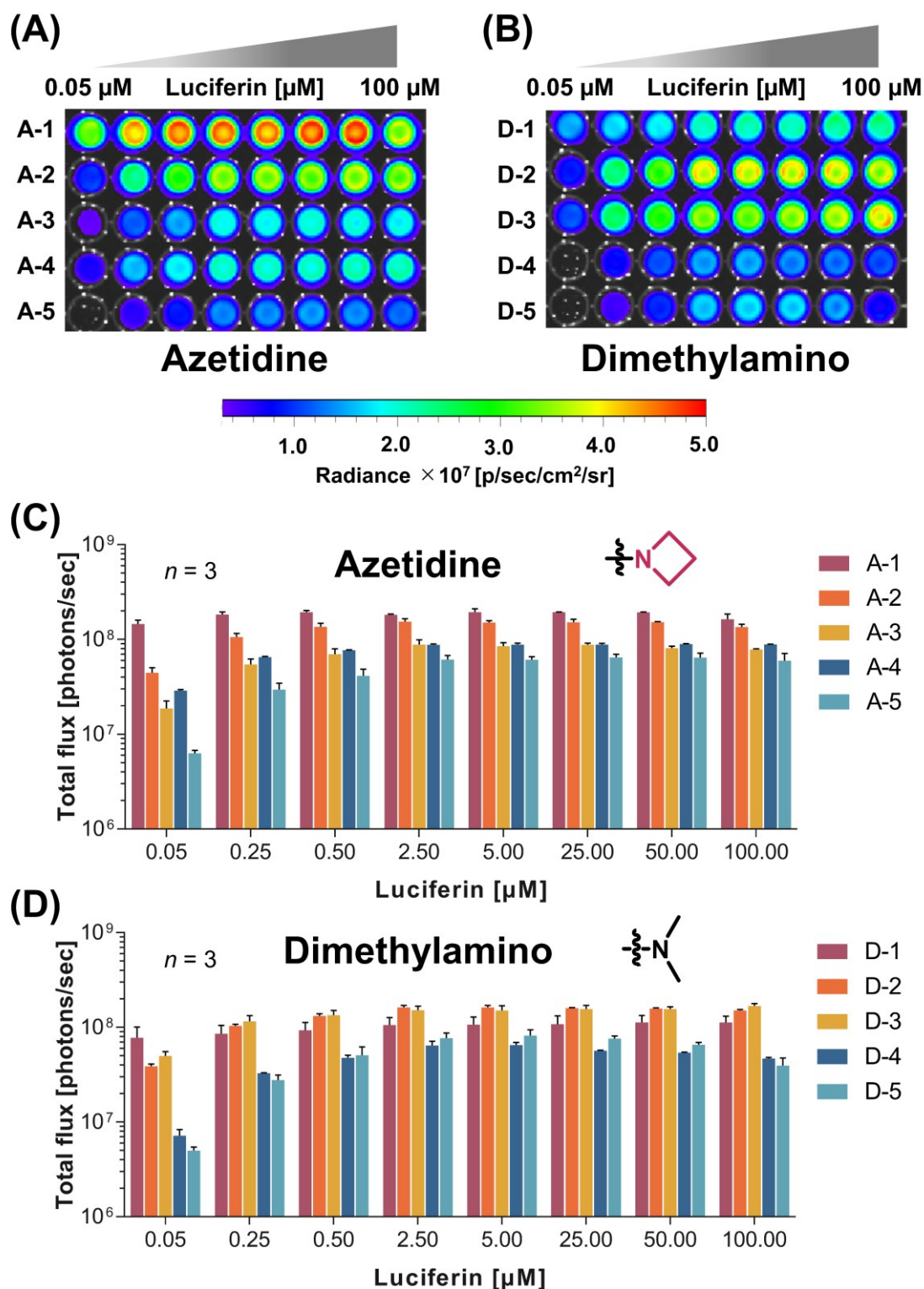


**Figure 3.2. Bioluminescence intensities for dimethylamino and azetidiny analogues.** (A and B) Images of dose-response bioluminescence photon production: 0.05-100  $\mu\text{M}$  luciferins were incubated with recombinant Fluc in the presence of ATP. (A) Azetidiny analogues, (B) Dimethylamino analogues. (C and D) Quantification of the photon flux from 0.05-100  $\mu\text{M}$  luciferins incubated with Fluc. (C) Azetidiny analogues, (D) Dimethylamino analogues. Error bars represent the standard deviation of the mean for triplicate experiments.

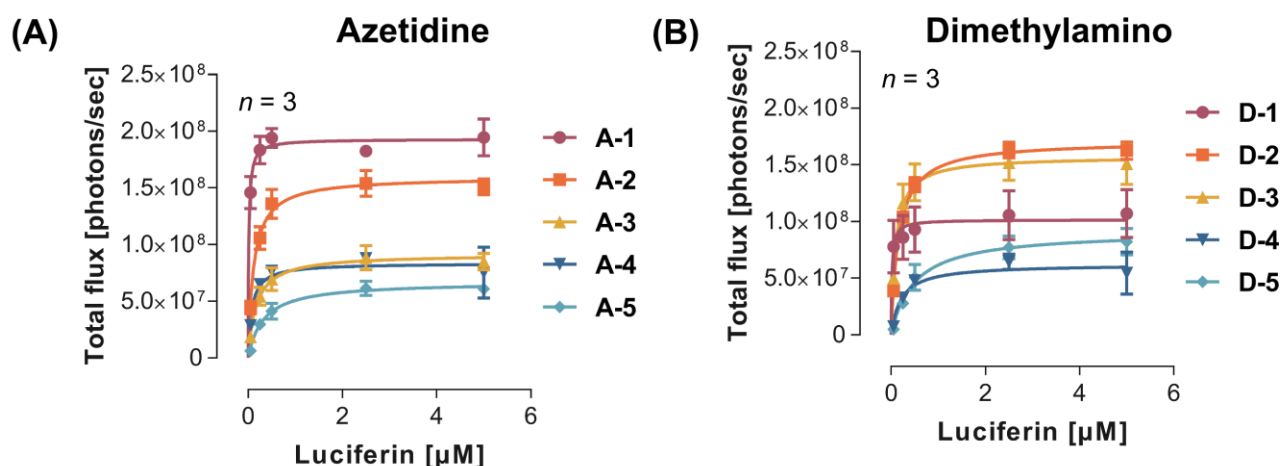


**Figure 3.3. Michaelis-Menten plots.** (A) Azetidino analogues. (B) Dimethylamino analogues.

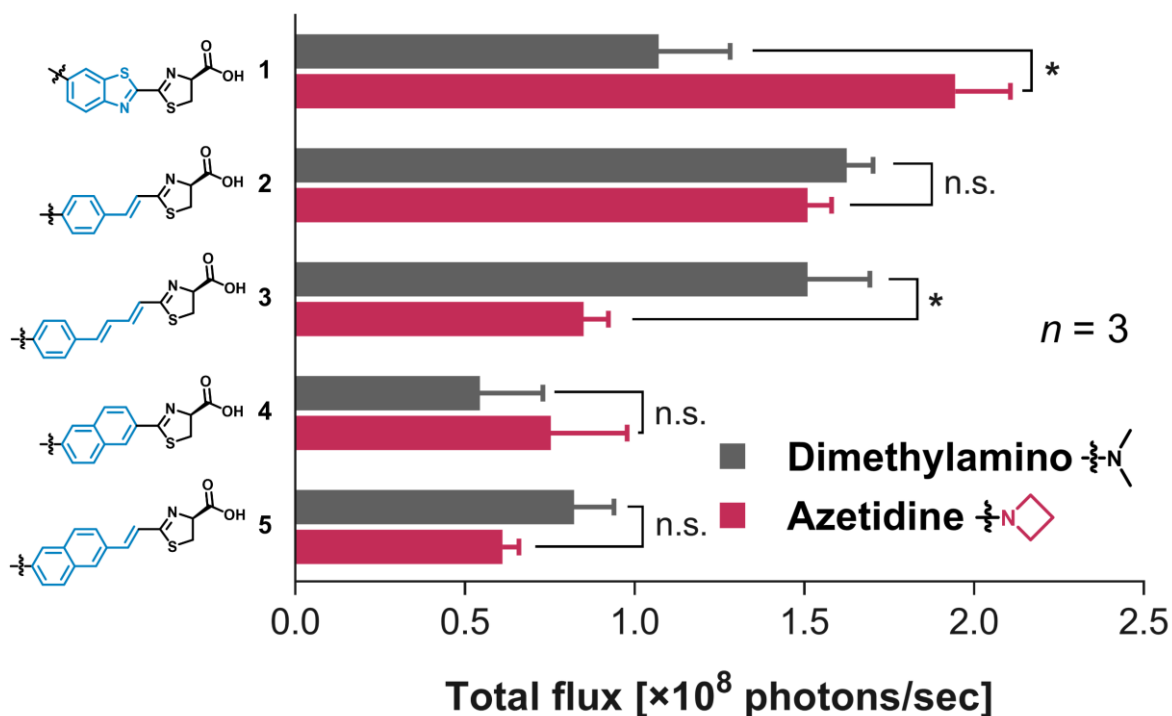
**Table 3.1. Characteristics of dimethylamino and azetidino luciferins.**

Luciferin core	Electron donor	$\lambda_{BL}^a$ [nm]	$K_m^b$ [ $\mu$ M]	$V_{max}^b$ [ $\times 10^7$ photons/sec]
1		620	$0.02 \pm 0.01$	$10.2 \pm 0.7$
		615	$0.02 \pm 0.00$	$19.3 \pm 0.5$
2		559	$0.16 \pm 0.01$	$17.1 \pm 0.3$
		563	$0.12 \pm 0.02$	$16.0 \pm 0.5$
3		675	$0.10 \pm 0.02$	$15.7 \pm 0.6$
		675	$0.17 \pm 0.04$	$9.16 \pm 0.41$
4		559	$0.21 \pm 0.09$	$6.23 \pm 0.58$
		562	$0.08 \pm 0.03$	$8.37 \pm 0.55$
5		684	$0.49 \pm 0.12$	$9.15 \pm 0.60$
		679	$0.32 \pm 0.06$	$6.72 \pm 0.31$

<sup>a</sup> Bioluminescence emission maxima with Fluc, <sup>b</sup>  $K_m$  and  $V_{max}$  were determined using nonlinear Michaelis-Menten regression analyses in GraphPad Prism (version 7.03 for Windows, GraphPad Software).

### 3.2.3. Verification of an azetidine-replacement effect

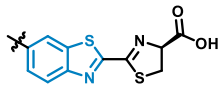
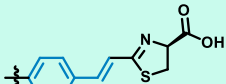
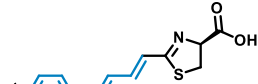
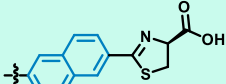
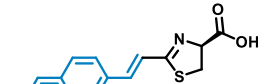
Subsequently, in order to clarify the aspect of the azetidine-substituent effect, the photon flux from dimethylamino and azetidinyl analogues were compared for each luciferin core structures. The photon flux at 5  $\mu\text{M}$  luciferin where the Fluc was sufficiently saturated ( $V_{\text{max}}$ ) were selected to be evaluated. As a result, two different core structural analogues, benzothiazole (**1**) and phenylbutadiene (**3**), were found to show the statistically significant differences ( $p < 0.05$ ,  $t$ -test) (**Figure 3.4**).



**Figure 3.4. Comparison of the photon flux from azetidinyl and dimethylamino analogues for each luciferin core structures at 5  $\mu\text{M}$  luciferin.** Error bars represent the standard deviation of the mean for triplicate experiments. \* $P < 0.05$  ( $t$ -test), n.s.; not significant ( $P > 0.05$ ).

Interestingly, in the benzothiazole core analogues (**A-1**, **D-1**), replacement of a dimethylamino group by an azetidine ring importantly improved the photon output as previously reported,<sup>15</sup> but the other cores (**2-5**) did not. The fluorescence quantum yields for all core analogues (**1-5**) in water (50 mM GTA buffer, pH 8.0) were then investigated by absolute measurements using a fluorometer equipped with an integrated sphere (**Table 3.2**). The results clearly indicated the difference in substituent effect between the benzothiazole (**1**) and the others core (**2-5**) on the fluorescence quantum yields. It was confirmed that an azetidine substituent contributed to the improvement of fluorescence quantum yields only in the benzothiazole (**1**) core. Further comparison of the fluorescence quantum yields for benzothiazole analogues (**A-1**, **D-1**) in various solvent (DMSO, acetonitrile, 2-propanol, methanol and water) demonstrated the TICT resistance on the azetidine-substituent analogue (**A-1**) in analogy to the previously

**Table 3.2. Comparison of the fluorescence quantum yields in buffer (pH 8.0).**

	Luciferin core	Electron donor	$\phi_{Fl}^a$ [-]
1			0.28
			0.65
2			0.015
			0.015
3			0.025
			0.029
4			0.23
			0.19
5			0.13
			0.11

<sup>a</sup> Absolute fluorescence quantum yield in 50 mM GTA buffer (pH 8.0).

reported work (**Figure 3.5**).<sup>20</sup> The relationship of the fluorescence quantum yields between luciferin and oxyluciferin, an actual light emitter, has not been clarified, but this substituent effect may be involved. In contrast, the reduced photon flux in the phenylbutadiene (**3**) core might be considered probably due to the reduced light-emitting reaction rate as a dominant factor.

In order to support TICT resistance by azetidine-substituent effect theoretically, I computed the potential energy surfaces of the oxidized form of benzothiazole core analogues (**A-1**, **D-1**) in water as a function of C-N bond rotation (**Figure 3.6**). The calculated results clearly showed the TICT formation faces a larger energy barrier in **A-1** (0.37 eV) than that in **D-1** (0.21 eV).

The bioluminescence spectra of dimethylamino and azetidinyl analogues with recombinant Fluc were recorded on a multichannel spectrometer equipped with charge-coupled devices (CCD) detector (**Figure 3.7**). As reported for fluorescent dyes, an azetidine substitution of a dimethylamino group did not affect their bioluminescence spectra except for the benzothiazole (**1**) core analogues. The azetidine substituted benzothiazole core analogue (**A-1**) showed a sharper spectrum width than that of corresponding dimethyl analogue (**D-1**), although their fluorescence spectra were completely identical (**Figure 3.8**). This behavior was also observed in the previous research about cyclic amino analogues reported by Hirano,<sup>14</sup> which presumably due to the suppression of free rotation of the C-N bond during bioluminescence reaction.

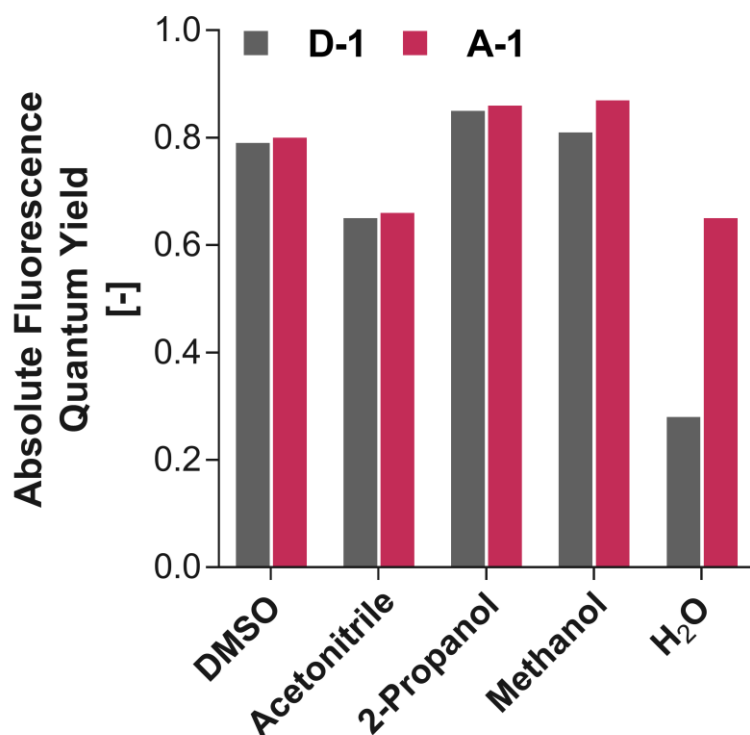


Figure 3.5. Absolute fluorescence quantum yields of D-1 and A-1 in various solvent (DMSO, acetonitrile, 2-propanol, methanol and water).

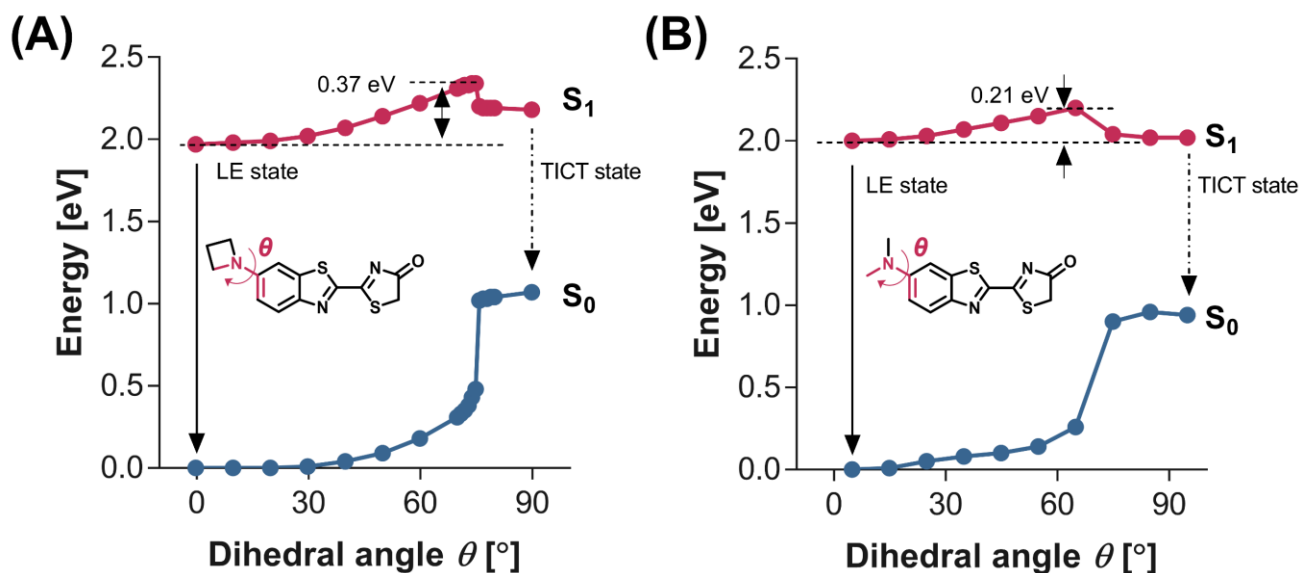


Figure 3.6. Calculated potential energy surfaces of benzothiazole core analogues in water.

(A) **A-1** (B) **D-1**. All quantum chemistry calculations are performed using Gaussian 16 software. The solvation effect is simulated through SMD solvent model.

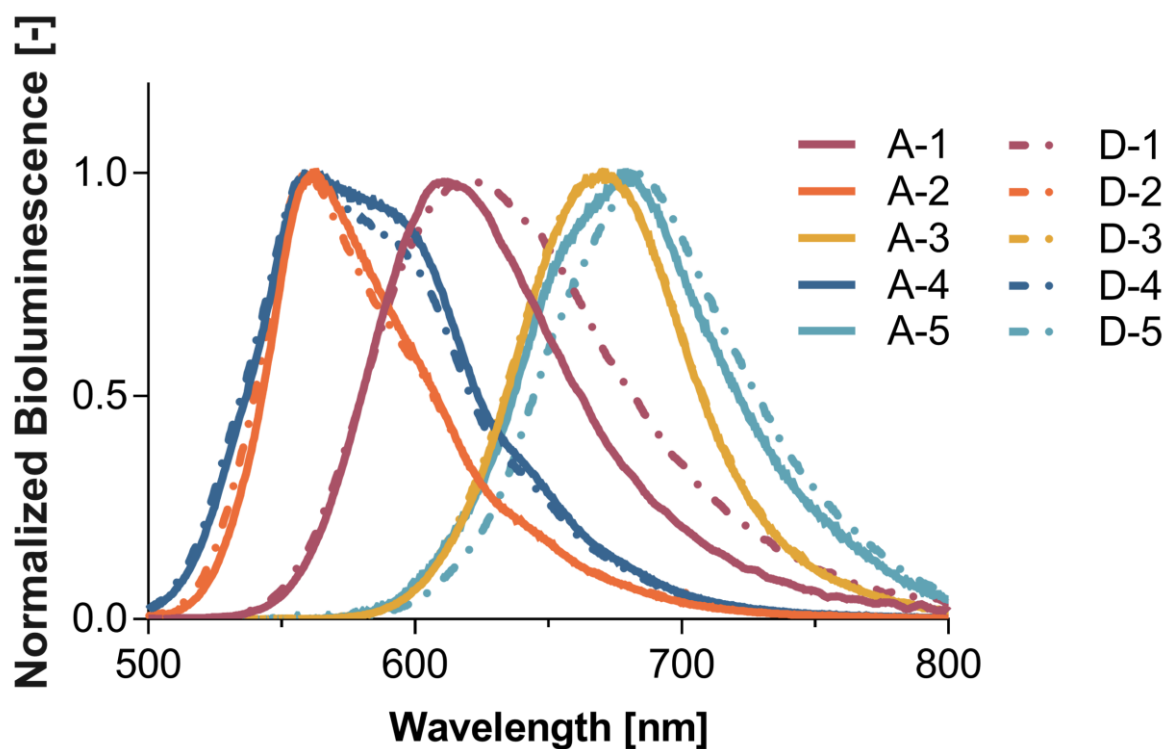


Figure 3.7. Bioluminescence spectra of azetidinyll (A, solid line) and dimethylamino (D, dotted line) analogues with Fluc.

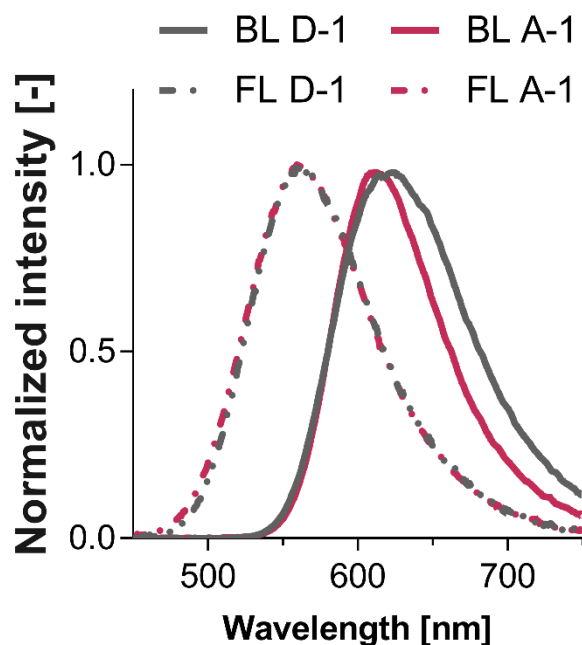
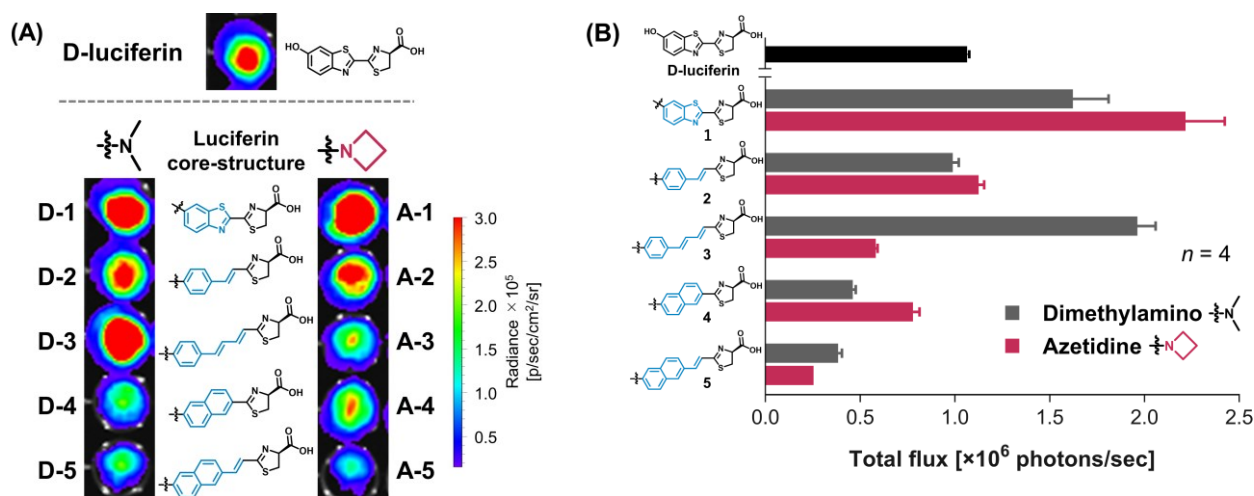


Figure 3.8. Comparison of the fluorescence and bioluminescence spectra for benzothiazole core analogues (D-1, A-1). The fluorescence spectra in water (50 mM GTA buffer, pH 8.0) were measured with the excitation light set to 375 nm.

### 3.2.4. Cellular bioluminescence applications

Finally, a cell-based application was performed to confirm that the analogues were sufficiently cell-membrane permeable and photon emitter even in cells for an imaging application. The 0.25-25  $\mu\text{M}$  of luciferins were incubated with stably Fluc expressing B16-F10 cells, a mouse melanoma cell line. The photon outputs were imaged 1 min after post luciferins addition. At saturating dose conditions (25  $\mu\text{M}$ ), The luciferins displayed sufficiently detectable signals (**Figure 3.9A**) and a similar emission trend described above *in vitro* results (**Figure 3.9B**). Once the luciferin concentrations were diluted 10 times (2.5  $\mu\text{M}$ ), 100 times (0.25  $\mu\text{M}$ ), meaning below  $K_m$ , the emission trend presented different behavior, especially for the benzothiazole (**1**) core analogues (**Figure 3.10**). This is thought to be due to the difference in the cell-membrane permeability of each luciferin. Time dependent imaging of the emitted photon revealed that the azetidine replacement did not affect the luminescent behavior over time (**Figure 3.11**).



**Figure 3.9. Photon flux from the Fluc-expressing cells.** (A) Bioluminescence image of Fluc-expressing B16F10 cells incubated with luciferins. Images were acquired 1 min after luciferin addition. (B) Quantitative analysis of the photon flux from cells. Error bars represent the standard error of the mean for quadruplicate experiments.

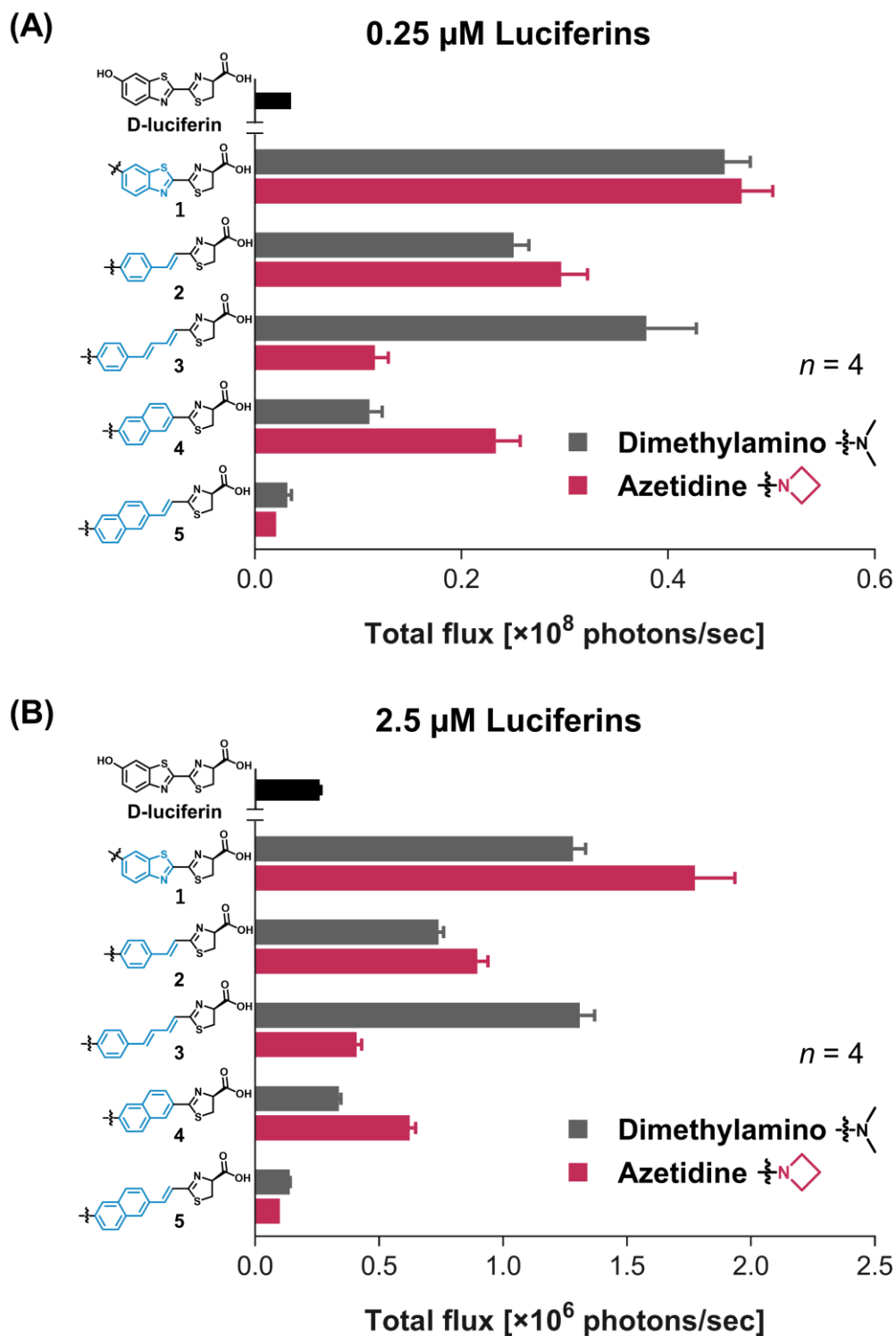


**Figure 3.10. Quantitative analysis of the photon flux from Fluc-expressing cells.** The cells were treated with (A) 0.25  $\mu$ M, (B) 2.5  $\mu$ M luciferins and imaged 1 min after post luciferin addition. Error bars represent the standard error of the mean for triplicate experiments.

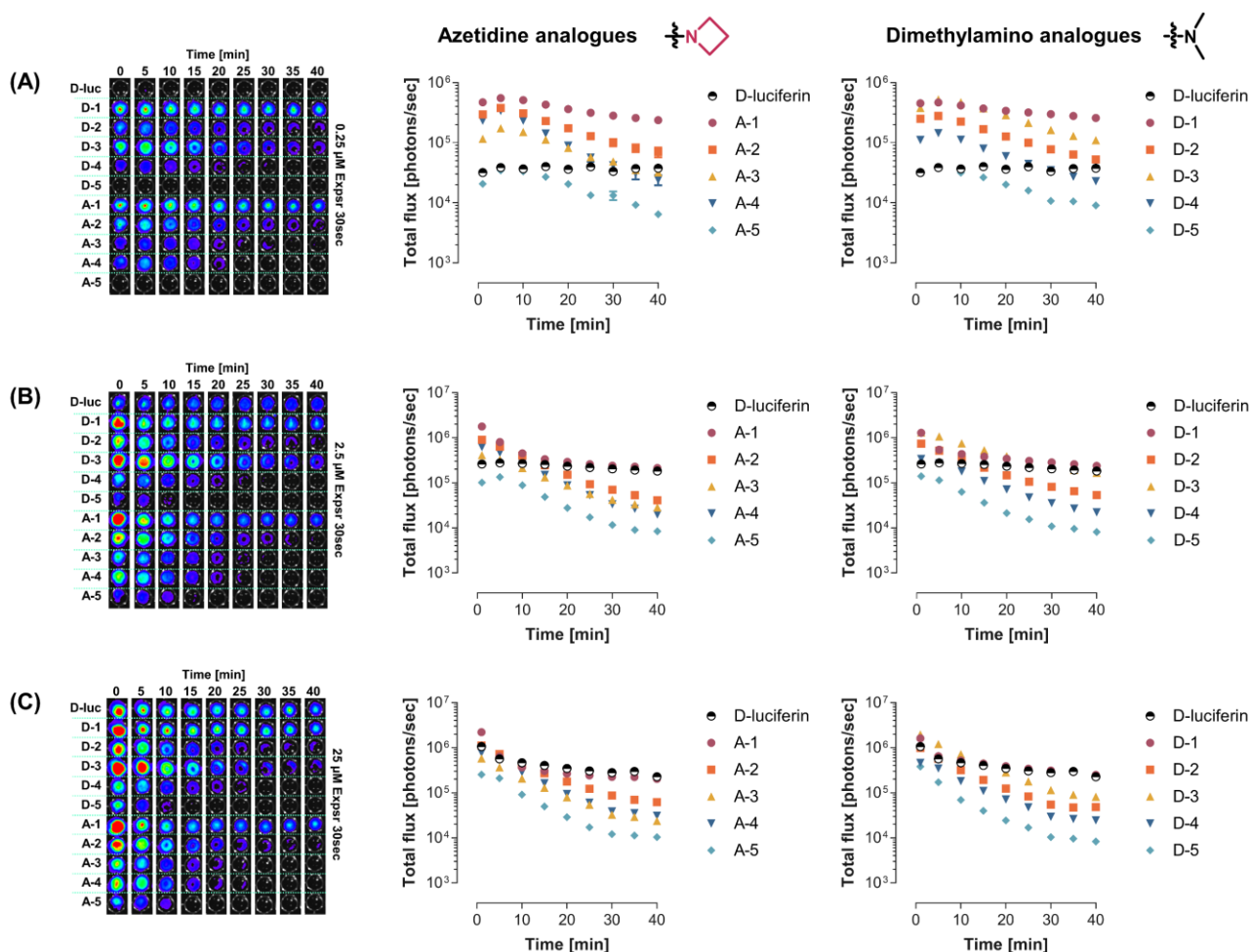


**Figure 3.11. Time courses of photon outputs from Fluc expressing B16F10 cells.** The cells were treated with (A) 0.25  $\mu\text{M}$ , (B) 2.5  $\mu\text{M}$ , (C) 25  $\mu\text{M}$  luciferins and imaged immediately post luciferin addition. The photon flux was measured over 40 minutes. Azetidinyl analogues (middle). Dimethylamino analogues (right). The photon flux was provided as log scale. Error bars represent the standard error of the mean for triplicate experiments.

## 3.3. Conclusions

In summary, an azetidine-substituent effect on firefly luciferin analogues has been investigated with the ten analogues having five different types of luciferin core. Unlike the previously published reports on classical fluorescent dyes,<sup>13, 20</sup> only the benzothiazole core analogue (**A-1**) benefited from an azetidine substitution and improved the bioluminescence compared to the corresponding *N,N*-dimethylamino analogue (**D-1**). After evaluation of fluorescence properties of luciferins in water, this enhancement is presumably due to an effective suppression of the TICT formation caused by the C-N bond rotation as reported in fluorescent dyes.<sup>13, 20</sup> In the live cells based assays, azetidine-substituent analogues were also cell-membrane permeable and potent light emitter. The azetidine-substituent strategy was not general for luciferins. However, this strategy offers an opportunity for enhancing photon production, and will inspire the rational design of brighter luciferin analogues through a synthetic approach.

## 3.4. Experimental Section

### 3.4.1. Material and methods

#### 3.4.1.1. General

Reagents and solvents were of the best grade available, supplied by Tokyo Chemical Industries (Japan), Wako Pure Chemical (Japan), Aldrich Chemical Co. (USA), Kanto Chemical Co. (Japan) or Watanabe Chemical Industries (Japan) and were used without further purification. NMR spectra were recorded on a JEOL ECA-500 instrument at 500 MHz for  $^1\text{H}$  NMR and at 125 MHz for  $^{13}\text{C}$  NMR. All chemical shifts ( $\delta$ ) are reported in ppm relative to tetramethyl silane ( $\delta = 0.0$  ppm) or residual non-deuterated NMR solvent  $\text{CDCl}_3$  (7.26 ppm for  $^1\text{H}$ , 77.16 ppm for  $^{13}\text{C}$ ),  $\text{CD}_3\text{OD}$  (3.31 ppm for  $^1\text{H}$ , 49.00 ppm for  $^{13}\text{C}$ ), or  $\text{DMSO-d}_6$  (2.50 ppm for  $^1\text{H}$ , 39.52 ppm for  $^{13}\text{C}$ ) and coupling constants ( $J$ ) are provided in Hz. Mass spectra (MS) were measured on a Waters LCT Premier XE (ESI-TOF). A 1.0 mg/mL stock solution of commercially available luciferase (Promega, QuantiLum<sup>®</sup> recombinant *Photinus pyralis* luciferase, E1701) in GTA buffer (50 mM, pH 8.0) containing 10% glycerol was prepared and stored at  $-80$  °C. The composition of the 50 mM GTA buffer is 50 mM 3,3-dimethylglutaric acid, 50 mM tris(hydroxymethyl)aminomethane, 50 mM 2-amino-2-methyl-1,3-propanediol and the pH was adjusted with 2 M HCl or 1 M NaOH solution. GraphPad Prism (version 7.03 for Windows, GraphPad Software) was used to analyze data and generate graphs.

#### 3.4.1.2. Bioluminescence spectra

The bioluminescence emission spectra for all luciferins were recorded on an AB-1850 spectrophotometer (ATTO, Japan). A solution of the luciferins (100  $\mu\text{M}$ ) in GTA buffer (50 mM, pH 8.0, 5  $\mu\text{L}$ ) and Fluc (1.0 mg/mL) in GTA buffer (50 mM, pH 8.0) containing 10% glycerol (5  $\mu\text{L}$ ) were placed in a polystyrene tube. The bioluminescence reaction was initiated by injection of 90  $\mu\text{L}$  of reaction buffer (4 mM ATP-2Na, 8 mM  $\text{MgSO}_4$  in 50 mM GTA buffer, pH 8.0). Emission data were collected for 60 s (slit width: 0.25 mm), and the luminescence intensities were normalized.

#### 3.4.1.3. Bioluminescence intensities and kinetic measurements

Measurements were acquired on an IVIS Spectrum (PerkinElmer, USA) with open filter. Reactions

were performed in a black 96-well flat-bottom plate. Solutions of luciferins in GTA buffer (50 mM, pH 7.0) were prepared (0.5  $\mu$ M - 1 mM luciferin), and 10  $\mu$ L was added to each well. Following the addition of Fluc (0.05 mg/mL) in GTA buffer (50 mM, pH 8.0) containing 10% glycerol (10  $\mu$ L), the luminescence reaction was initiated by addition of 80  $\mu$ L of reaction buffer (4 mM ATP-2Na, 8 mM MgSO<sub>4</sub> in 50 mM GTA buffer, pH 8.0). Emission data was recorded over a 30 sec period. Samples were analyzed in triplicate and three runs of each compound-enzyme pair were performed. Initial velocities were estimated as integrated values of the light emission intensities for 30 s.  $K_m$  and relative  $V_{max}$  values were determined using nonlinear regression analyses and robust fit outlier removal in GraphPad Prism (version 7.03 for Windows, GraphPad Software).

#### 3.4.1.4. Fluorescence measurements

The fluorescence spectra for luciferins (10  $\mu$ M) in 50 mM GTA buffer (pH 8.0) were measured using a VARIOSKAN FLASH (Thermo Scientific, USA) microplate reader with the excitation light and excitation/emission slit widths set to 375 nm and 1 nm, respectively. Spectral data were recorded at 25 °C in a clear bottom 96-well microplate over the wavelength range of 400-750 nm. The absolute fluorescence quantum yields were collected using a Quantaurus-QY (Hamamatsu Photonics, Japan) with the excitation light set to 375 nm.

#### 3.4.1.5. Computational quantum chemical calculations

All quantum chemistry calculations are performed using Gaussian 16 software. The solvation effect is simulated through SMD solvent model. The ground and excited state geometries are optimized using density functional theory (DFT) and time-dependent density functional theory (TD-DFT) at the B3LYP/6-31+G(d) levels of theory in water, respectively. Frequency checks were carried out after each geometry optimization to ensure that the minima on the potential energy surfaces (PES) were found.

#### 3.4.1.6. Cellular bioluminescence assays

The B16-F10 cells expressing luciferase (B16-F10/CMV-Luc#2 cells) were obtained from the Japanese Collection of Research Bioresources Cell Bank (Ibaraki, Japan). Transiently transfected B16-F10/CMV-Luc cells were cultured in DMEM medium supplemented with FBS (10%), penicillin (100 U/mL) and streptomycin (100  $\mu$ g/mL) at 37 °C in 5% CO<sub>2</sub>. For bioluminescence emission assays, approximately  $4.5 \times 10^5$  cells/well were plated in black 96-well plates in 75  $\mu$ L of DMEM containing 10% FBS. The cells were then incubated with 75  $\mu$ L of luciferins (0.5-500  $\mu$ M) in PBS. Bioluminescence images were acquired on an IVIS Spectrum (PerkinElmer, USA) imaging system equipped with a cooled CCD camera with the following settings: open filter; exposure time: 30 sec; binning: medium 8; and  $f$ /stop: 1. The bioluminescence images were analyzed by Living Image 4.4 software (PerkinElmer, USA).

### 3.4.2. Synthetic procedures

All dimethylamino analogues except for **D-5**, and azetidinyl analogues (**A-1** and **A-2**) have been reported previously.<sup>15, 17</sup>

**4-(Azetidin-1-yl)benzaldehyde (8):** To a solution of 4-fluorobenzaldehyde (1.75 g, 14.1 mmol) in anhydrous DMSO (40 mL) was added K<sub>2</sub>CO<sub>3</sub> (5.82 g, 42.1 mmol, 3.0 eq.) followed by addition of azetidine hydrochloride (1.98 g, 21.2 mmol, 1.5 eq.) with stirring at 110 °C overnight. After cooling to room temperature, the reaction was diluted with water (200 mL) and extracted with EtOAc (3×100 mL). The combined organic layer was washed with brine, dried over Na<sub>2</sub>SO<sub>4</sub> and filtered. The filtrate was concentrated under reduced pressure. The crude material was purified by silica gel column chromatography (20% ethyl acetate/*n*-hexane) to afford title compound **8** (919 mg, 40%) as a pale yellow solid. <sup>1</sup>H-NMR (500 MHz, CDCl<sub>3</sub>) δ 9.72 (s, 1H), 7.71 (d, *J* = 8.5 Hz, 2H), 6.39 (d, *J* = 8.5 Hz, 2H), 4.04 (t, *J* = 7.3 Hz, 4H), 2.45 (quint, *J* = 7.3 Hz, 2H) ppm; <sup>13</sup>C-NMR (125 MHz, CDCl<sub>3</sub>) δ 190.5, 155.2, 132.1, 125.9, 109.9, 51.5, 16.6 ppm; HRMS (ESI+) calcd for C<sub>10</sub>H<sub>12</sub>NO [M+H]<sup>+</sup> : 162.0919, found: *m/z* 162.0942.

**Ethyl (E)-3-(4-(azetidin-1-yl)phenyl)acrylate (9):** To a solution of **8** (471 mg, 2.92 mmol) in benzene (10.0 mL) was added (carbethoxymethylene)triphenylphosphorane (1.23 g, 3.53 mmol, 1.2 eq.) and the mixture was stirred at reflux temperature for 3 h. After cooling to room temperature, the reaction was concentrated under reduced pressure. The crude material was purified by silica gel column chromatography (5-10% ethyl acetate/*n*-hexane) to afford title compound **9** (384 mg, 57%) as a light yellow crystalline solid. <sup>1</sup>H-NMR (400 MHz, CDCl<sub>3</sub>) δ 7.61 (d, *J* = 15.6 Hz, 1H), 7.39 (d, *J* = 8.8 Hz, 2H), 6.37 (d, *J* = 8.8 Hz, 2H), 6.21 (d, *J* = 15.6 Hz, 1H), 4.23 (q, *J* = 7.2 Hz, 2H), 3.94 (t, *J* = 7.4 Hz, 4H), 2.39 (quint, *J* = 7.2 Hz, 2H), 1.32 (t, *J* = 7.2 Hz, 3H) ppm; <sup>13</sup>C-NMR (100 MHz, CDCl<sub>3</sub>) δ 168.0, 153.2, 145.3, 129.7, 123.2, 112.9, 110.9, 60.2, 52.0, 16.8, 14.6 ppm; HRMS (ESI+) calcd for C<sub>14</sub>H<sub>18</sub>NO<sub>2</sub> [M+H]<sup>+</sup> : 232.1332, found: *m/z* 232.1334.

**Ethyl (2E,4E)-5-(4-(azetidin-1-yl)phenyl)penta-2,4-dienoate (10):** To a suspension of 60% NaH (205 mg, 5.13 mmol, 1.5 eq.) in anhydrous THF (10.0 mL) at 0 °C was added triethyl 4-phosphonocrotonate (1.28 g, 5.13 mmol, 1.5 eq.). Stirring for 20 min yielded an orange colored solution. To this solution was added **8** (551 mg, 3.42 mmol) in anhydrous THF (2.0 mL) dropwise over 5 min at 0 °C. The reaction was stirred for 3 h at room temperature, quenched with water (ca. 20 mL) and extracted with EtOAc (3×50 mL). The combined organic layer was washed with brine, dried over Na<sub>2</sub>SO<sub>4</sub> and filtered. The filtrate was concentrated under reduced pressure. The crude material was purified by silica gel column chromatography (11-32% ethyl acetate/*n*-hexane) to afford title compound **10** (560 mg, 64%) as a yellow solid. <sup>1</sup>H-NMR (500 MHz, CDCl<sub>3</sub>) δ 7.43 (dd, *J* = 15.5, 11.5 Hz, 1H), 7.32 (d, *J* = 8.5 Hz, 2H), 6.82 (d, *J* = 15.5 Hz, 1H), 6.68 (dd, *J* = 15.5, 11.0 Hz, 1H), 6.38 (d, *J* = 9.0 Hz, 2H), 5.87 (d, *J* = 15.0 Hz, 1H), 4.21 (q, *J* = 7.0 Hz,

2H), 3.93 (t,  $J = 7.3$  Hz, 4H), 2.39 (quint,  $J = 7.3$  Hz, 2H), 1.31 (t,  $J = 7.0$  Hz, 1H) ppm;  $^{13}\text{C}$ -NMR (125 MHz,  $\text{CDCl}_3$ )  $\delta$  167.7, 152.5, 145.8, 141.4, 128.6, 125.1, 122.1, 118.5, 111.2, 60.2, 52.2, 16.9, 14.5 ppm; HRMS (ESI<sup>+</sup>) calcd for  $\text{C}_{16}\text{H}_{20}\text{NO}_2$   $[\text{M}+\text{H}]^+$  : 258.1494, found:  $m/z$  258.1467.

**(E)-3-(4-(Azetidin-1-yl)phenyl)acrylic acid (11):** To a solution of **9** (330 mg, 1.43 mmol) in *iso*-PrOH (8.0 mL) was added 1 M NaOH aqueous solution (2.90 mL), and the mixture was stirred at reflux temperature for 8 h. After cooling to room temperature, *iso*-PrOH was removed under reduced pressure. The residue was acidified with 1 N HCl aqueous solution, and extracted with  $\text{CHCl}_3$  (3×50 mL). The combined organic layer was washed with brine, dried over  $\text{Na}_2\text{SO}_4$  and filtered. The filtrate was concentrated under reduced pressure to afford title compound **11** (279 mg, 96%) as a yellow solid. This crude product was used for the next reaction without further purification.  $^1\text{H}$ -NMR (400 MHz,  $\text{CD}_3\text{OD}$ )  $\delta$  7.57 (d,  $J = 16.0$  Hz, 1H), 7.41 (d,  $J = 8.8$  Hz, 2H), 6.42 (d,  $J = 8.8$  Hz, 2H), 6.20 (d,  $J = 15.6$  Hz, 1H), 3.93 (t,  $J = 7.4$  Hz, 4H), 2.40 (quint,  $J = 7.4$  Hz, 2H) ppm; HRMS (ESI<sup>+</sup>) calcd for  $\text{C}_{12}\text{H}_{14}\text{NO}_2$   $[\text{M}+\text{H}]^+$  : 204.1025, found:  $m/z$  204.1026.

**(2E,4E)-5-(4-(azetidin-1-yl)phenyl)penta-2,4-dienoic acid (12):** **12** was synthesized in the same manner as described for the preparation of **11**; yield 86%, a yellow solid.  $^1\text{H}$ -NMR (500 MHz,  $\text{DMSO-d}_6$ )  $\delta$  7.37 (d,  $J = 8.0$  Hz, 2H), 7.28 (dd,  $J = 15.0, 11.0$  Hz, 1H), 6.90 (d,  $J = 15.5$  Hz, 1H), 6.82 (dd,  $J = 15.5, 11.0$  Hz, 1H), 6.38 (d,  $J = 8.0$  Hz, 2H), 5.85 (d,  $J = 15.0$  Hz, 1H), 3.85 (t,  $J = 7.0$  Hz, 4H), 2.32 (quint,  $J = 7.0$  Hz, 2H) ppm;  $^{13}\text{C}$ -NMR (125 MHz,  $\text{DMSO-d}_6$ )  $\delta$  167.9, 152.2, 145.2, 140.8, 130.2, 128.4, 124.5, 121.8, 110.9, 51.7, 16.2 ppm; HRMS (ESI<sup>+</sup>) calcd for  $\text{C}_{14}\text{H}_{16}\text{NO}_2$   $[\text{M}+\text{H}]^+$  : 230.1181, found:  $m/z$  230.1171.

**Methyl (E)-N-(3-(4-(azetidin-1-yl)phenyl)acryloyl)-S-trityl-D-cysteinate (13):** To a solution of **11** (121 mg, 0.595 mmol) and H-D-Cys-S(Trt)-OMe hydrochloric acid (281 mg, 0.744 mmol, 1.3 eq.) in anhydrous DMF (2.0 mL) were added DMT-MM (198 mg, 0.716 mmol, 1.2 eq.) and TEA (100  $\mu\text{L}$ , 0.717 mmol, 1.2 eq.), and the mixture was stirred at 0 °C for 4.5 h. The reaction was diluted with water (ca. 20 mL) at 0 °C, and then extracted with EtOAc (3×50 mL). The combined organic layer was washed with brine, dried over  $\text{Na}_2\text{SO}_4$  and filtered. The crude material was purified by silica gel column chromatography (25-40% ethyl acetate/*n*-hexane) to afford title compound **13** (322 mg, 96%) as a yellow solid.  $^1\text{H}$ -NMR (500 MHz,  $\text{CDCl}_3$ )  $\delta$  7.39-7.21 (m, 18H), 6.39 (d,  $J = 8.5$ , 2H), 6.14 (d,  $J = 15.5$  Hz, 1H), 4.79-4.76 (m, 1H), 3.95 (t,  $J = 7.3$  Hz, 4H), 3.73 (s, 3H), 2.76-2.68 (m, 2H), 2.40 (quint,  $J = 7.3$  Hz, 2H) ppm;  $^{13}\text{C}$ -NMR (125 MHz,  $\text{CDCl}_3$ )  $\delta$  171.3, 166.2, 153.0, 144.5, 142.5, 129.6, 129.4, 128.1, 127.0, 123.5, 114.9, 111.0, 67.0, 52.8, 52.1, 51.2, 34.3, 16.8 ppm; HRMS (ESI<sup>+</sup>) calcd for  $\text{C}_{14}\text{H}_{18}\text{NO}_2$   $[\text{M}+\text{H}]^+$  : 563.2363, found:  $m/z$  563.2354.

**Methyl *N*-((2*E*,4*E*)-5-(4-(azetidin-1-yl)phenyl)penta-2,4-dienoyl)-*S*-trityl-*D*-cysteinate (**14**):** **14** was synthesized in the same manner as described for the preparation of **13**; yield 81%, a yellow solid. <sup>1</sup>H-NMR (500 MHz, CDCl<sub>3</sub>) δ 7.39-7.20 (m, 17H), 6.80 (d, *J* = 15.5 Hz, 1H), 6.67 (dd, *J* = 15.5, 11.0 Hz, 1H), 6.39 (d, *J* = 8.5 Hz, 2H), 5.96 (d, *J* = 7.5 Hz, 1H), 5.83 (d, *J* = 15.0 Hz, 1H), 4.77-4.73 (m, 1H), 3.93 (t, *J* = 7.3 Hz, 4H), 3.72 (s, 3H), 2.73-2.66 (m, 2H), 2.39 (quint, *J* = 7.3 Hz, 2H) ppm; <sup>13</sup>C-NMR (125 MHz, CDCl<sub>3</sub>) δ 171.3, 166.0, 152.4, 144.5, 143.0, 140.8, 129.6, 128.5, 128.1, 127.0, 125.4, 122.1, 120.4, 111.2, 67.0, 66.8, 52.8, 52.2, 51.2, 16.9 ppm; HRMS (ESI+) calcd for C<sub>37</sub>H<sub>37</sub>N<sub>2</sub>O<sub>3</sub>S [M+H]<sup>+</sup> : 589.2525, found: *m/z* 589.2497.

**Methyl (*S*,*E*)-2-(4-(azetidin-1-yl)styryl)-4,5-dihydrothiazole-4-carboxylate (**A-2-OMe**):** To a solution of triphenylphosphine oxide (350 mg, 1.26 mmol, 3.0 eq.) in anhydrous CH<sub>2</sub>Cl<sub>2</sub> (5.0 mL) was added trifluoromethane sulfonic anhydride (99.0 μL, 0.604 mmol, 1.5 eq.) slowly dropwise at 0 °C. After stirring for 30 min, this solution was added to a solution of **13** (225 mg, 0.401 mmol, 1.0 eq.) in anhydrous CH<sub>2</sub>Cl<sub>2</sub> (4.0 mL) dropwise carefully at 0 °C, at which point the reaction solution turned deep red in color, and the reaction mixture was stirred for 2 h. The reaction was quenched with saturated NaHCO<sub>3</sub> solution and extracted with CH<sub>2</sub>Cl<sub>2</sub> (100 mL). The combined organic layer was washed with brine, dried over Na<sub>2</sub>SO<sub>4</sub> and filtered. The filtrate was concentrated under reduced pressure. The crude material was purified by silica gel column chromatography (30% ethyl acetate/*n*-hexane) to afford the **A-2-OMe** (40.1 mg, 33%) as a yellow solid. <sup>1</sup>H-NMR (500 MHz, CDCl<sub>3</sub>) δ 7.35 (d, *J* = 8.5, 2H), 7.05 (d, *J* = 16.0 Hz, 1H), 6.90 (d, *J* = 16.0 Hz, 1H), 6.38 (d, *J* = 9.0 Hz, 2H), 5.17 (t, *J* = 9.3 Hz, 1H), 3.94 (t, *J* = 7.3 Hz, 4H), 3.83 (s, 3H), 3.62-3.52 (m, 2H), 2.39 (quint, *J* = 7.3 Hz, 2H) ppm; <sup>13</sup>C-NMR (125 MHz, CDCl<sub>3</sub>) δ 171.7, 170.7, 152.9, 143.1, 129.1, 123.9, 117.6, 111.1, 77.9, 52.9, 52.1, 34.6, 16.8 ppm; HRMS (ESI<sup>+</sup>) calcd for C<sub>16</sub>H<sub>19</sub>N<sub>2</sub>O<sub>2</sub>S [M+H]<sup>+</sup> : 303.1167, found: *m/z* 303.1162.

**Methyl (*S*)-2-((1*E*,3*E*)-4-(4-(azetidin-1-yl)phenyl)buta-1,3-dien-1-yl)-4,5-dihydrothiazole-4-carboxylate (**A-3-OMe**):** **A-3-OMe** was synthesized in the same manner as described for the preparation of **A-2-OMe**; yield 74%, a yellow solid. <sup>1</sup>H-NMR (500 MHz, CDCl<sub>3</sub>) δ 7.32 (d, *J* = 8.5 Hz, 2H), 6.92 (dd, *J* = 15.5, 10.0 Hz, 1H), 6.75 (d, *J* = 15.5 Hz, 1H), 6.69 (dd, *J* = 15.5, 10.0 Hz, 1H), 6.53 (d, *J* = 15.5 Hz, 1H), 6.37 (d, *J* = 8.5 Hz, 2H), 5.16 (t, *J* = 9.0 Hz, 1H), 3.92 (t, *J* = 7.3 Hz, 4H), 3.81 (s, 3H), 3.60-3.50 (m, 2H), 2.38 (quint, *J* = 7.3 Hz, 2H) ppm; <sup>13</sup>C-NMR (125 MHz, CDCl<sub>3</sub>) δ 171.6, 170.3, 152.4, 143.8, 139.7, 130.5, 128.5, 125.3, 122.9, 111.2, 78.0, 52.9, 52.2, 34.7, 16.9 ppm; HRMS (ESI+) calcd for C<sub>18</sub>H<sub>21</sub>N<sub>2</sub>O<sub>2</sub>S [M+H]<sup>+</sup> : 329.1324, found: *m/z* 329.1297.

**Methyl 6-(azetidin-1-yl)-2-naphthoate (**16**):** A round bottom flask was charged with methyl-6-bromo-2-naphthoate (780 mg, 2.94 mmol), azetidine hydrochloride (331 mg, 3.54 mmol, 1.2 eq.), tris(dibenzylideneacetone)palladium (135 mg, 0.147 mmol), xantphos (170 mg, 0.294 mmol), Cs<sub>2</sub>CO<sub>3</sub> (1.91 g, 5.86 mmol, 2.0 eq.) and toluene (8.0 mL) under argon. The resulting solution was heated at 100 °C with rapid stirring for 24 h. The reaction mixture was allowed to cool to room temperature and then diluted with water (10 mL) and extracted with ethyl acetate (3×50 mL). The combined organic layer was washed with brine, dried over Na<sub>2</sub>SO<sub>4</sub> and filtered. The filtrate was concentrated under reduced pressure. The crude

material was purified by silica gel column chromatography (0-10% ethyl acetate/*n*-hexane) to afford title compound **16** (193 mg, 27%) as a yellow solid.  $^1\text{H-NMR}$  (400 MHz,  $\text{CDCl}_3$ )  $\delta$  8.44 (s, 1H), 7.93 (dd,  $J = 8.4, 1.6$  Hz, 1H), 7.76 (d,  $J = 8.8$  Hz, 1H), 7.60 (d,  $J = 8.4$  Hz, 1H), 6.80 (dd,  $J = 8.8, 2.4$  Hz, 1H), 6.61 (d,  $J = 2.0$  Hz, 1H), 4.02 (t,  $J = 7.4$  Hz, 4H), 3.94 (s, 3H), 2.43 (quint,  $J = 7.3$  Hz, 2H) ppm;  $^{13}\text{C-NMR}$  (100 MHz,  $\text{CDCl}_3$ )  $\delta$  167.8, 151.4, 137.4, 131.4, 130.6, 126.0, 125.9, 125.8, 123.2, 114.9, 104.1, 52.2, 52.1, 16.9 ppm; HRMS (ESI+) calcd for  $\text{C}_{15}\text{H}_{16}\text{NO}_2$   $[\text{M}+\text{H}]^+$  : 242.1181, found:  $m/z$  242.1161.

**6-(Azetidin-1-yl)-2-naphthoic acid (17):** **17** was synthesized in the same manner as described for the preparation of **11**; yield quantitative, a yellow solid. This crude product was used for next reaction directly.  $^1\text{H-NMR}$  (400 MHz,  $\text{CDCl}_3 + \text{CD}_3\text{OD}$ )  $\delta$  8.43 (s, 1H), 7.91 (dd,  $J = 8.4, 1.6$  Hz, 1H), 7.78 (d,  $J = 8.8$  Hz, 1H), 7.62 (d,  $J = 8.8$  Hz, 1H), 6.85 (dd,  $J = 8.8, 2.0$  Hz, 1H), 6.67 (d,  $J = 2.0$  Hz, 1H), 4.04 (t,  $J = 7.3$  Hz, 4H), 3.94 (s, 3H), 2.46 (quint,  $J = 7.3$  Hz, 2H) ppm. HRMS (ESI+) calcd for  $\text{C}_{14}\text{H}_{14}\text{NO}_2$   $[\text{M}+\text{H}]^+$  : 228.1025, found:  $m/z$  228.1035.

**Methyl N-(6-(azetidin-1-yl)-2-naphthoyl)-S-trityl-D-cysteinate (18):** **18** was synthesized in the same manner as described for the preparation of **13**; yield 90%, a yellow solid.  $^1\text{H-NMR}$  (500 MHz,  $\text{CDCl}_3$ )  $\delta$  8.17 (s, 1H), 7.80 (d,  $J = 8.5$  Hz, 1H), 7.73 (d,  $J = 9.0$  Hz, 1H), 7.67 (d,  $J = 9.0$  Hz, 1H), 7.44-7.38 (m, 5H), 7.29-7.16 (m, 9H), 6.86 (dd,  $J = 8.5, 1.5$  Hz, 1H), 6.79 (d,  $J = 7.5$  Hz, 1H), 6.67 (s, 1H), 4.95-4.91 (m, 1H), 4.06 (t,  $J = 7.3$  Hz, 4H), 3.79 (s, 3H), 2.84 (dd,  $J = 12.5, 5.5$  Hz, 1H), 2.79 (dd,  $J = 12.5, 5.0$  Hz, 1H), 2.47 (quint,  $J = 7.1$  Hz, 2H) ppm;  $^{13}\text{C-NMR}$  (125 MHz,  $\text{CDCl}_3$ )  $\delta$  171.4, 167.2, 151.1, 144.4, 136.8, 130.3, 129.6, 128.2, 128.1, 127.0, 126.7, 126.1, 126.0, 124.4, 115.2, 104.2, 67.1, 52.9, 52.3, 51.5, 34.4, 16.9, ppm. HRMS (ESI+) calcd for  $\text{C}_{37}\text{H}_{35}\text{N}_2\text{O}_2\text{S}$   $[\text{M}+\text{H}]^+$  : 587.2368, found:  $m/z$  587.2357.

**Methyl (S)-2-(6-(azetidin-1-yl)naphthalen-2-yl)-4,5-dihydrothiazole-4-carboxylate (A-4-OMe):** **A-4-OMe** was synthesized in the same manner as described for the preparation of **A-2-OMe**; yield 46%, an orange solid.  $^1\text{H-NMR}$  (500 MHz,  $\text{CDCl}_3$ )  $\delta$  8.14 (s, 1H), 7.88 (dd,  $J = 8.5, 1.0$  Hz, 1H), 7.73 (d,  $J = 8.5$  Hz, 1H), 7.59 (d,  $J = 8.5$  Hz, 1H), 6.79 (dd,  $J = 8.5, 1.5$  Hz, 1H), 6.61 (d,  $J = 1.5$  Hz, 1H), 5.31 (t,  $J = 9.0$  Hz, 1H), 4.01 (t,  $J = 7.3$  Hz, 4H), 3.84 (s, 3H), 3.74-3.62 (m, 2H), 2.42 (quint,  $J = 7.3$  Hz, 2H) ppm;  $^{13}\text{C-NMR}$  (125 MHz,  $\text{CDCl}_3$ )  $\delta$  171.8, 171.2, 151.1, 136.8, 130.2, 130.1, 126.2, 126.1, 126.0, 125.6, 115.0, 104.3, 78.5, 52.9, 52.3, 35.4, 16.9 ppm; HRMS (ESI+) calcd for  $\text{C}_{18}\text{H}_{19}\text{N}_2\text{O}_2\text{S}$   $[\text{M}+\text{H}]^+$  : 327.1167, found:  $m/z$  327.1168.

**(6-(Azetidin-1-yl)naphthalen-2-yl)methanol (19):** To a solution of  $\text{LiAlH}_4$  (37.1 mg, 0.977 mmol, 1.5 eq.) in anhydrous THF (4.0 mL) was added a solution of **16** (157 mg, 0.651 mmol) in anhydrous THF (10.0 mL) dropwise carefully at  $-78$  °C, and the mixture was stirred at room temperature overnight. The reaction was diluted with water (40 mL), 10% NaOH (40 mL) and water (120 mL) at  $0$  °C, and then a gray precipitate was formed. After the filtration through celite pad, the filtrate was concentrated under reduced pressure. The crude material was purified by silica gel column chromatography (20-50% ethyl acetate/*n*-hexane) to afford title compound **19** (123 mg, 89%) as a beige solid.  $^1\text{H-NMR}$  (500 MHz,  $\text{CDCl}_3$ )  $\delta$  7.67 (m, 3H), 7.37 (dd,  $J =$

8.5, 1.5 Hz, 1H), 6.80 (dd,  $J = 8.5, 2.5$  Hz, 1H), 6.66 (d,  $J = 2.0$  Hz, 1H), 4.76 (s, 2H), 3.98 (t,  $J = 7.0$  Hz, 4H), 2.41 (quint,  $J = 7.0$  Hz, 2H), 1.73 (br, 1H) ppm;  $^{13}\text{C}$ -NMR (125 MHz,  $\text{CDCl}_3$ )  $\delta$  150.2, 134.5, 134.4, 128.9, 127.1, 126.5, 126.1, 126.0, 114.9, 105.0, 65.9, 52.6, 17.1 ppm; HRMS (ESI+) calcd for  $\text{C}_{14}\text{H}_{16}\text{NO}$   $[\text{M}+\text{H}]^+$  : 214.1232, found:  $m/z$  214.1208.

**6-(Azetidin-1-yl)-2-naphthaldehyde (20):** To a solution of **19** (124 mg, 0.579 mmol), NMO (102 mg, 0.869 mmol, 1.5 eq.) and activated molecular sieves 4A (MS4A) in anhydrous  $\text{CH}_2\text{Cl}_2$  (5.0 mL) was added TPAP (10.2 mg, 29.0  $\mu\text{mol}$ , 5 mol%), and the mixture was stirred at room temperature 3.5 h. After the filtration through celite pad to remove MS4A, the filtrate was concentrated under reduced pressure. The crude material was purified by silica gel column chromatography (10-20% ethyl acetate/*n*-hexane) to afford title compound **20** (84.1 mg, 69%) as a yellow solid.  $^1\text{H}$ -NMR (500 MHz,  $\text{CDCl}_3$ )  $\delta$  10.00 (s, 1H), 8.14 (s, 1H), 7.82 (dd,  $J = 8.5, 1.5$  Hz, 1H), 7.79 (d,  $J = 9.0$  Hz, 1H), 7.63 (d,  $J = 8.0$  Hz, 1H), 6.81 (dd,  $J = 9.0, 2.5$  Hz, 1H), 6.60 (d,  $J = 2.0$  Hz, 1H), 4.05 (t,  $J = 7.3$  Hz, 4H), 2.45 (quint,  $J = 7.3$  Hz, 2H) ppm;  $^{13}\text{C}$ -NMR (125 MHz,  $\text{CDCl}_3$ )  $\delta$  192.0, 166.0, 151.9, 138.5, 135.2, 131.0, 126.7, 125.7, 123.8, 115.0, 104.2, 52.1, 16.8 ppm; HRMS (ESI+) calcd for  $\text{C}_{14}\text{H}_{14}\text{NO}$   $[\text{M}+\text{H}]^+$  : 212.1075, found:  $m/z$  212.1081.

**Ethyl (E)-3-(6-(azetidin-1-yl)naphthalen-2-yl)acrylate (21):** **21** was synthesized in the same manner as described for the preparation of **9**; yield 84%, a yellow solid.  $^1\text{H}$ -NMR (500 MHz,  $\text{CDCl}_3$ )  $\delta$  7.79 (d,  $J = 15.5$  Hz, 1H), 7.76 (s, 1H), 7.67 (d,  $J = 9.0$  Hz, 1H), 7.58 (d,  $J = 8.5$  Hz, 1H), 7.55 (dd,  $J = 8.5, 1.5$  Hz, 1H), 6.77 (dd,  $J = 9.0, 2.0$  Hz, 1H), 6.60 (d,  $J = 2.0$  Hz, 1H), 6.44 (d,  $J = 16.0$  Hz, 1H), 4.27 (q,  $J = 7.2$  Hz, 2H), 4.00 (t,  $J = 7.3$  Hz, 4H), 2.42 (quint,  $J = 7.3$  Hz, 2H), 1.34 (t,  $J = 7.3$  Hz, 3H) ppm;  $^{13}\text{C}$ -NMR (125 MHz,  $\text{CDCl}_3$ )  $\delta$  167.7, 150.9, 145.4, 136.0, 130.5, 129.8, 128.2, 126.7, 126.6, 124.2, 115.9, 114.9, 104.6, 60.4, 52.3, 16.9, 14.5 ppm; HRMS (ESI+) calcd for  $\text{C}_{18}\text{H}_{20}\text{NO}_2$   $[\text{M}+\text{H}]^+$  : 282.1494, found:  $m/z$  282.1474.

**(E)-3-(6-(Azetidin-1-yl)naphthalen-2-yl)acrylic acid (22):** **22** was synthesized in the same manner as described for the preparation of **11**; yield quantitative, a yellow solid. This crude product was used for next reaction directly. HRMS (ESI+) calcd for  $\text{C}_{16}\text{H}_{16}\text{NO}_2$   $[\text{M}+\text{H}]^+$  : 254.1181, found:  $m/z$  254.1174.

**Methyl (E)-N-(3-(6-(azetidin-1-yl)naphthalen-2-yl)acryloyl)-S-trityl-D-cysteinate (23):** **23** was synthesized in the same manner as described for the preparation of **13**; yield 90%, a yellow solid.  $^1\text{H}$ -NMR (500 MHz,  $\text{CDCl}_3$ )  $\delta$  7.73 (s, 1H), 7.71-7.67 (m, 2H), 7.59 (d,  $J = 8.5$  Hz, 1H), 7.54 (dd,  $J = 8.5, 1.5$  Hz, 1H), 7.43-7.37 (m, 7H), 7.29-7.19 (m, 7H), 6.78 (dd,  $J = 8.5, 2.0$  Hz, 1H), 6.61 (d,  $J = 2.0$  Hz, 1H), 6.36 (d,  $J = 15.5$  Hz, 1H), 6.11 (d,  $J = 8.0$  Hz, 1H), 4.81-4.78 (m, 1H), 4.00 (t,  $J = 7.5$  Hz, 4H), 3.73 (s, 3H), 2.77 (dd,  $J = 12.5, 5.0$  Hz, 1H), 2.72 (dd,  $J = 12.5, 5.0$  Hz, 1H), 2.42 (quint,  $J = 7.3$  Hz, 2H) ppm;  $^{13}\text{C}$ -NMR (125 MHz,  $\text{CDCl}_3$ )  $\delta$  171.2, 165.8, 150.8, 144.4, 142.6, 135.8, 130.1, 129.8, 129.7, 129.6, 128.1, 128.0, 127.0, 126.6, 124.2, 117.8, 114.9, 104.7, 67.1, 52.8, 52.4, 51.3, 34.2 17.0 ppm; HRMS (ESI+) calcd for  $\text{C}_{39}\text{H}_{37}\text{N}_2\text{O}_3\text{S}$   $[\text{M}+\text{H}]^+$  : 613.2525, found:  $m/z$  613.2512.

**Methyl (S,E)-2-(2-(6-(azetidin-1-yl)naphthalen-2-yl)vinyl)-4,5-dihydrothiazole-4-carboxylate (A-5-OMe):** **A-5-OMe** was synthesized in the same manner as described for the preparation of **A-2-OMe**; yield 33%, a yellow solid. <sup>1</sup>H-NMR (500 MHz, CDCl<sub>3</sub>) δ 7.72 (s, 1H), 7.67 (d, *J* = 8.5 Hz, 1H), 7.58 (d, *J* = 8.5 Hz, 1H), 7.54 (dd, *J* = 8.5, 1.5 Hz, 1H), 7.23 (d, *J* = 15.0 Hz, 1H), 7.11 (d, *J* = 16.0 Hz, 1H), 6.78 (dd, *J* = 9.0, 2.0 Hz, 1H), 6.61 (d, *J* = 2.0 Hz, 1H), 5.21 (t, *J* = 9.0 Hz, 1H), 4.01 (t, *J* = 7.3 Hz, 4H), 3.84 (s, 3H), 3.64 (dd, *J* = 11.0, 9.0 Hz, 1H), 3.57 (dd, *J* = 11.0, 9.0 Hz, 1H), 2.43 (quint, *J* = 7.3 Hz, 2H) ppm; <sup>13</sup>C-NMR (125 MHz, CDCl<sub>3</sub>) δ 171.6, 170.6, 150.8, 143.2, 135.7, 129.7, 129.6, 128.8, 126.8, 126.7, 123.9, 120.3, 115.0, 104.7, 78.0, 53.0, 52.4, 34.7, 17.0 ppm; HRMS (ESI<sup>+</sup>) calcd for C<sub>20</sub>H<sub>21</sub>N<sub>2</sub>O<sub>2</sub>S [M+H]<sup>+</sup> : 353.1324, found: *m/z* 353.1336.

**(S,E)-2-(4-(Azetidin-1-yl)styryl)-4,5-dihydrothiazole-4-carboxylic acid (A-2):** To a solution of **A-2-OMe** (40.1 mg, 0.132 mmol) in THF (5.0 mL) were added 0.1 M sodium phosphate buffer (2.0 mL, pH 6.8) and lipase acrylic resin (8.40 mg), and the clear yellow mixture was stirred at 37 °C for 44 h. After filtration through celite pad, the filtrate was concentrated under reduced pressure. The residue was purified by flash column chromatography (RP: 10-90% CH<sub>3</sub>CN/H<sub>2</sub>O) to afford the **A-2** (19.4 mg, 51%) as an orange solid. This compound has been already synthesized through a different synthetic route.<sup>17</sup> <sup>1</sup>H-NMR (500 MHz, CD<sub>3</sub>OD) δ 7.39 (d, *J* = 8.5, 2H), 7.07 (d, *J* = 16.0 Hz, 1H), 6.88 (d, *J* = 16.0 Hz, 1H), 6.42 (d, *J* = 8.5 Hz, 2H), 4.97 (t, *J* = 9.3 Hz, 1H), 3.92 (t, *J* = 7.3 Hz, 4H), 3.61-3.47 (m, 2H), 2.39 (quint, *J* = 7.3 Hz, 2H) ppm; <sup>13</sup>C-NMR (125 MHz, CD<sub>3</sub>OD) δ 154.6, 144.3, 130.1, 125.3, 117.9, 113.2, 112.2, 81.2, 53.0, 40.3, 36.5, 17.6 ppm; HRMS (ESI<sup>+</sup>) calcd for C<sub>15</sub>H<sub>17</sub>N<sub>2</sub>O<sub>2</sub>S [M+H]<sup>+</sup> : 289.1011, found: *m/z* 289.1103.

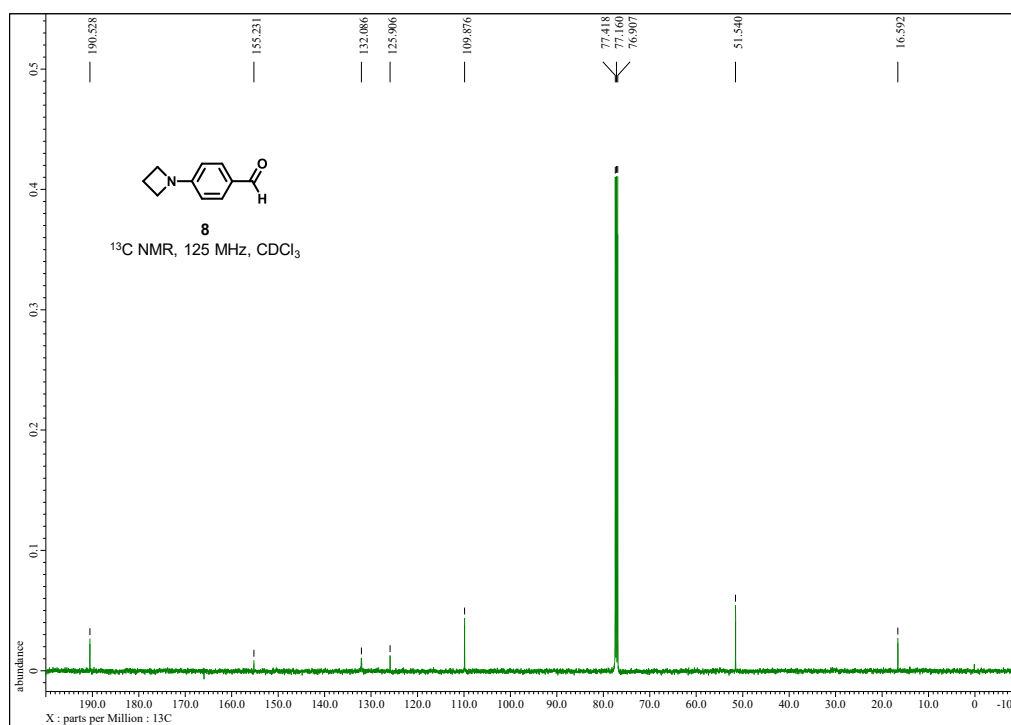
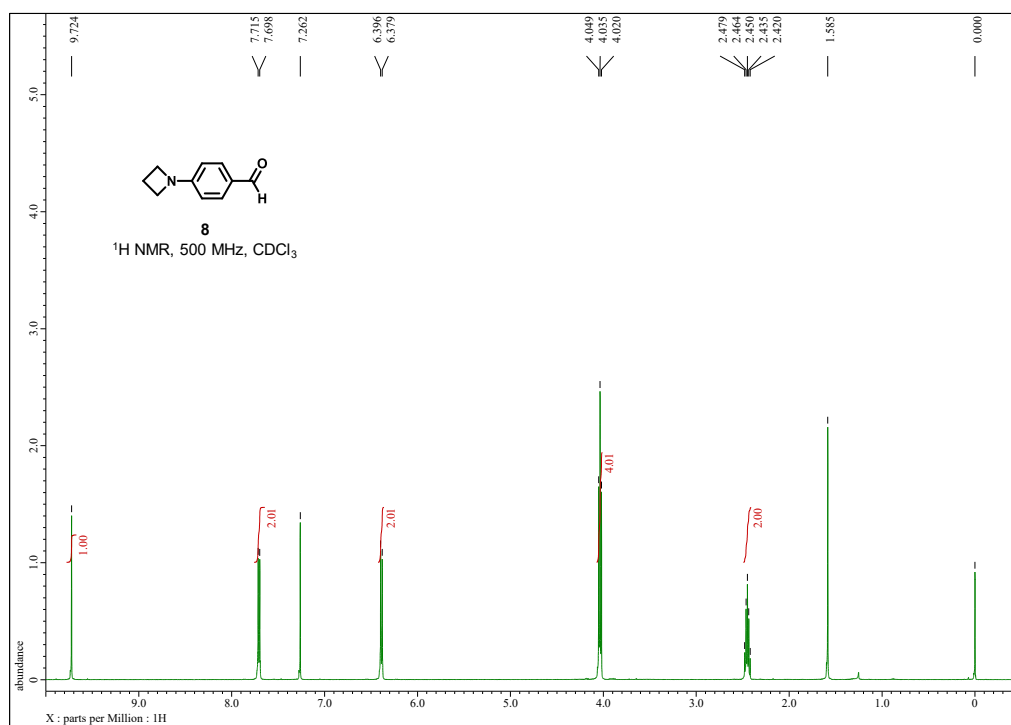
**(S)-2-((1E,3E)-4-(4-(Azetidin-1-yl)phenyl)buta-1,3-dien-1-yl)-4,5-dihydrothiazole-4-carboxylic acid (A-3):** **A-3** was synthesized in the same manner as described for the preparation of **A-2**; yield 82%, a red solid. <sup>1</sup>H-NMR (500 MHz, CD<sub>3</sub>OD + Acetone-d<sub>6</sub>) δ 7.38 (d, *J* = 8.5 Hz, 2H), 7.14 (dd, *J* = 15.0, 10.0 Hz, 1H), 6.91 (d, *J* = 15.5 Hz, 1H), 6.83 (dd, *J* = 15.5, 10.0 Hz, 1H), 6.53 (d, *J* = 15.0 Hz, 1H), 6.41 (d, *J* = 8.5 Hz, 2H), 5.08 (t, *J* = 8.8 Hz, 1H), 3.92 (t, *J* = 7.3 Hz, 4H), 3.70-3.60 (m, 2H), 2.39 (quint, *J* = 7.3 Hz, 2H) ppm; <sup>13</sup>C-NMR (125 MHz, CD<sub>3</sub>OD + Acetone-d<sub>6</sub>) δ 175.3, 174.5, 154.3, 147.9, 143.7, 130.0, 126.5, 123.4, 120.7, 112.2, 76.9, 53.1, 35.6, 17.6 ppm; HRMS (ESI<sup>+</sup>) calcd for C<sub>17</sub>H<sub>19</sub>N<sub>2</sub>O<sub>2</sub>S [M+H]<sup>+</sup> : 315.1167, found: *m/z* 315.1141.

**(S)-2-(6-(Azetidin-1-yl)naphthalen-2-yl)-4,5-dihydrothiazole-4-carboxylic acid (A-4):** **A-4** was synthesized in the same manner as described for the preparation of **A-2**; yield 80%, a yellow solid. <sup>1</sup>H-NMR (500 MHz, CD<sub>3</sub>OD) δ 8.02 (s, 1H), 7.78 (dd, *J* = 8.5, 1.0 Hz, 1H), 7.64 (d, *J* = 9.0 Hz, 1H), 7.50 (d, *J* = 8.5 Hz, 1H), 6.74 (dd, *J* = 8.5, 1.5 Hz, 1H), 6.57 (d, *J* = 1.5 Hz, 1H), 5.00 (t, *J* = 9.3 Hz, 1H), 3.88 (t, *J* = 7.3 Hz, 4H), 3.61-3.48 (m, 2H), 2.31 (quint, *J* = 7.3 Hz, 2H) ppm; <sup>13</sup>C-NMR (125 MHz, CD<sub>3</sub>OD) δ 178.6, 171.1, 152.7, 137.9, 131.0, 130.7, 128.1, 127.6, 126.9, 126.3, 116.1, 105.5, 83.1, 53.3, 37.4, 17.7 ppm; HRMS (ESI<sup>+</sup>) calcd for C<sub>17</sub>H<sub>17</sub>N<sub>2</sub>O<sub>2</sub>S [M+H]<sup>+</sup> : 313.1011, found: *m/z* 313.1009.

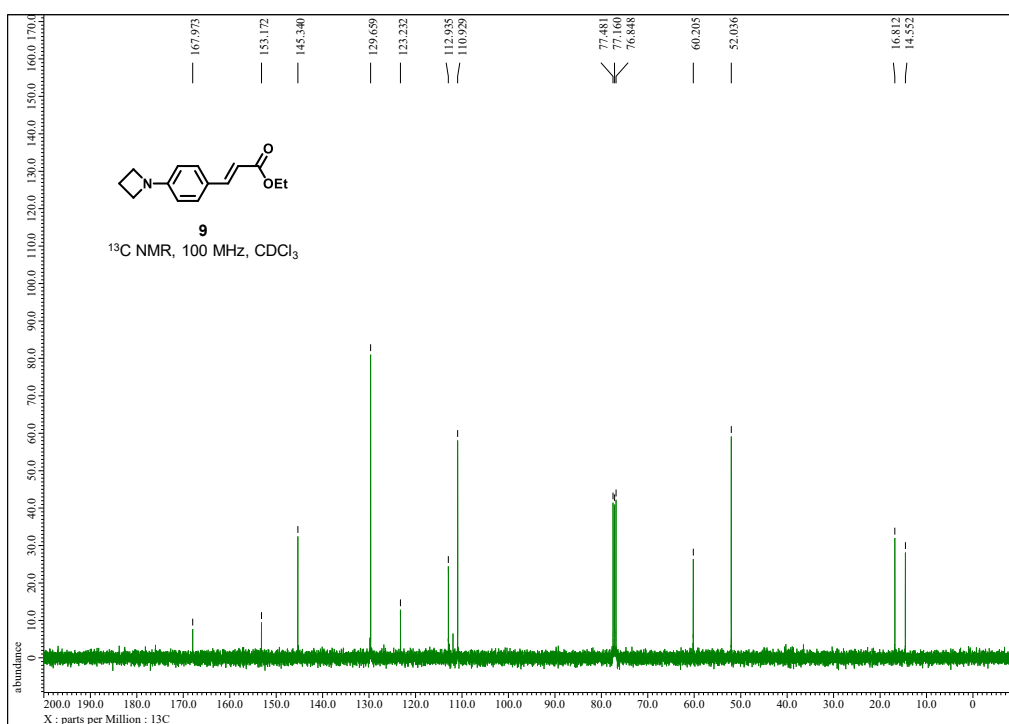
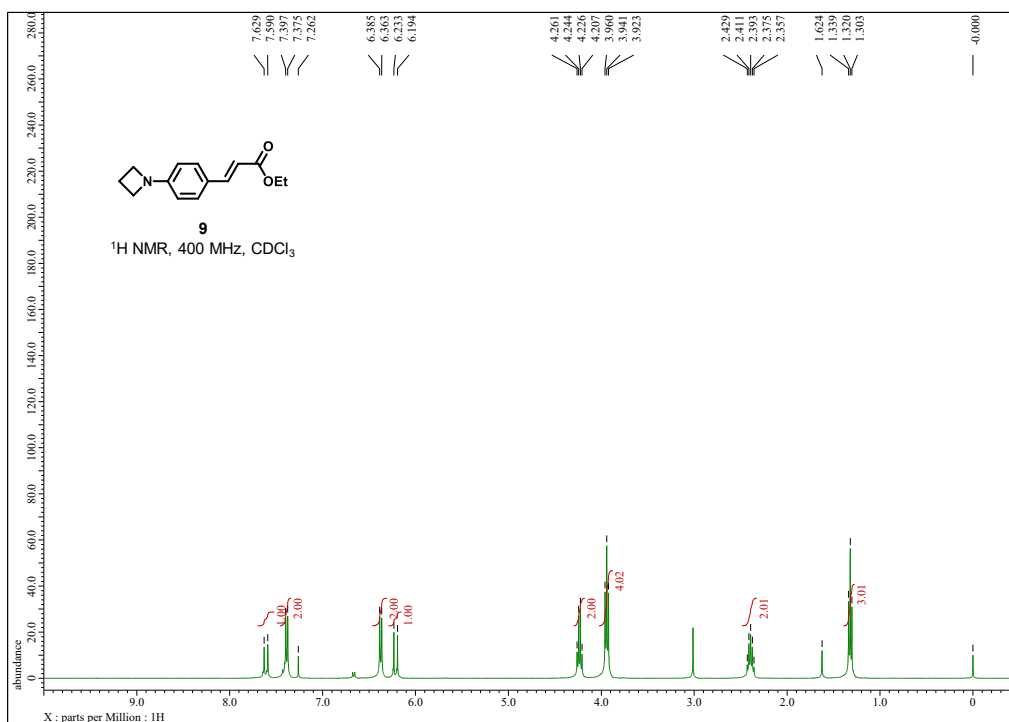
**(S,E)-2-(2-(6-(Azetidin-1-yl)naphthalen-2-yl)vinyl)-4,5-dihydrothiazole-4-carboxylic acid (A-5):** **A-5** was synthesized in the same manner as described for the preparation of **A-2**; yield 53%, a yellow solid.  $^1\text{H-NMR}$  (500 MHz,  $\text{CD}_3\text{OD}$ )  $\delta$  7.69 (s, 1H), 7.61 (d,  $J = 8.5$  Hz, 1H), 7.51 (br, 2H), 7.16 (d,  $J = 16.0$  Hz, 1H), 7.02 (d,  $J = 15.5$  Hz, 1H), 6.73 (dd,  $J = 8.5, 2.0$  Hz, 1H), 6.57 (d,  $J = 2.0$  Hz, 1H), 4.91 (t,  $J = 9.5$  Hz, 1H), 3.89 (t,  $J = 7.5$  Hz, 4H), 3.54-3.50 (m, 1H), 3.45-3.41 (m, 1H), 2.33 (quint,  $J = 7.3$  Hz, 2H) ppm;  $^{13}\text{C-NMR}$  (125 MHz,  $\text{CD}_3\text{OD}$ )  $\delta$  178.7, 171.9, 149.6, 143.8, 136.5, 130.7, 130.4, 130.2, 128.6, 127.8, 124.9, 121.1, 116.6, 107.2, 81.2, 53.9, 36.7, 17.7 ppm; HRMS (ESI $^+$ ) calcd for  $\text{C}_{19}\text{H}_{19}\text{N}_2\text{O}_2\text{S}$   $[\text{M}+\text{H}]^+$  : 339.1167, found:  $m/z$  339.1173.

### 3.4.3. NMR spectra

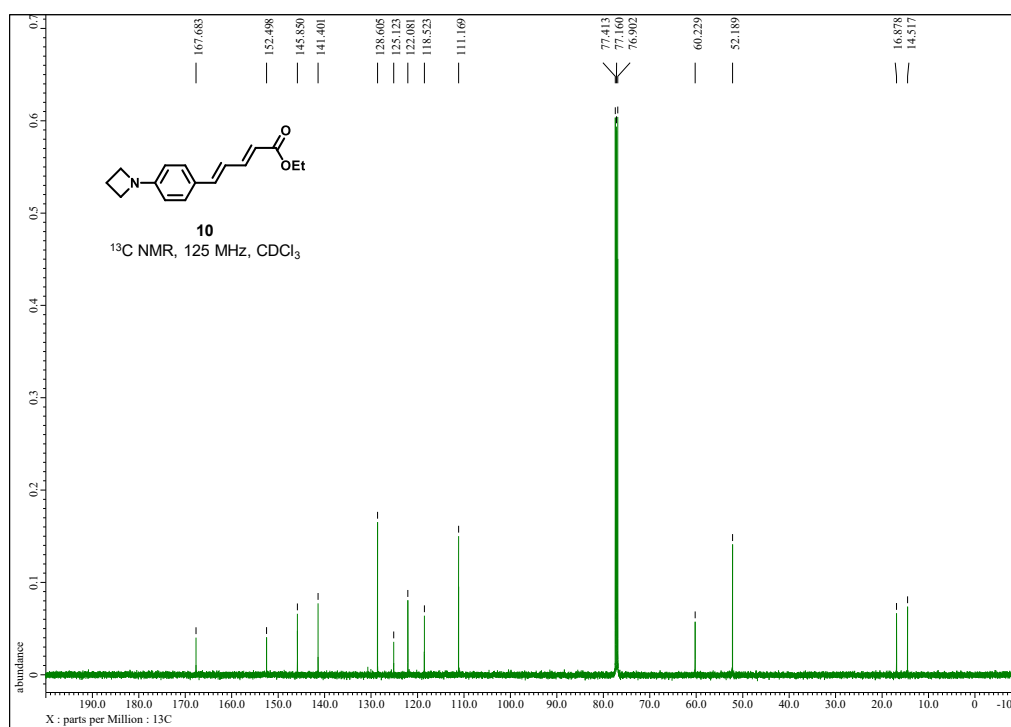
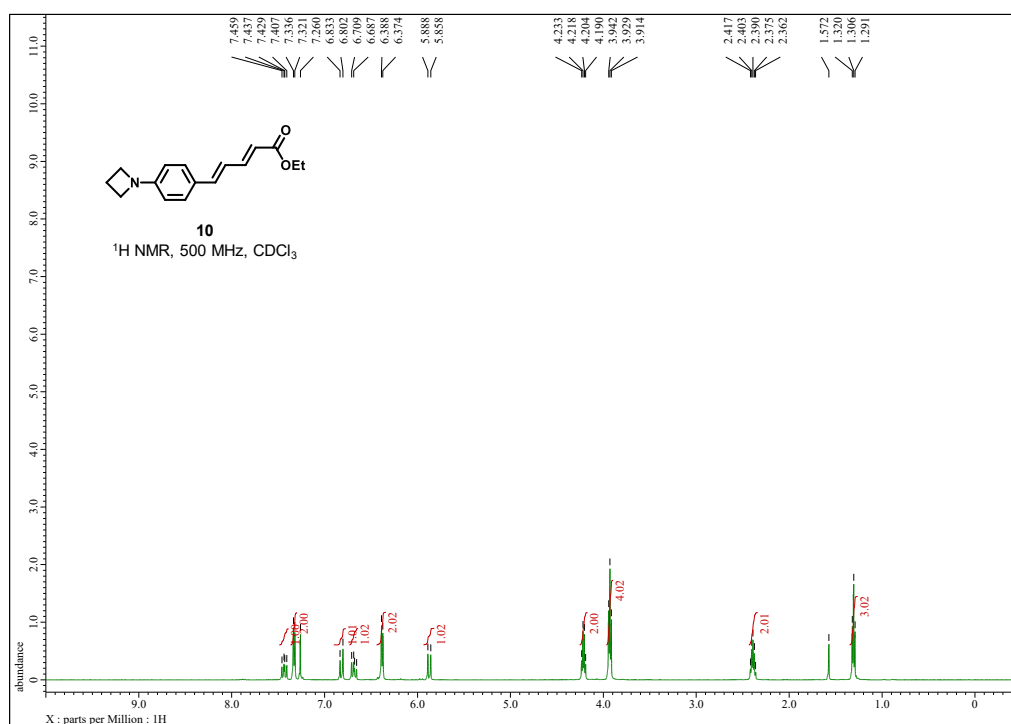
#### Compound 8



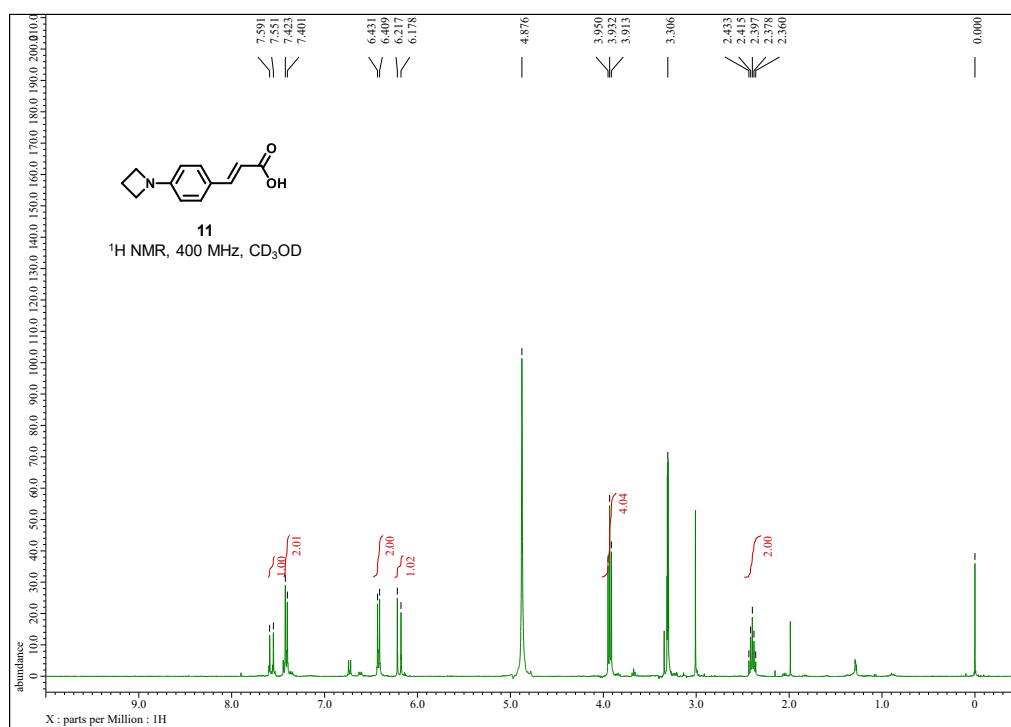
## Compound 9



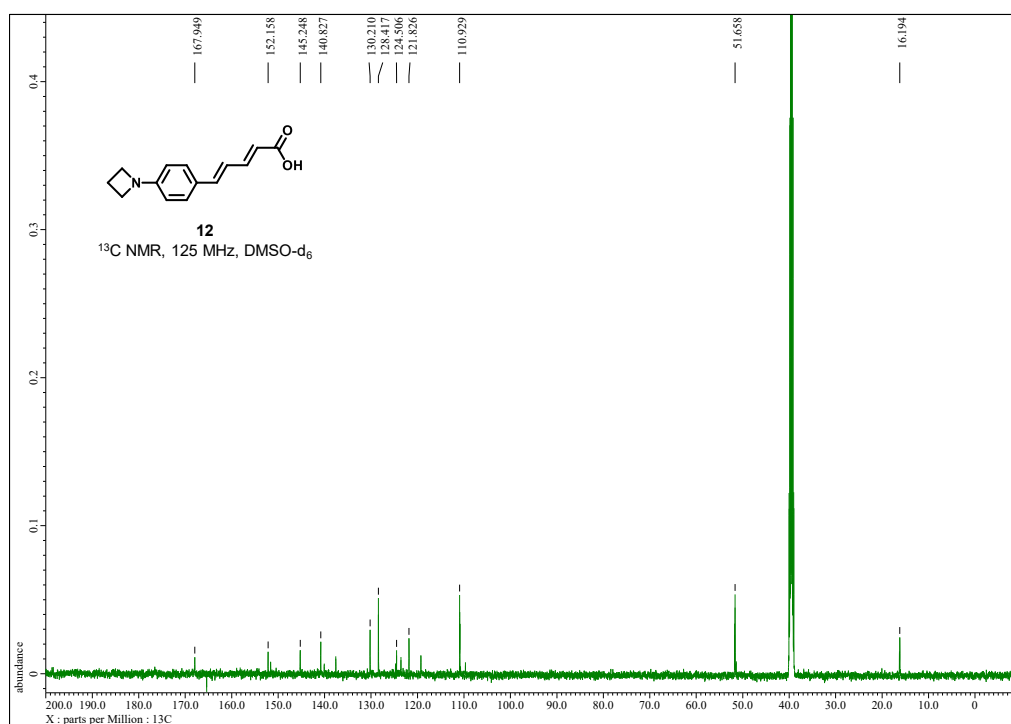
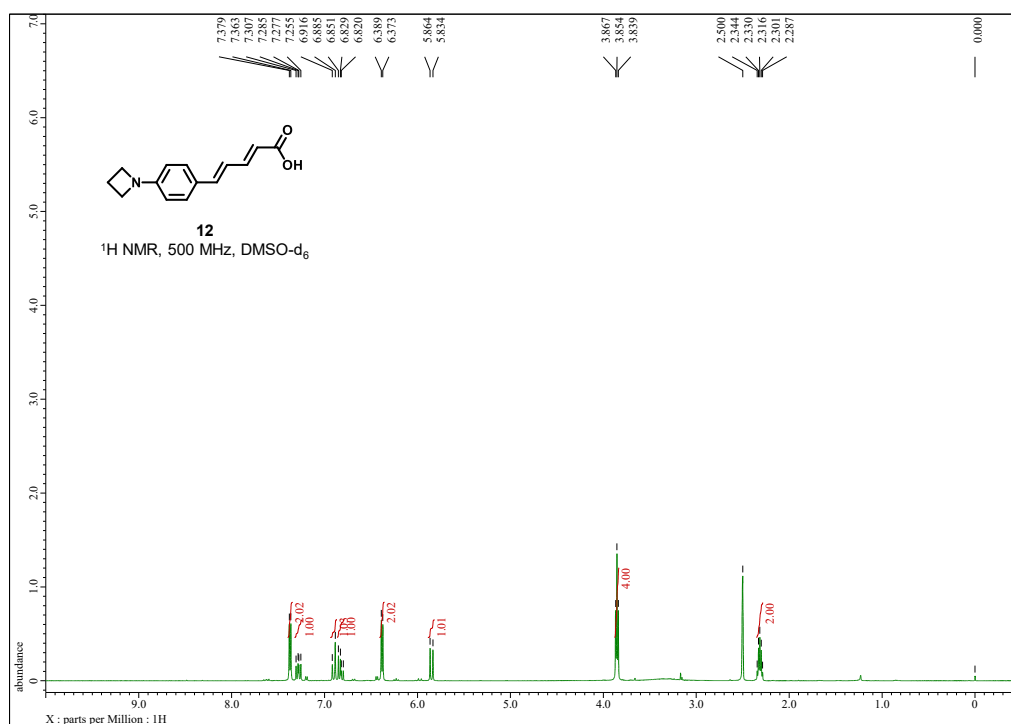
## Compound 10



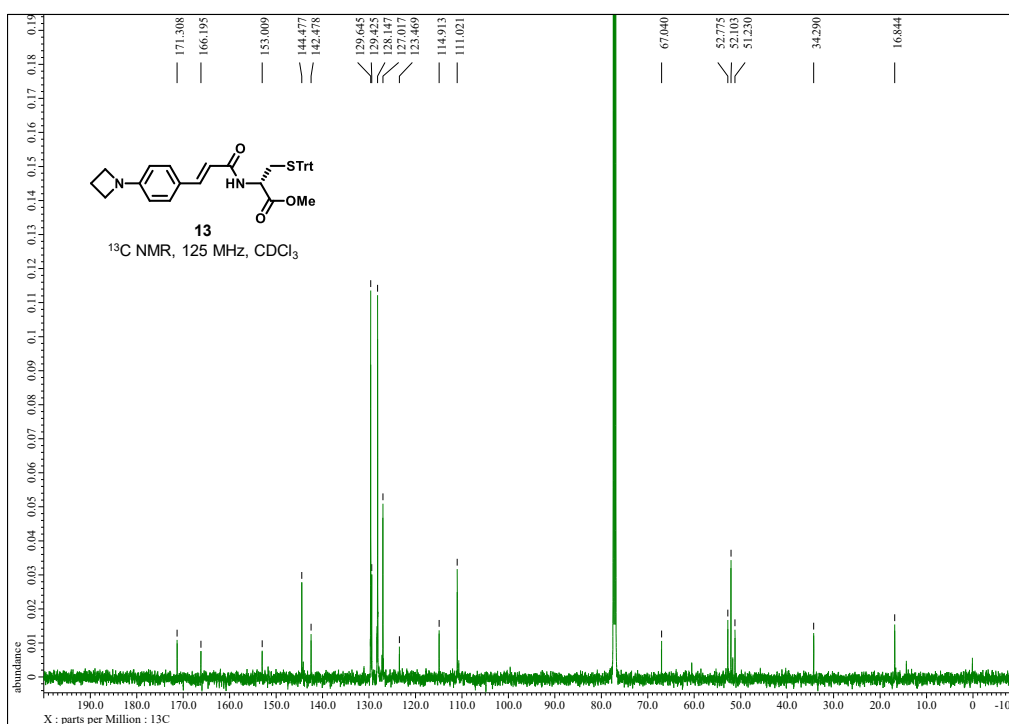
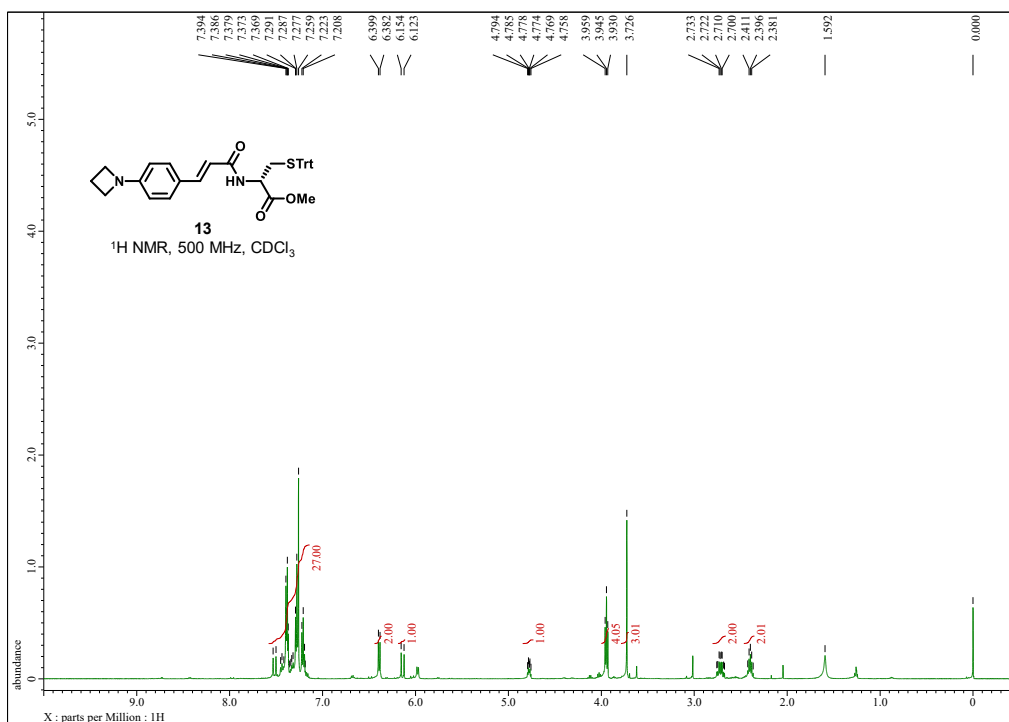
## Compound 11



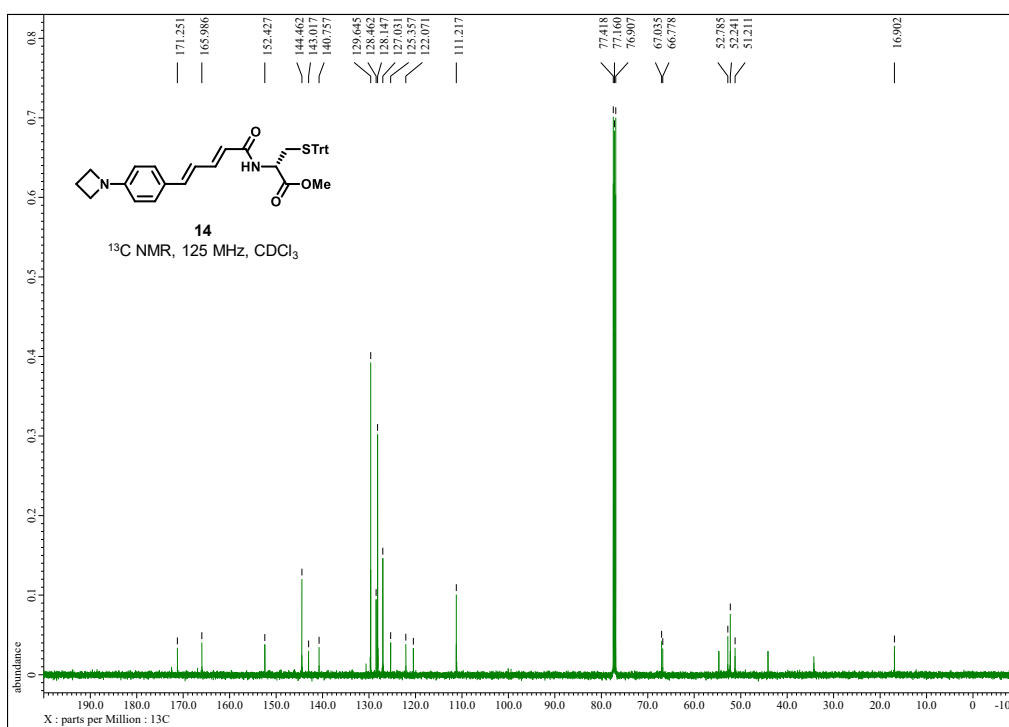
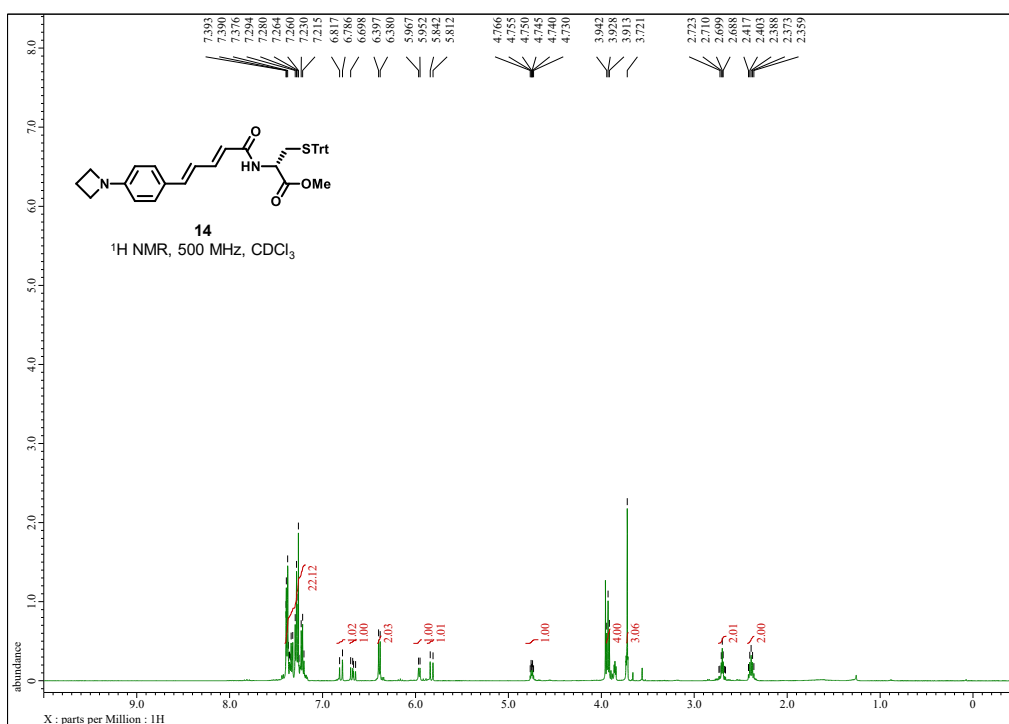
## Compound 12



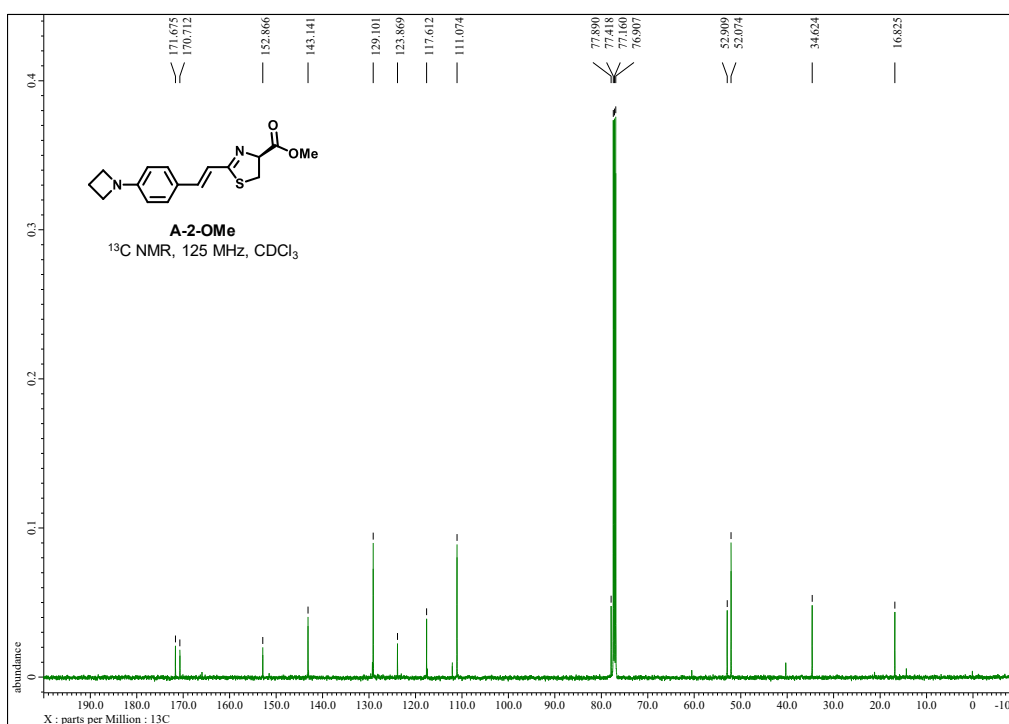
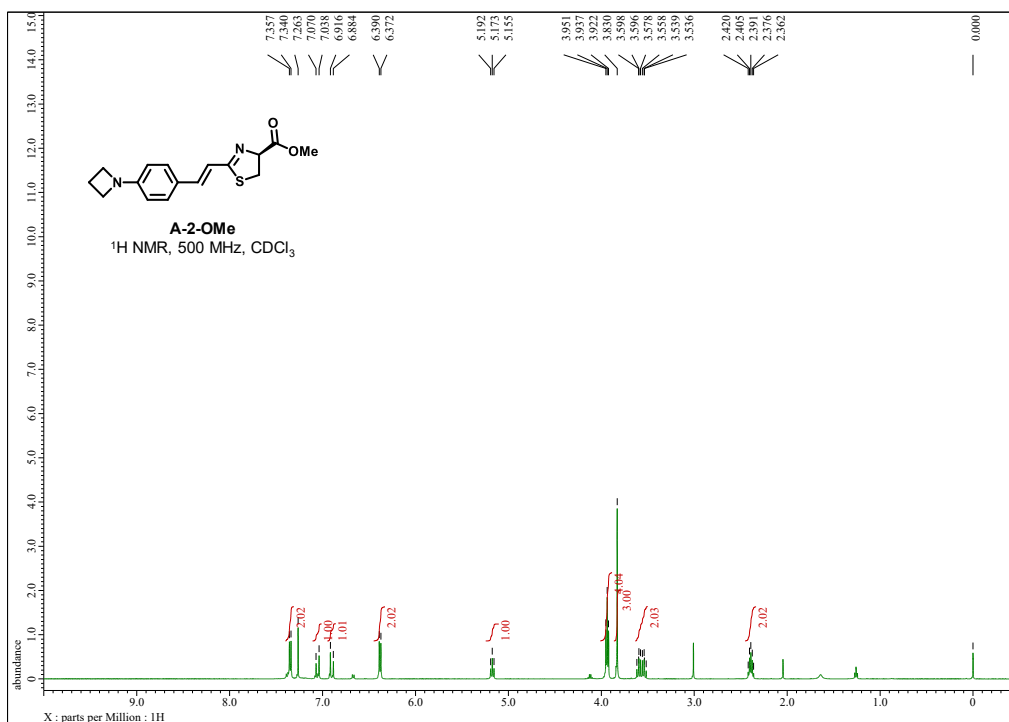
## Compound 13



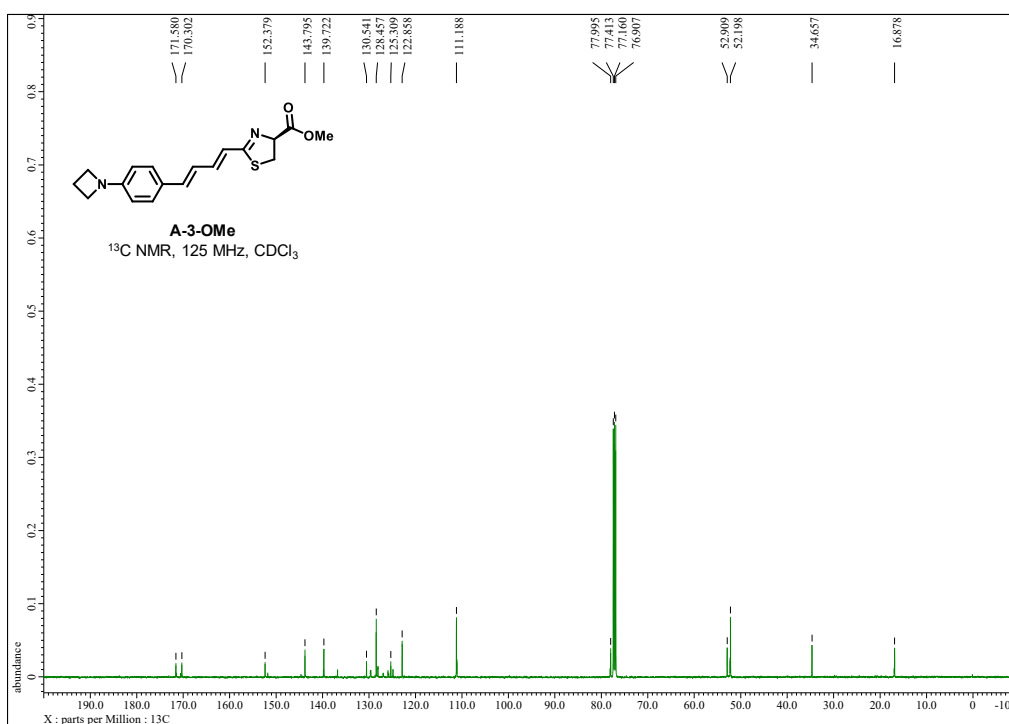
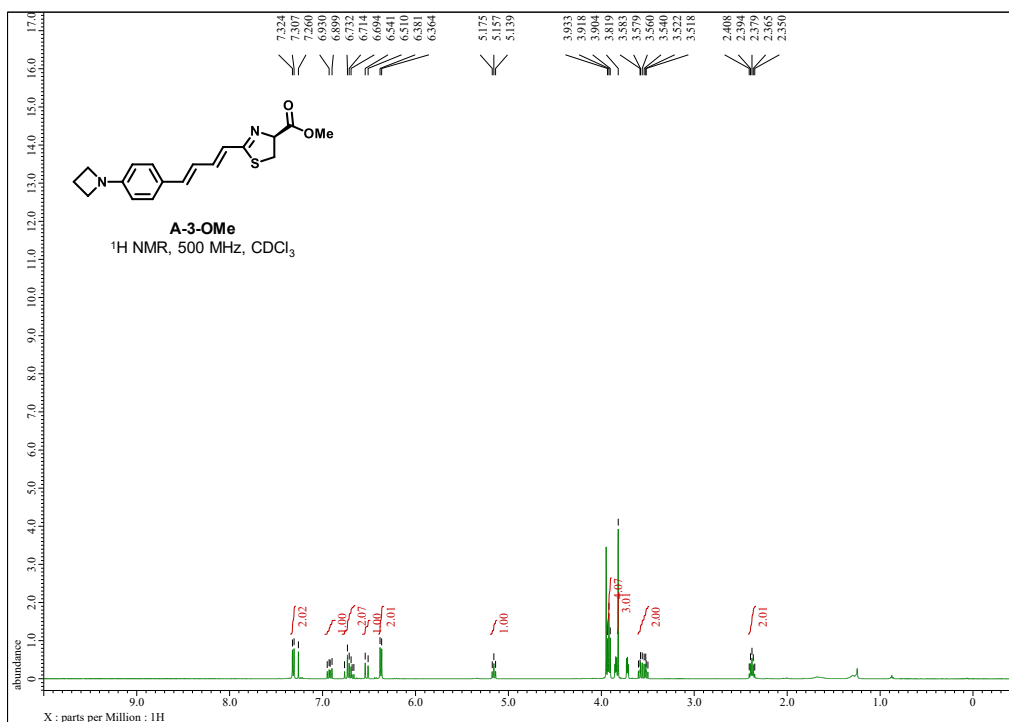
## Compound 14



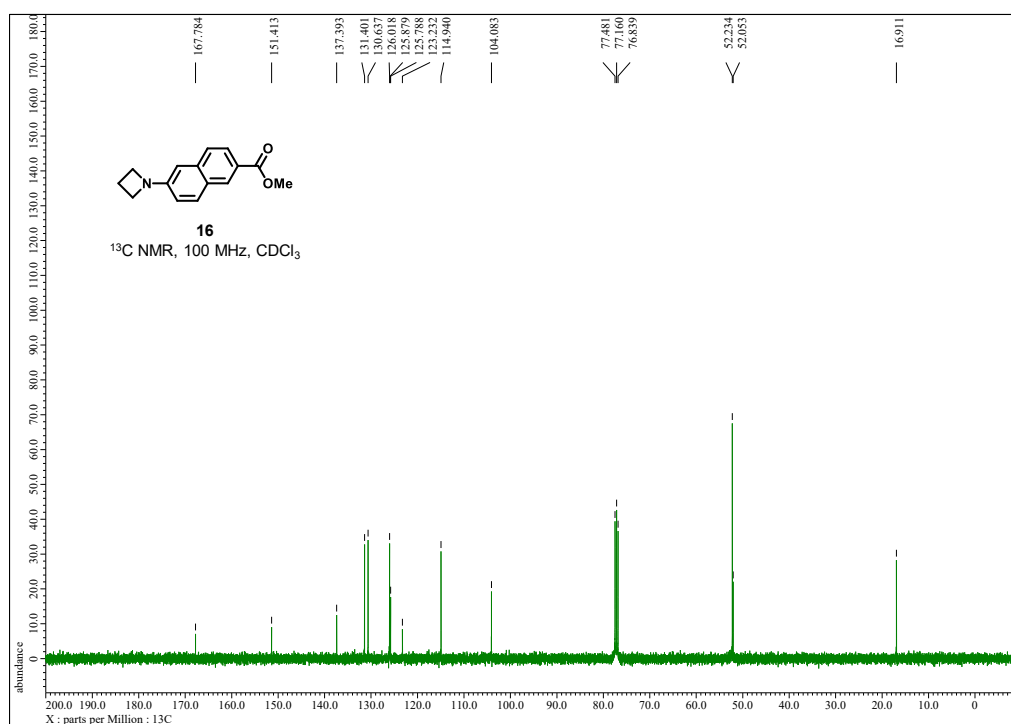
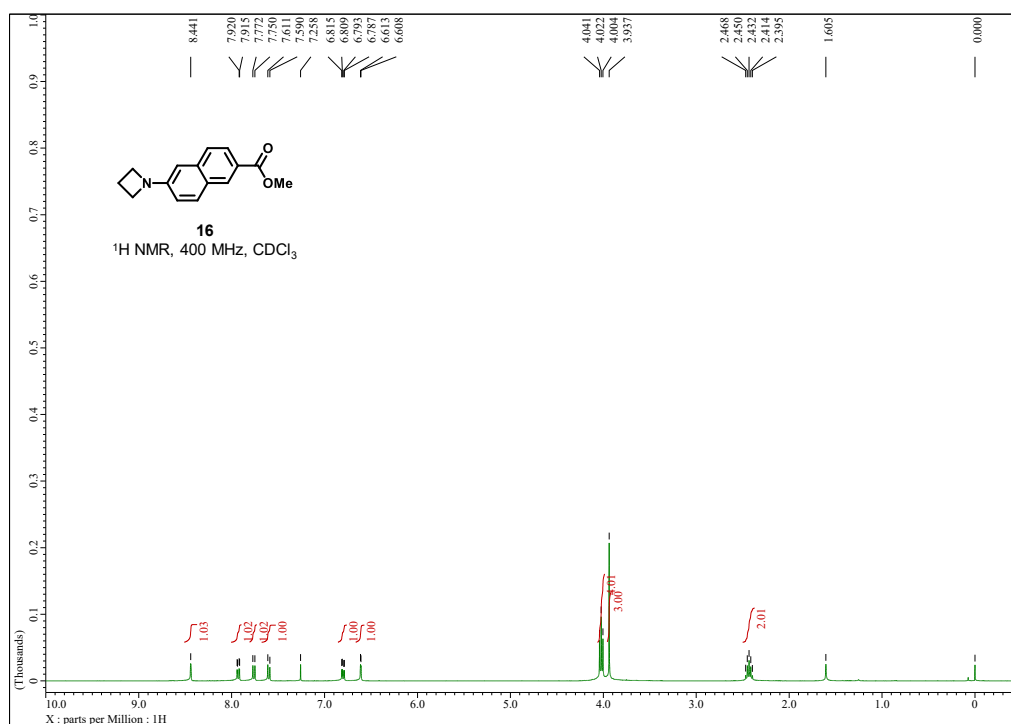
## A-2-OMe



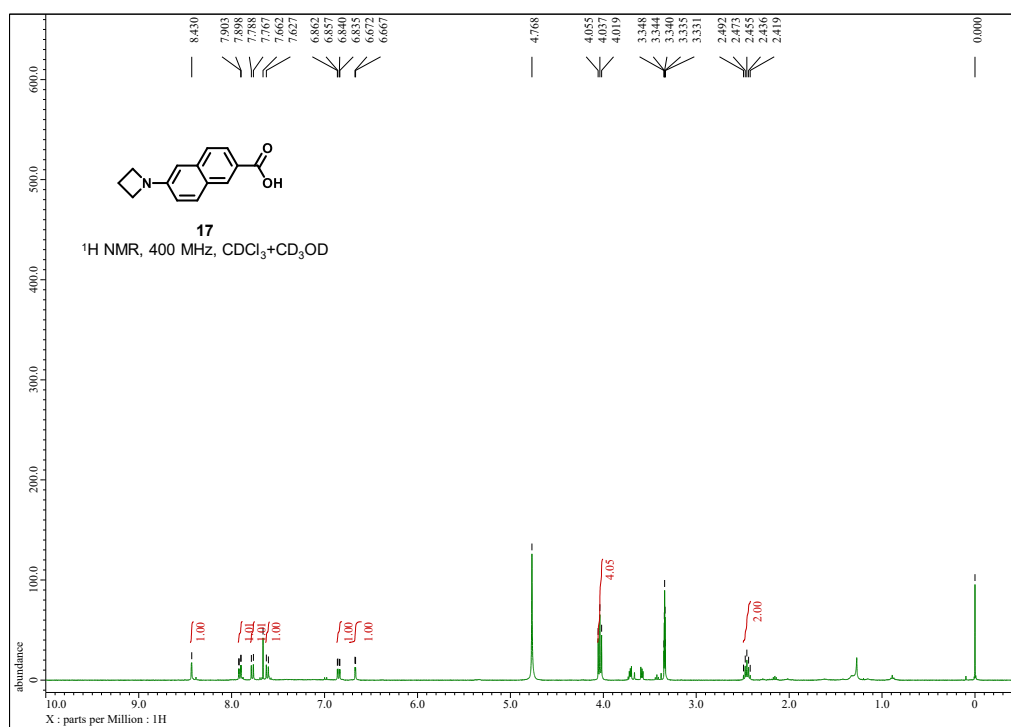
## A-3-OMe



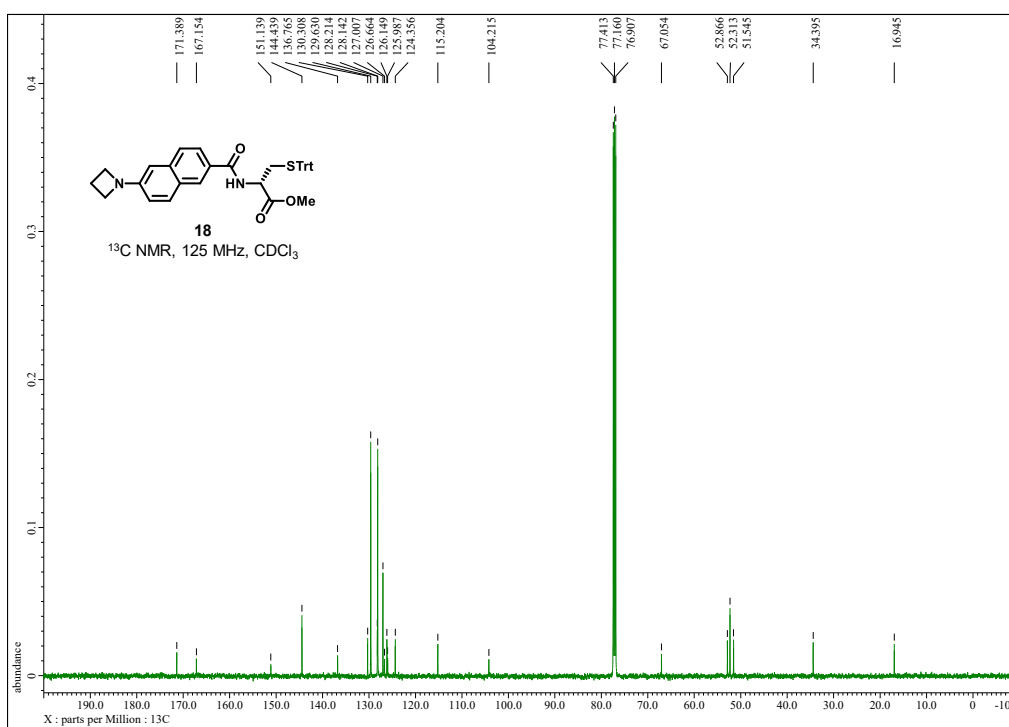
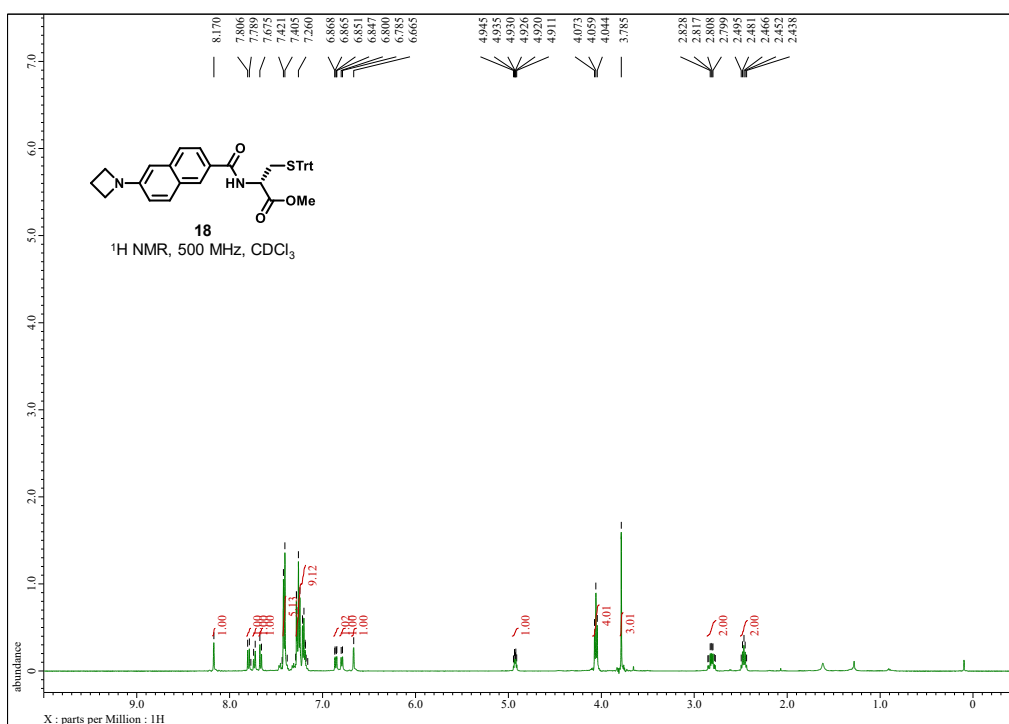
## Compound 16



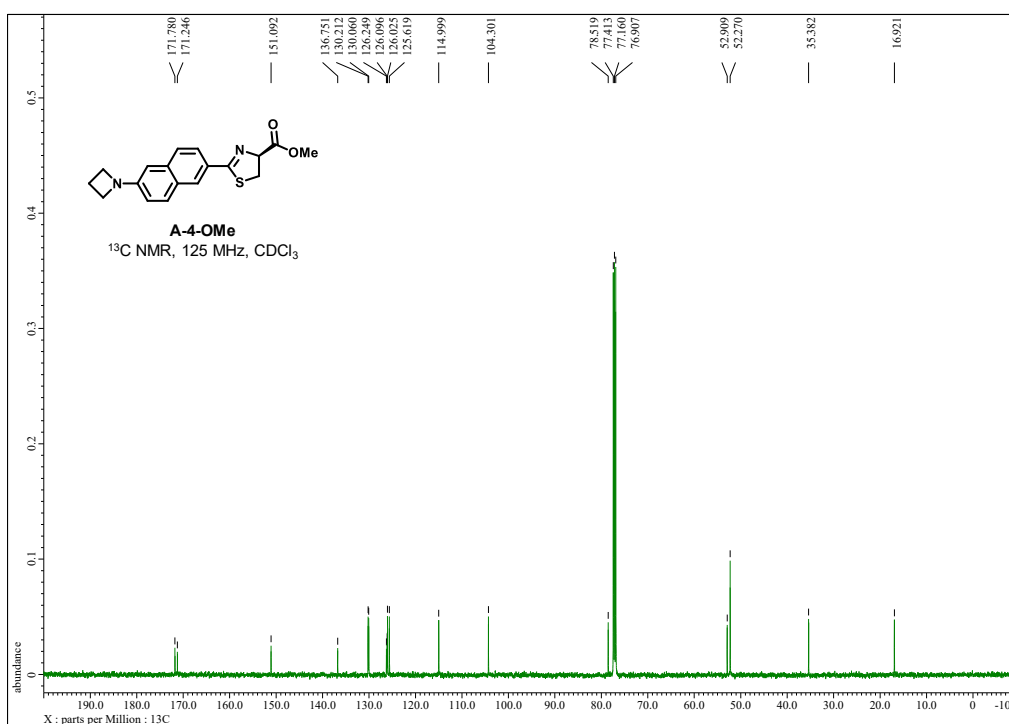
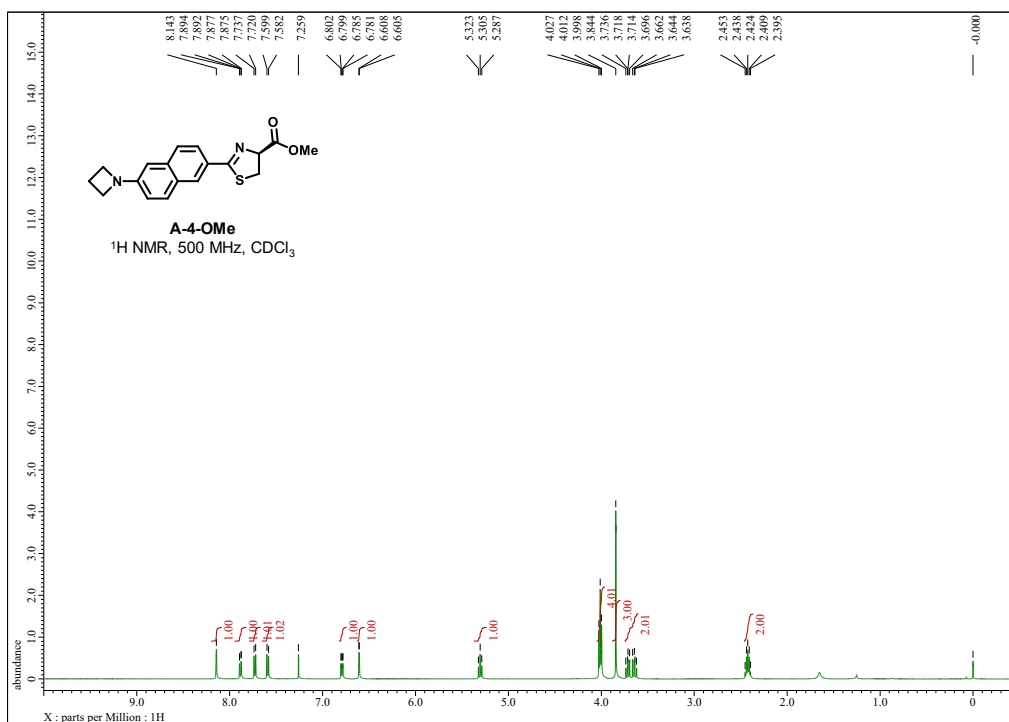
## Compound 17



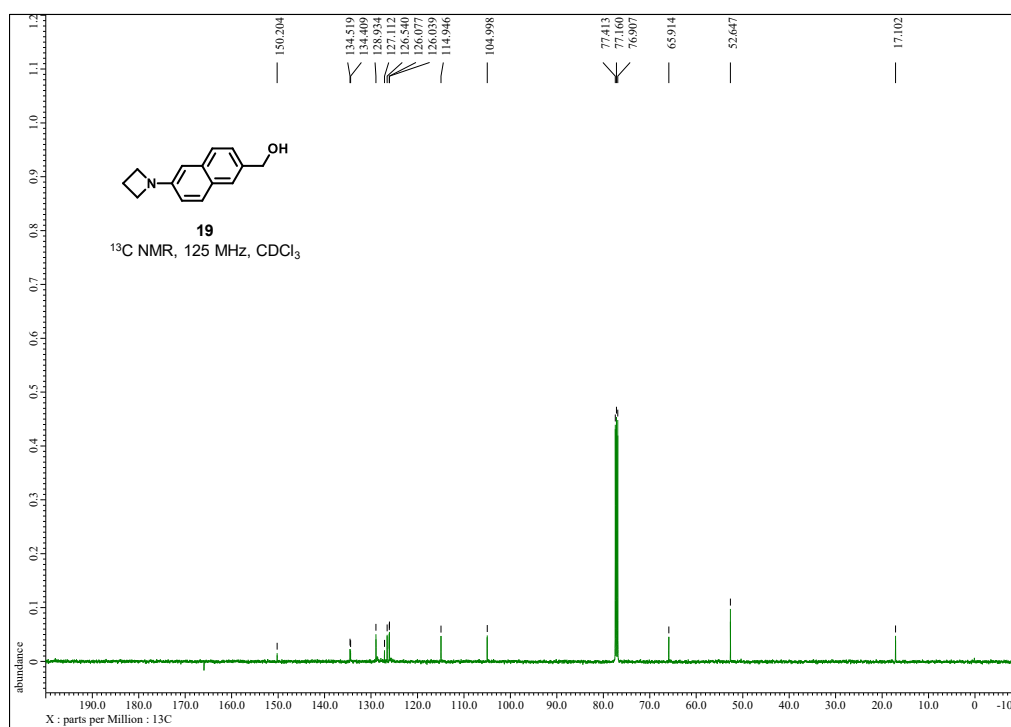
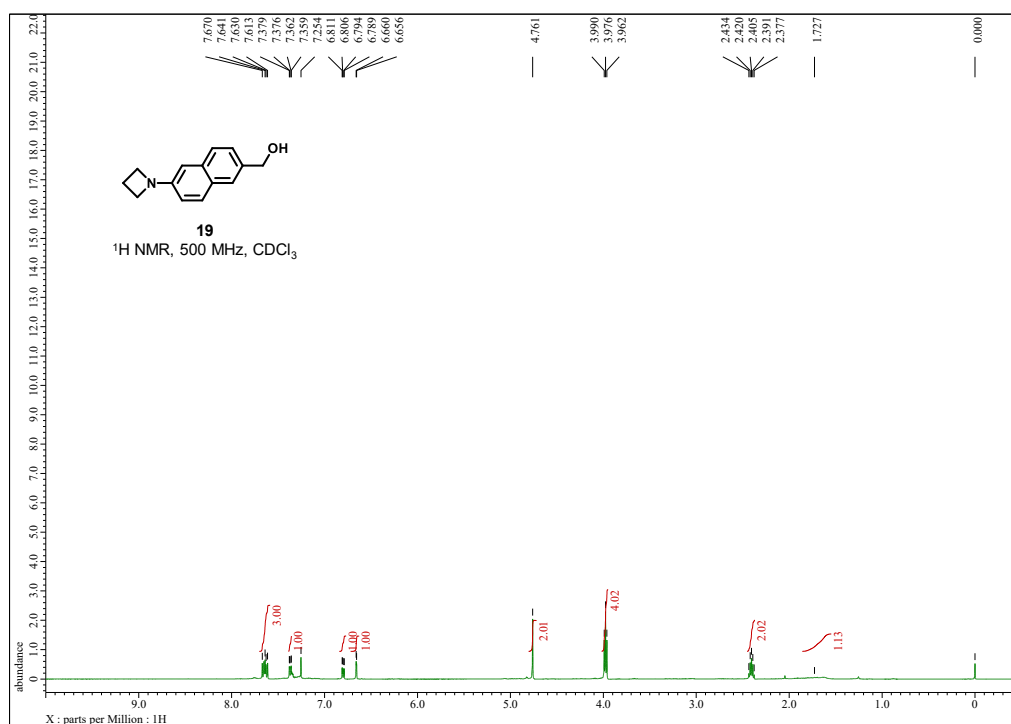
## Compound 18



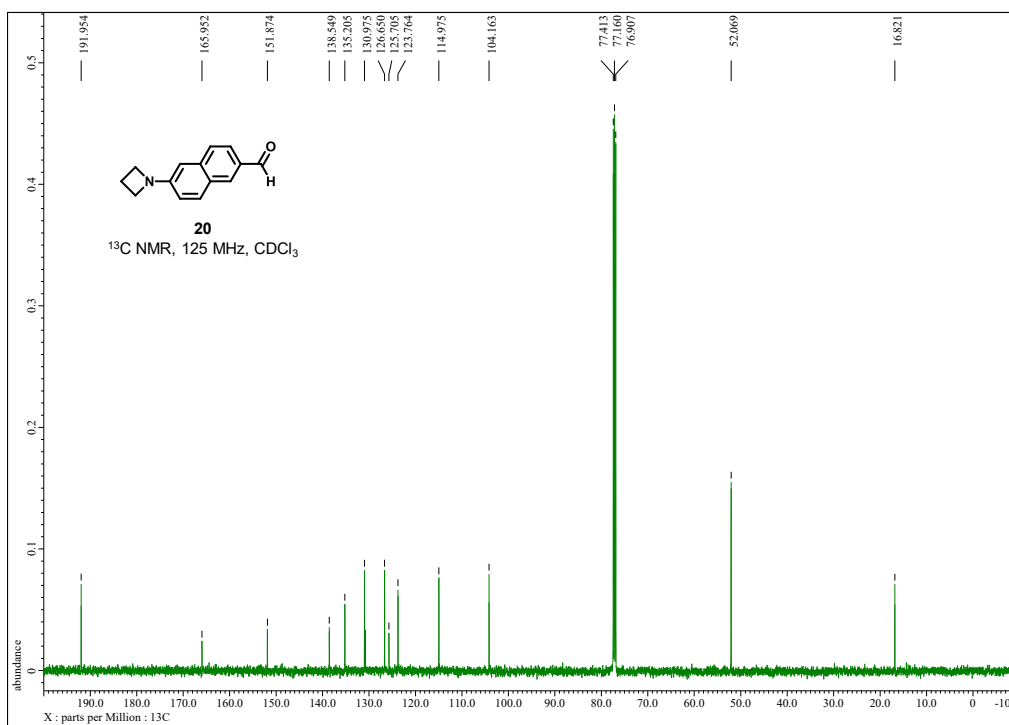
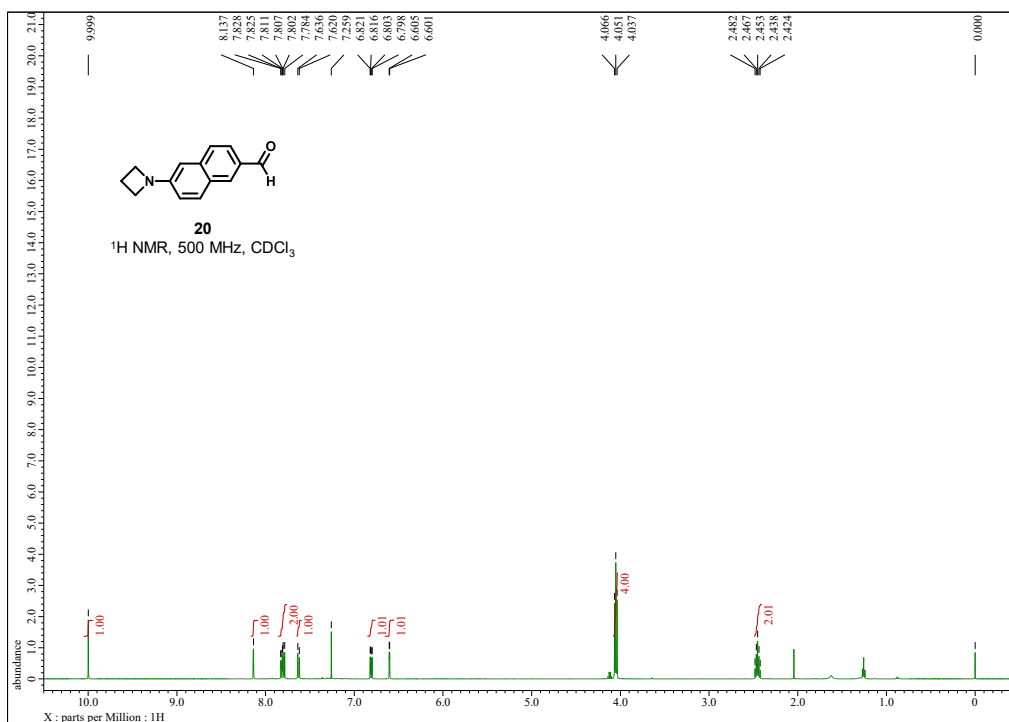
## A-4-OMe



## Compound 19

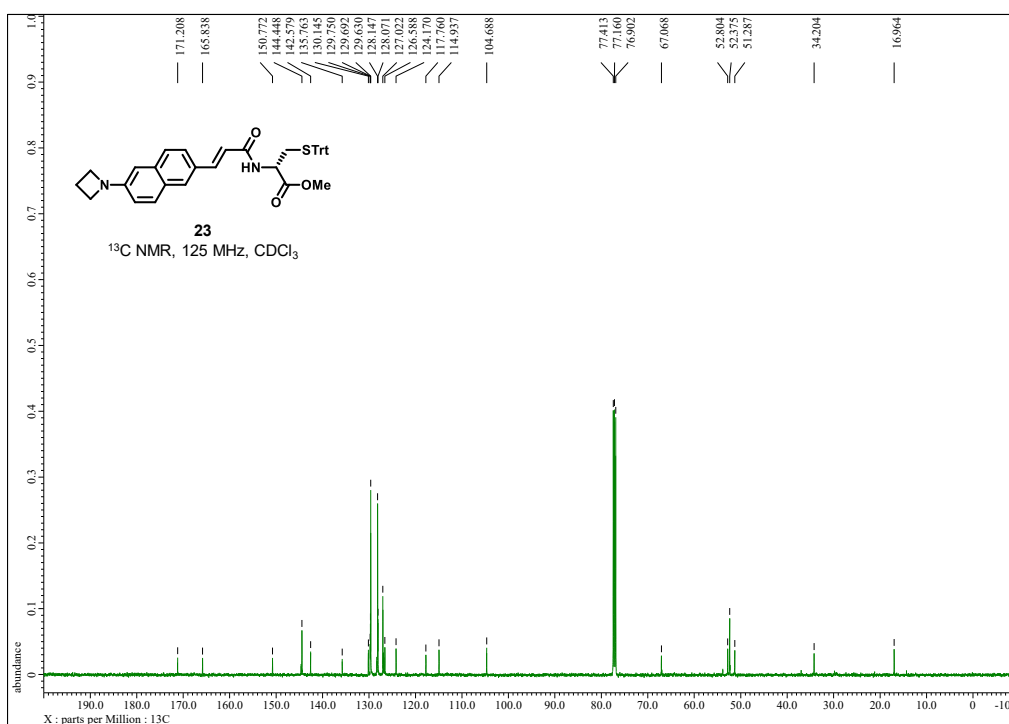
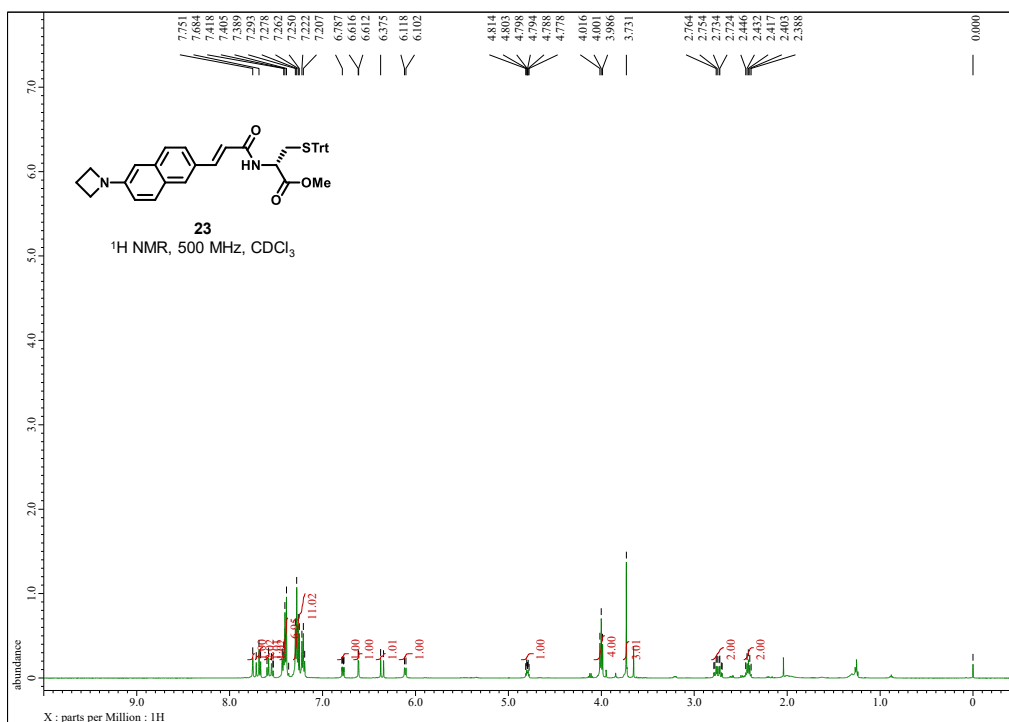


## Compound 20

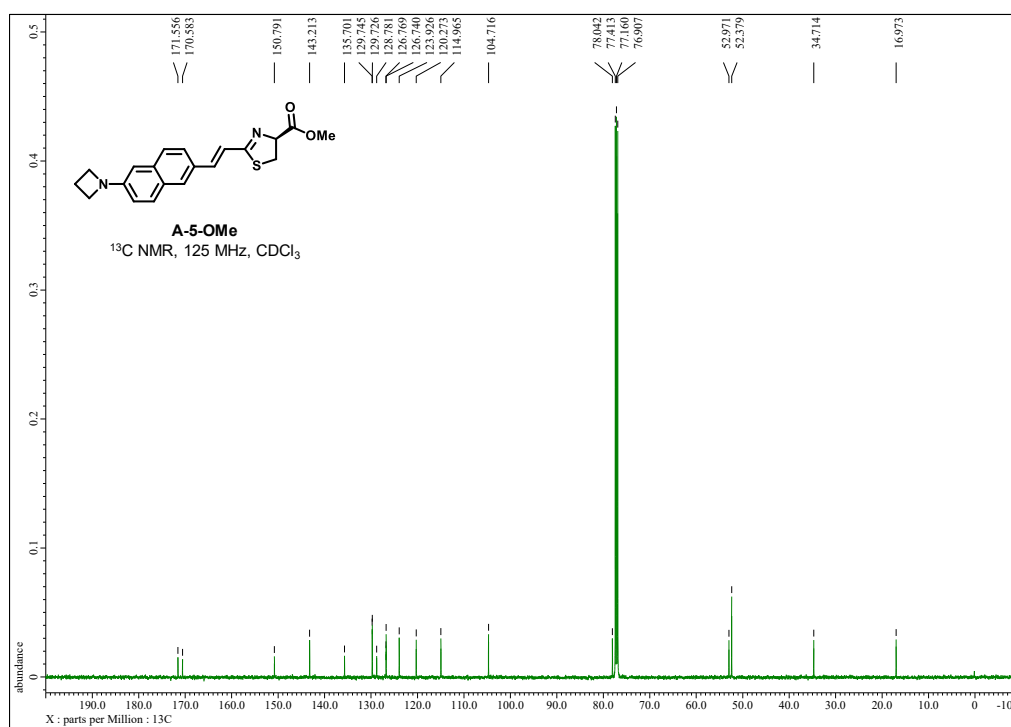
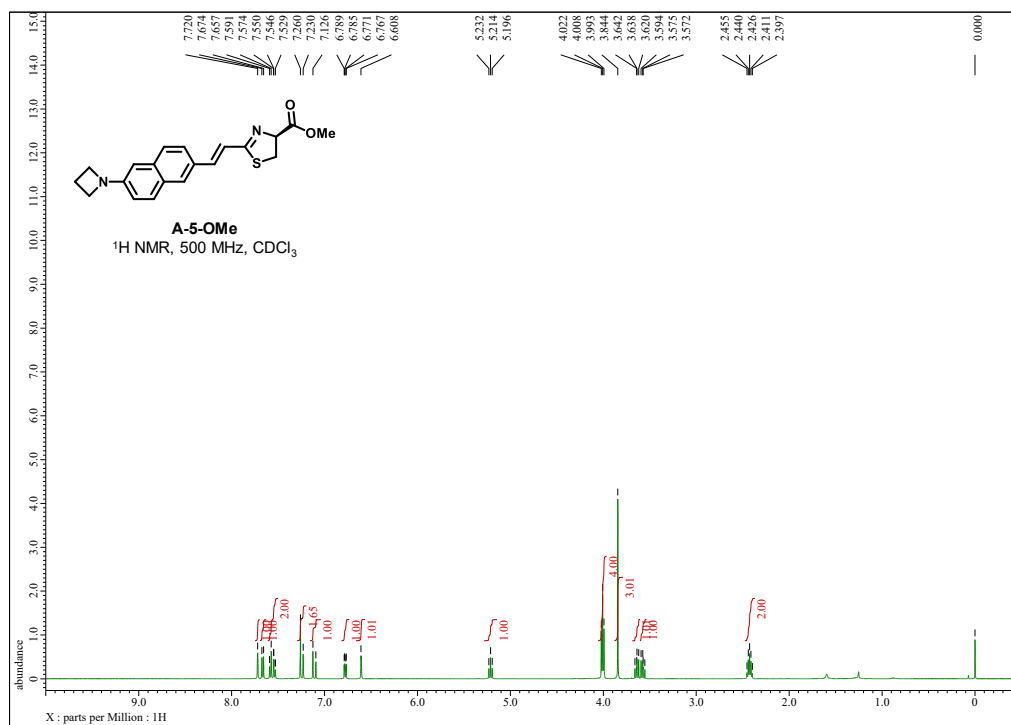




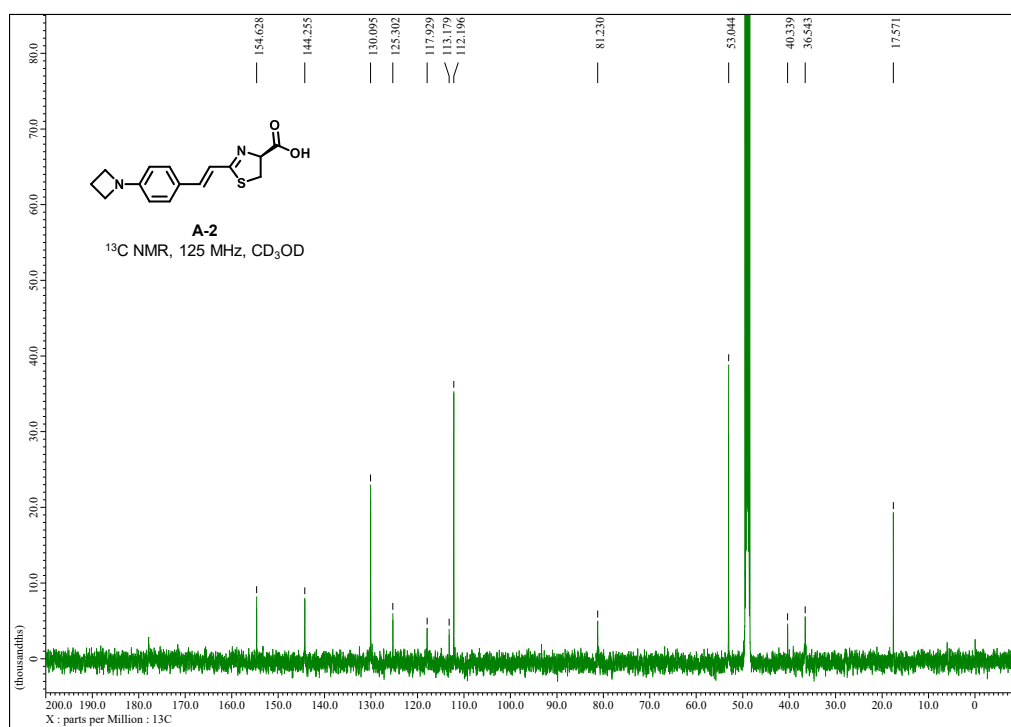
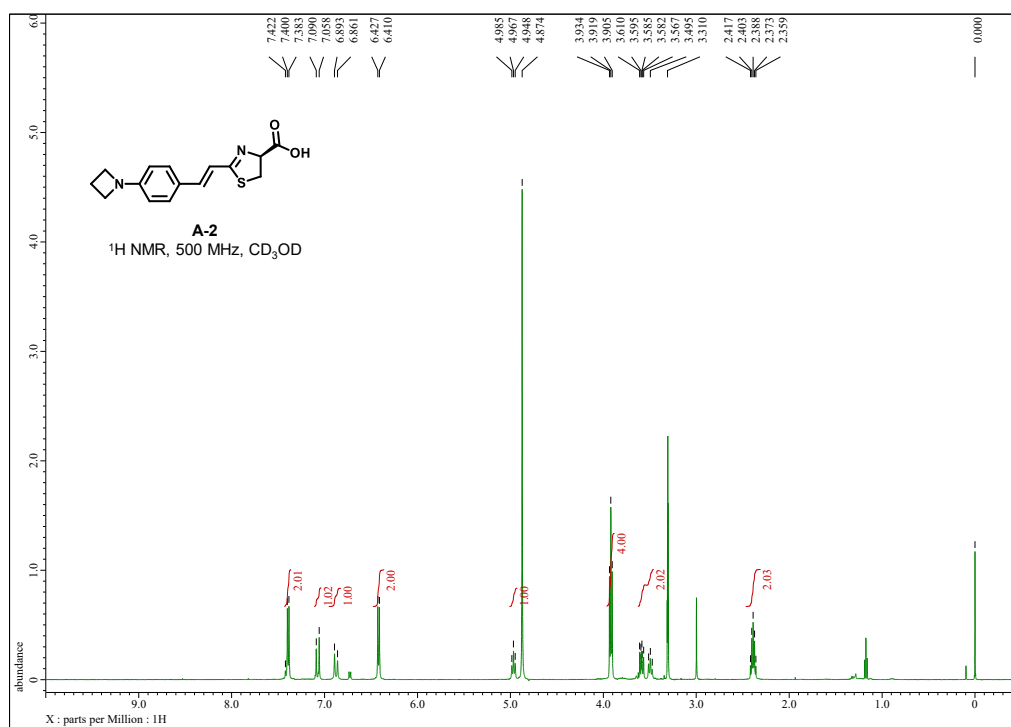
## Compound 23



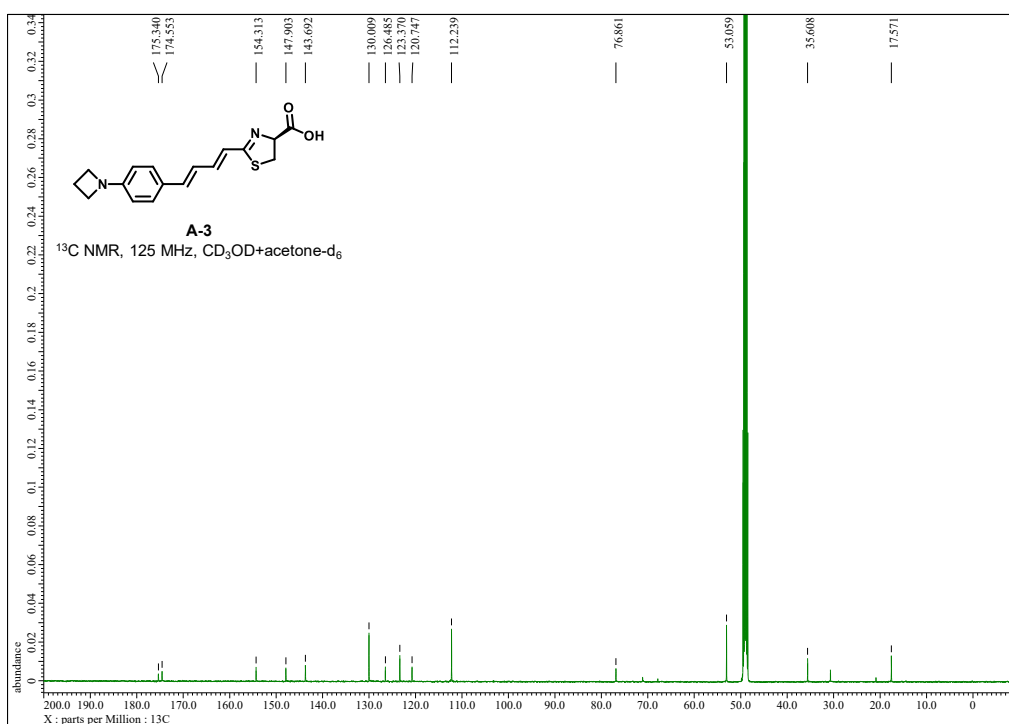
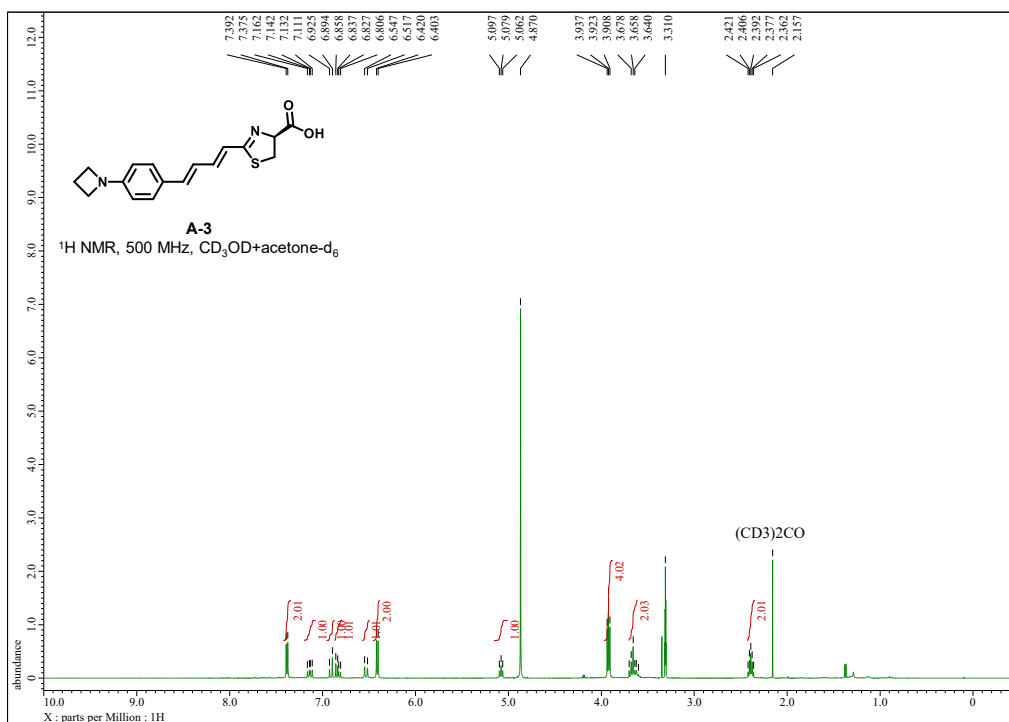
## A-5-OMe



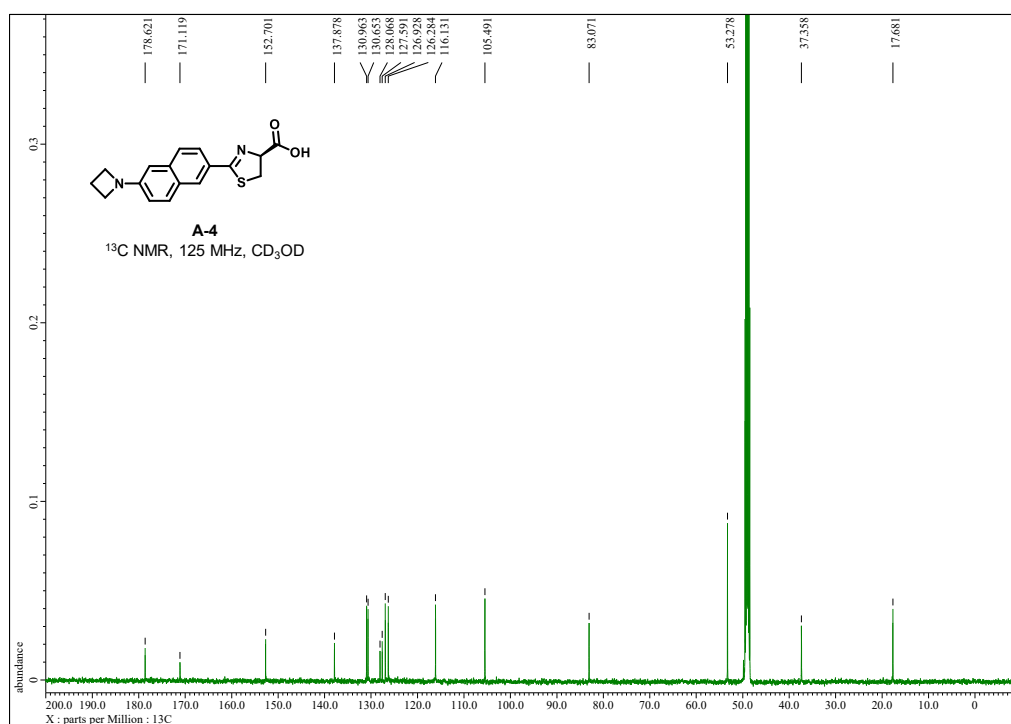
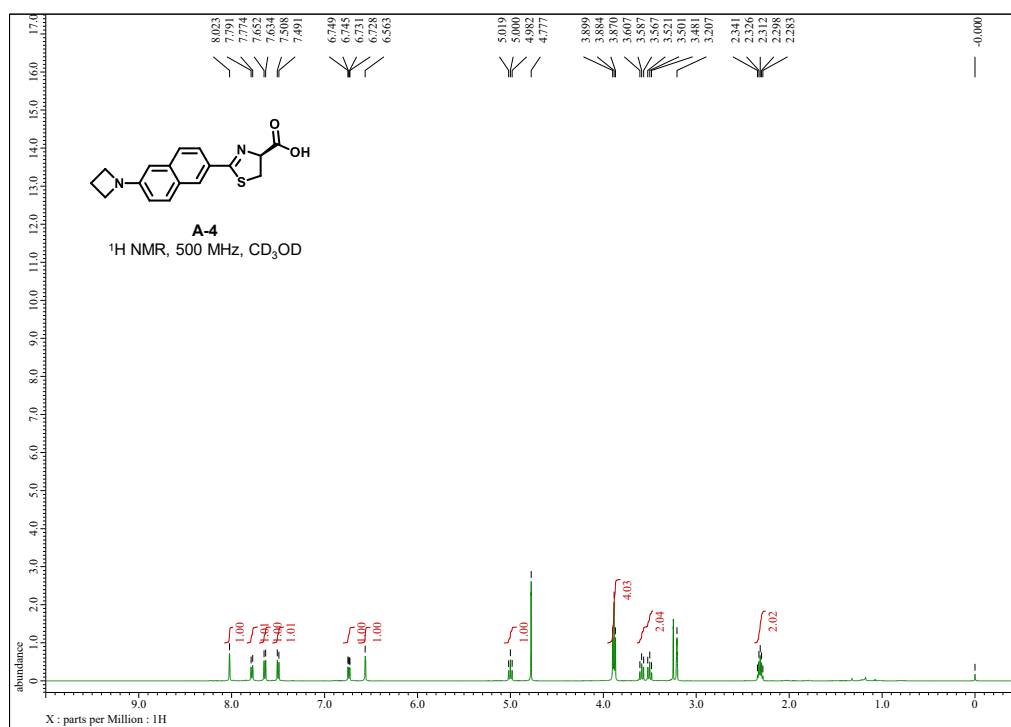
## A-2



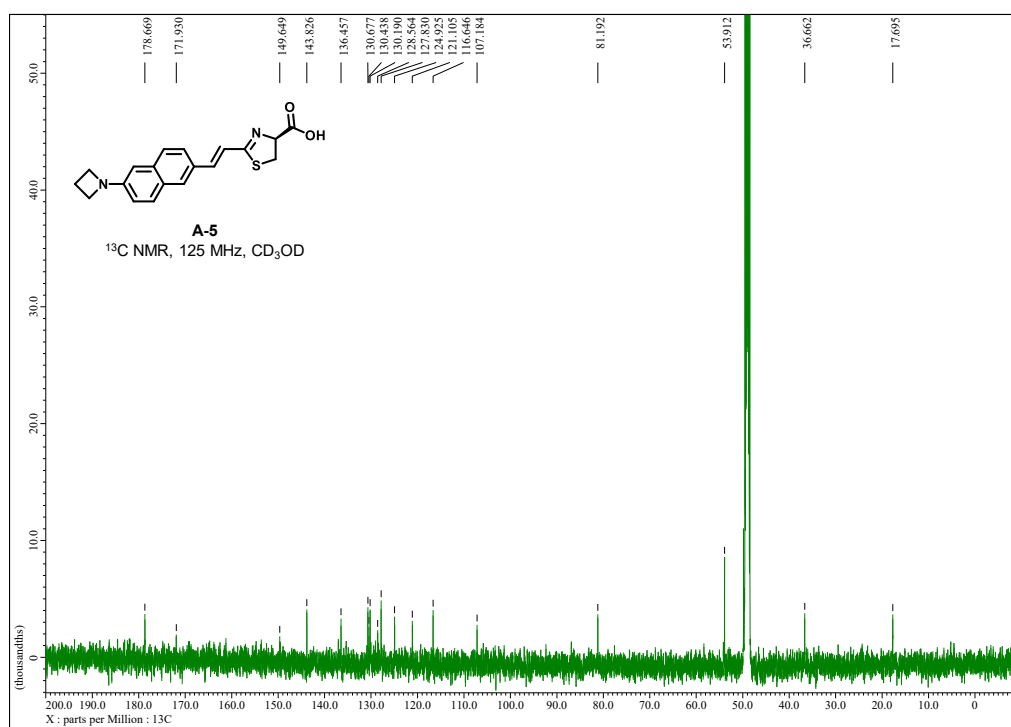
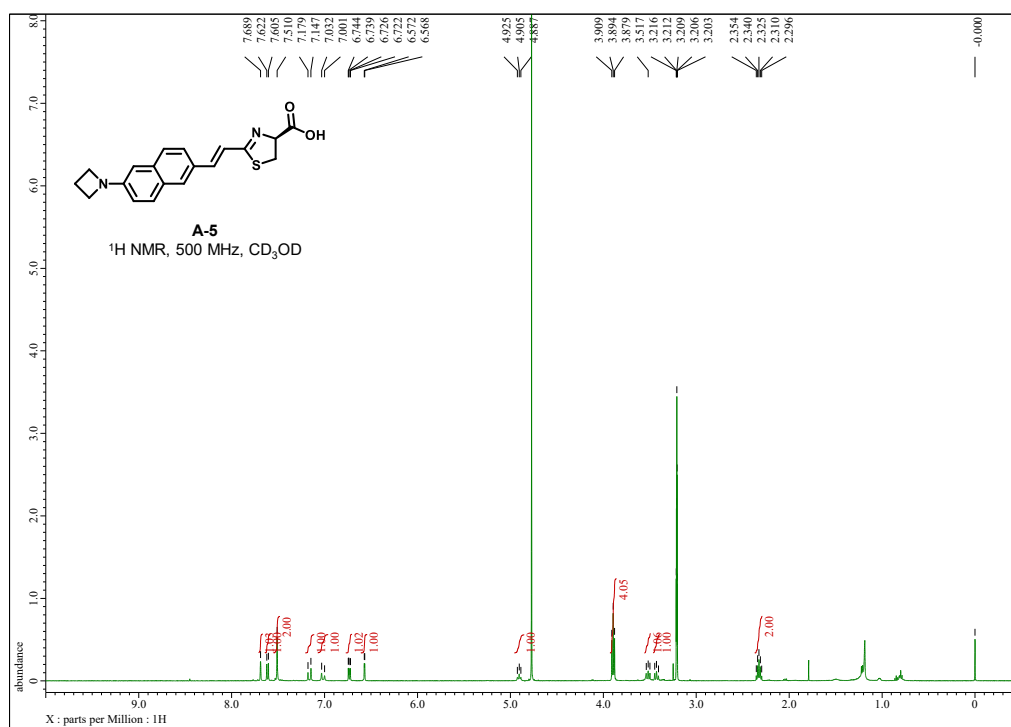
## A-3



## A-4



## A-5



## References

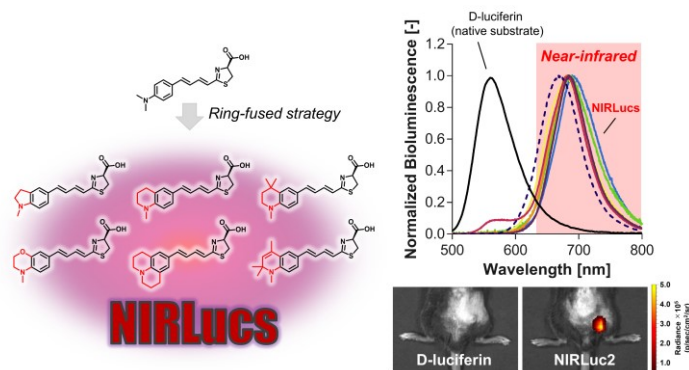
1. Iwano, S., Sugiyama, M., Hama, H., Watakabe, A., Hasegawa, N., Kuchimaru, T., Tanaka, K. Z., Takahashi, M., Ishida, Y., Hata, J., Shimozono, S., Namiki, K., Fukano, T., Kiyama, M., Okano, H., Kizaka-Kondoh, S., McHugh, T. J., Yamamori, T., Hioki, H., Maki, S. and Miyawaki, A., "Single-cell bioluminescence imaging of deep tissue in freely moving animals", *Science*, **2018**, 359, 935-939.
2. Yao, Z., Zhang, B. S. and Prescher, J. A., "Advances in bioluminescence imaging: new probes from old recipes", *Curr. Opin. Chem. Biol.*, **2018**, 45, 148-156.
3. Iwano, S., Obata, R., Miura, C., Kiyama, M., Hama, K., Nakamura, M., Amano, Y., Kojima, S., Hirano, T., Maki, S. and Niwa, H., "Development of simple firefly luciferin analogs emitting blue, green, red, and near-infrared biological window light", *Tetrahedron*, **2013**, 69, 3847-3856.
4. Wu, W., Su, J., Tang, C., Bai, H., Ma, Z., Zhang, T., Yuan, Z., Li, Z., Zhou, W., Zhang, H., Liu, Z., Wang, Y., Zhou, Y., Du, L., Gu, L. and Li, M., "cybLuc: An Effective Aminoluciferin Derivative for Deep Bioluminescence Imaging", *Anal. Chem.*, **2017**, 89, 4808-4816.
5. Hall, M. P., Woodroffe, C. C., Wood, M. G., Que, I., Van't Root, M., Ridwan, Y., Shi, C., Kirkland, T. A., Encell, L. P., Wood, K. V., Lowik, C. and Mezzanotte, L., "Click beetle luciferase mutant and near infrared naphthyl-luciferins for improved bioluminescence imaging", *Nat. Commun.*, **2018**, 9, 132-143.
6. Ikeda, Y., Saitoh, T., Niwa, K., Nakajima, T., Kitada, N., Maki, S. A., Sato, M., Citterio, D., Nishiyama, S. and Suzuki, K., "An allylated firefly luciferin analogue with luciferase specific response in living cells", *Chem. Commun.*, **2018**, 54, 1774-1777.
7. Williams, S. J. and Prescher, J. A., "Building Biological Flashlights: Orthogonal Luciferases and Luciferins for *in Vivo* Imaging", *Acc. Chem. Res.*, **2019**, Article ASAP.
8. Shinde, R., Perkins, J. and Contag, C. H., "Luciferin derivatives for enhanced *in vitro* and *in vivo* bioluminescence assays", *Biochemistry*, **2006**, 45, 11103-11112.
9. Woodroffe, C. C., Shultz, J. W., Wood, M. G., Osterman, J., Cali, J. J., Daily, W. J., Meisenheimer, P. L. and Klaubert, D. H., "N-Alkylated 6'-aminoluciferins are bioluminescent substrates for Ultra-Glo and QuantiLum luciferase: new potential scaffolds for bioluminescent assays", *Biochemistry*, **2008**, 47, 10383-10393.
10. Takakura, H., Kojima, R., Kamiya, M., Kobayashi, E., Komatsu, T., Ueno, T., Terai, T., Hanaoka, K., Nagano, T. and Urano, Y., "New class of bioluminogenic probe based on bioluminescent enzyme-induced electron transfer: BioLeT", *J. Am. Chem. Soc.*, **2015**, 137, 4010-4013.
11. Reddy, G. R., Thompson, W. C. and Miller, S. C., "Robust light emission from cyclic alkylaminoluciferin substrates for firefly luciferase", *J. Am. Chem. Soc.*, **2010**, 132, 13586-13587.

12. Mofford, D. M., Reddy, G. R. and Miller, S. C., "Aminoluciferins extend firefly luciferase bioluminescence into the near-infrared and can be preferred substrates over D-luciferin", *J. Am. Chem. Soc.*, **2014**, *136*, 13277-13282.
13. Grimm, J. B., English, B. P., Chen, J., Slaughter, J. P., Zhang, Z., Revyakin, A., Patel, R., Macklin, J. J., Normanno, D., Singer, R. H., Lionnet, T. and Lavis, L. D., "A general method to improve fluorophores for live-cell and single-molecule microscopy", *Nat. Methods*, **2015**, *12*, 244-250.
14. Kakiuchi, M., Ito, S., Kiyama, M., Goto, F., Matsushashi, T., Yamaji, M., Maki, S. and Hirano, T., "Electronic and Steric Effects of Cyclic Amino Substituents of Luciferin Analogues on a Firefly Luciferin–Luciferase Reaction", *Chem. Lett.*, **2017**, *46*, 1090-1092.
15. Sharma, D. K., Adams, S. T., Jr., Liebmann, K. L. and Miller, S. C., "Rapid Access to a Broad Range of 6'-Substituted Firefly Luciferin Analogues Reveals Surprising Emitters and Inhibitors", *Org. Lett.*, **2017**, *19*, 5836-5839.
16. Ikeda, Y., Nomoto, T., Hiruta, Y., Nishiyama, N. and Citterio, D., "Ring-fused Firefly Luciferins: Expanded Palette of Near-infrared Emitting Bioluminescent Substrates". *Anal. Chem.*, **2019**, *submitted*.
17. Mofford, D. M., Liebmann, K. L., Sankaran, G. S., Reddy, G., Reddy, G. R. and Miller, S. C., "Luciferase Activity of Insect Fatty Acyl-CoA Synthetases with Synthetic Luciferins", *ACS Chem. Biol.*, **2017**, *12*, 2946-2951.
18. Takakura, H., Kojima, R., Urano, Y., Terai, T., Hanaoka, K. and Nagano, T., "Aminoluciferins as functional bioluminogenic substrates of firefly luciferase", *Chem. Asian. J.*, **2011**, *6*, 1800-1810.
19. Takakura, H., Sasakura, K., Ueno, T., Urano, Y., Terai, T., Hanaoka, K., Tsuboi, T. and Nagano, T., "Development of luciferin analogues bearing an amino group and their application as BRET donors", *Chem. Asian. J.*, **2010**, *5*, 2053-2061.
20. Liu, X., Qiao, Q., Tian, W., Liu, W., Chen, J., Lang, M. J. and Xu, Z., "Aziridinyl Fluorophores Demonstrate Bright Fluorescence and Superior Photostability by Effectively Inhibiting Twisted Intramolecular Charge Transfer". *J. Am. Chem. Soc.*, **2016**, *138*, 6960-6963.

## Chapter 4

# Ring-Fused Firefly Luciferins: Expanded Palette of Near-Infrared Emitting Bioluminescent Substrates

This chapter is based on "Ring-Fused Firefly Luciferins: Expanded Palette of Near-Infrared Emitting Bioluminescent Substrates, [Yuma Ikeda](#), Takahiro Nomoto, Yuki Hiruta, Nobuhiro Nishiyama and Daniel Citterio, *Anal. Chem.*, **2020**, accepted (DOI: 10.1021/acs.analchem.9b04562).



## Summary

One limitation in firefly bioluminescence imaging is the limited variety of luciferins emitting in the near-infrared (NIR) region (650–900 nm), where tissue penetration is high. Herein, I describe a series of structure-inherent NIR emitting firefly luciferin analogues, **NIRLucs**, designed through a ring fusion strategy. This strategy resulted in pH-independent structure-inherent NIR emission with a native firefly luciferase, which was theoretically supported by quantum chemical calculations of the oxidized form of each luciferin. When applied to cells, **NIRLucs** displayed dose-independent improved NIR emission even at low concentrations where the native D-luciferin substrate does not emit. Additionally, excellent blood retention and brighter photon flux (7-fold overall, 16-fold in the NIR spectral range) than in the case of D-luciferin have been observed with one of the **NIRLucs** in mice bearing subcutaneous tumors. I believe that these synthetic luciferins provide a solution to the longstanding limitation in the variety of NIR emitting luciferins, and pave the way to the further development of NIR bioluminescence imaging platforms.

## 4.1. Introduction

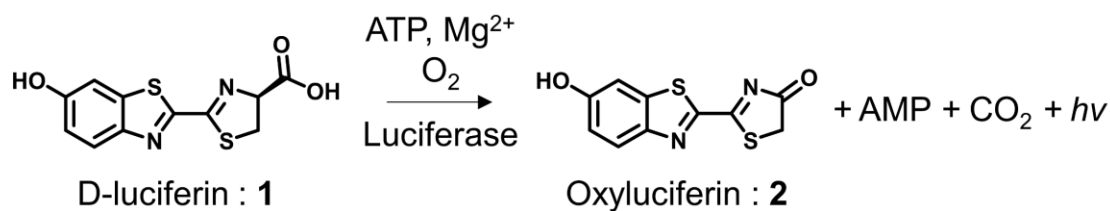
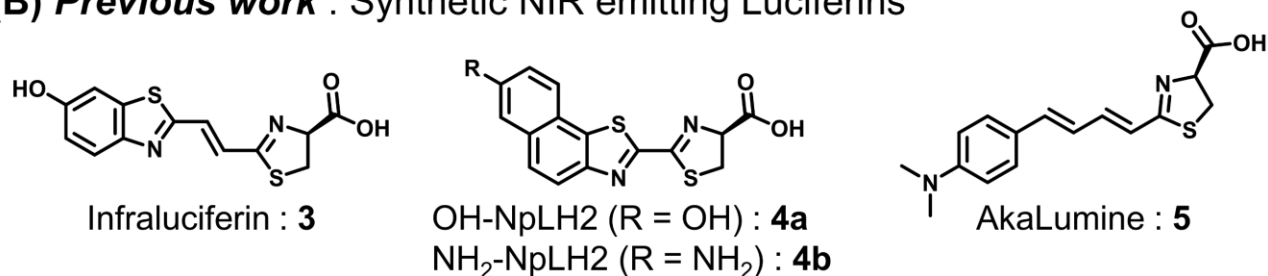
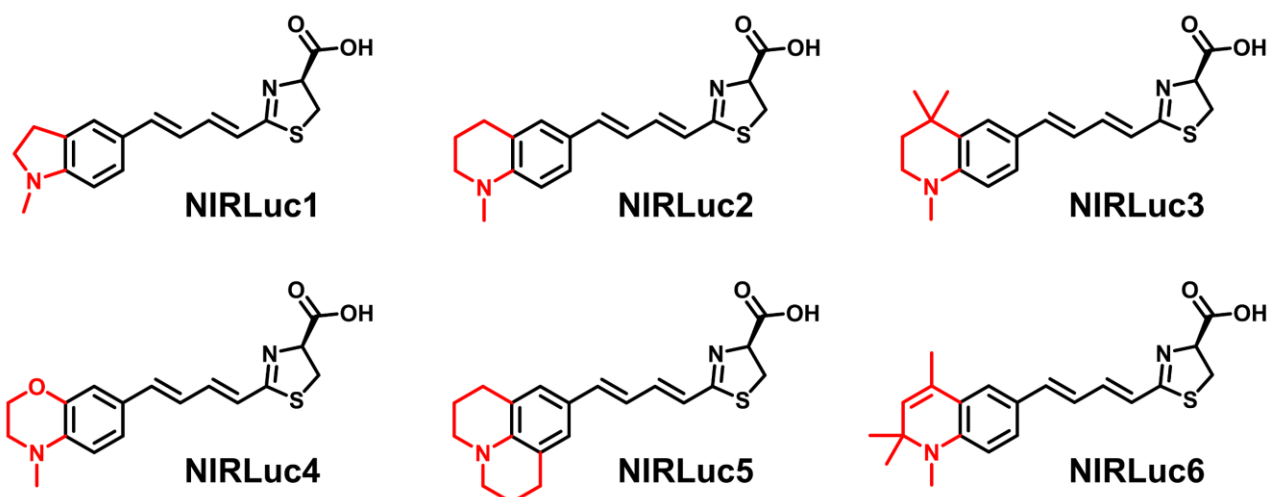
Optical imaging technologies play important roles in the biomedical research field. Nowadays, bioluminescence has become a standard non-invasive modality to trace biological functions *in vivo* without having to sacrifice animals, which for example enables the spatiotemporally monitoring of cancer metastasis over time.<sup>1-2</sup> The light emitting process relies on the enzymatic reaction catalyzed by a luciferase to yield the excited-state oxyluciferin, which emits light upon relaxation to the ground state (**Figure 4.1A**). The most commonly used luciferin-luciferase pairs in these assays originate from insects, such as the firefly and click beetles. These bioluminescent systems consist of D-luciferin (**1**) and the corresponding insect luciferases, for example Fluc from *photinus pylalis*. They emit yellow-green to red light (560-620 nm) depending on the luciferase type and the environment surrounding the luciferase active site, such as pH, metal ions and temperature.<sup>3</sup>

Although D-luciferin (**1**) has been routinely adopted as a reliable reporter for *in vitro* and *in vivo* imaging, it is sometimes not the ideal substrate for *in vivo* imaging, especially in deep tissues such as mouse lung, liver or brain. The light emitted from D-luciferin suffers from strong light absorption by blood components and tissue, making *in vivo* imaging difficult.<sup>4</sup> In optical imaging, particularly in deep tissues, emission in the near-infrared (NIR) region, called the "bio-optical window" ranging from 650-900 nm, is desirable.<sup>5</sup> Mutations to luciferases have successfully afforded red-shifted light production utilizing D-luciferin (**1**) as a substrate, but were not an effective strategy to achieve NIR emission. This is potentially due to the inherent limitation in electronic energy level differences between excited and ground states of the oxidized form of D-luciferin, the light emitting molecule in firefly bioluminescence.<sup>6</sup> Fortunately, luciferases also tolerate synthetic luciferins to catalyze light emitting reactions.<sup>7</sup> Recent studies have seen a great surge of interest in accessing synthetic luciferins emitting in the NIR region to improve bioluminescence imaging resolution for deep tissues (**Figure 4.1B**).<sup>8</sup> In 2014, James and co-workers synthesized the  $\pi$ -extended firefly luciferin analogue, infraluciferin (**3**), that emits NIR bioluminescence (706 nm) with a Fluc mutant.<sup>9</sup> Infraluciferin (**3**) showed weaker bioluminescence output compared to other synthetic luciferins, but 95% of the light from infraluciferin (**3**) was above 600 nm, where less attenuation by blood components occurs.<sup>9</sup> Another success story of luciferin development are naphthyl-luciferins (**4a**, **b**), which have an additional phenyl ring fused to the luciferin benzothiazole core of the D-luciferin to increase conjugation. These synthetic luciferins showed remarkable red-shifted NIR emission (**4a**: 743 nm, **4b**: 730 nm) with CBR2opt, which is a mutant luciferase from click beetle. Less scattering of signals from naphthyl-luciferin (**4b**) enabled

highly resolved bioluminescence imaging combined with a precise tomography.<sup>10</sup> However, these synthetic luciferins (**3**, **4a** and **4b**) show much lower photon production *in vivo* than D-luciferin (**1**). Maki and co-workers replaced the benzothiazole fragment with a  $\pi$ -conjugated phenyl group, and successfully developed a significantly red-shifted analogue, AkaLumine (**5**), whose emission maximum with native Fluc is located in the NIR (675 nm).<sup>11-12</sup> More recently, Iwano and co-workers have created a highly optimized engineered luciferase for AkaLumine (**5**), named Akaluc. The bioluminescence wavelength of the AkaLumine (**5**)/Akaluc pair is slightly blue-shifted, but still in the NIR region (650 nm). This fully-engineered bioluminescence imaging system known as "AkaBLI" allowed imaging of single-cells trapped in the mouse lung vasculature.<sup>13</sup> Hence, it can be said that the creation of both synthetic luciferins and mutant luciferases offers the potential to generate improved bioluminescence systems.

Although NIR bioluminescence imaging opens up the possibilities of *in vivo* deep tissue imaging even at single cell level, there is still less variety in NIR luciferins compared to the development of artificial luciferases.<sup>7</sup> Therefore, creation of a broad pallet of NIR luciferins would promote the expansion of bioluminescence applications as *in vivo* reporter systems. In particular AkaLumine (**5**) is a promising scaffold for bioluminescence imaging, since NIR emission is achieved with Fluc, the most commonly utilized luciferase. Although there is the possibility of additional structural modifications to AkaLumine (**5**), the structural elements required for NIR emission of AkaLumine still remain unclear. Some researchers have developed new analogues based on AkaLumine (**5**), but they have achieved only one further red-shifted analogue with significantly reduced bioluminescence activity.<sup>14-16</sup>

This chapter describes the expanded palette of NIR emitting luciferins in order to clarify the possibility of further red-shifted emission of AkaLumine (**5**)-based luciferins. I designed and synthesized a series of synthetic NIR luciferins (NIRLucs) via a ring fusion strategy, using AkaLumine (**5**) as a framework (**Figure 4.1C**). We also evaluated the basic and theoretical characteristics of NIRLucs and found that effective suppression of free rotation of the C-N bond of AkaLumine (**5**) resulted in a new class of structure-inherent NIR emitting luciferins with further bathochromic shift. NIRLucs were cell-membrane permeable and displayed dose-independent NIR emission when applied to cells expressing luciferase even at low concentrations where D-luciferin (**1**) does not emit. Finally, we demonstrated the *in vivo* application with one of the NIRLucs in mice bearing subcutaneous tumors. This work provides a variety of NIR emitting luciferins and is expected to have the potential for expanding *in vivo* bioluminescence imaging applications.

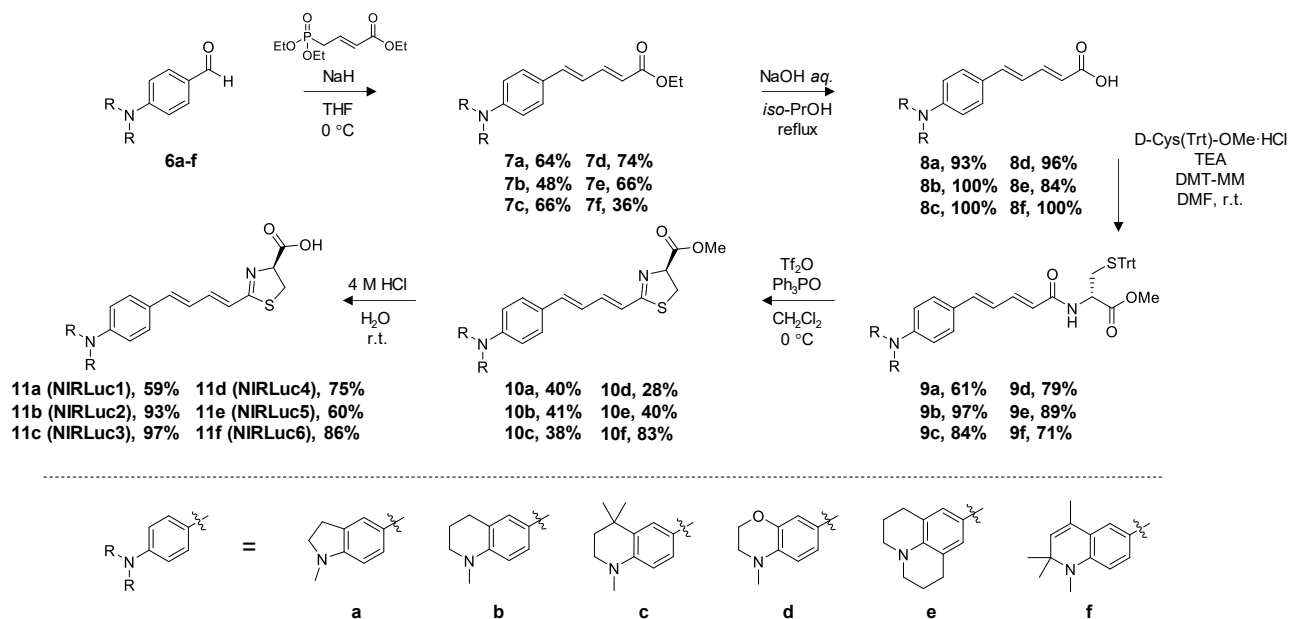
**(A) Firefly Bioluminescence****(B) Previous work** : Synthetic NIR emitting Luciferins**(C) This work** : Expanded NIR Luciferin Palette

**Figure 4.1. Reaction of firefly luciferin and chemical structures of NIR emitting luciferins.** (A) Firefly bioluminescence: Luciferase catalyzes the adenylation and oxidation of luciferin to release a photon. (B) Previously reported synthetic NIR emitting luciferins. (C) Newly synthesized NIR emitting analogues based on the AkaLumine (**5**) scaffold.

## 4.2. Results and Discussion

### 4.2.1. Design and synthesis of NIRLucs

It is well known that the thiazoline fragment in firefly luciferin plays a crucial role in light emission.<sup>17</sup> In fact, most successful luciferin analogues retain the thiazoline moiety in their structure.<sup>7, 18-20</sup> Contrariwise, the benzothiazole fragment is the moiety tolerant to chemical modification, controlling the emission wavelength. A wide variety of luciferin analogues, including those with NIR emission, have been developed based on alterations to this subunit. I selected the AkaLumine (**5**) structure, one of the successful NIR emitting analogues, as the framework for the development of a series of NIR emitting luciferins. Previous studies revealed that a minor alteration of the *N,N*-dimethyl amino group in AkaLumine (**5**) might retain the NIR emission *in vitro*.<sup>15</sup> In order to develop the pallet of structure-inherent NIR luciferins, I focused on the ring fusion strategy in anticipation of further extension of the bioluminescence emission into the deeper NIR. In classical xanthene dyes such as rhodamine, Atto and Alexa fluorophores, it has been reported that red-shifted fluorescence emission can be achieved by introducing cyclization of the aryl amine.<sup>21</sup> This is explained by a decrease in the HOMO-LUMO energy gap due to the extension of the conjugated system. A similar modification has also been reported for firefly luciferin by Miller and co-workers and led to successful extension of bioluminescence emission up to 648 nm.<sup>22-23</sup> It was speculated that increased rigidity of the luciferin would lead to NIR bioluminescence emission. With all of these previous results in mind, it was envisioned that a panel of novel luciferins emitting in the NIR range beyond 675 nm (maximal emission wavelength for AkaLumine (**5**)/Fluc) can be developed based on the ring fusion structure. The **NIRLucs** have been prepared from the corresponding benzaldehydes according to the reported scheme (**Scheme 4.1**).<sup>15</sup> Olefination of each aldehyde via Horner-Wadsworth-Emmons reaction furnished the desired stereoselective diene esters (**7**), which were hydrolyzed under alkaline condition to give carboxylic acid products (**8**). The condensation reaction with *S*-trityl protected D-cysteine methyl ester afforded amides (**9**). The thiazoline ring (**10**) was formed via Tf<sub>2</sub>O-TPPO mediated intramolecular cyclization. Finally, acid catalyzed hydrolysis gave luciferins (**11**) as a single pure product with acceptable enantiopurity (>80% e.r.).



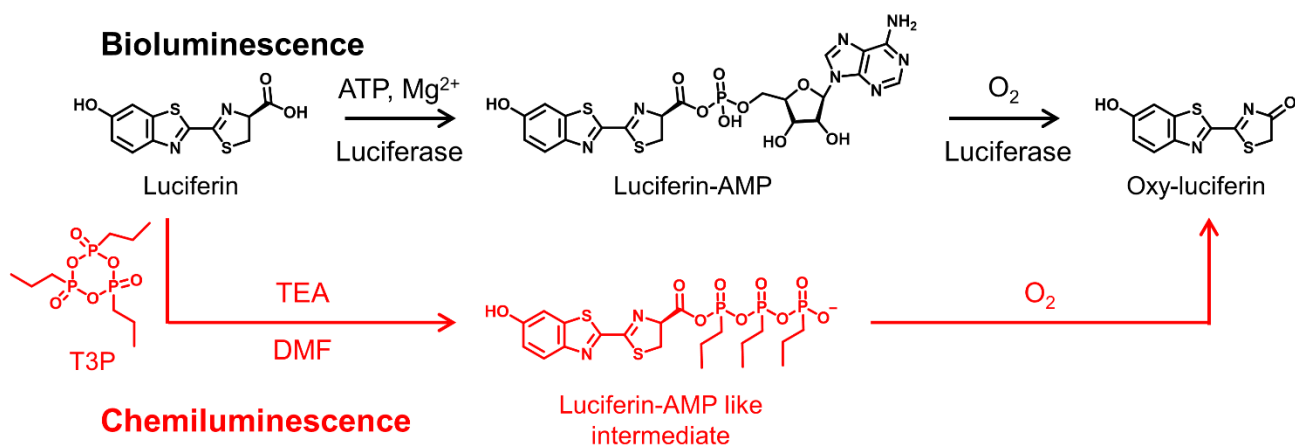
Scheme 4.1. Synthesis of NIRLucs

## 4.2.2. Evaluation of light emitting potential of NIRLucs

With the synthesized analogues in hand, I firstly evaluated the light emitting potential of the synthetic luciferins. Firefly luciferin is known to glow chemiluminescence induced by *n*-propylphosphonic anhydride (T3P) and triethyl amine (TEA) in DMF.<sup>24</sup> This non-enzymatic light production involves the formation of an activated acyl-phosphonic acid intermediate followed by oxidative reaction, which mimics the luciferase catalyzed bioluminescence reaction (**Figure 4.2A**). Once T3P was added into luciferin solutions, robust light emission was observed from all synthesized analogues. Their chemiluminescence emission wavelengths were found to be located in the NIR region as expected (**Figure 4.2B, Table 4.1**). In addition, all ring fusion luciferins showed up to 32 nm longer emission wavelength (**NIRLuc5**: 697 nm) than the non-fused luciferin, AkaLumine (**5**). These results suggested that further bathochromically-shifted bioluminescence emission might be elicited on the basis of the AkaLumine (**5**) scaffold through effective restriction of the freely rotatable C-N bond.

In order to clarify whether these wavelength shifts are an inherent capacity of the luciferins, fluorescence spectroscopic assays were performed. Previous studies revealed that fluorescence and bioluminescence emission are well correlated, meaning that the photophysical properties of the luciferin are an important factor to determine the potential emission color.<sup>22</sup> In the luminescence reaction, the actual light emitter is the oxidized form of the luciferin. However, firefly oxyluciferin is known to be chemically unstable, and it is difficult to evaluate. Hirano and co-workers have reported that there is a strong correlation between fluorescence properties of luciferins and oxyluciferins.<sup>25</sup> Instead of evaluation of oxyluciferin, it was decided to study the fluorescence properties of the

(A)



(B)

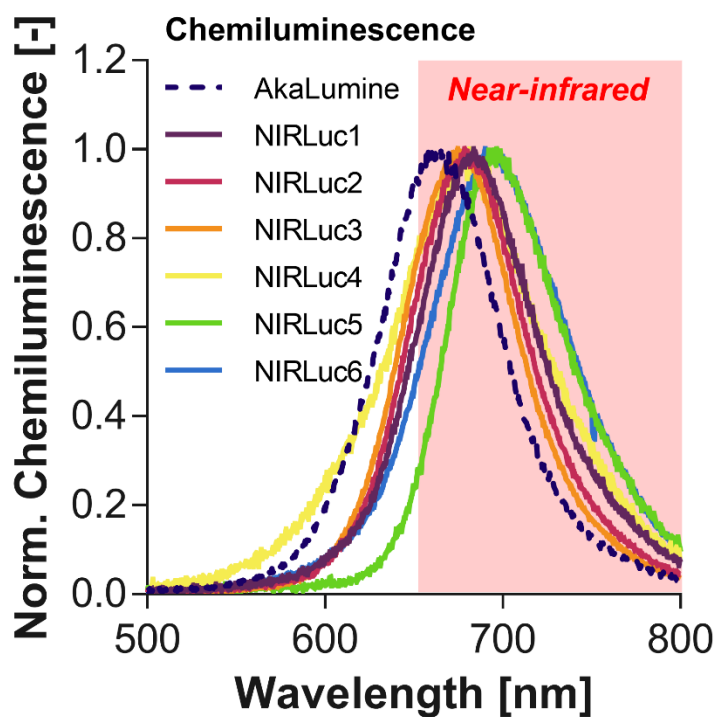


**Figure 4.2. Chemiluminescence of NIRLucs.** (A) Chemical conversion pathways of luciferin to oxyluciferin in bioluminescence (black) and chemiluminescence (red). (B) Normalized chemiluminescence spectra of AkaLumine (5) and the **NIRLucs** with T3P and TEA in DMF.

luciferins. When determining their fluorescence emission wavelength in 50 mM GTA buffer (pH 8.0), it was found that all analogues show longer fluorescence wavelength than AkaLumine (**5**), similar to the chemiluminescence spectra (**Figure 4.3, Table 4.1**). Therefore, each luciferin were evaluated. Bioluminescence quantum yield  $\varphi_{BL}$ , indicating the number of photons emitted in the bioluminescence reaction, is expressed by the following equation (eq. 1):

$$\varphi_{BL} = \varphi_{FI}\varphi_R\varphi_{ES} \quad (1)$$

where  $\varphi_{FI}$  is the fluorescence quantum yield of the oxyluciferin,  $\varphi_R$  is the reaction yield of the oxyluciferin formation from the corresponding luciferin, and  $\varphi_{ES}$  is the production yield of oxyluciferin in the excited state.<sup>26-27</sup> Therefore, the fluorescence quantum yield of the oxyluciferin is one of the dominant factors determining the photon output. It has been reported that styrenyl analogues show much lower fluorescence quantum yields than benzothiazole-type luciferins such as native D-luciferin (**1**).<sup>15</sup> I simply evaluated the fluorescence quantum yields of **NIRLucs** compared to AkaLumine (**5**) in order to confirm the effect of restriction of C-N bond rotation. The fluorescence quantum yields of each luciferin were determined by absolute measurements using a fluorometer equipped with an integral sphere. Against all expectations, the fluorescence quantum yields of ring-fused luciferins remained unchanged as compared to AkaLumine (**5**), even though C-N bond rotation was suppressed by the rigid chemical structure (**Table 4.1**). Therefore, the restriction of freely rotatable C-N bond was not considered to be a dominant factor in the reduced fluorescence quantum yield of the styrenyl analogues.

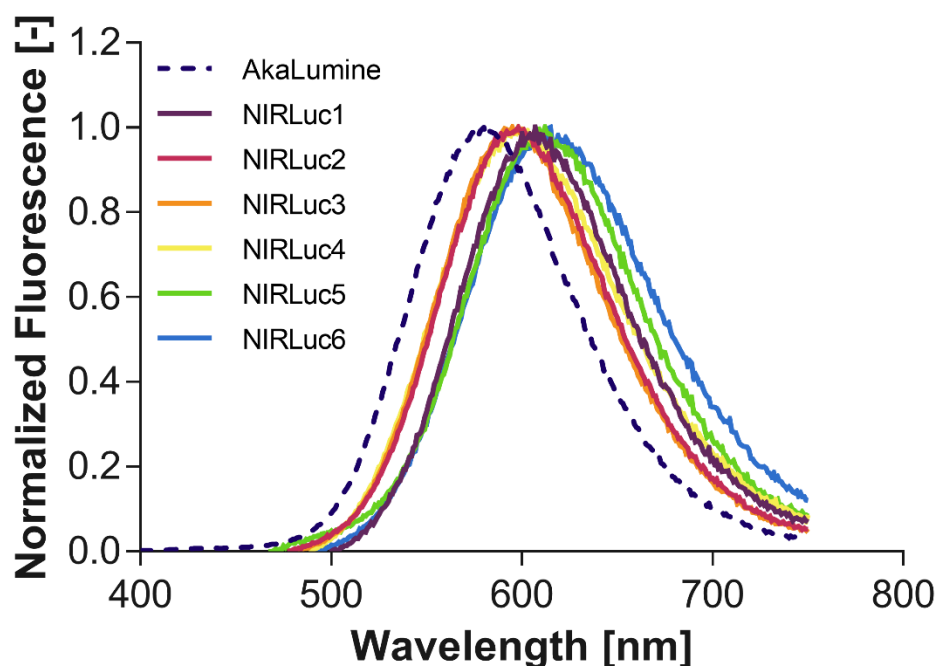


**Figure 4.3. Normalized fluorescence emission spectra of AkaLumine and NIRLucs in 50 mM GTA buffer (pH 8.0).**  $\lambda_{Ex} = 375$  nm

### 4.2.3. Bioluminescence activity *in vitro*

The bioluminescence emission wavelengths of **NIRLucs** with Fluc were evaluated. The results clearly indicate that all synthetic luciferins are competent light emitters and can be accommodated by native Fluc, like the native D-luciferin (**1**) substrate. As expected, peak bioluminescence emission for **NIRLucs** was almost identical to chemiluminescence emission wavelengths and ranged from 680 nm to 690 nm, which is longer than the wavelength of AkaLumine (**5**) (**Figure 4.4, Table 4.1**). It should be noted that the near-infrared emission of **NIRLucs** is of significance when it comes to light transmission through biological tissues. **NIRLuc2** displayed a smaller blue-shifted peak emission around 560 nm, in addition to the NIR peak. This minor peak suggests that the light emitter of **NIRLuc2** produced inside the active site of the luciferase has two different conformations. Similar behavior has been reported for other synthetic luciferins.<sup>10, 15</sup>

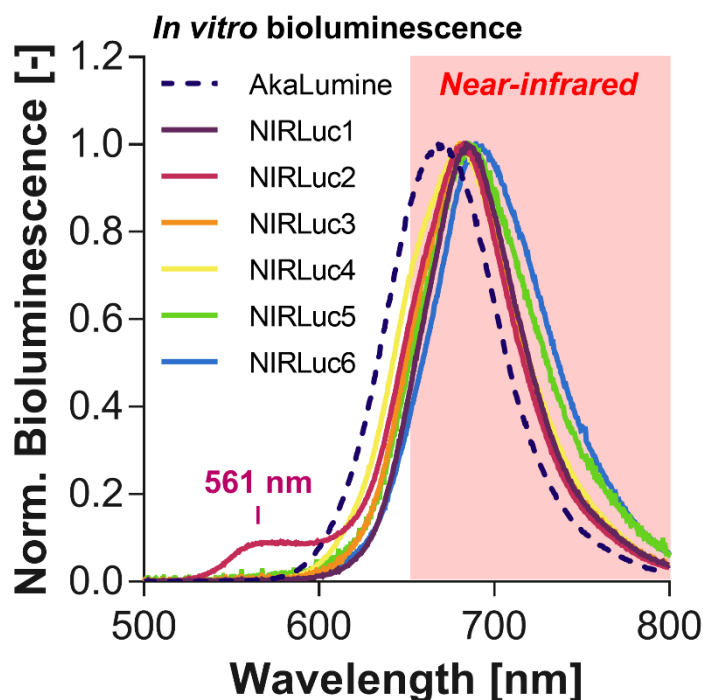


**Figure 4.4.** Bioluminescence emission spectra of AkaLumine (**5**) and the NIRLucs with native Fluc.

Dose-dependent bioluminescent emission intensities were measured using a PMT-based luminometer. As a result, with the luciferin concentration increased, emission intensities integrated over 60 sec were enhanced and reached saturation around at 1  $\mu$ M (**Figure 4.5**). Although **NIRLuc2** and **NIRLuc4** showed robust light emission, **NIRLuc3**, **NIRLuc5** and **NIRLuc6** gave particularly weaker (less than one tenth) light output than the other compounds. These analogues have a relatively bulky

chemical structure, which could likely inhibit the luciferase catalyzed light emitting reaction. As with other firefly luciferins, **NIRLucs** displayed a sharp increase in photon output after addition of ATP-Mg<sup>2+</sup> solution (**Figure 4.6**). AkaLumine (**5**), **NIRLuc1** and **NIRLuc4** showed an immediate onset of light emission reduction. This is presumably due to product inhibition as previously discussed for synthetic luciferins.<sup>22-23, 28</sup> In contrast, **NIRLuc2**, **NIRLuc3**, **NIRLuc5** and **NIRLuc6** emitted a relatively sustained emission. In particular, **NIRLuc2** exhibited more stable emission rates compared to those of AkaLumine (**5**).

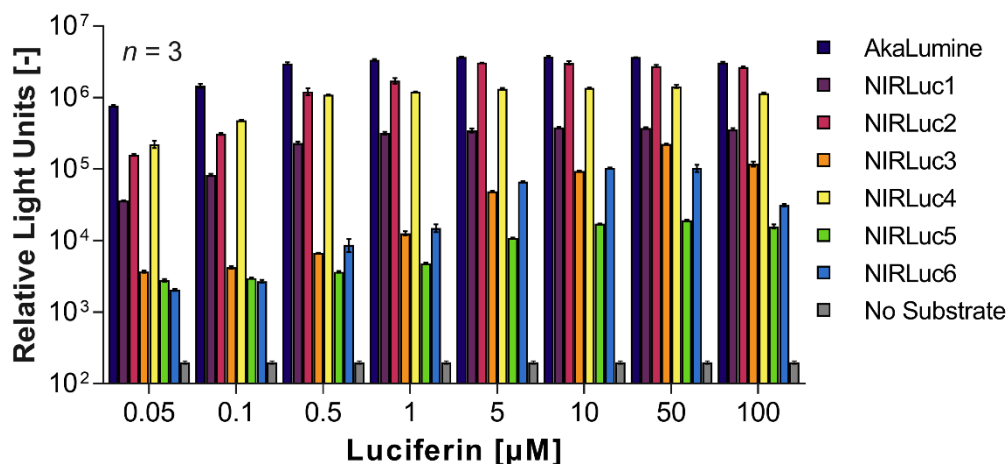


**Figure 4.5. Dose-dependent bioluminescent emission intensities:** 0.05-100  $\mu\text{M}$  luciferins incubated with 5.0  $\mu\text{g}/\text{mL}$  native Fluc in 50 mM GTA buffer (pH 8.0). Integrated values of the light emission intensities for the first 60 sec post addition of an ATP-Mg solution. Error bars represent the standard deviation of the mean for triplicate experiments.

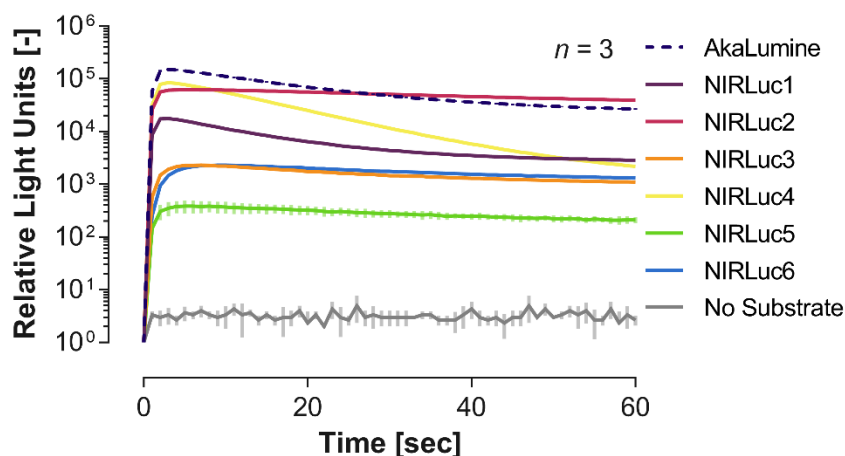


**Figure 4.6. Burst kinetic profiles of 10  $\mu\text{M}$  of each luciferin with 5.0  $\mu\text{g}/\text{mL}$  native Fluc in 50 mM GTA buffer (pH 8.0).** The bioluminescence reaction was initiated by addition of ATP-Mg<sup>2+</sup>, and monitored every 1 sec for 60 sec. The background signal in the absence of substrate is shown as a reference. Error bars represent the standard deviation of the mean for triplicate experiments.

The kinetic analysis revealed that **NIRLuc3**, **NIRLuc5** and **NIRLuc6** had relatively larger apparent  $K_m$  values and reduced  $V_{max}$  values (**Figure 4.7**, **Table 4.1**). As mentioned earlier, steric modification might hamper the efficiency of the light emission reaction process. The  $K_m$  value for **NIRLuc1** was comparable to that of AkaLucine (**5**), but it showed a 10-fold reduced  $V_{max}$  value. This result suggests that NIRLuc1 fits inside the luciferase, but the catalytic luminescence reaction might be hindered. Although **NIRLuc2** and **NIRLuc4** have slightly inferior  $K_m$  and  $V_{max}$  values, respectively, they are latent light emitters that can be used for imaging applications.

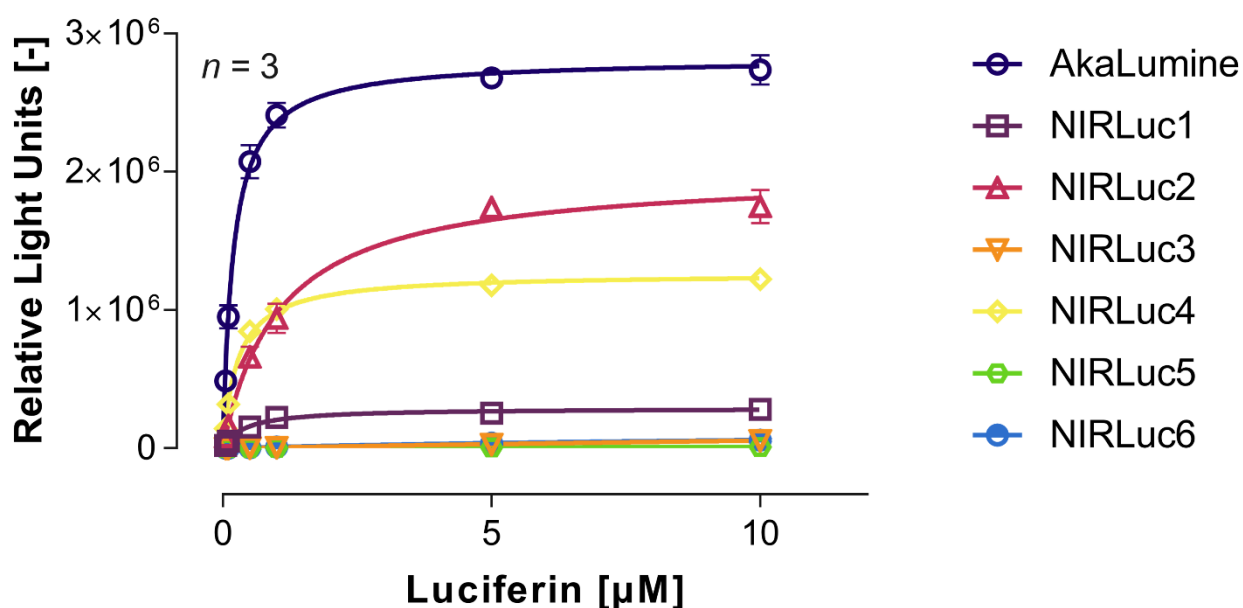


**Figure 4.7. Luciferin saturation assay with increasing concentration of luciferins (0.05-10 μM).** The  $K_m$  and  $V_{max}$  values of each luciferin were determined by Michaelis–Menten nonlinear regression analyses in GraphPad Prism (version 7.03 for Windows, GraphPad Software). The theoretical equation is described as follows:

$$v = \frac{V_{max}[S]}{K_m + [S]} \quad (2)$$

Error bars represent the standard deviation of the mean for triplicate experiments.

For practical applications, the emission spectra were also investigated under physiological pH conditions. It is widely known that bioluminescence spectra of D-luciferin (**1**) are strongly affected by pH values.<sup>29</sup> pH-Insensitivity of the emission wavelength is most desirable, because pH-dependent spectral shifts are sometimes problematic for imaging applications. The bioluminescence emission of AkaLucine (**5**) and **NIRLucs** was measured at various pH values ranging from 5.5-8.5. Consequently, all **NIRLucs** exhibited similar emission trends across the physiological pH range (**Figure 4.8**, **4.9**).

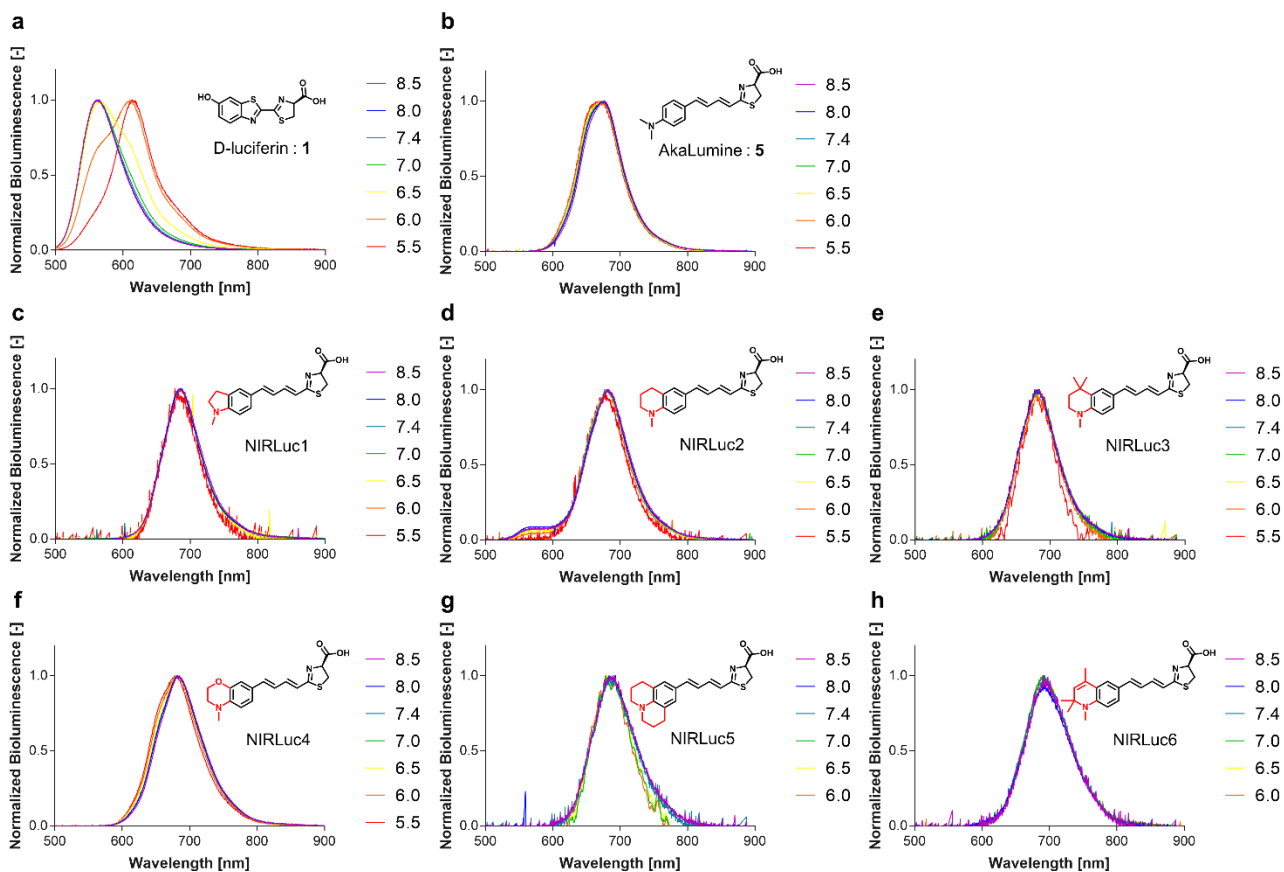


**Figure 4.8. pH-Dependence of bioluminescence spectra of D-luciferin (a), AkaLumine (b) and NIRLucs (c-h) with Fluc in 50 mM GTA buffer (pH 5.5-8.5).** The emission wavelength of D-luciferin with Fluc changes from green to red under acidic condition. In contrast, the bioluminescence emission wavelengths of AkaLumine and NIRLucs were pH independent. The spectra for NIRLuc5 and NIRLuc6 at pH 5.5 could not be obtained due to poor light emission.

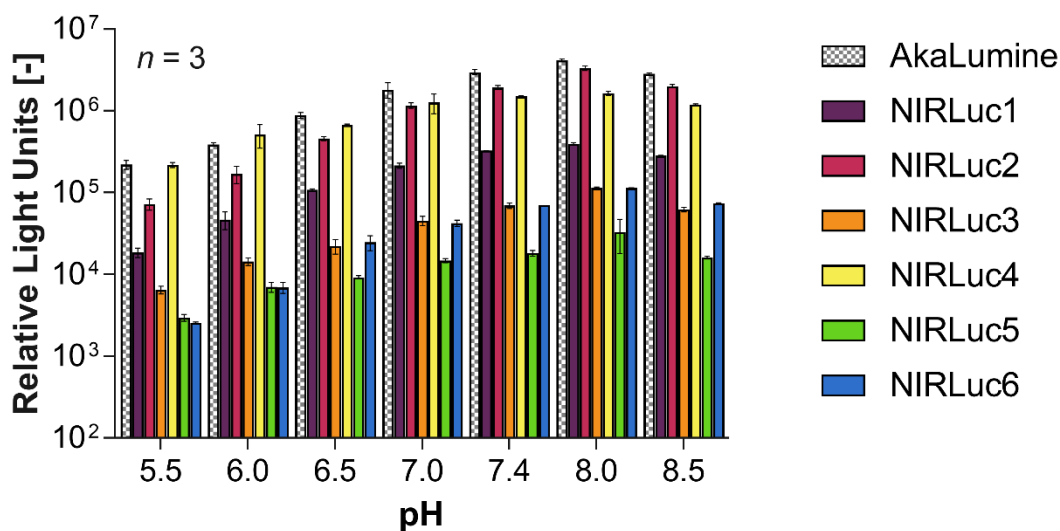


**Figure 4.9. pH-Dependence of bioluminescence emission intensities:** 10  $\mu$ M luciferins incubated with 5.0  $\mu$ g/mL native Fluc in 50 mM GTA buffer (pH 5.5-8.5). Light emission intensities integrated over 60 s. Error bars represent the standard deviation of the mean for triplicate experiments.

**Table 4.1. Characteristics of AkaLumine (5) and NIRLucs.**

Compound	$\lambda_{Fl}^a$ [nm]	$\varphi_{Fl}^b$ [-]	$\lambda_{CL}^c$ [nm]	$\lambda_{BL}^d$ [nm]	$K_m^e$ [ $\mu$ M]	$V_{max}^e$ [ $\times 10^5$ ]
AkaLumine	583	0.025	665	675	0.20 $\pm$ 0.01	28.2 $\pm$ 0.4
NIRLuc1	606	0.017	684	684	0.41 $\pm$ 0.05	2.90 $\pm$ 0.07
NIRLuc2	594	0.029	679	561*, 683**	1.05 $\pm$ 0.10	20.0 $\pm$ 0.5
NIRLuc3	601	0.030	675	684	29.1 $\pm$ 1.2	2.17 $\pm$ 0.04
NIRLuc4	596	0.021	682	680	0.28 $\pm$ 0.02	12.6 $\pm$ 0.2
NIRLuc5	613	0.021	697	686	3.55 $\pm$ 1.65	0.13 $\pm$ 0.02
NIRLuc6	613	0.025	690	690	13.8 $\pm$ 1.5	1.43 $\pm$ 0.10

<sup>a</sup>  $\lambda_{Ex}$  = 375 nm, <sup>b</sup> Absolute fluorescence quantum yield in 50 mM GTA buffer (pH 8.0), <sup>c</sup> Chemiluminescence emission maxima, <sup>d</sup> Bioluminescence emission maxima with native Fluc, <sup>e</sup>  $K_m$  and  $V_{max}$  values were determined using nonlinear Michaelis -Menten regression analyses in GraphPad Prism (version 7.03 for Windows, GraphPad Software). \* minor peak, \*\* major peak.

#### 4.2.4. Theoretical calculation of oxy-NIRLucs

In order to theoretically support the cause of the red-shifted emission of **NIRLucs**, density functional theory (DFT) and time-dependent density functional theory (TD-DFT) calculations were employed. Quantum chemical calculations of the oxidized form of each luciferin were carried out at the B3LYP/6-31+G (d) level theory (**Figure 4.10, 4.11**). The results showed that restriction of the conformational flexibility of the rotatable *N,N*-dimethyl amino group in AkaLumine (**5**) tends to greatly influence the HOMO energy level. (**Figure 4.10, Table 4.2**). The electron distributions for the HOMO and LUMO of **NIRLucs** are similar to those of AkaLumine (**5**), suggesting that they exhibit charge-transfer characteristics during the light emitting process as previously reported.<sup>16</sup> The theoretically calculated transition wavelengths ( $\lambda_{tr}$ ) between HOMO-LUMO are also support the trend towards red-shifted emission as in the spectroscopic measurements of **NIRLucs** shown above. The computationally calculated wavelengths correlated with the experimentally observed values (**Figure 4.12**). Thus, the structure-inherent bathochromic-shifts in **NIRLucs** are theoretically supported through quantum chemical calculations.

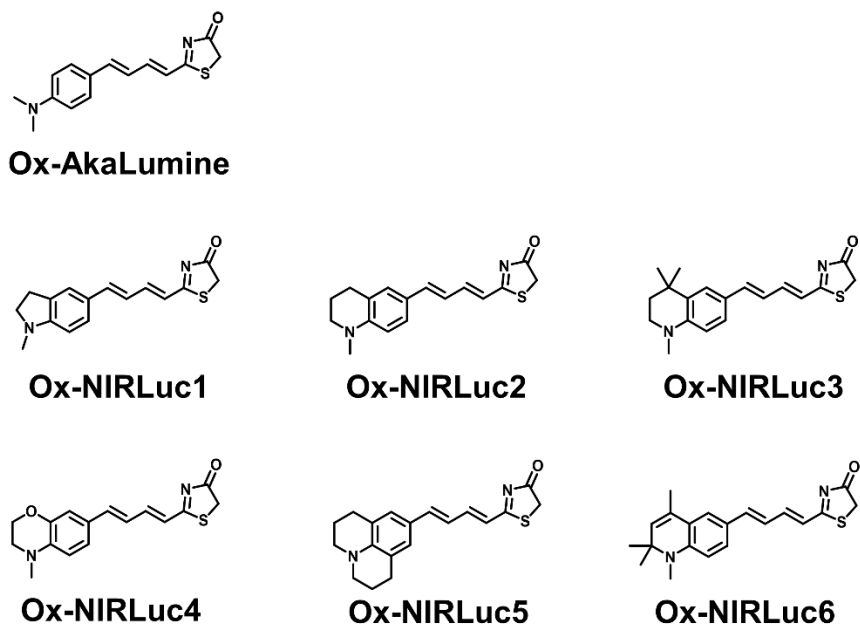


Figure 4.10. Chemical structures of oxidized forms of AkaLumine (5) and NIRLucs.

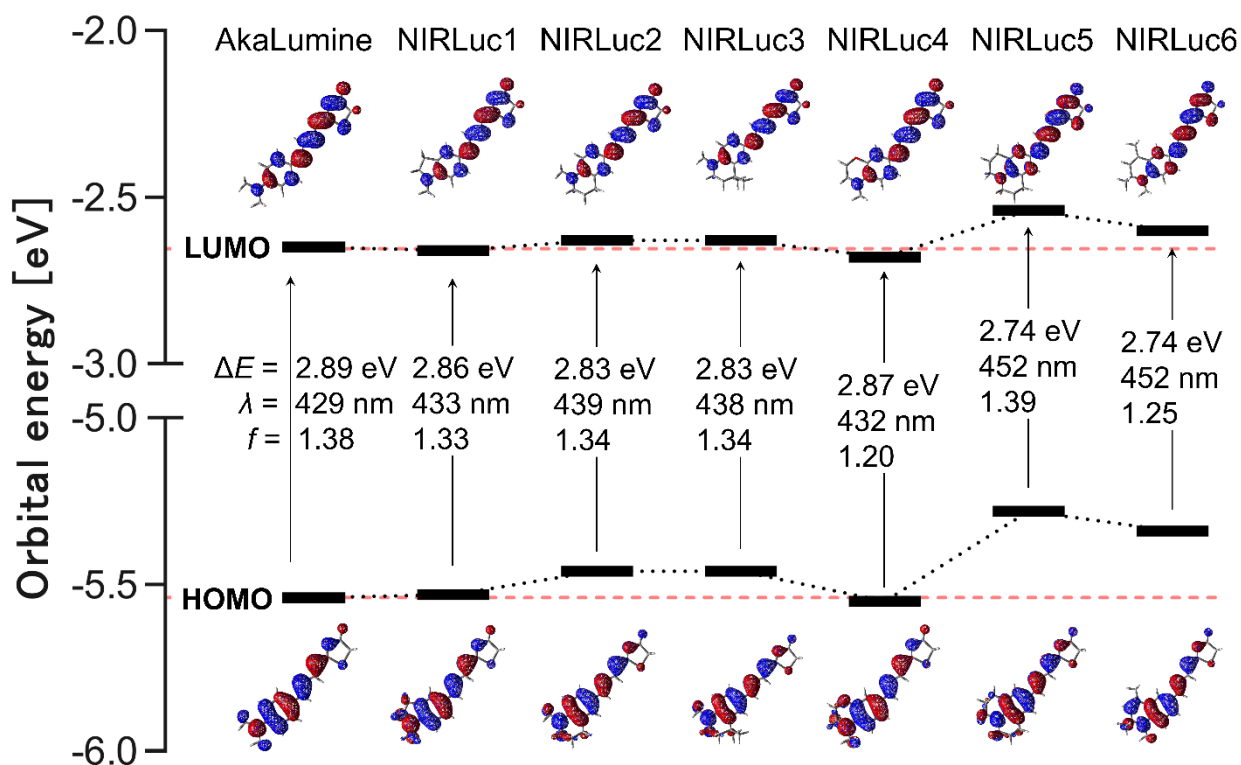
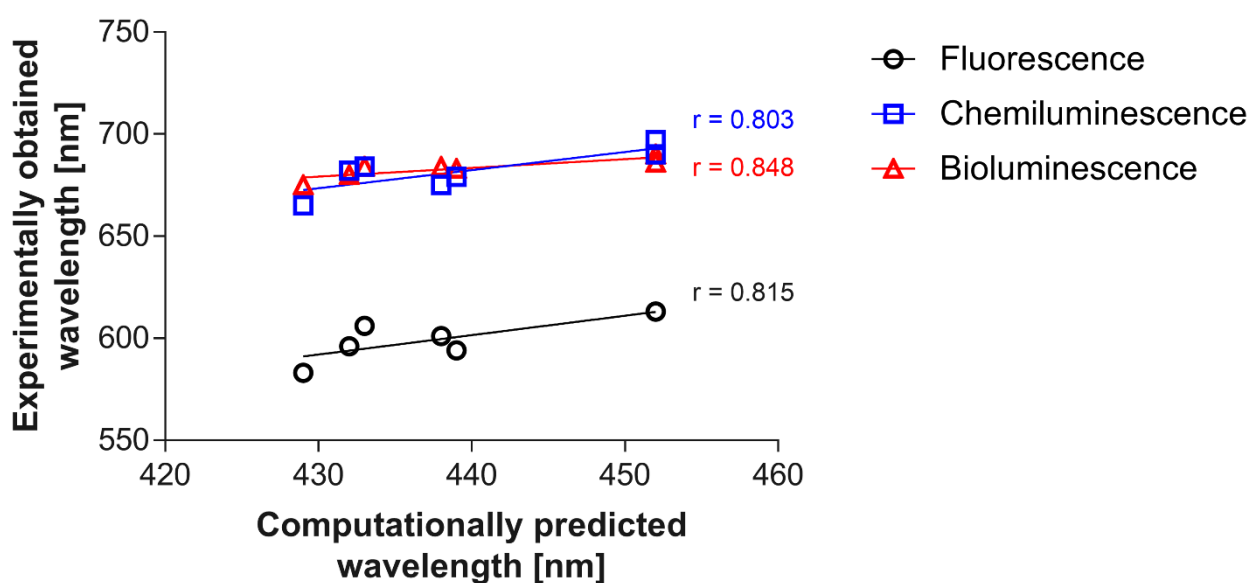


Figure 4.11. Comparison of HOMO (bottom) and LUMO (top) energy levels for the oxidized form of AkaLumine (5) and NIRLucs, calculated at the B3LYP/6-31+G (d) level. Red dashed lines indicate the HOMO and LUMO energy level of AkaLumine (5).

**Table 4.2. Calculated Frontier orbitals and oscillator strengths of AkaLucime (5) and NIRLucs at the basis of B3LYP/6-31+G(d).**

Compound	HOMO [eV]	LUMO [eV]	$\Delta E^a$ [eV]	$\lambda_{tr}^b$ [nm]	Oscillation strength [-]	$\varphi_{Fl}^c$ [-]
AkaLucime	-5.54	-2.65	2.89	429	1.38	0.025
NIRLuc1	-5.53	-2.66	2.86	433	1.33	0.017
NIRLuc2	-5.46	-2.63	2.83	439	1.34	0.029
NIRLuc3	-5.46	-2.63	2.83	438	1.34	0.030
NIRLuc4	-5.55	-2.68	2.87	432	1.20	0.021
NIRLuc5	-5.28	-2.54	2.74	452	1.39	0.021
NIRLuc6	-5.34	-2.60	2.74	452	1.25	0.025

<sup>a</sup> Energy band gap between HOMO-LUMO, <sup>b</sup> calculated transition wavelengths from energy band gap, <sup>c</sup> Absolute fluorescence quantum yield in 50 mM GTA buffer (pH 8.0).

**Figure 4.12. Correlation between calculated wavelengths and experimentally obtained wavelengths.**

Computationally predicted wavelengths were calculated at the B3LYP/6-31+G(d) level without inclusion of solvent effects using the Gaussian 09 program. r: Pearson correlation value.

### 4.2.5. Light emission in luciferase-expressing live cells

Encouraged by the *in vitro* results, the utility of **NIRLucs** as optical reporter in more practical applications was examined. For this purpose, stably luciferase expressing B16-F10 cells, a mouse melanoma cell line forming malignant melanoma, were selected. The **NIRLucs** were compared with AkaLumine (**5**) and the conventionally utilized native D-luciferin (**1**) substrate in live cells. When used as optical reporters, the light output from luciferins should reflect the luciferase expression level. It was first confirmed that the photon flux from **NIRLucs** showed a linear correlation with increasing number of luciferase-expressing B16-F10 cells (**Figure 4.13**).

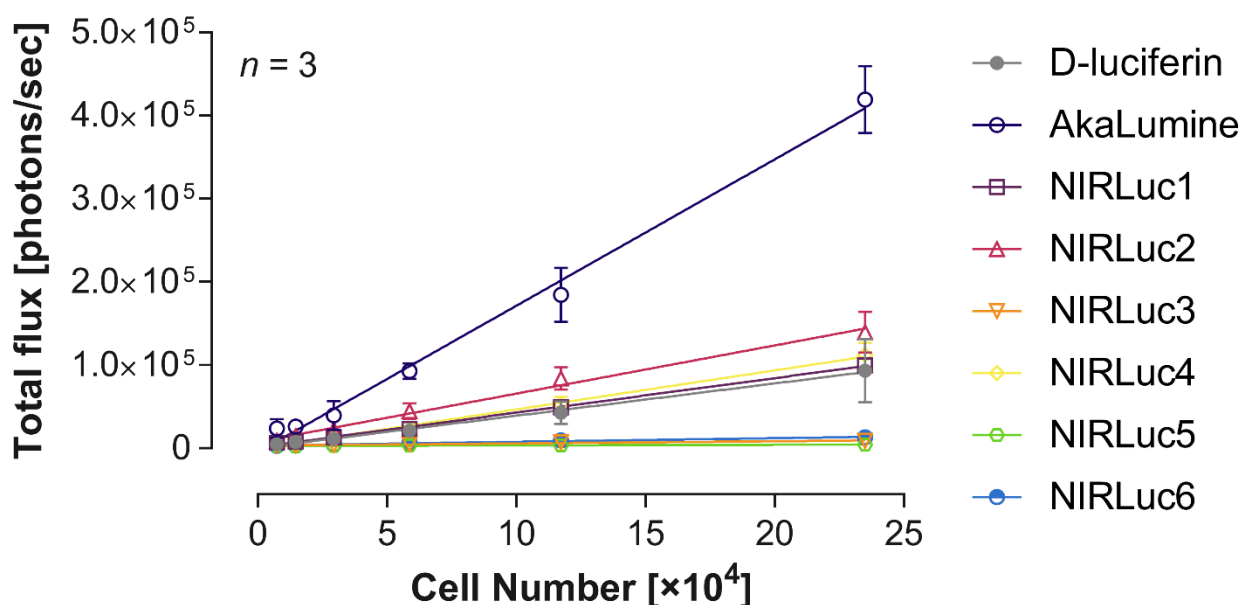


**Figure 4.13. Cell number-dependent bioluminescence of stably luciferase-expressing B16F10 cells with 25  $\mu\text{M}$  luciferins.** Error bars represent the standard error of the mean. Exposure time: 180 sec.

Then, the dose-dependent photon output after treatment of B16-F10 cells with different concentrations of luciferins (0.25-250  $\mu\text{M}$ ) was assessed in a black 96-well clear bottom plate by photon flux imaging. The photon output generated by AkaLumine (**5**) and **NIRLucs** displayed less dose-dependency, whereas the signals from D-luciferin (**1**) showed significant decrease as the substrate concentration was lowered (**Figure 4.14A**). Compared to D-luciferin (**1**), **NIRLuc1** (7-fold), **NIRLuc2** (22-fold) and **NIRLuc4** (16-fold) presented brighter signals at  $<2.5 \mu\text{M}$  concentration. This is due to their relatively lower  $K_m$  values, which leads to saturation of luciferase inside cells at much lower concentrations. In fact, the bioluminescence emission from **NIRLucs** with relatively higher  $K_m$

values such as **NIRLuc3**, **NIRLuc5** and **NIRLuc6** were dramatically reduced below 250  $\mu\text{M}$  substrate concentration. This dose-independency of photon output is a suitable feature for a luminescent reporter, since the *in vivo* luciferin concentrations commonly reach low values. The bioluminescence emission in the NIR range, where tissue is more light transparent, was also evaluated using a  $680 \pm 10$  nm band pass filter. The signals emitted in the NIR range from **NIRLuc1**, **NIRLuc2** and **NIRLuc4** were also less dose-dependent, and clearly stronger than that of D-luciferin (**1**) even at a substrate concentration as low as 0.25  $\mu\text{M}$ , owing to their structure-inherent NIR emission (Figure 4.14B). From time dependent imaging of luminescence signals, it was found that the light output of **NIRLuc4** was greatly reduced to less than 25% of its initial level already 5 min after substrate addition, despite **NIRLuc4** showing a high initial rate of light emission (**Figure 4.15**). This effect was also observed in *in vitro* experiments (**Figure 4.6**) and presumed to be due to product inhibition as the primary factor.<sup>22</sup> The results from cellular experiments strongly support the advantage of **NIRLucs**, which appear to be preferable substrates compared to D-luciferin (**1**) especially for *in vivo* imaging, as they work at lower doses (0.25  $\mu\text{M}$ ) and show NIR emission (684~698 nm).

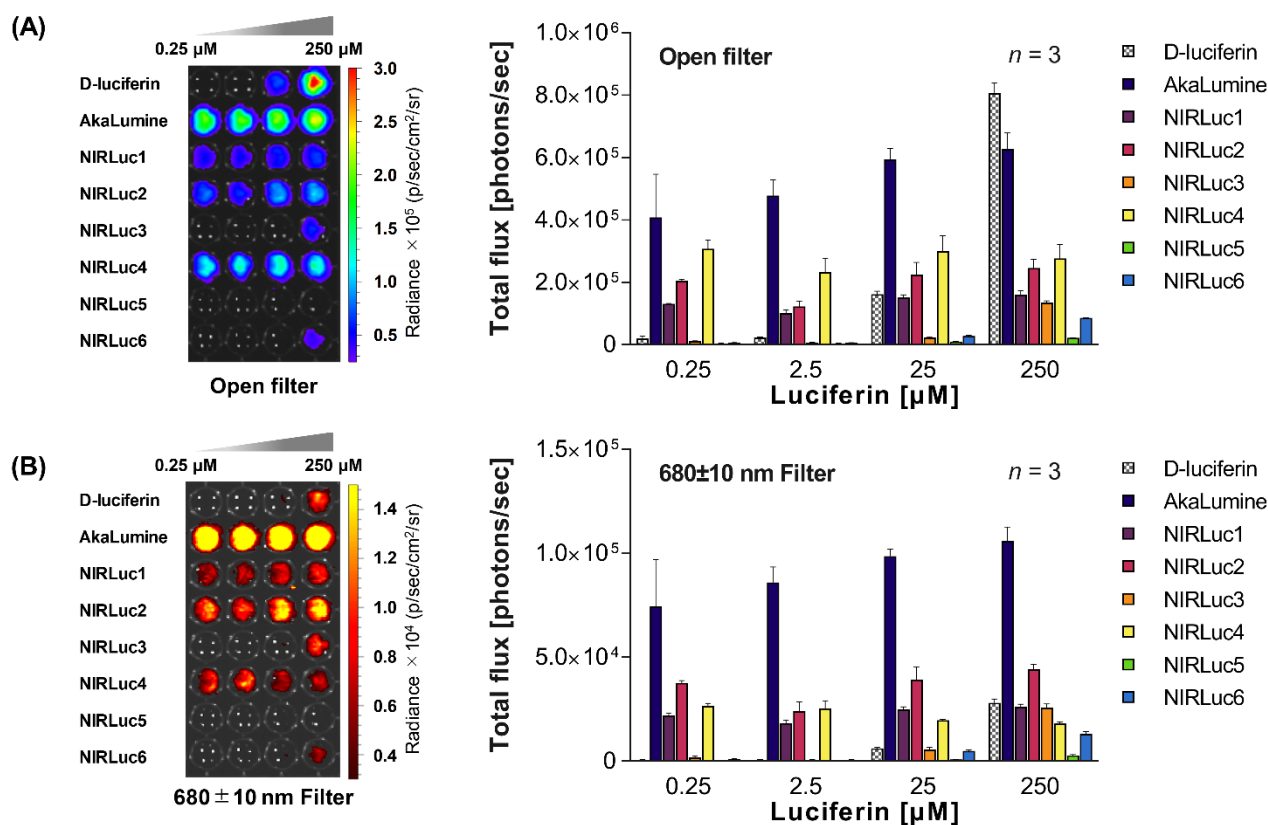


**Figure 4.14. Dose-response photon flux from luciferase-expressing cells:** 0.25-250  $\mu\text{M}$  luciferins were incubated into stably luciferase-expressing B16-F10 cells with open filter (A) or NIR (680  $\pm$  10 nm) filter (B). Error bars represent the standard error of the mean for triplicate experiments. Exposure time: 60 sec.

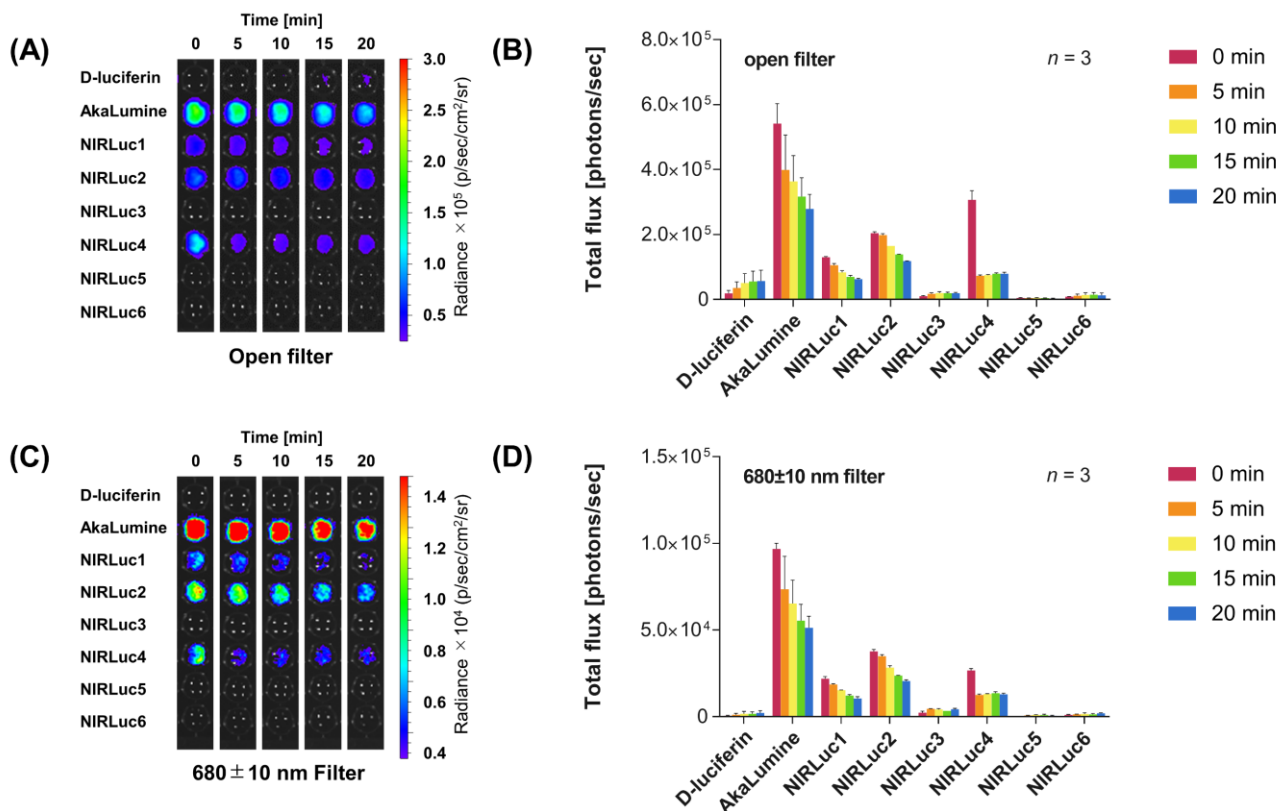


**Figure 4.15. Time-dependent photon output from stably Fluc-expressing B16F10 cells treated with 0.25 μM luciferins.** (A, C) Bioluminescence imaging of cells with open filter (A) or NIR (680±10 nm) filter (C). (B, D) Quantification of the imaged bioluminescent signals with open filter (B) or NIR (680±10 nm) filter (D). Error bars represent the standard error of the mean for triplicate experiments. Exposure time: 60 sec.

#### 4.2.6. *In vivo* applications of NIRLuc2 to mice bearing subcutaneous tumors

Comprehensively considering the *in vitro* and *in cellulo* performance, **NIRLuc2** was selected as a preferred candidate for *in vivo* applications and studied accordingly. Firstly, the blood retention of **NIRLuc2** was evaluated in comparison with D-luciferin (**1**) and AkaLumine (**5**) by intravenous injection of 5 mM of each luciferin solution (100 μL) in PBS (-) into ICR mice. The blood was sampled from the tail vein and mixed with Fluc to produce bioluminescence signals. It is noteworthy that the blood retention of **NIRLuc2** was relatively longer ( $t_{1/2} = 17.8$  min) than that of D-luciferin (**1**) ( $t_{1/2} = 3.5$  min) and AkaLumine (**5**) ( $t_{1/2} = 7.9$  min) (**Figure 4.16**). This different behavior might be due to the differences in pharmacokinetics depending on the hydrophobicity of each luciferin. The luciferins are considered to be predominantly existing in the carboxylate form in blood (pH ≈ 7.4).<sup>30</sup> The ClogP values estimated for the carboxylate form of luciferins are -0.02 for D-luciferin (**1**), 1.27 for AkaLumine (**5**) and 1.93 for **NIRLuc2**, respectively, suggesting a correlation with blood retention.

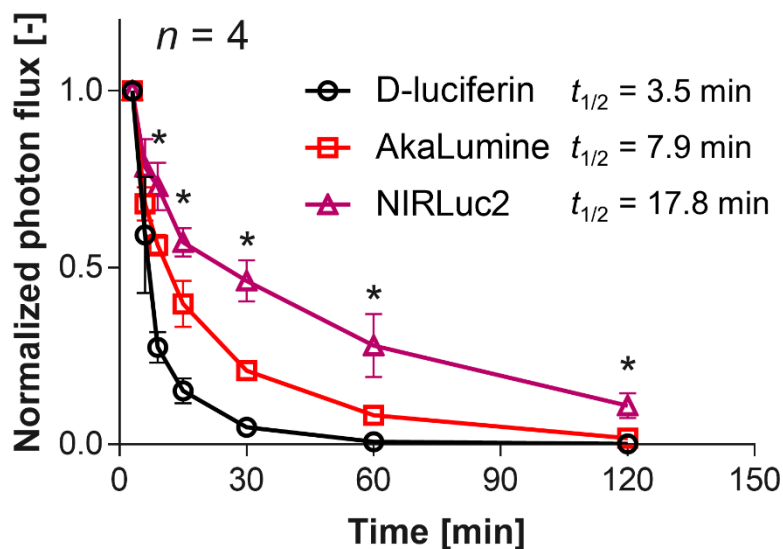


**Figure 4.16. Blood retention of NIRLuc2, D-luciferin (1) and AkaLumine (5) in ICR mice ( $n = 4$ ).**  $*P < 0.05$  ( $t$ -test), compared to AkaLumine (5). Error bars represent the standard error of the mean for quadruplicate experiments.

Finally, a comparative bioluminescence imaging study in mice bearing subcutaneous tumors was conducted to evaluate the performance of **NIRLuc2** *in vivo*.  $5 \times 10^5$  stably luciferase expressing B16-F10 cells were subcutaneously implanted to the right dorsolateral side of C57BL/6J mice and grown tumors were monitored 2 weeks later. The luciferins (5 mM, 100  $\mu$ L) were intravenously injected to the tumor bearing mice and the bioluminescence signals imaged. **NIRLuc2** also displayed structure-inherent NIR bioluminescence from subcutaneous tumors as well as the reaction with recombinant Fluc *in vitro* (**Figure 4.17**). The photon flux from D-luciferin (1) significantly decreased over time after intravenous injection, whereas those from AkaLumine (5) and **NIRLuc2** reached a peak 6 min after administration (**Figure 4.18**). Moreover, the photon output from **NIRLuc2** was less strongly time-dependent than that from AkaLumine (5), presumably owing to longer blood retention and higher affinity to the luciferase. Quantitative analysis revealed that the photon flux of **NIRLuc2** from tumors 15 min after intravenous injection outperformed the one from D-luciferin (1) (7-fold for open filter, 16-fold for NIR) and was not statistically different ( $P > 0.05$ ,  $t$ -test) from that of AkaLumine (5) (**Figure 4.19**). This imaging data illustrates the utility of **NIRLuc2** as a new class of NIR emitting bioluminescent probe.

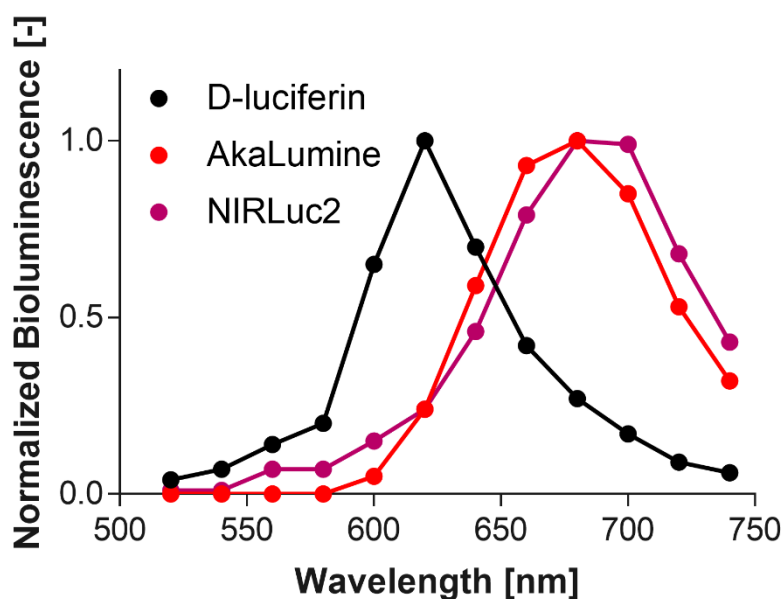


**Figure 4.17.** Bioluminescence spectra from subcutaneous tumors of B16-F10-Fluc cells. Data is representative of four independent experiments.

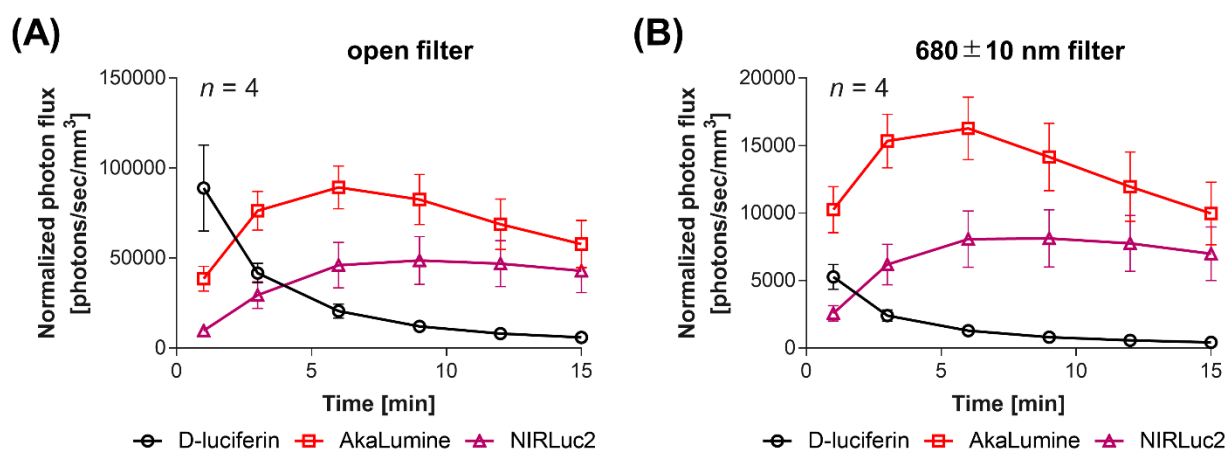


**Figure 4.18.** Time course of bioluminescent photon flux from subcutaneous tumors *in vivo* with open filter (A) or NIR (680 ± 10 nm) filter (B). Error bars represent the standard error of the mean for quadruplicate experiments. Photon flux was normalized by tumor volume.

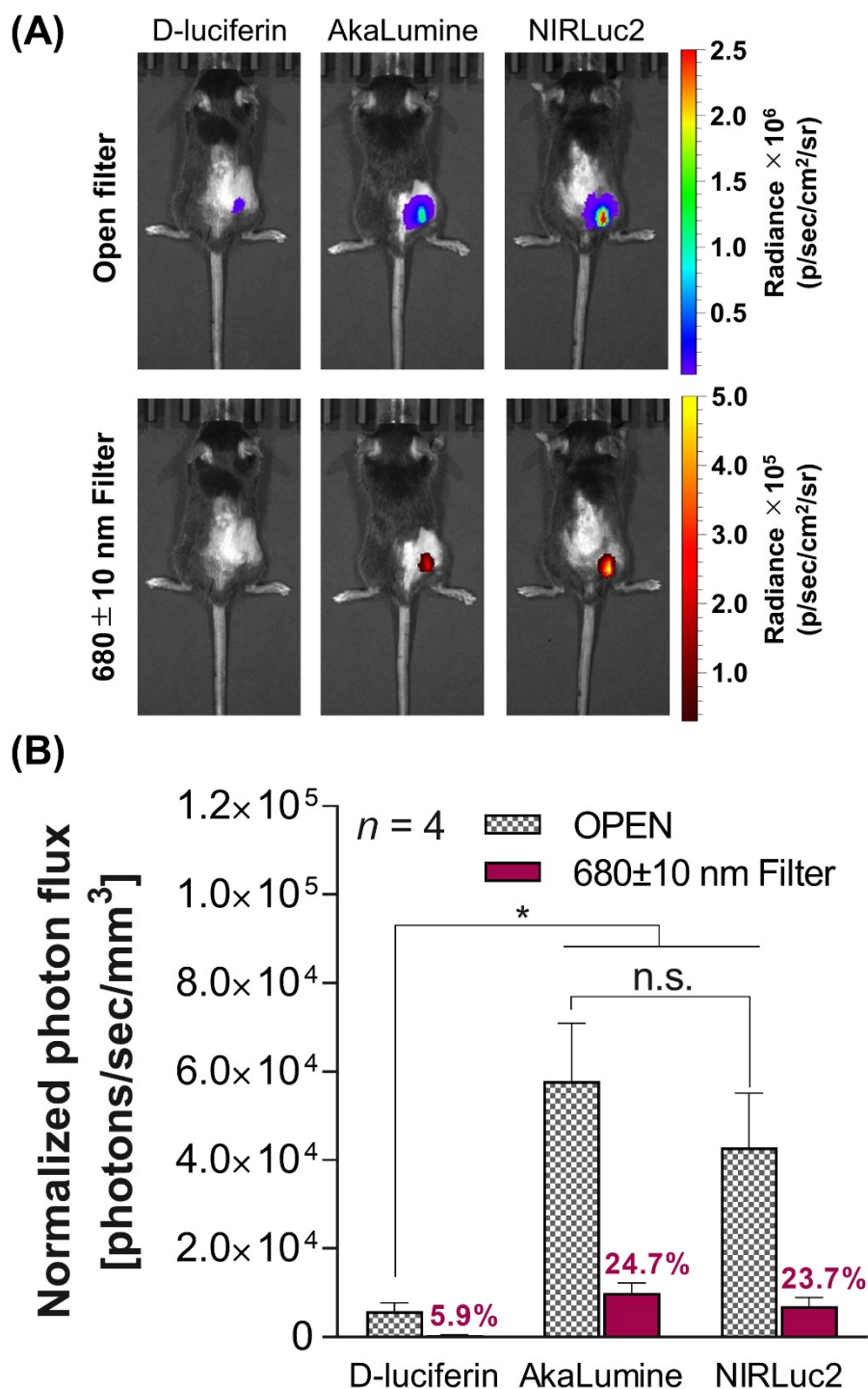


**Figure 4.19. Tumor bioluminescence imaging with NIRLuc2 *in vivo*.** (A) Bioluminescence images of C57BL/6J mice bearing subcutaneous tumors of B16-F10-Fluc cells with open filter (upper) or NIR (680 ± 10 nm) filter (bottom) recorded 15 min after intravenous injection of luciferins. (B) Quantitative analysis of the photon flux from subcutaneous tumors ( $n = 4$ ). Photon flux was normalized by tumor volume. \* $P < 0.05$  ( $t$ -test), compared to D-luciferin (1). n.s.; not significant ( $P > 0.05$ ). Error bars represent the standard error of the mean for quadruplicate experiments. The number on the red purple bars indicate the ratio of NIR emission (680 nm filter) relative to the total emission (OPEN).

## 4.3. Conclusions

In summary, a panel of luminogenic luciferins, **NIRLucs**, emitting NIR photons suitable for *in vivo* imaging has been developed. **NIRLucs** were synthesized based on the NIR emitting firefly luciferin analogue AkaLumine (**5**) through a ring fusion strategy. This strategy resulted in theoretically supported pH-independent structure-inherent NIR emission with the commonly used native luciferase Fluc. When applied to cellular imaging, **NIRLucs** showed cell-membrane permeability and linear correlation between the photon flux and the cell-number, suggesting their utility as bioluminescent reporters. Their photon flux was dose-independent with NIR emission even at 1000-times diluted concentration compared to D-luciferin (**1**). Furthermore, an initial comparative *in vivo* application was performed with **NIRLuc2** as a candidate. **NIRLuc2** displayed noteworthy blood retention and 16-fold brighter NIR photon flux in mice bearing subcutaneous tumors compared to that of native substrate D-luciferin (**1**). It was also shown that photon production of **NIRLuc2** was less time-dependent after intravenous injection owing to the long half-life in blood and high affinity to luciferase. In total, our approach provides a solution to the longstanding limitation in variety of NIR emitting luciferins. This study also suggests the possibility of multi-component NIR bioluminescence imaging in combination with mutant luciferases.

## 4.4. Experimental Section

### 4.4.1. Material and methods

#### 4.4.1.1. General

Reagents and solvents were of the best grade available, supplied by Tokyo Chemical Industries (Japan), Wako Pure Chemical (Japan), Aldrich Chemical Co. (USA), Kanto Chemical Co. (Japan) or Watanabe Chemical Industries (Japan) and were used without further purification. NMR spectra were recorded on a JEOL ECA-500 instrument at 500 MHz for  $^1\text{H}$  NMR and at 125 MHz for  $^{13}\text{C}$  NMR. All chemical shifts ( $\delta$ ) are reported in ppm relative to tetramethylsilane ( $\delta = 0.0$  ppm) or residual non-deuterated NMR solvent  $\text{CDCl}_3$  (7.26 ppm for  $^1\text{H}$ , 77.16 ppm for  $^{13}\text{C}$ ),  $\text{CD}_3\text{OD}$  (3.31 ppm for  $^1\text{H}$ , 49.00 ppm for  $^{13}\text{C}$ ), or  $\text{DMSO-d}_6$  (2.50 ppm for  $^1\text{H}$ , 39.52 ppm for  $^{13}\text{C}$ ) and coupling constants ( $J$ ) are provided in Hz. Mass spectra (MS) were measured on a Waters LCT Premier XE (ESI-TOF). A 1.0 mg/mL stock solution of commercially available luciferase (Promega, QuantiLum<sup>®</sup> recombinant *Photinus pyralis* luciferase, E1701) in GTA buffer (50 mM, pH 8.0) containing 10% glycerol was prepared and stored at  $-80$  °C. The composition of the 50 mM GTA buffer is 50 mM 3,3-dimethylglutaric acid, 50 mM tris(hydroxymethyl)aminomethane, 50 mM 2-amino-2-methyl-1,3-propanediol and the pH was adjusted with 2 M HCl or 1 M NaOH solution. The enantiopurity was analyzed on an analytical HPLC (Agilent 1100 Series, USA) using Chiralcel<sup>®</sup> OD-3R (150 X 4.6 mm ID, DAICEL, Japan) with a linear gradient of 10%-90%  $\text{CH}_3\text{CN}$  in  $\text{H}_2\text{O}$  over 30 min (flow rate 0.6 mL/min) as eluent. A UV detector set at 370 nm was used for peak detection. GraphPad Prism (version 7.03 for Windows, GraphPad Software) was used to analyze data and generate graphs. The calculated logP (ClogP) values were calculated by ChemDraw 13.0.

#### 4.4.1.2. Chemiluminescence spectra

The chemiluminescence emission spectra for all luciferins with *n*-propylphosphonic anhydride (T3P) and triethylamine (TEA) in DMF were measured on an AB-1850 spectrophotometer (ATTO, Japan). A solution of the luciferins (2 mM) in DMF (20  $\mu\text{L}$ ) and TEA (2 M) in DMF (20  $\mu\text{L}$ ) were placed in a polystyrene tube. This solution was treated with T3P (110 mM) in DMF (60  $\mu\text{L}$ ), which was injected with a syringe, to initiate the chemiluminescence reaction. Emission data were collected for 5 s (slit width: 1.0 mm), and the luminescence intensities were normalized.

### 4.4.1.3. Fluorescence spectroscopy

The fluorescence spectra for luciferins (10  $\mu\text{M}$ ) in 50 mM GTA buffer (pH 8.0) were measured using a VARIOSKAN FLASH (Thermo Scientific, USA) microplate reader with the excitation light and excitation/emission slit widths set to 375 nm and 1 nm, respectively. Spectral data were recorded at 25 °C in a clear bottom 96-well microplate over the wavelength range of 400-750 nm. The absolute fluorescence quantum yields were collected using a Quantaury-QY (Hamamatsu Photonics, Japan) with the excitation light set to 375 nm.

### 4.4.1.4. Bioluminescence spectra

The bioluminescence emission spectra for all luciferins were recorded on an AB-1850 spectrophotometer (ATTO, Japan). A solution of the luciferins (100  $\mu\text{M}$ ) in GTA buffer (50 mM, pH 8.0, 5  $\mu\text{L}$ ) and Fluc (1.0 mg/mL) in GTA buffer (50 mM, pH 8.0) containing 10% glycerol (5  $\mu\text{L}$ ) were placed in a polystyrene tube. The bioluminescence reaction was initiated by injection of 90  $\mu\text{L}$  of reaction buffer (4 mM ATP-2Na, 8 mM  $\text{MgSO}_4$  in 50 mM GTA buffer, pH 8.0). Emission data were collected for 60 s (slit width: 0.25 mm), and the luminescence intensities were normalized. The pH dependence of the spectra was assessed in a similar manner in GTA buffer (50 mM, pH5.5-8.5).

### 4.4.1.5. Bioluminescence kinetic measurements

Measurements were acquired on a TriStar<sup>2</sup> LB942 luminometer (BERTHOLD, Germany) without filter. Reactions were performed in white 96-well flat-bottom plates (Grenier). Solutions of luciferins in GTA buffer (50 mM, pH 7.0) were prepared (0.5  $\mu\text{M}$  - 100  $\mu\text{M}$  luciferin), and 10  $\mu\text{L}$  was added to each well. Following the addition of Fluc (0.05 mg/mL) in GTA buffer (50 mM, pH 8.0) containing 10% glycerol (10  $\mu\text{L}$ ), the luminescence reaction was initiated by injection of 80  $\mu\text{L}$  of reaction buffer (4 mM ATP-2Na, 8 mM  $\text{MgSO}_4$  in 50 mM GTA buffer, pH 8.0). Emission data was recorded every 1 s over a 60 s period. Samples were analyzed in triplicate and three runs of each compound-enzyme pair were performed. Initial velocities were estimated as integrated values of the light emission intensities for 30 s.  $K_m$  and relative  $V_{\text{max}}$  values were determined using nonlinear regression analyses and robust fit outlier removal in GraphPad Prism (version 7.03 for Windows, GraphPad Software). The pH dependence of luminescence intensities was assessed with 10  $\mu\text{M}$  luciferins in GTA buffer (50 mM, pH5.5-8.5).

#### 4.4.1.6. Quantum chemical calculations

All calculations of HOMO and LUMO energy levels were carried out using the Gaussian 09 program. The geometries of the ground state and excited state structures were optimized using Density Functional Theory (DFT) and Time-Dependent Density Functional Theory (TD-DFT) at the B3LYP level. The 6-31+G(d) basis set was adopted for all atoms.

#### 4.4.1.7. Cellular bioluminescence assays

B16-F10 cells expressing luciferase (B16-F10/CMV-Luc#2 cells) were obtained from Japanese Collection of Research Bioresources Cell Bank (Ibaraki, Japan). Transiently transfected B16-F10/CMV-Luc cells were cultured in DMEM medium supplemented with FBS (10%), penicillin (100 U/mL) and streptomycin (100 µg/mL) at 37 °C in 5% CO<sub>2</sub>. For bioluminescence emission assays, approximately  $3.5 \times 10^5$  cells/well were plated in black 96-well plates in 75 µL of DMEM containing 10% FBS. The cells then incubated with 75 µL of luciferins (0.5-500 µM) in PBS (-). Bioluminescence images were acquired on an IVIS Spectrum (PerkinElmer, USA) system equipped with a cooled CCD camera with following conditions; OPEN for total or 680±10 nm emission filter for NIR bioluminescence, exposure time: 180 sec, binning: medium 8, and *f*/stop: 1. The bioluminescence images were analyzed by Living Image 4.4 software (PerkinElmer, USA).

For cell number-dependent assays,  $7.5 \times 10^3$  -  $2.4 \times 10^5$  cells/well were plated in black 96-well plates in 50 µL of DMEM containing 10% FBS. The cells then incubated with 50 µL of luciferins (50 µM) in PBS. Bioluminescence images were acquired 1 min after adding the luciferins and analyzed as above.

#### 4.4.1.8. Mice

The ICR mice (female, 4 weeks old) and C57BL/6J mice (female, 4 weeks old) were obtained from Japan SLC, Inc (Hamamatsu, Japan). The mice were provided access to food and water *ad libitum*. All the animal experiments were approved by the Animal Care and Use Committee of Tokyo Institute of Technology. The experiments were performed in accordance with the Guidelines for the Care and Use of Laboratory Animals as stated by Tokyo Institute of Technology.

#### 4.4.1.9. Measurements of blood retention

100 µL of luciferins (5 mM) in PBS (-) containing 5% DMSO were intravenously injected to ICR mice (female, 4 weeks old). 5 µL of blood was sampled from tail vein at each time point and then mixed with 45 µL of PBS (-) in a black 96-well plate. The bioluminescence was initiated by adding 25 µL of ATP-Mg (80 µM) and 25 µL of Fluc (20 µg/mL) and the bioluminescence images were taken immediately on an IVIS Spectrum (PerkinElmer, USA) system equipped with a cooled CCD camera with following conditions; OPEN, exposure time: 10 sec, binning: medium 8, and *f*/stop: 1. The

bioluminescence images were analyzed by Living Image 4.4 software (PerkinElmer, USA). The results were normalized by the photon flux at the 3 min after intravenous injection in each individual.

#### 4.4.1.10. *In vivo* subcutaneous tumor imaging

A subcutaneous tumor model was prepared by subcutaneously inoculating a C57BL/6J mouse with B16-F10/CMV-Luc cells ( $5 \times 10^5$  cells/mouse). The experiments were performed 14 days after engraftment. The mice were anesthetized with 2% isoflurane and placed on a temperature-controlled stage. 100  $\mu$ L of luciferins (5 mM) in PBS (-) containing 5% DMSO were intravenously injected to mice and bioluminescence images were acquired on an IVIS Spectrum (PerkinElmer, USA) system equipped with a cooled CCD camera with following conditions; OPEN for total or  $680 \pm 10$  nm emission filter for NIR bioluminescence, exposure time: 60 sec, binning: medium 8, and  $f$ /stop: 1. The bioluminescence images were analyzed by Living Image 4.4 software (PerkinElmer, USA).

The photon flux from a subcutaneous tumor were normalized by the tumor volume ( $V$ ) estimated by the following equation:

$$V = a \times b^2 / 2 \quad (3)$$

where  $a$  and  $b$  are the major and minor axes of the tumor, respectively, as measured by a caliper. The statistical significance was determined by two-tailed Student's  $t$ -test. The results were considered statistically significance if the  $P$ -values were lower than 0.05.

#### 4.4.2. Synthetic procedures

The **NIRLucs** have been successfully accessed from the corresponding benzaldehydes according to the reported scheme (Scheme 4.1).<sup>15</sup> The benzaldehydes (**6**) were synthesized as previously reported (**6a**,<sup>31</sup>, **6c**,<sup>32</sup>, **6d**,<sup>33</sup>, **6f**,<sup>34</sup>). Compound **6e** is commercially available from Tokyo Chemical Industries (Japan).

**Compound 7a:** To a suspension of 60% NaH (273 mg, 6.83 mmol, 2.0 eq.) in anhydrous THF (3.8 mL) at 0 °C was added triethyl 4-phosphonocrotonate (1.28 g, 5.13 mmol, 1.5 eq.). Stirring for 20 min yielded an orange colored solution. To this solution was added **6a** (548 mg, 3.40 mmol) in anhydrous THF (3.0 mL) dropwise over 5 min at 0 °C. The reaction was stirred for 3 h at room temperature, quenched with water (ca. 20 mL) and extracted with EtOAc (3  $\times$  50 mL). The combined organic layer was washed with brine, dried over Na<sub>2</sub>SO<sub>4</sub> and filtered. The filtrate was concentrated under reduced pressure. The crude material was purified by silica gel column chromatography (11–32% ethyl acetate/*n*-hexane) to afford **7a** (561 mg, 64%) as a yellow solid. <sup>1</sup>H NMR (500 MHz, CDCl<sub>3</sub>)  $\delta$  7.43 (dd,  $J$  = 15.0, 11.0 Hz, 1H), 7.24 (s, 1H), 7.16 (d,  $J$  = 8.0 Hz, 1H), 6.81 (d,  $J$  = 15.5 Hz, 1H), 6.66 (dd,  $J$  = 15.5, 11.0 Hz, 1H), 6.38 (d,  $J$  = 8.0 Hz, 1H), 5.85 (d,  $J$  = 15.5 Hz, 1H), 4.21 (q,  $J$  = 7.2 Hz, 2H), 3.39 (t,  $J$  = 8.0 Hz, 2H), 2.97 (t,  $J$  = 8.0 Hz, 2H), 2.79 (s, 3H), 1.31 (t,  $J$  = 7.0 Hz, 3H) ppm; <sup>13</sup>C NMR (125 MHz, CDCl<sub>3</sub>)  $\delta$  167.8, 154.5, 146.0, 141.8, 131.0, 128.9, 125.9, 122.7, 121.6, 118.2, 106.4, 60.2, 55.7, 35.4, 28.3, 14.5 ppm; HRMS (ESI+) calcd for C<sub>16</sub>H<sub>20</sub>NO<sub>2</sub> [M+H]<sup>+</sup> : 258.1494, found:  $m/z$

258.1484.

**Compound 7b: 7b** was synthesized in the same manner as described for the preparation of **7a**; yield 48%, a yellow oil.  $^1\text{H}$  NMR (500 MHz,  $\text{CDCl}_3$ )  $\delta$  7.43 (dd,  $J = 15.0, 11.0$  Hz, 1H), 7.18 (dd,  $J = 8.0, 2.0$  Hz, 1H), 7.09 (s, 1H), 6.78 (d,  $J = 15.0$  Hz, 1H), 6.66 (dd,  $J = 15.0, 11.0$  Hz, 1H), 6.51 (d,  $J = 8.0$  Hz, 1H), 5.85 (d,  $J = 15.0$  Hz, 1H), 4.21 (q,  $J = 7.2$  Hz, 2H), 3.28 (t,  $J = 5.8$  Hz, 2H), 2.92 (s, 3H), 2.75 (t,  $J = 6.5$  Hz, 2H), 1.97 (quint,  $J = 6.1$  Hz, 2H), 1.30 (t,  $J = 7.2$  Hz, 3H) ppm;  $^{13}\text{C}$  NMR (125 MHz,  $\text{CDCl}_3$ )  $\delta$  167.8, 147.6, 146.1, 141.6, 127.8, 127.4, 123.9, 122.7, 121.4, 117.8, 110.6, 60.2, 51.3, 39.0, 27.9, 22.2, 14.5 ppm; HRMS (ESI+) calcd for  $\text{C}_{17}\text{H}_{22}\text{NO}_2$   $[\text{M}+\text{H}]^+$  : 272.1651, found:  $m/z$  272.1638.

**Compound 7c: 7c** was synthesized in the same manner as described for the preparation of **7a**; yield 66%, a yellow oil.  $^1\text{H}$  NMR (500 MHz,  $\text{CDCl}_3$ )  $\delta$  7.44 (dd,  $J = 15.0, 11.0$  Hz, 1H), 7.29 (d,  $J = 2.0$  Hz, 1H), 7.20 (dd,  $J = 8.5, 2.5$  Hz, 1H), 6.81 (d,  $J = 15.0$  Hz, 1H), 6.67 (dd,  $J = 15.0, 11.0$  Hz, 1H), 6.52 (d,  $J = 8.5$  Hz, 1H), 5.86 (d,  $J = 15.0$  Hz, 1H), 4.21 (q,  $J = 7.2$  Hz, 2H), 3.30 (t,  $J = 6.0$  Hz, 2H), 2.95 (s, 3H), 1.75 (t,  $J = 6.0$  Hz, 2H), 1.32-1.27 (m, 9H) ppm;  $^{13}\text{C}$  NMR (125 MHz,  $\text{CDCl}_3$ )  $\delta$  167.8, 146.4, 146.2, 142.0, 131.4, 126.8, 125.1, 123.8, 121.2, 117.8, 110.8, 60.2, 47.7, 39.2, 36.9, 32.1, 30.6, 14.5 ppm; HRMS (ESI+) calcd for  $\text{C}_{19}\text{H}_{26}\text{NO}_2$   $[\text{M}+\text{H}]^+$  : 300.1964, found:  $m/z$  300.1960.

**Compound 7d: 7d** was synthesized in the same manner as described for the preparation of **7a**; yield 74%, a yellow oil.  $^1\text{H}$  NMR (500 MHz,  $\text{CDCl}_3$ )  $\delta$  7.42 (dd,  $J = 15.0, 11.0$  Hz, 1H), 6.95 (dd,  $J = 8.0, 2.0$  Hz, 1H), 6.92 (d,  $J = 2.0$  Hz, 1H), 6.77 (d,  $J = 15.5$  Hz, 1H), 6.66 (dd,  $J = 15.0, 11.0$  Hz, 1H), 6.60 (d,  $J = 8.5$  Hz, 1H), 5.88 (d,  $J = 15.0$  Hz, 1H), 4.28 (t,  $J = 4.5$  Hz, 2H), 4.21 (q,  $J = 7.0$  Hz, 2H), 3.32 (t,  $J = 4.5$  Hz, 2H), 2.93 (s, 3H), 1.30 (t,  $J = 7.3$  Hz, 3H) ppm;  $^{13}\text{C}$  NMR (125 MHz,  $\text{CDCl}_3$ )  $\delta$  167.6, 145.6, 144.1, 141.0, 137.8, 126.2, 122.8, 122.2, 118.9, 113.9, 111.9, 64.7, 60.2, 49.1, 38.6, 14.5 ppm; HRMS (ESI+) calcd for  $\text{C}_{16}\text{H}_{20}\text{NO}_3$   $[\text{M}+\text{H}]^+$  : 274.1443, found:  $m/z$  274.1438.

**Compound 7e: 7e** was synthesized in the same manner as described for the preparation of **7a**; yield 66%, an orange solid.  $^1\text{H}$  NMR (500 MHz,  $\text{CDCl}_3$ )  $\delta$  7.42 (dd,  $J = 15.0, 10.5$  Hz, 1H), 6.92 (s, 2H), 6.73 (d,  $J = 15.0$  Hz, 1H), 6.62 (dd,  $J = 15.0, 10.5$  Hz, 1H), 5.82 (d,  $J = 15.0$  Hz, 1H), 4.20 (q,  $J = 7.0$  Hz, 2H), 3.20 (t,  $J = 5.6$  Hz, 4H), 2.73 (t,  $J = 6.3$  Hz, 4H), 1.98-1.93 (m, 4H), 1.30 (t,  $J = 7.0$  Hz, 3H) ppm;  $^{13}\text{C}$  NMR (125 MHz,  $\text{CDCl}_3$ )  $\delta$  167.9, 146.3, 144.0, 141.8, 126.6, 123.3, 121.3, 121.0, 117.5, 60.1, 50.1, 27.8, 21.9, 14.5 ppm; HRMS (ESI+) calcd for  $\text{C}_{19}\text{H}_{24}\text{NO}_2$   $[\text{M}+\text{H}]^+$  : 298.1807, found:  $m/z$  298.1794.

**Compound 7f: 7f** was synthesized in the same manner as described for the preparation of **7a**; yield 36%, a yellow oil.  $^1\text{H}$  NMR (500 MHz,  $\text{CDCl}_3$ )  $\delta$  7.44 (dd,  $J = 15.0, 11.0$  Hz, 1H), 7.22 (dd,  $J = 8.5, 2.0$  Hz, 1H), 7.15 (d,  $J = 2.0$  Hz, 1H), 6.81 (d,  $J = 15.5$  Hz, 1H), 6.68 (dd,  $J = 15.0, 11.0$  Hz, 1H), 6.47 (d,  $J = 8.5$  Hz, 1H), 5.87 (d,  $J = 15.0$  Hz, 1H), 5.31 (d,  $J = 1.5$  Hz, 1H), 4.21 (q,  $J = 7.2$  Hz, 2H), 2.84 (s, 3H), 2.01 (d,  $J = 1.5$  Hz, 3H), 1.32 (s, 6H), 1.31 (t,  $J = 7.0$  Hz, 3H) ppm;  $^{13}\text{C}$  NMR (125 MHz,  $\text{CDCl}_3$ )  $\delta$  167.8, 146.4, 146.0, 141.6, 130.3, 128.8, 127.7,

124.0, 122.9, 122.3, 121.6, 118.1, 110.5, 60.2, 56.9, 31.0, 28.0, 18.8, 14.5 ppm; HRMS (ESI+) calcd for  $C_{20}H_{26}NO_2$   $[M+H]^+$  : 312.1964, found:  $m/z$  312.1955.

**Compound 8a:** To a solution of **7a** (499 mg, 1.94 mmol) in *iso*-PrOH (15.6 mL) was added 1 M NaOH aqueous solution (3.9 mL), and the mixture was stirred at reflux temperature for 8 h. After cooling to room temperature, *iso*-PrOH was removed under reduced pressure. The residue was acidified with 1 N HCl aqueous solution, and extracted with  $CHCl_3$  (3×50 mL). The combined organic layer was washed with brine, dried over  $Na_2SO_4$  and filtered. The filtrate was concentrated under reduced pressure to afford **8a** (445 mg, 93%) as a yellow-brown solid. This crude product was used for the next reaction without further purification.  $^1H$  NMR (500 MHz,  $DMSO-d_6$ )  $\delta$  7.23 (s, 1H), 7.10 (d,  $J$  = 8.0 Hz, 1H), 6.84 (dd,  $J$  = 15.0, 11.0 Hz, 1H), 6.66 (dd,  $J$  = 15.5, 11.0 Hz, 1H), 6.55 (d,  $J$  = 15.5 Hz, 1H), 6.43 (d,  $J$  = 8.0 Hz, 1H), 5.79 (d,  $J$  = 15.0 Hz, 1H), 3.28 (t,  $J$  = 8.0 Hz, 2H), 2.87 (t,  $J$  = 8.0 Hz, 2H), 2.71 (s, 3H) ppm;  $^{13}C$  NMR (125 MHz,  $DMSO-d_6$ )  $\delta$  167.9, 154.2, 145.6, 141.4, 130.1, 128.7, 125.2, 122.5, 121.2, 118.6, 106.2, 55.0, 34.9, 27.6 ppm; HRMS (ESI+) calcd for  $C_{14}H_{16}NO_2$   $[M+H]^+$  : 230.1181, found:  $m/z$  230.1180.

**Compound 8b:** **8b** was synthesized in the same manner as described for the preparation of **8a**; yield 100%, a yellow solid.  $^1H$  NMR (500 MHz,  $DMSO-d_6$ )  $\delta$  12.00 (br, 1H), 7.29 (dd,  $J$  = 15.0, 11.0 Hz, 1H), 7.19 (dd,  $J$  = 8.5, 2.0 Hz, 1H), 7.12 (s, 1H), 6.85 (d,  $J$  = 15.0 Hz, 1H), 6.78 (dd,  $J$  = 15.5, 10.5 Hz, 1H), 6.54 (d,  $J$  = 8.5 Hz, 1H), 5.81 (d,  $J$  = 15.0 Hz, 1H), 3.25 (t,  $J$  = 5.5 Hz, 2H), 2.87 (s, 3H), 2.68 (t,  $J$  = 6.3 Hz, 2H), 1.86 (quint,  $J$  = 6.0 Hz, 2H) ppm;  $^{13}C$  NMR (125 MHz,  $DMSO-d_6$ )  $\delta$  168.0, 147.3, 145.6, 141.2, 127.5, 127.3, 123.3, 122.2, 121.0, 118.3, 110.4, 50.4, 38.5, 27.2, 21.6 ppm; HRMS (ESI+) calcd for  $C_{15}H_{18}NO_2$   $[M+H]^+$  : 244.1338, found:  $m/z$  244.1330.

**Compound 8c:** **8c** was synthesized in the same manner as described for the preparation of **8a**; yield 100%, a yellow solid.  $^1H$  NMR (500 MHz,  $DMSO-d_6$ )  $\delta$  12.00 (br, 1H), 7.34 (d,  $J$  = 2.0 Hz, 1H), 7.29 (dd,  $J$  = 15.0, 10.5 Hz, 1H), 7.21 (dd,  $J$  = 8.5, 2.0 Hz, 1H), 6.89 (d,  $J$  = 15.5 Hz, 1H), 6.82 (dd,  $J$  = 15.0, 10.5 Hz, 1H), 6.54 (d,  $J$  = 9.0 Hz, 1H), 5.83 (d,  $J$  = 15.0 Hz, 1H), 3.26 (t,  $J$  = 6.0 Hz, 2H), 2.90 (s, 3H), 1.68 (t,  $J$  = 6.0 Hz, 2H), 1.24 (s, 6H) ppm;  $^{13}C$  NMR (125 MHz,  $DMSO-d_6$ )  $\delta$  168.0, 146.1, 145.7, 141.5, 130.8, 126.7, 124.9, 123.3, 120.9, 118.3, 110.7, 46.8, 38.8, 36.3, 31.6, 30.4 ppm; HRMS (ESI+) calcd for  $C_{17}H_{22}NO_2$   $[M+H]^+$  : 272.1651, found:  $m/z$  272.1644.

**Compound 8d:** **8d** was synthesized in the same manner as described for the preparation of **8a**; yield 96%, a brown solid.  $^1H$  NMR (500 MHz,  $DMSO-d_6$ )  $\delta$  12.07 (br, 1H), 7.28 (dd,  $J$  = 15.0, 9.5 Hz, 1H), 6.97 (dd,  $J$  = 8.0, 2.0 Hz, 1H), 6.91 (d,  $J$  = 1.5 Hz, 1H), 6.87-6.79 (m, 2H), 6.66 (d,  $J$  = 8.5 Hz, 1H), 5.85 (d,  $J$  = 15.0 Hz, 1H), 4.20 (t,  $J$  = 4.5 Hz, 2H), 3.29 (t,  $J$  = 4.5 Hz, 2H), 2.87 (s, 3H) ppm;  $^{13}C$  NMR (125 MHz,  $DMSO-d_6$ )  $\delta$  167.9, 145.3, 143.6, 140.7, 137.8, 125.3, 122.4, 122.1, 119.3, 113.3, 111.9, 64.2, 48.2, 38.0 ppm; HRMS (ESI+) calcd for  $C_{14}H_{16}NO_3$   $[M+H]^+$  : 246.1130, found:  $m/z$  246.1125.

**Compound 8e:** **8e** was synthesized in the same manner as described for the preparation of **8a**; yield 84%, a deep red solid.  $^1\text{H}$  NMR (500 MHz, DMSO- $d_6$ )  $\delta$  11.90 (br, 1H), 7.27 (dd,  $J = 15.0, 10.5$  Hz, 1H), 6.93 (s, 2H), 6.76 (d,  $J = 7.5$  Hz, 1H), 6.72 (dd,  $J = 15.0, 10.5$  Hz, 1H), 5.78 (d,  $J = 15.0$ , 1H), 3.17 (t,  $J = 5.5$  Hz, 4H), 2.66 (t,  $J = 6.3$  Hz, 4H), 1.88-1.83 (m, 4H) ppm;  $^{13}\text{C}$  NMR (125 MHz, DMSO- $d_6$ )  $\delta$  168.0, 145.7, 143.6, 141.4, 126.3, 122.5, 120.6, 120.6, 117.9, 49.2, 27.1, 21.2 ppm; HRMS (ESI+) calcd for  $\text{C}_{17}\text{H}_{20}\text{NO}_2$   $[\text{M}+\text{H}]^+$  : 270.1494, found:  $m/z$  270.1483.

**Compound 8f:** **8f** was synthesized in the same manner as described for the preparation of **8a**; yield 100%, a yellow solid.  $^1\text{H}$  NMR (500 MHz,  $\text{CDCl}_3$ )  $\delta$  7.54 (dd,  $J = 15.0, 11.0$  Hz, 1H), 7.24 (dd,  $J = 8.5, 2.0$  Hz, 1H), 7.16 (d,  $J = 2.5$  Hz, 1H), 6.86 (d,  $J = 15.0$  Hz, 1H), 6.71 (dd,  $J = 15.5, 11.0$  Hz, 1H), 6.48 (d,  $J = 8.5$  Hz, 1H), 5.88 (d,  $J = 15.0$  Hz, 1H), 5.32 (d,  $J = 1.0$  Hz, 1H), 2.85 (s, 3H), 2.02 (d,  $J = 1.0$  Hz, 3H), 1.33 (s, 6H) ppm;  $^{13}\text{C}$  NMR (125 MHz,  $\text{CDCl}_3$ )  $\delta$  172.9, 148.4, 146.6, 142.9, 130.3, 129.2, 127.6, 123.8, 122.9, 122.5, 121.3, 116.9, 110.5, 57.0, 31.0, 28.1, 18.8 ppm; HRMS (ESI+) calcd for  $\text{C}_{18}\text{H}_{22}\text{NO}_2$   $[\text{M}+\text{H}]^+$  : 284.1651, found:  $m/z$  284.1655.

**Compound 9a:** To a solution of **8a** (304 mg, 1.33 mmol) and D-Cys(Trt)-OMe hydrochloric acid (658 mg, 1.59 mmol, 1.2 eq.) in anhydrous DMF (13.3 mL) were added DMT-MM (442 mg, 1.60 mmol, 1.2 eq.) and TEA (0.22 mL, 1.58 mmol, 1.2 eq.), and the mixture was stirred at 0 °C for 3 h. The reaction was diluted with water (ca. 20 mL) at 0 °C and then extracted with EtOAc (3×100 mL). The combined organic layer was washed with brine, dried over  $\text{Na}_2\text{SO}_4$  and filtered. The crude material was purified by silica gel column chromatography (30-50% ethyl acetate/*n*-hexane) to afford **9a** (477 mg, 61%) as a yellow solid.  $^1\text{H}$  NMR (500 MHz,  $\text{CDCl}_3$ )  $\delta$  7.39-7.16 (m, 17H), 6.80 (d,  $J = 15.0$ , 1H), 6.65 (dd,  $J = 15.5, 11.0$  Hz, 1H), 6.39 (d,  $J = 8.0$  Hz, 1H), 5.96 (d,  $J = 7.5$  Hz, 1H), 5.81 (d,  $J = 14.5$ , 1H), 4.76-4.73 (m, 1H), 3.72 (s, 3H), 3.39 (t,  $J = 8.5$  Hz, 2H), 2.97 (t,  $J = 8.5$  Hz, 2H), 2.79 (s, 3H), 2.73-2.66 (m, 2H) ppm;  $^{13}\text{C}$  NMR (125 MHz,  $\text{CDCl}_3$ )  $\delta$  171.3, 166.1, 154.3, 144.4, 143.2, 141.1, 131.0, 129.6, 128.6, 128.1, 127.0, 126.1, 122.6, 121.6, 120.1, 106.4, 67.0, 55.8, 52.8, 51.2, 35.5, 34.2, 28.4 ppm; HRMS (ESI+) calcd for  $\text{C}_{37}\text{H}_{37}\text{N}_2\text{O}_3\text{S}$   $[\text{M}+\text{H}]^+$  : 589.2525, found:  $m/z$  589.2528.

**Compound 9b:** **9b** was synthesized in the same manner as described for the preparation of **9a**; yield 97%, a yellow solid.  $^1\text{H}$  NMR (500 MHz,  $\text{CDCl}_3$ )  $\delta$  7.39-7.18 (m, 16H), 7.09 (s, 1H), 6.76 (d,  $J = 15.5$ , 1H), 6.64 (dd,  $J = 15.5, 11.0$  Hz, 1H), 6.52 (d,  $J = 8.5$  Hz, 1H), 5.95 (d,  $J = 8.0$  Hz, 1H), 5.80 (d,  $J = 15.0$ , 1H), 4.76-4.73 (m, 1H), 3.71 (s, 3H), 3.28 (t,  $J = 5.7$  Hz, 2H), 2.93 (s, 3H), 2.76 (t,  $J = 6.4$  Hz, 2H), 2.73-2.66 (m, 2H), 1.97 (quint,  $J = 6.4$  Hz, 2H) ppm;  $^{13}\text{C}$  NMR (125 MHz,  $\text{CDCl}_3$ )  $\delta$  171.3, 166.1, 147.5, 144.5, 143.3, 141.0, 129.6, 128.1, 127.7, 127.2, 127.0, 124.2, 122.7, 121.4, 119.8, 110.6, 67.0, 52.8, 51.3, 51.2, 39.0, 34.3, 27.9, 22.3 ppm; HRMS (ESI+) calcd for  $\text{C}_{38}\text{H}_{39}\text{N}_2\text{O}_3\text{S}$   $[\text{M}+\text{H}]^+$  : 603.2681, found:  $m/z$  603.2675.

**Compound 9c:** **9c** was synthesized in the same manner as described for the preparation of **9a**; yield 84%, a yellow solid.  $^1\text{H}$  NMR (500 MHz,  $\text{CDCl}_3$ )  $\delta$  7.39-7.20 (m, 17H), 6.80 (d,  $J = 15.5$ , 1H), 6.66 (dd,  $J = 15.0, 11.0$  Hz, 1H), 6.53 (d,  $J = 8.5$  Hz, 1H), 5.97 (d,  $J = 8.0$  Hz, 1H), 5.82 (d,  $J = 14.5$ , 1H), 4.77-4.73 (m, 1H), 3.72 (s, 3H), 3.30 (t,  $J = 6.0$  Hz, 2H), 2.95 (s, 3H), 2.73-2.66 (m, 2H), 1.76 (t,  $J = 6.0$  Hz, 2H), 1.30 (s, 6H) ppm;  $^{13}\text{C}$  NMR

(125 MHz, CDCl<sub>3</sub>)  $\delta$  171.3, 166.1, 146.2, 144.5, 143.3, 141.3, 131.4, 129.6, 128.1, 127.0, 126.5, 125.1, 124.0, 121.2, 119.7, 110.9, 67.0, 52.8, 51.2, 47.7, 39.3, 36.9, 34.3, 32.1, 30.6 ppm; HRMS (ESI+) calcd for C<sub>40</sub>H<sub>43</sub>N<sub>2</sub>O<sub>3</sub>S [M+H]<sup>+</sup> : 631.2994, found: *m/z* 631.2981.

**Compound 9d: 9d** was synthesized in the same manner as described for the preparation of **9a**; yield 79%, a yellow solid. <sup>1</sup>H NMR (500 MHz, CDCl<sub>3</sub>)  $\delta$  7.39-7.20 (m, 16H), 6.93 (s, 1H), 6.75 (d, *J* = 15.5, 1H), 6.65 (dd, *J* = 15.0, 10.5 Hz, 1H), 6.60 (d, *J* = 8.0 Hz, 1H), 5.95 (d, *J* = 7.5 Hz, 1H), 5.82 (d, *J* = 14.5, 1H), 4.75-4.72 (m, 1H), 4.28 (t, *J* = 4.5 Hz, 2H), 3.71 (s, 3H), 3.31 (t, *J* = 4.5 Hz, 2H), 2.92 (s, 3H), 2.73-2.66 (m, 2H) ppm; <sup>13</sup>C NMR (125 MHz, CDCl<sub>3</sub>)  $\delta$  171.2, 165.9, 144.5, 144.2, 142.8, 140.3, 137.6, 129.6, 128.1, 127.0, 126.4, 122.8, 122.1, 120.8, 113.8, 112.0, 67.0, 64.7, 52.8, 51.2, 49.1, 38.6, 34.2 ppm; HRMS (ESI+) calcd for C<sub>22</sub>H<sub>27</sub>N<sub>2</sub>O<sub>2</sub>S [M+H]<sup>+</sup> : 605.2474, found: *m/z* 605.2495.

**Compound 9e: 9e** was synthesized in the same manner as described for the preparation of **9a**; yield 89%, a yellow solid. <sup>1</sup>H NMR (500 MHz, CDCl<sub>3</sub>)  $\delta$  7.38-7.18 (m, 15H), 6.90 (s, 2H), 6.70 (d, *J* = 15.0, 1H), 6.59 (dd, *J* = 15.5, 11.0 Hz, 1H), 5.91 (d, *J* = 8.0 Hz, 1H), 5.76 (d, *J* = 15.0 Hz, 1H), 4.75-4.71 (m, 1H), 3.70 (s, 3H), 3.18 (t, *J* = 5.8 Hz, 4H), 2.72 (t, *J* = 6.3 Hz, 4H), 2.70-2.64 (m, 2H), 1.94 (quint, *J* = 6.1 Hz, 4H) ppm; <sup>13</sup>C NMR (125 MHz, CDCl<sub>3</sub>)  $\delta$  171.3, 166.2, 144.5, 143.9, 143.4, 141.2, 129.7, 128.2, 127.0, 126.4, 123.5, 121.3, 121.0, 119.5, 67.1, 52.7, 51.2, 50.1, 34.3, 27.8, 22.0 ppm; HRMS (ESI+) calcd for C<sub>40</sub>H<sub>41</sub>N<sub>2</sub>O<sub>3</sub>S [M+H]<sup>+</sup> : 629.2838, found: *m/z* 629.2822.

**Compound 9f: 9f** was synthesized in the same manner as described for the preparation of **9a**; yield 71%, a yellow solid. <sup>1</sup>H NMR (500 MHz, CDCl<sub>3</sub>)  $\delta$  7.39-7.20 (m, 16H), 7.15 (d, *J* = 2.0, 1H), 6.80 (d, *J* = 15.5 Hz, 1H), 6.67 (dd, *J* = 15.5, 11.0 Hz, 1H), 6.48 (d, *J* = 8.5 Hz, 1H), 5.97 (d, *J* = 7.5, 1H), 5.83 (d, *J* = 15.0 Hz, 1H), 5.32 (d, *J* = 1.5 Hz, 1H), 4.77-4.73 (m, 1H), 3.72 (s, 3H), 2.84 (s, 3H), 2.73-2.67 (m, 2H), 2.02 (d, *J* = 1.0 Hz, 3H), 1.33 (s, 6H) ppm; <sup>13</sup>C NMR (125 MHz, CDCl<sub>3</sub>)  $\delta$  171.3, 166.1, 146.2, 144.5, 143.2, 141.0, 130.3, 129.6, 128.6, 128.1, 127.8, 127.0, 124.2, 122.9, 122.3, 121.6, 120.0, 110.6, 67.0, 56.9, 52.8, 51.2, 34.3, 31.0, 27.9, 18.8 ppm; HRMS (ESI+) calcd for C<sub>41</sub>H<sub>43</sub>N<sub>2</sub>O<sub>3</sub>S [M+H]<sup>+</sup> : 643.2994, found: *m/z* 643.3004.

**Compound 10a:** To a solution of triphenylphosphine oxide (TPPO) (213 mg, 0.765 mmol, 3.0 eq.) in anhydrous CH<sub>2</sub>Cl<sub>2</sub> (2.5 mL) was added trifluoromethane sulfonic anhydride (Tf<sub>2</sub>O) (63.0  $\mu$ L, 0.384 mmol, 1.5 eq.) slowly dropwise at 0 °C. After stirring for 30 min, a solution of **9a** (150 mg, 0.255 mmol, 1.0 eq.) in anhydrous CH<sub>2</sub>Cl<sub>2</sub> (2.7 mL) was added dropwise carefully at 0 °C, at which point the reaction solution turned deep red in color, and the reaction mixture was stirred for 10 min. The reaction was quenched with saturated aqueous NaHCO<sub>3</sub> solution and extracted with CH<sub>2</sub>Cl<sub>2</sub> (3 $\times$ 50 mL). The combined organic layer was washed with brine, dried over Na<sub>2</sub>SO<sub>4</sub> and filtered. The filtrate was concentrated under reduced pressure. The crude material was purified by silica gel column chromatography (47-68% ethyl acetate/*n*-hexane) to afford **10a** (33.1 mg, 40%) as a yellow oil. <sup>1</sup>H NMR (500 MHz, CDCl<sub>3</sub>)  $\delta$  7.25 (s, 1H), 7.15 (dd, *J* = 8.0, 1.5 Hz, 1H), 6.93 (dd, *J* = 15.5, 10.0 Hz, 1H), 6.75 (d, *J* = 15.5 Hz, 1H), 6.68 (dd, *J* = 15.5, 10.0 Hz, 1H), 6.52 (d, *J* =

15.0 Hz, 1H), 6.38 (d,  $J = 8.0$  Hz, 1H), 5.16 (t,  $J = 9.0$  Hz, 1H), 3.82 (s, 3H), 3.60-3.50 (m, 2H), 3.39 (t,  $J = 8.3$  Hz, 2H), 2.97 (t,  $J = 8.3$  Hz, 2H), 2.79 (s, 3H) ppm;  $^{13}\text{C}$  NMR (125 MHz,  $\text{CDCl}_3$ )  $\delta$  171.6, 170.4, 154.3, 144.0, 140.1, 131.0, 128.7, 126.0, 122.6, 122.5, 122.4, 106.4, 78.0, 55.7, 52.9, 35.4, 34.7, 28.3 ppm; HRMS (ESI+) calcd for  $\text{C}_{18}\text{H}_{21}\text{N}_2\text{O}_2\text{S}$   $[\text{M}+\text{H}]^+$  : 329.1324, found:  $m/z$  329.1308.

**Compound 10b:** **10b** was synthesized in the same manner as described for the preparation of **10a**; yield 41%, a yellow oil.  $^1\text{H}$  NMR (500 MHz,  $\text{CDCl}_3$ )  $\delta$  7.17 (dd,  $J = 8.0, 1.5$  Hz, 1H), 7.09 (s, 1H), 6.93 (dd,  $J = 15.5, 9.5$  Hz, 1H), 6.73-6.64 (m, 2H), 6.52 (d,  $J = 3.0$  Hz, 1H), 6.50 (d,  $J = 4.0$  Hz, 1H), 5.15 (t,  $J = 9.0$  Hz, 1H), 3.82 (s, 3H), 3.60-3.50 (m, 2H), 3.28 (t,  $J = 5.6$  Hz, 2H), 2.93 (s, 3H), 2.76 (t,  $J = 6.3$  Hz, 2H), 1.97 (quint,  $J = 6.0$  Hz, 2H) ppm;  $^{13}\text{C}$  NMR (125 MHz,  $\text{CDCl}_3$ )  $\delta$  171.6, 170.4, 147.5, 144.1, 139.9, 127.6, 127.3, 124.1, 122.8, 122.3, 122.2, 110.6, 78.0, 52.9, 51.2, 39.0, 34.6, 27.9, 22.3 ppm; HRMS (ESI+) calcd for  $\text{C}_{19}\text{H}_{23}\text{N}_2\text{O}_2\text{S}$   $[\text{M}+\text{H}]^+$  : 343.1480, found:  $m/z$  343.1483.

**Compound 10c:** **10c** was synthesized in the same manner as described for the preparation of **10a**; yield 38%, a yellow oil.  $^1\text{H}$  NMR (500 MHz,  $\text{CDCl}_3$ )  $\delta$  7.28 (d,  $J = 1.5$  Hz, 1H), 7.20 (dd,  $J = 8.5, 1.5$  Hz, 1H), 6.94 (dd,  $J = 15.5, 10.0$  Hz, 1H), 6.75 (d,  $J = 15.0$  Hz, 1H), 6.67 (dd,  $J = 15.5, 10.0$  Hz, 1H), 6.53-6.50 (m, 2H), 5.16 (t,  $J = 9.0$  Hz, 1H), 3.82 (s, 3H), 3.60-3.50 (m, 2H), 3.30 (t,  $J = 6.0$  Hz, 2H), 2.95 (s, 3H), 1.75 (t,  $J = 6.0$  Hz, 2H), 1.30 (s, 6H) ppm;  $^{13}\text{C}$  NMR (125 MHz,  $\text{CDCl}_3$ )  $\delta$  171.6, 170.4, 146.2, 144.2, 140.3, 131.4, 126.7, 125.0, 124.0, 122.1, 121.9, 110.8, 78.0, 52.9, 47.6, 39.2, 36.9, 34.6, 32.1, 30.6 ppm; HRMS (ESI+) calcd for  $\text{C}_{21}\text{H}_{27}\text{N}_2\text{O}_2\text{S}$   $[\text{M}+\text{H}]^+$  : 371.1793, found:  $m/z$  371.1784.

**Compound 10d:** **10d** was synthesized in the same manner as described for the preparation of **10a**; yield 28%, a yellow oil.  $^1\text{H}$  NMR (500 MHz,  $\text{CDCl}_3$ )  $\delta$  6.95 (dd,  $J = 8.0, 2.0$  Hz, 1H), 6.93-6.89 (m, 2H), 6.72-6.64 (m, 2H), 6.60 (d,  $J = 8.0$  Hz, 1H), 6.53 (d,  $J = 15.0$  Hz, 1H), 5.16 (t,  $J = 9.0$  Hz, 1H), 4.28 (t,  $J = 4.5$  Hz, 1H), 3.82 (s, 3H), 3.61-3.50 (m, 2H), 3.32 (t,  $J = 4.5$  Hz, 2H), 2.92 (s, 3H) ppm;  $^{13}\text{C}$  NMR (125 MHz,  $\text{CDCl}_3$ )  $\delta$  171.6, 170.3, 144.1, 143.6, 139.3, 137.6, 126.4, 123.6, 123.2, 122.0, 113.9, 112.0, 78.0, 64.7, 51.9, 49.1, 38.6, 34.7 ppm; HRMS (ESI+) calcd for  $\text{C}_{18}\text{H}_{21}\text{N}_2\text{O}_3\text{S}$   $[\text{M}+\text{H}]^+$  : 345.1273, found:  $m/z$  345.1270.

**Compound 10e:** **10e** was synthesized in the same manner as described for the preparation of **10a**; yield 40%, an orange oil.  $^1\text{H}$  NMR (500 MHz,  $\text{CDCl}_3$ )  $\delta$  6.94-6.89 (comp, 3H), 6.68-6.64 (m, 2H), 6.49 (d,  $J = 15.0, 1.5$  Hz, 1H), 5.15 (t,  $J = 9.0$  Hz, 1H), 3.82 (s, 3H), 3.57 (dd,  $J = 11.0, 9.0$  Hz, 1H), 3.51 (dd,  $J = 11.0, 9.0$  Hz, 1H), 3.19 (t,  $J = 5.6$  Hz, 4H), 2.73 (t,  $J = 6.4$  Hz, 4H), 1.99-1.92 (m, 4H) ppm;  $^{13}\text{C}$  NMR (125 MHz,  $\text{CDCl}_3$ )  $\delta$  171.7, 170.4, 144.2, 143.9, 140.1, 126.4, 123.5, 122.0, 121.8, 121.3, 78.0, 52.9, 50.1, 34.7, 27.8, 21.9 ppm; HRMS (ESI+) calcd for  $\text{C}_{21}\text{H}_{25}\text{N}_2\text{O}_2\text{S}$   $[\text{M}+\text{H}]^+$  : 369.1637, found:  $m/z$  369.1625.

**Compound 10f:** **10f** was synthesized in the same manner as described for the preparation of **10a**; yield 83%, a yellow oil.  $^1\text{H}$  NMR (500 MHz,  $\text{CDCl}_3$ )  $\delta$  7.21 (dd,  $J = 8.5, 2.0$  Hz, 1H), 7.14 (d,  $J = 2.0$  Hz, 1H), 6.94 (dd,  $J = 15.5, 10.0$  Hz, 1H), 6.75 (d,  $J = 15.0$  Hz, 1H), 6.68 (dd,  $J = 15.5, 10.0$  Hz, 1H), 6.52 (d,  $J = 15.0$  Hz, 1H), 6.46

(d,  $J = 8.5$  Hz, 1H), 5.31 (d,  $J = 1.0$ , 1H), 5.16 (t,  $J = 9.0$  Hz, 1H), 3.82 (s, 3H), 3.60-3.50 (m, 2H), 2.83 (s, 3H), 2.01 (d,  $J = 1.5$  Hz, 3H), 1.32 (s, 6H) ppm;  $^{13}\text{C}$  NMR (125 MHz,  $\text{CDCl}_3$ )  $\delta$  171.6, 170.4, 146.2, 144.0, 140.0, 130.3, 128.7, 127.7, 124.2, 122.9, 122.4, 122.3, 122.2, 110.5, 78.0, 56.9, 52.9, 34.6, 31.0, 27.9, 18.8 ppm; HRMS (ESI+) calcd for  $\text{C}_{22}\text{H}_{27}\text{N}_2\text{O}_2\text{S}$   $[\text{M}+\text{H}]^+$  : 383.1793, found:  $m/z$  383.1790.

**Compound 11a (NIRLuc1):** Luciferin ester **10a** (33.1 mg, 0.101 mmol) was treated with 4 M HCl aq. (1.5 mL) at room temperature for 24 h. The reaction mixture was neutralized by the addition of saturated  $\text{NaHCO}_3$  aq. at 0 °C, and concentrated under reduced pressure. The residue was purified by ODS column chromatography (20-100% acetonitrile/ $\text{H}_2\text{O}$ ) to afford **11a** (18.8 mg, 59%) as a yellow solid.  $^1\text{H}$  NMR (500 MHz,  $\text{CD}_3\text{OD}$ )  $\delta$  7.26 (s, 1H), 7.17 (dd,  $J = 8.0, 1.5$  Hz, 1H), 6.93 (td,  $J = 10.0, 5.2$  Hz, 1H), 6.79-6.73 (m, 2H), 6.50 (d,  $J = 15.0$  Hz, 1H), 6.43 (d,  $J = 8.5$  Hz, 1H), 4.94 (t,  $J = 9.3$  Hz, 1H), 3.57 (dd,  $J = 10.9, 9.2$  Hz, 1H), 3.47 (dd,  $J = 10.7, 9.6$  Hz, 1H), 3.33 (t,  $J = 8.0$  Hz, 2H), 2.93 (t,  $J = 8.2$  Hz, 2H), 2.77 (s, 3H) ppm;  $^{13}\text{C}$  NMR (125 MHz,  $\text{CD}_3\text{OD}$ )  $\delta$  178.3, 170.9, 155.6, 144.5, 141.0, 132.3, 129.5, 127.8, 123.6, 123.5, 107.8, 107.7, 82.1, 56.8, 36.7, 35.8, 29.1 ppm; HRMS (ESI+) calcd for  $\text{C}_{17}\text{H}_{19}\text{N}_2\text{O}_2\text{S}$   $[\text{M}+\text{H}]^+$  : 315.1167, found:  $m/z$  315.1158; The optical purity was determined by CSP HPLC analysis (Chiracel OZ-3R, eluent: 10-90%  $\text{CH}_3\text{CN}/\text{H}_2\text{O}$ , flow 0.6 mL/min) 67% e.e. [ $t_{\text{R}}$  (minor) = 14.8 min,  $t_{\text{R}}$  (major) = 16.1 min].

**Compound 11b (NIRLuc2):** **11b** was synthesized in the same manner as described for the preparation of **11a**; yield 93%, a yellow solid.  $^1\text{H}$  NMR (500 MHz,  $\text{CD}_3\text{OD}$ )  $\delta$  7.16 (dd,  $J = 8.5, 2.0$  Hz, 1H), 7.07 (s, 1H), 6.92 (dd,  $J = 15.0, 8.5$  Hz, 1H), 6.76-6.68 (m, 2H), 6.54 (d,  $J = 8.5$  Hz, 1H), 6.49 (d,  $J = 15.5$  Hz, 1H), 4.94 (t,  $J = 9.0$  Hz, 1H), 3.56 (dd,  $J = 10.5, 9.0$  Hz, 1H), 3.46 (dd,  $J = 10.5, 9.5$  Hz, 1H), 3.26 (t,  $J = 5.8$  Hz, 2H), 2.90 (s, 3H), 2.73 (t,  $J = 6.5$  Hz, 2H), 1.94 (quint,  $J = 6.0$  Hz, 2H) ppm;  $^{13}\text{C}$  NMR (125 MHz,  $\text{CD}_3\text{OD}$ )  $\delta$  178.4, 170.9, 148.7, 144.6, 140.9, 128.6, 128.0, 125.7, 123.9, 123.2, 123.1, 111.7, 82.1, 52.2, 39.1, 36.7, 28.8, 23.4 ppm; HRMS (ESI+) calcd for  $\text{C}_{18}\text{H}_{21}\text{N}_2\text{O}_2\text{S}$   $[\text{M}+\text{H}]^+$  : 329.1324, found:  $m/z$  329.1325; The optical purity was determined by CSP HPLC analysis (Chiracel OZ-3R, eluent: 10-90%  $\text{CH}_3\text{CN}/\text{H}_2\text{O}$ , flow 0.6 mL/min) 76% e.e. [ $t_{\text{R}}$  (minor) = 16.6 min,  $t_{\text{R}}$  (major) = 18.3 min].

**Compound 11c (NIRLuc3):** **11c** was synthesized in the same manner as described for the preparation of **11a**; yield 97%, a yellow solid.  $^1\text{H}$  NMR (500 MHz,  $\text{CD}_3\text{OD}$ )  $\delta$  7.31 (d,  $J = 2.0$  Hz, 1H), 7.20 (dd,  $J = 8.5, 2.0$  Hz, 1H), 6.94 (td,  $J = 10.0, 5.2$  Hz, 1H), 6.75 (d,  $J = 5.0$  Hz, 1H), 6.56 (d,  $J = 8.5$  Hz, 1H), 6.50 (d,  $J = 15.0$  Hz, 1H), 4.94 (t,  $J = 9.0$  Hz, 1H), 3.57 (dd,  $J = 10.5, 9.0$  Hz, 1H), 3.47 (dd,  $J = 10.5, 9.5$  Hz, 1H), 3.29 (t,  $J = 6.0$  Hz, 2H), 2.93 (s, 3H), 1.75 (t,  $J = 6.0$  Hz, 2H), 1.28 (s, 6H) ppm;  $^{13}\text{C}$  NMR (125 MHz,  $\text{CD}_3\text{OD}$ )  $\delta$  178.3, 171.0, 147.5, 144.6, 141.1, 132.5, 127.5, 126.1, 125.6, 123.2, 123.0, 112.0, 82.0, 39.4, 38.1, 36.7, 32.9, 31.3, 31.0 ppm; HRMS (ESI+) calcd for  $\text{C}_{20}\text{H}_{25}\text{N}_2\text{O}_2\text{S}$   $[\text{M}+\text{H}]^+$  : 357.1637, found:  $m/z$  357.1630; The optical purity was determined by CSP HPLC analysis (Chiracel OZ-3R, eluent: 10-90%  $\text{CH}_3\text{CN}/\text{H}_2\text{O}$ , flow 0.6 mL/min) 98% e.e. [ $t_{\text{R}}$  (minor) = 18.6 min,  $t_{\text{R}}$  (major) = 20.2 min].

**Compound 11d (NIRLuc4):** **11d** was synthesized in the same manner as described for the preparation of

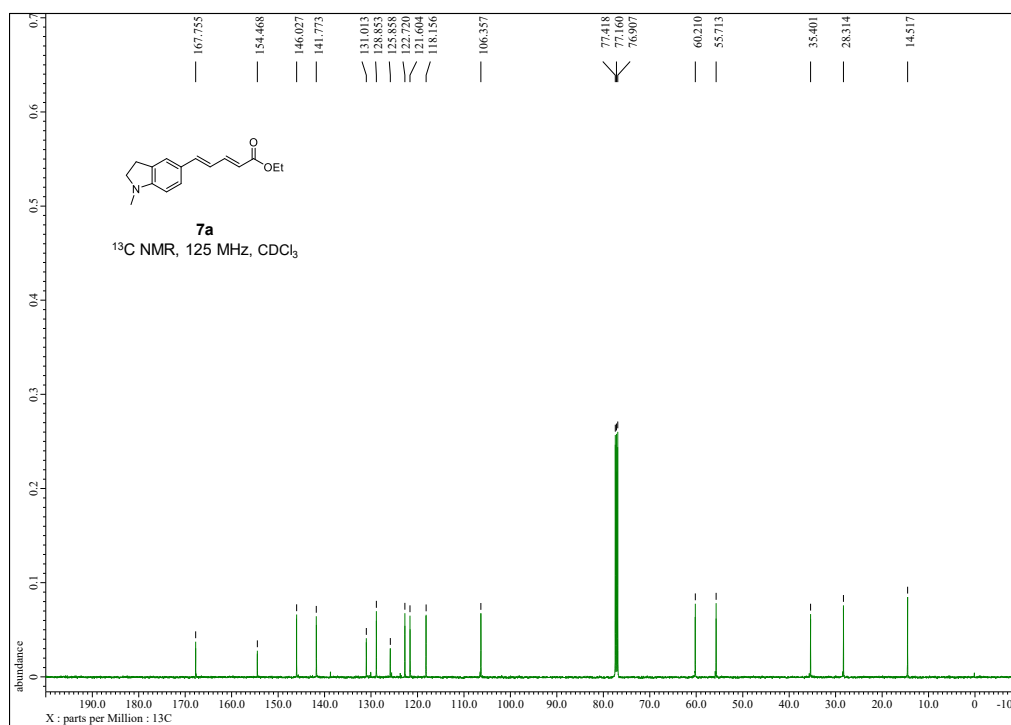
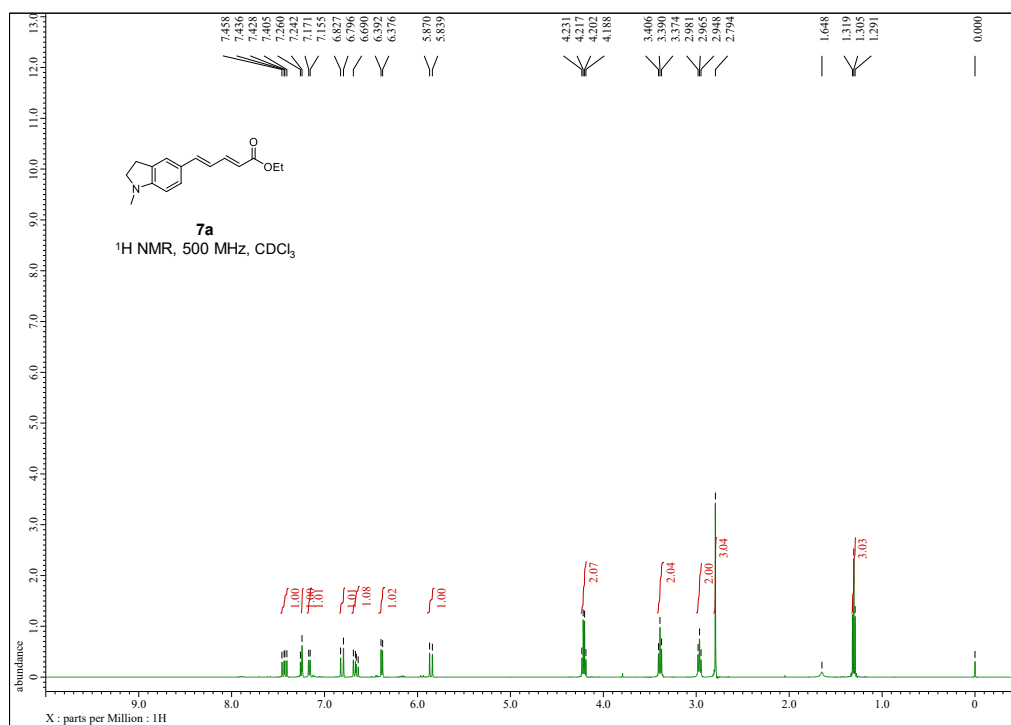
**11a**; yield 75%, a yellow solid.  $^1\text{H}$  NMR (500 MHz,  $\text{CD}_3\text{OD}$ )  $\delta$  6.95-6.87 (m, 3H), 6.74 (dd,  $J = 15.5, 9.5$  Hz, 1H), 6.69 (d,  $J = 15.0$  Hz, 1H), 6.63 (d,  $J = 8.5$  Hz, 1H), 6.52 (d,  $J = 15.5$  Hz, 1H), 4.94 (t,  $J = 9.3$  Hz, 1H), 4.23 (t,  $J = 4.5$  Hz, 2H), 3.56 (dd,  $J = 10.6, 9.2$  Hz, 1H), 3.47 (dd,  $J = 10.7, 9.6$  Hz, 1H), 3.28 (t,  $J = 4.3$  Hz, 2H), 2.90 (s, 3H) ppm;  $^{13}\text{C}$  NMR (125 MHz,  $\text{CD}_3\text{OD}$ )  $\delta$  178.3, 170.7, 145.5, 144.1, 140.3, 139.0, 127.7, 124.4, 124.1, 122.9, 114.6, 113.1, 82.2, 65.8, 50.0, 38.6, 36.7 ppm; HRMS (ESI+) calcd for  $\text{C}_{17}\text{H}_{19}\text{N}_2\text{O}_3\text{S}$   $[\text{M}+\text{H}]^+$  : 331.1116, found:  $m/z$  331.1104; The optical purity was determined by CSP HPLC analysis (Chiracel OZ-3R, eluent: 10-90%  $\text{CH}_3\text{CN}/\text{H}_2\text{O}$ , flow 0.6 mL/min) 81% e.e. [ $t_{\text{R}}$  (minor) = 13.2 min,  $t_{\text{R}}$  (major) = 14.3 min].

**Compound 11e (NIRLuc5): 11e** was synthesized in the same manner as described for the preparation of **11a**; yield 60%, a yellow solid.  $^1\text{H}$  NMR (500 MHz,  $\text{CD}_3\text{OD}$ )  $\delta$  6.90 (dd,  $J = 15.5, 10.0$  Hz, 1H), 6.88 (s, 2H), 6.68 (dd,  $J = 15.0, 9.5$  Hz, 1H), 6.63 (d,  $J = 15.5$  Hz, 1H), 6.46 (d,  $J = 15.5$  Hz, 1H), 4.93 (t,  $J = 9.2$  Hz, 1H), 3.55 (dd,  $J = 10.7, 9.0$  Hz, 1H), 3.46 (dd,  $J = 10.7, 9.6$  Hz, 1H), 3.18 (t,  $J = 5.6$  Hz, 4H), 2.70 (t,  $J = 6.4$  Hz, 4H), 1.97-1.89 (m, 4H) ppm;  $^{13}\text{C}$  NMR (125 MHz,  $\text{CD}_3\text{OD}$ )  $\delta$  178.3, 170.9, 144.9, 144.7, 141.2, 127.3, 125.1, 122.9, 122.6, 122.5, 82.1, 51.0, 36.7, 28.7, 23.0 ppm; HRMS (ESI+) calcd for  $\text{C}_{20}\text{H}_{23}\text{N}_2\text{O}_2\text{S}$   $[\text{M}+\text{H}]^+$  : 355.1480, found:  $m/z$  355.1480; The optical purity was determined by CSP HPLC analysis (Chiracel OZ-3R, eluent: 10-90%  $\text{CH}_3\text{CN}/\text{H}_2\text{O}$ , flow 0.6 mL/min) 85% e.e. [ $t_{\text{R}}$  (minor) = 19.9 min,  $t_{\text{R}}$  (major) = 22.9 min].

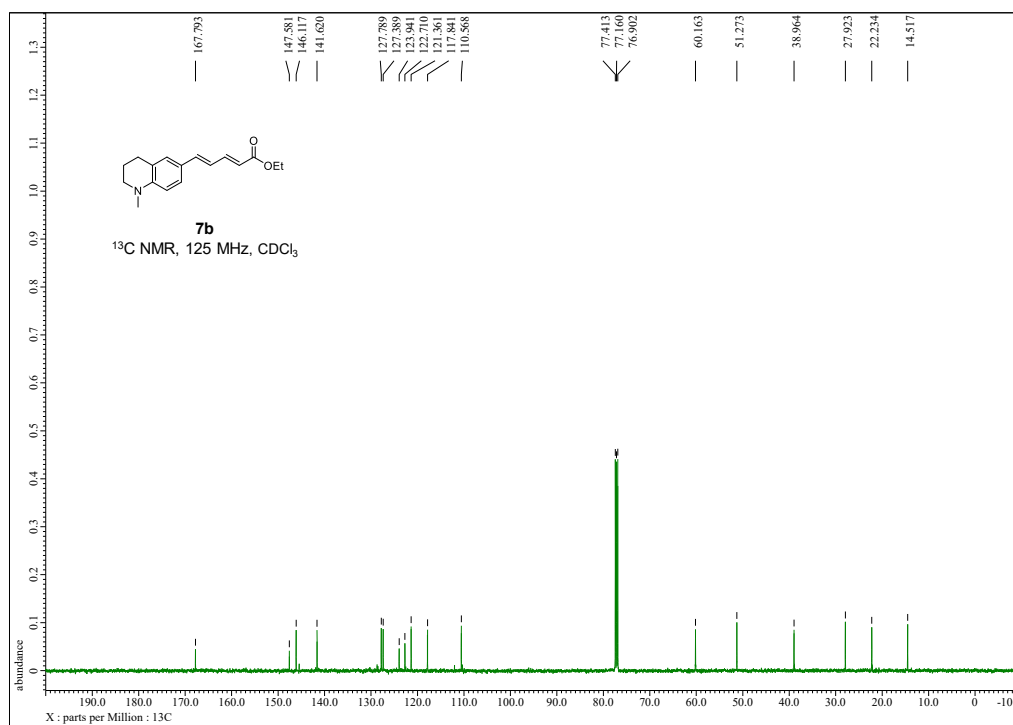
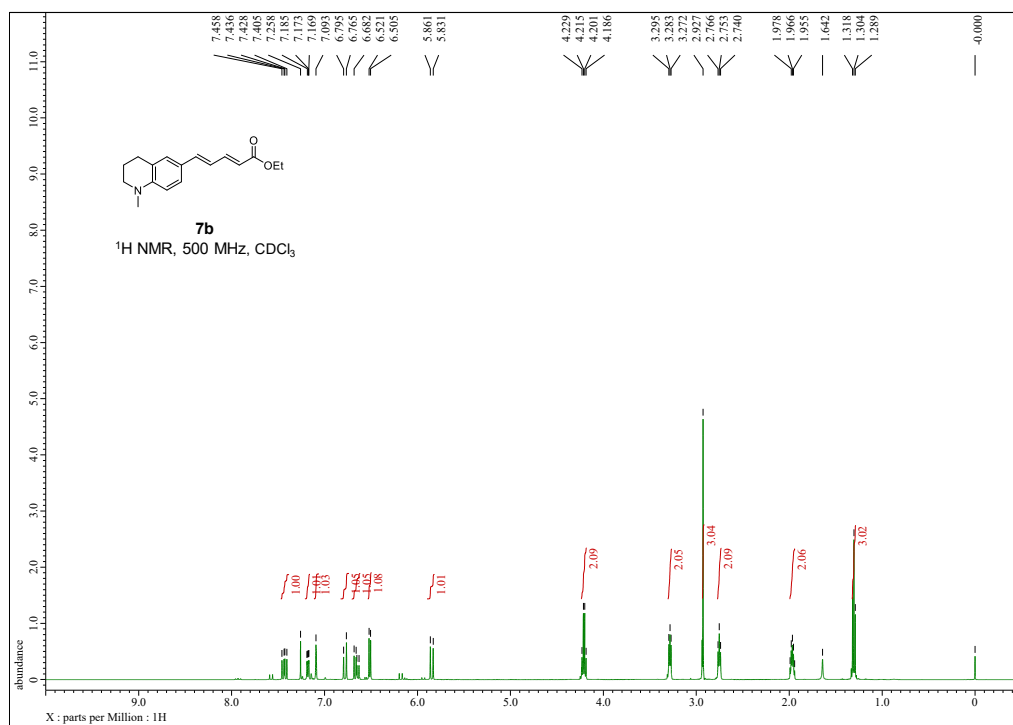
**Compound 11f (NIRLuc6): 11f** was synthesized in the same manner as described for the preparation of **11a**; yield 86%, a yellow solid.  $^1\text{H}$  NMR (500 MHz,  $\text{CD}_3\text{OD}$ )  $\delta$  7.23 (dd,  $J = 8.5, 2.0$ , 1H), 7.16 (d,  $J = 2.0$  Hz, 1H), 6.99-6.90 (m, 1H), 6.81-6.70 (m, 2H), 6.56-6.46 (m, 2H), 5.35 (d,  $J = 1.0$ , 1H), 4.95 (t,  $J = 9.5$  Hz, 1H), 3.57 (dd,  $J = 10.9, 9.2$  Hz, 1H), 3.47 (dd,  $J = 10.7, 9.7$  Hz, 1H), 2.83 (s, 3H), 1.99 (d,  $J = 1.0$  Hz, 3H), 1.31 (s, 6H) ppm;  $^{13}\text{C}$  NMR (125 MHz,  $\text{CD}_3\text{OD}$ )  $\delta$  178.3, 170.9, 147.5, 144.5, 140.7, 131.3, 129.6, 128.8, 125.7, 124.1, 123.5, 123.4, 123.1, 111.6, 82.0, 57.8, 36.7, 31.2, 27.9, 18.8 ppm; HRMS (ESI+) calcd for  $\text{C}_{21}\text{H}_{25}\text{N}_2\text{O}_2\text{S}$   $[\text{M}+\text{H}]^+$  : 369.1637, found:  $m/z$  369.1648; The optical purity was determined by CSP HPLC analysis (Chiracel OZ-3R, eluent: 10-90%  $\text{CH}_3\text{CN}/\text{H}_2\text{O}$ , flow 0.6 mL/min) 96% e.e. [ $t_{\text{R}}$  (minor) = 19.5 min,  $t_{\text{R}}$  (major) = 20.1 min].

### 4.4.3. NMR spectra

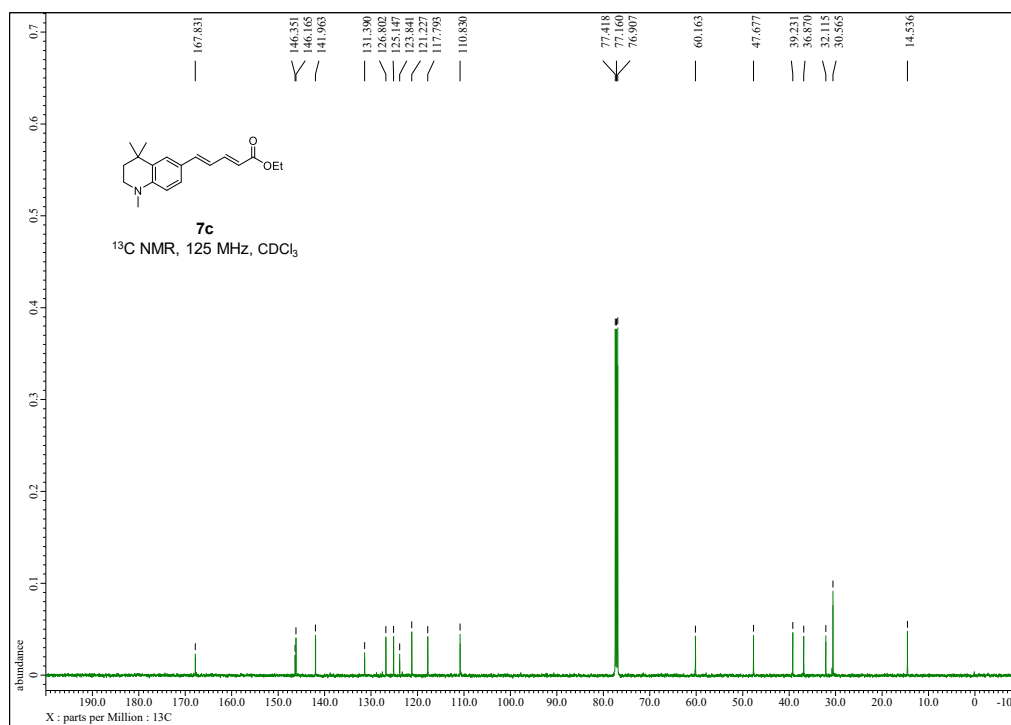
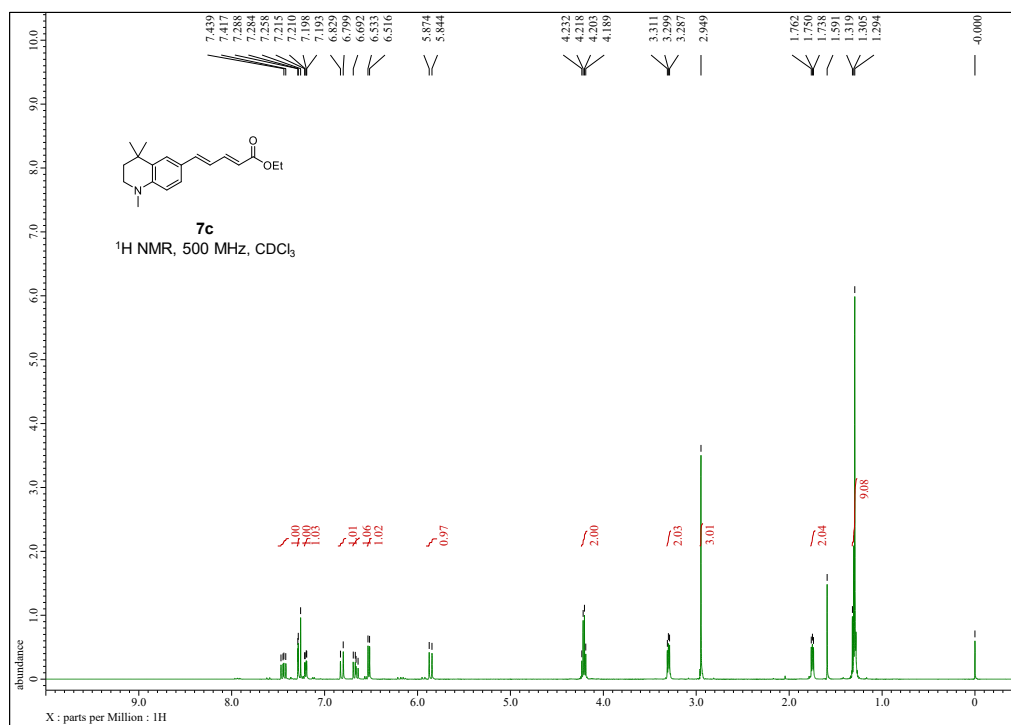
#### Compound 7a



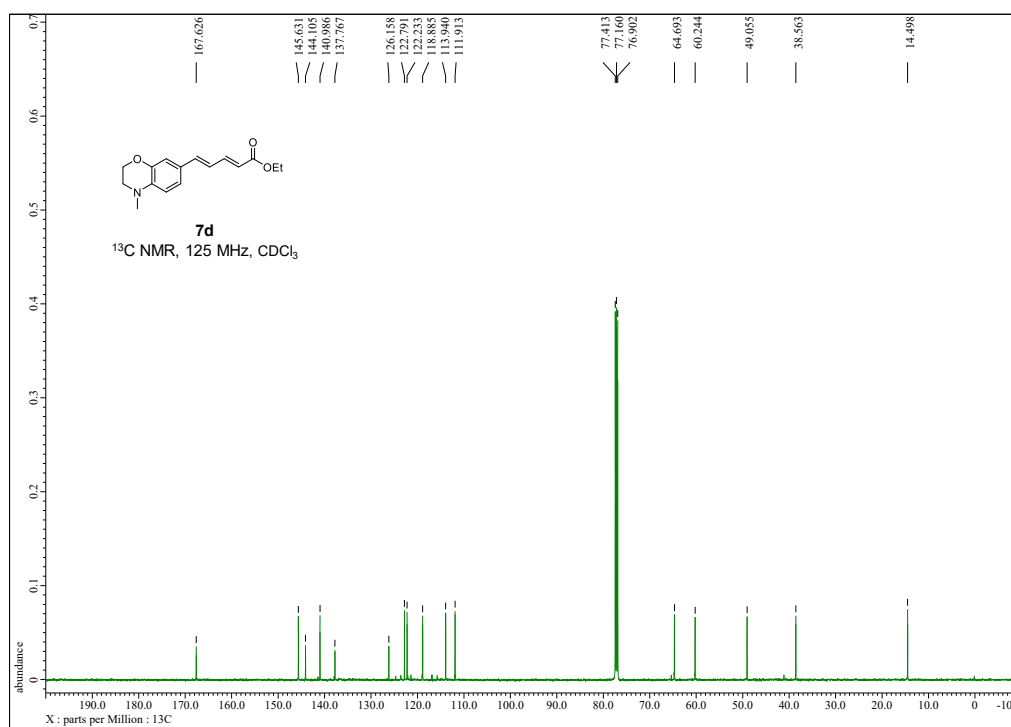
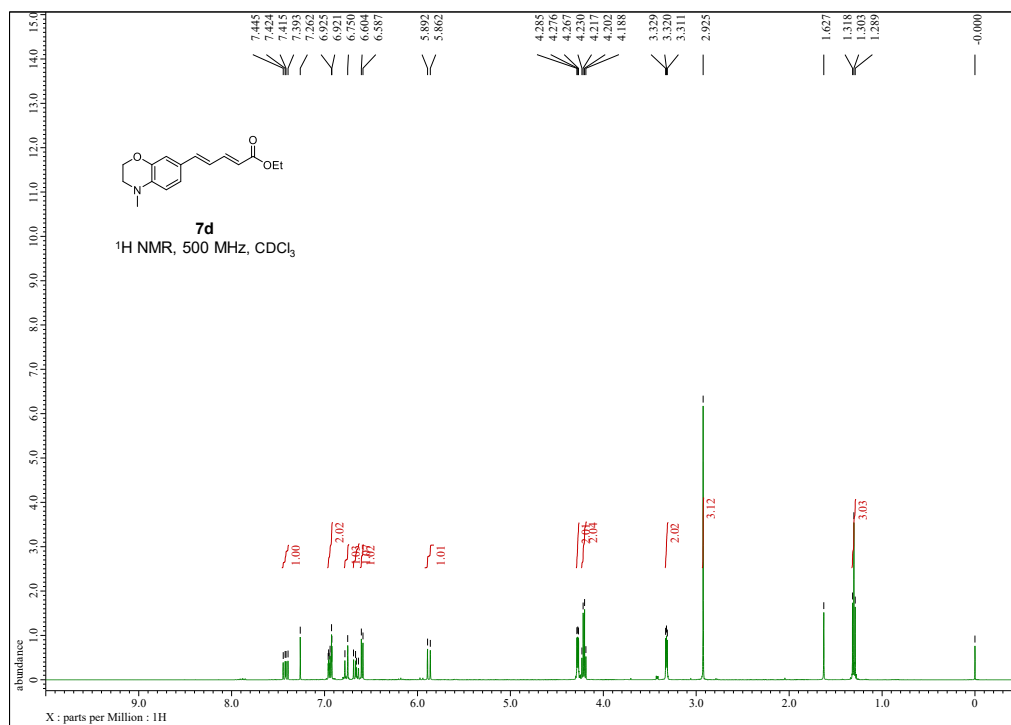
## Compound 7b

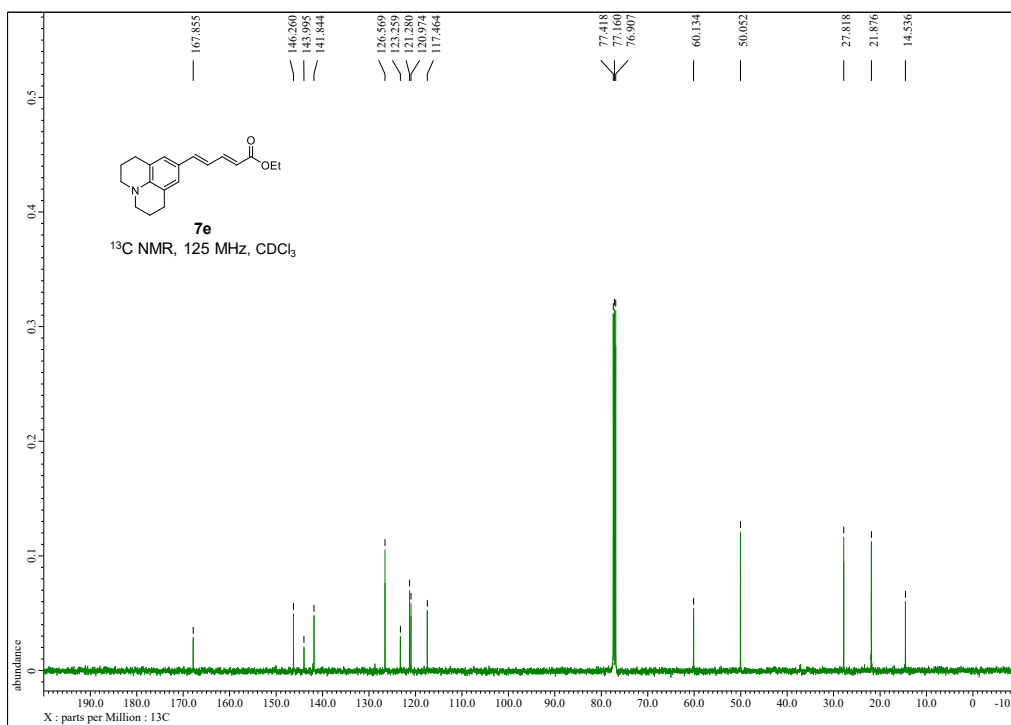
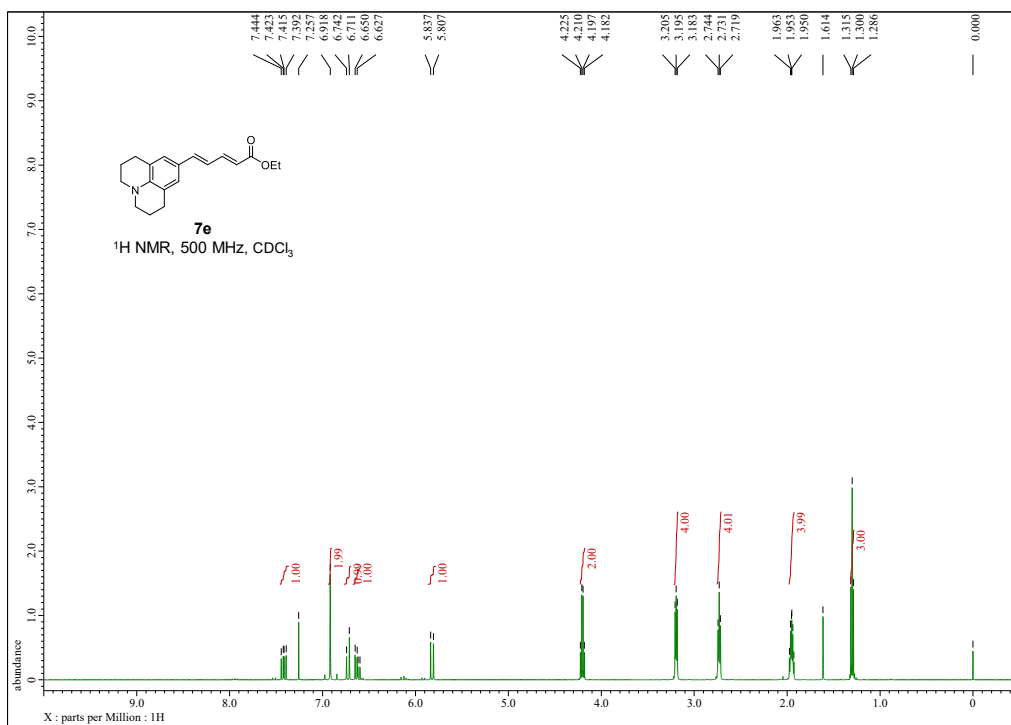


## Compound 7c

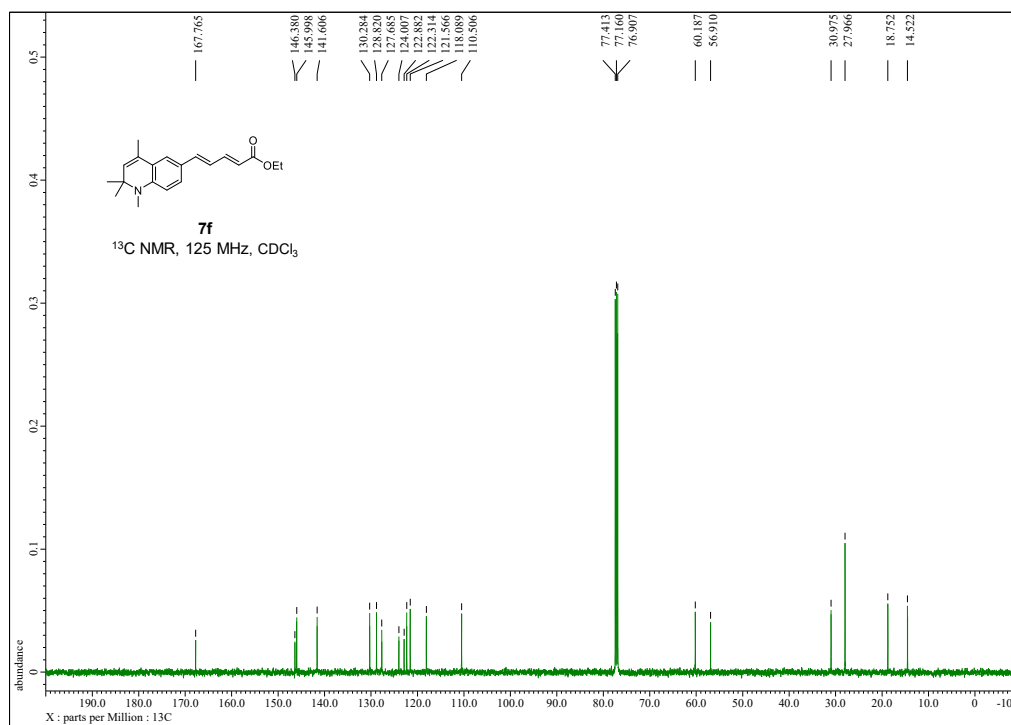
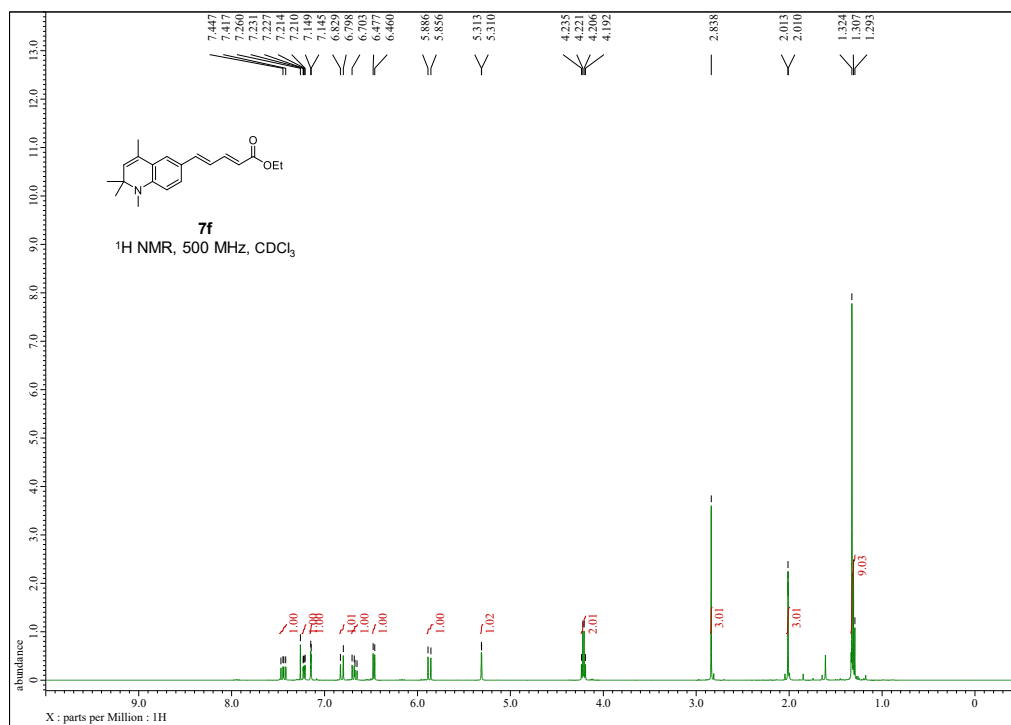


## Compound 7d

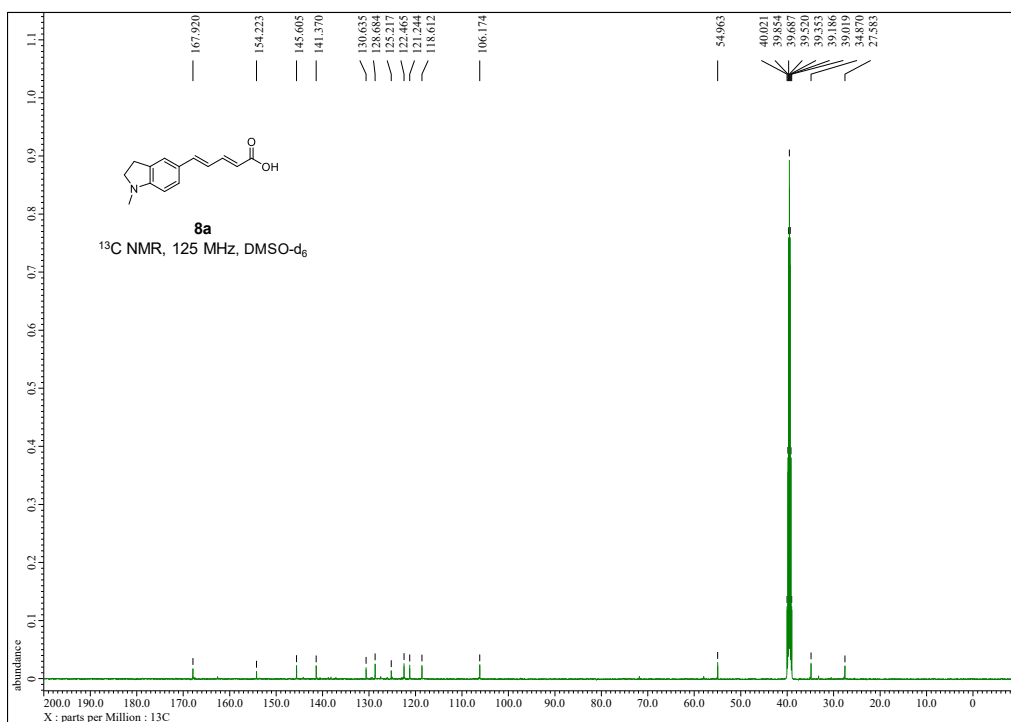
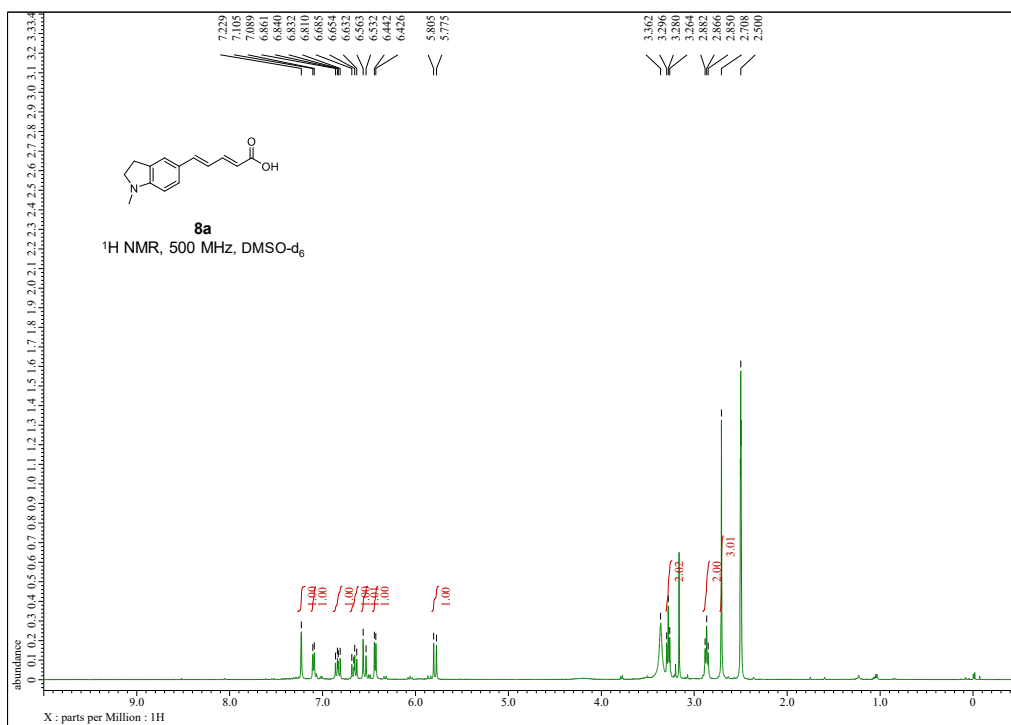


Compound **7e**

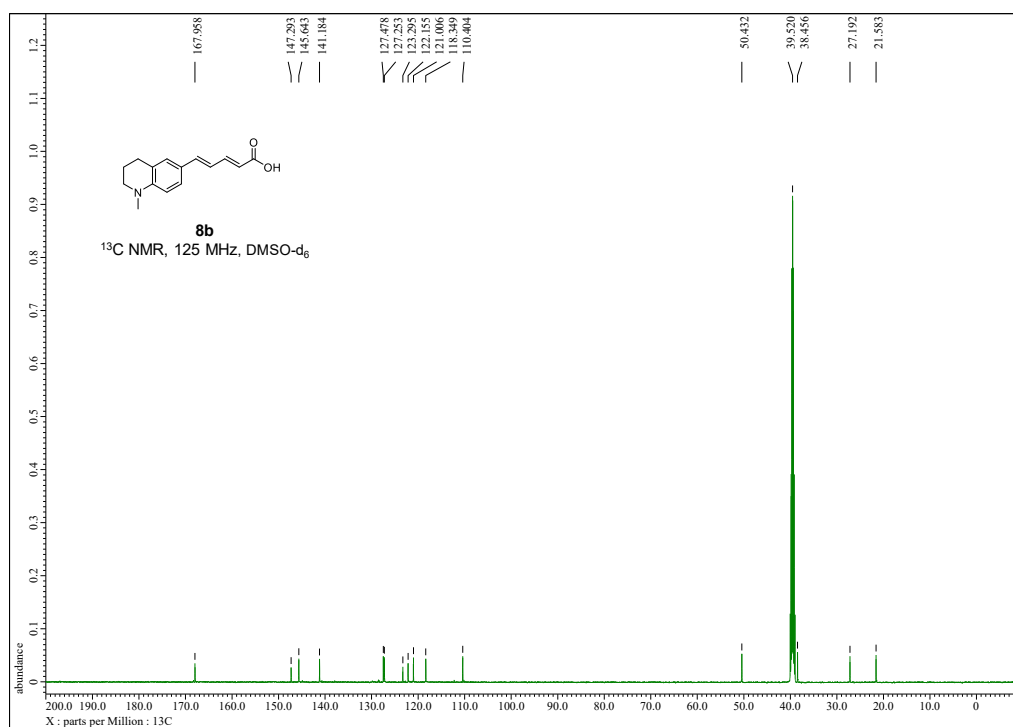
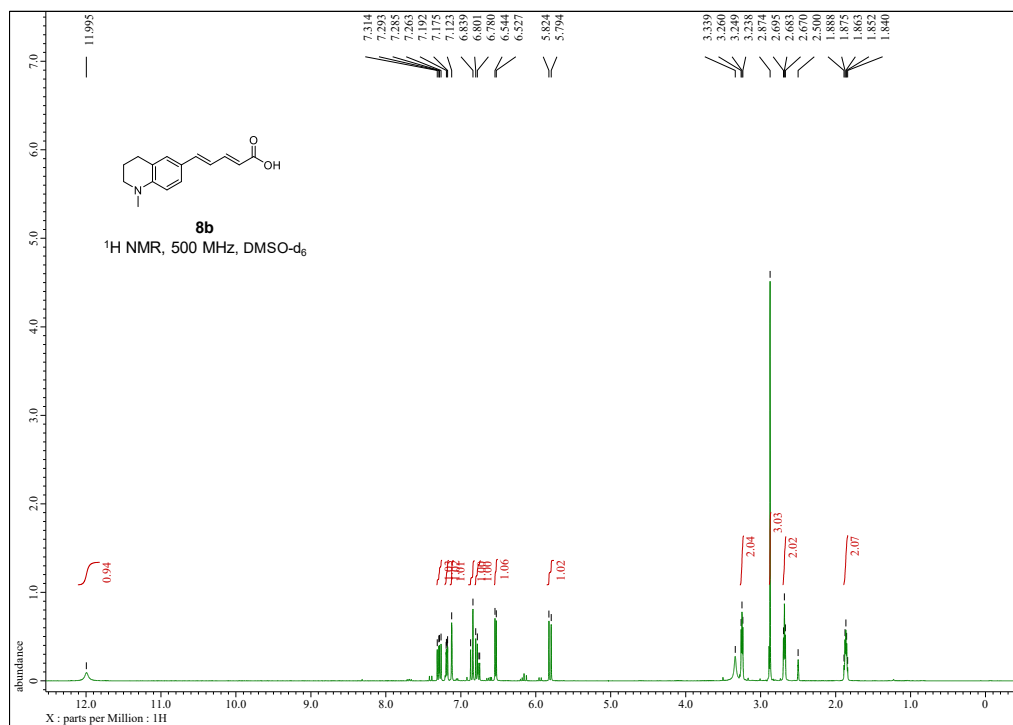
## Compound 7f



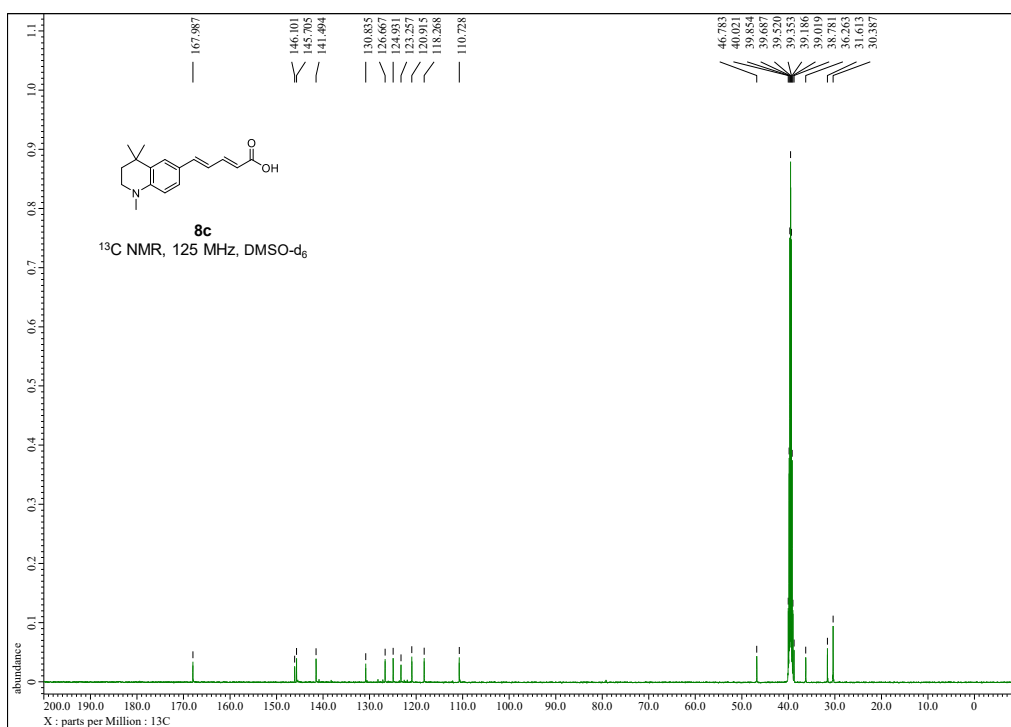
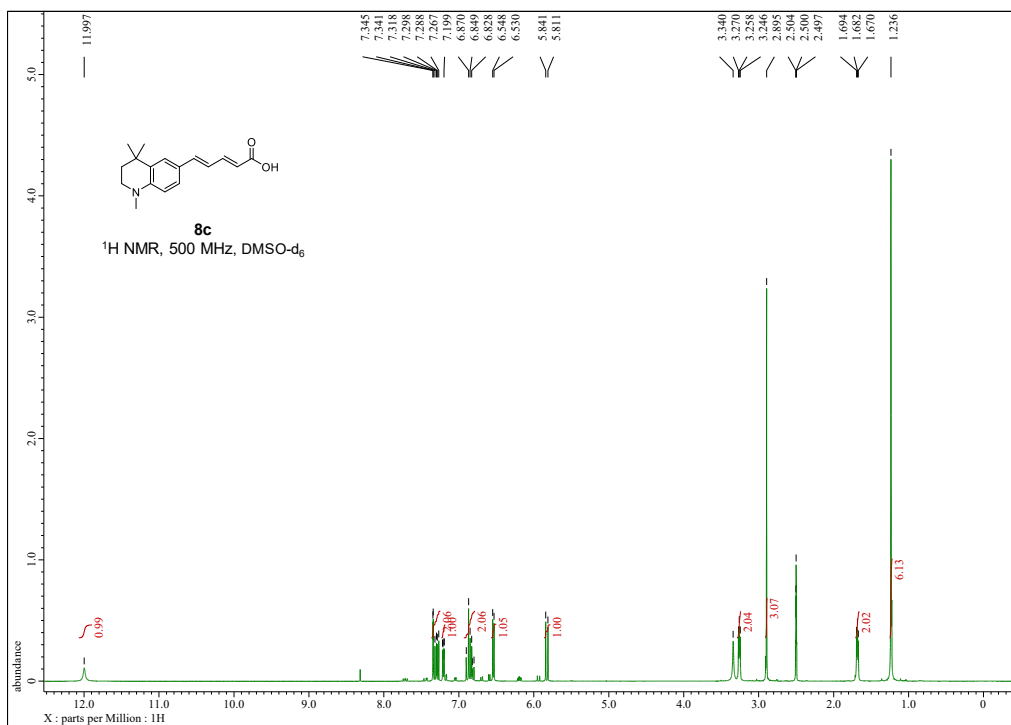
## Compound 8a



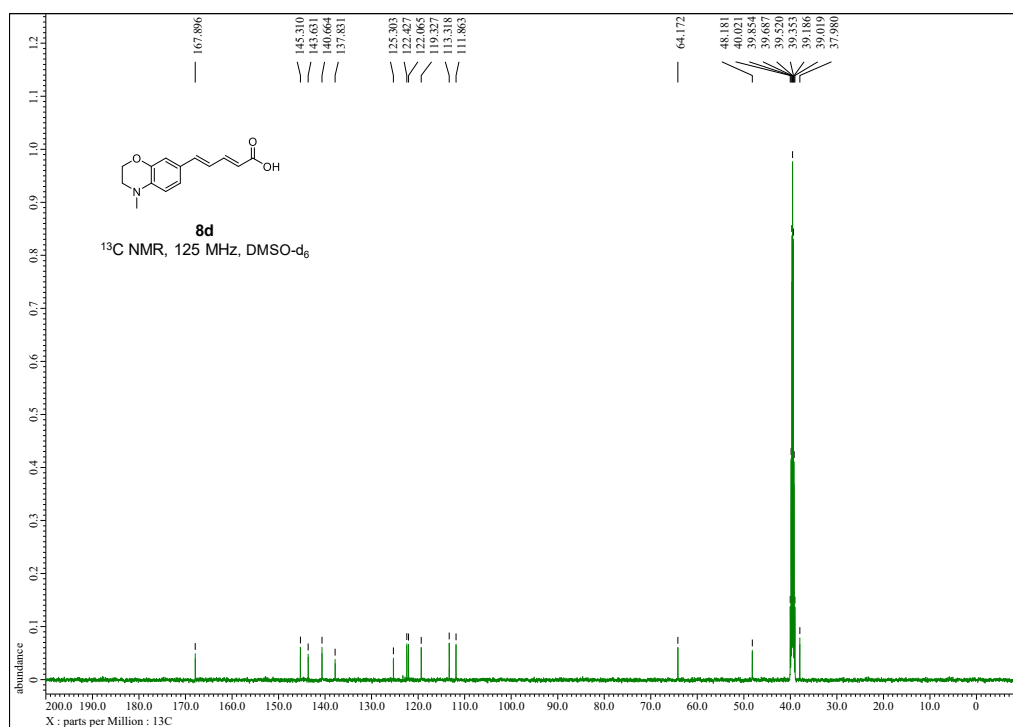
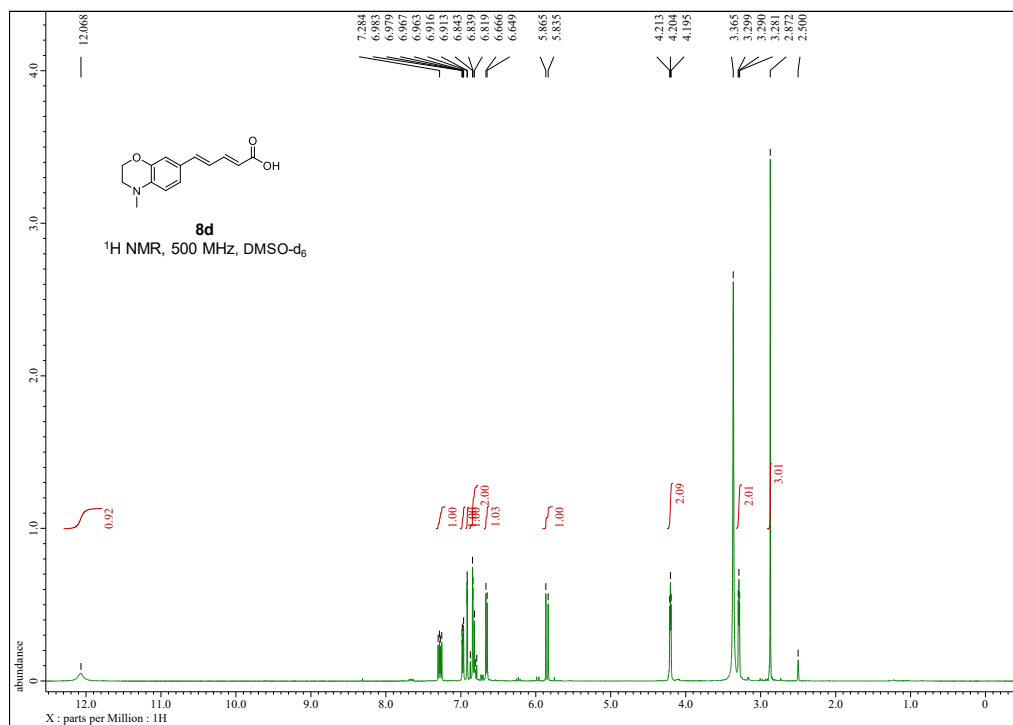
## Compound 8b



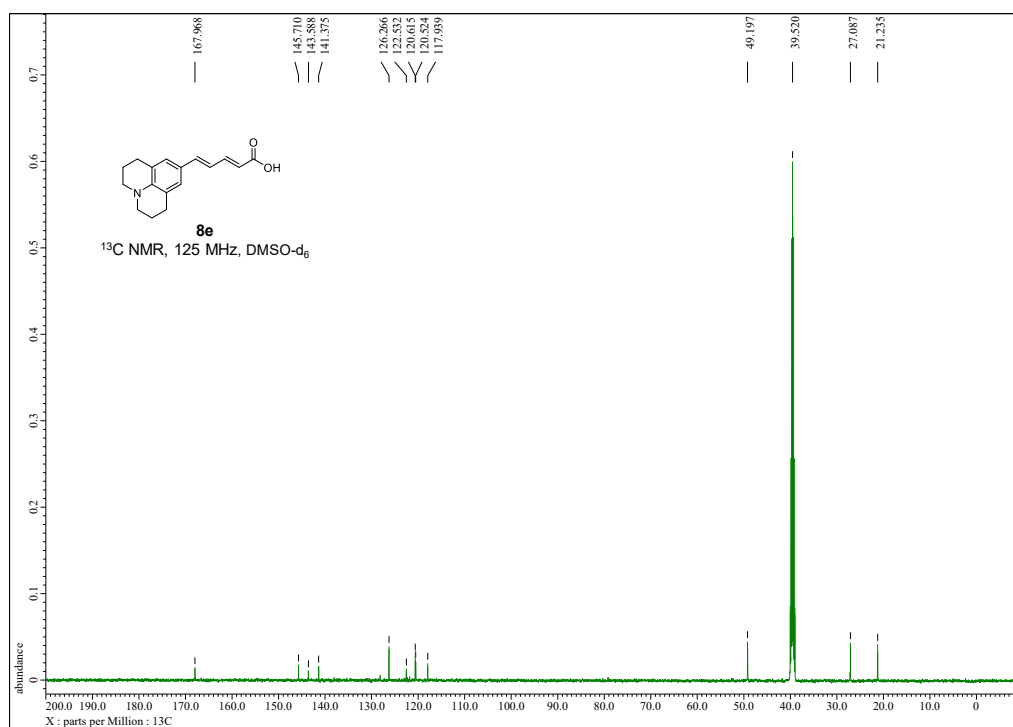
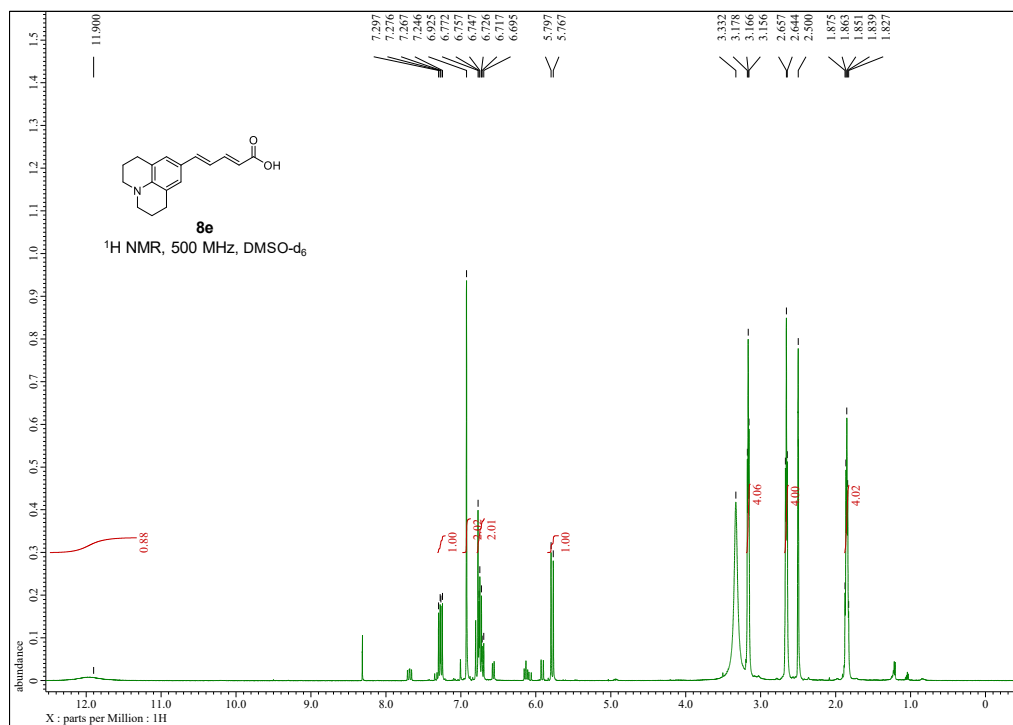
## Compound 8c



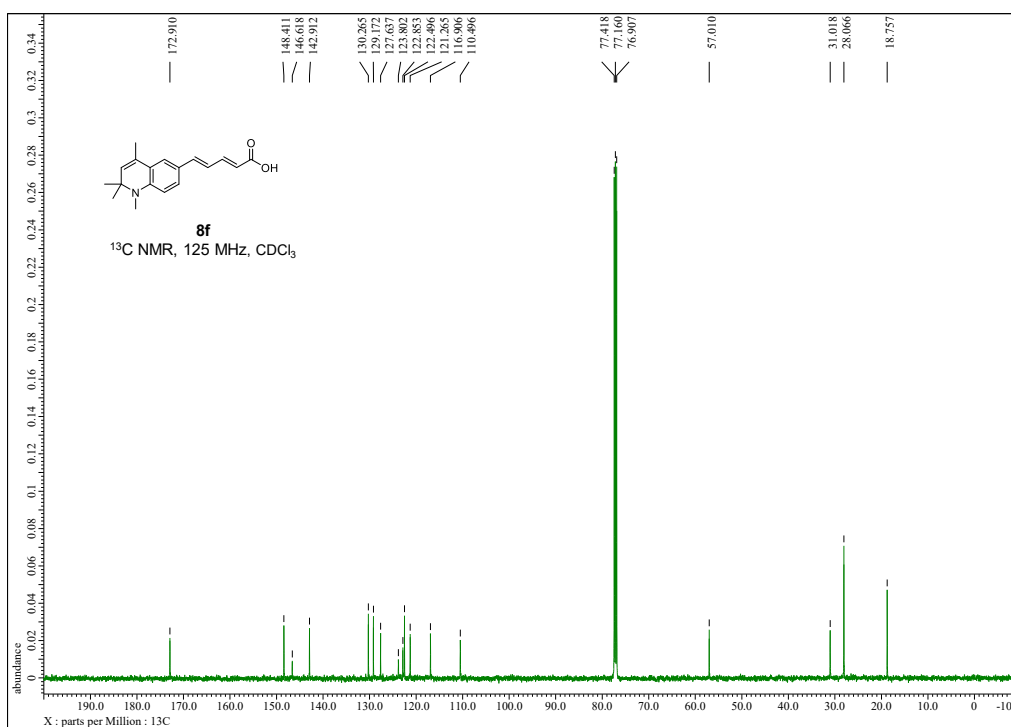
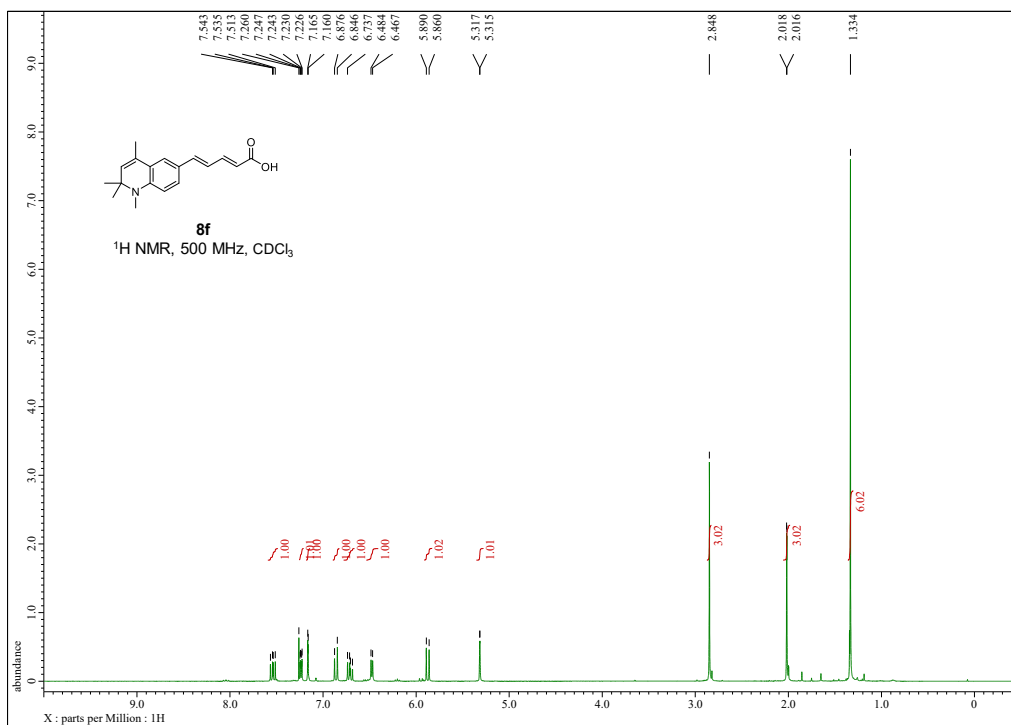
## Compound 8d



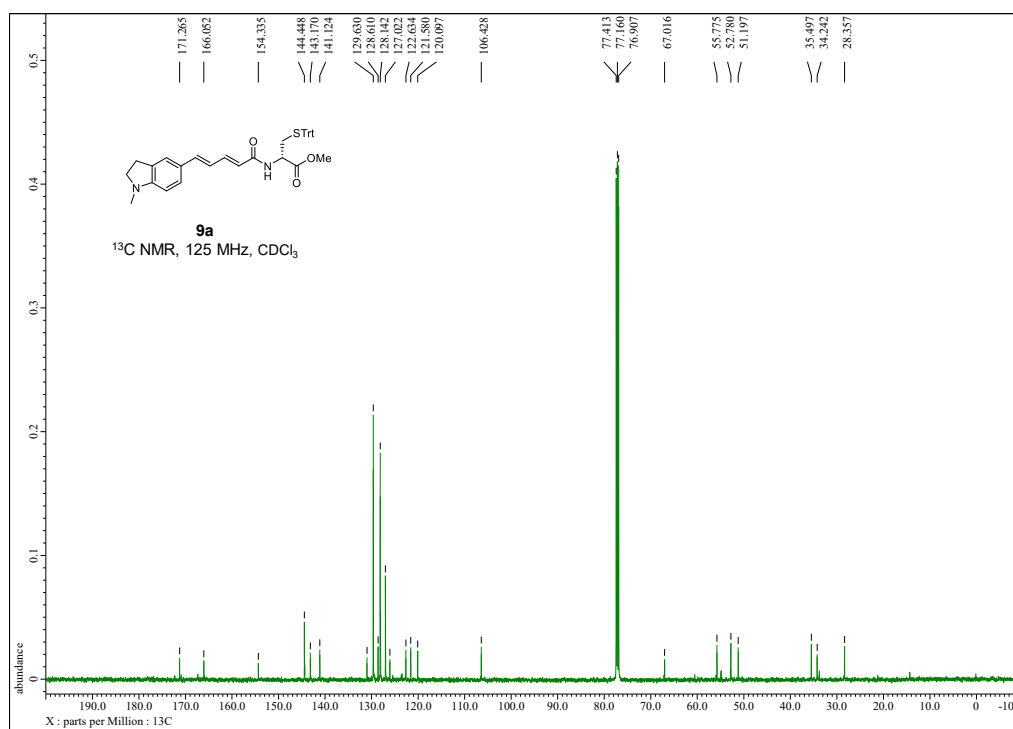
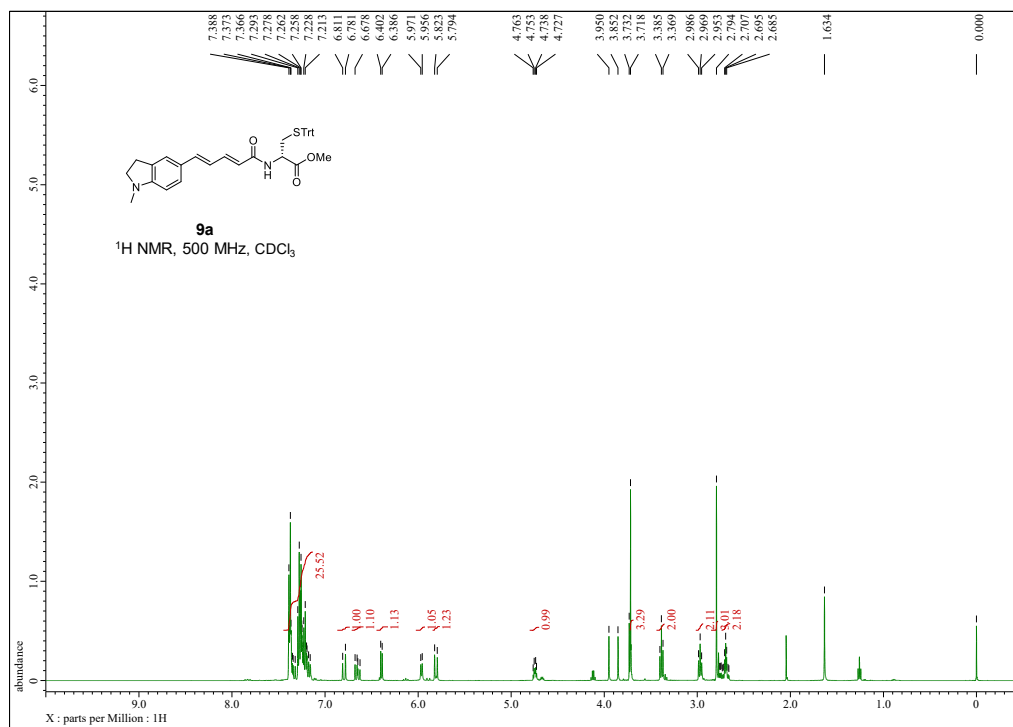
## Compound 8e



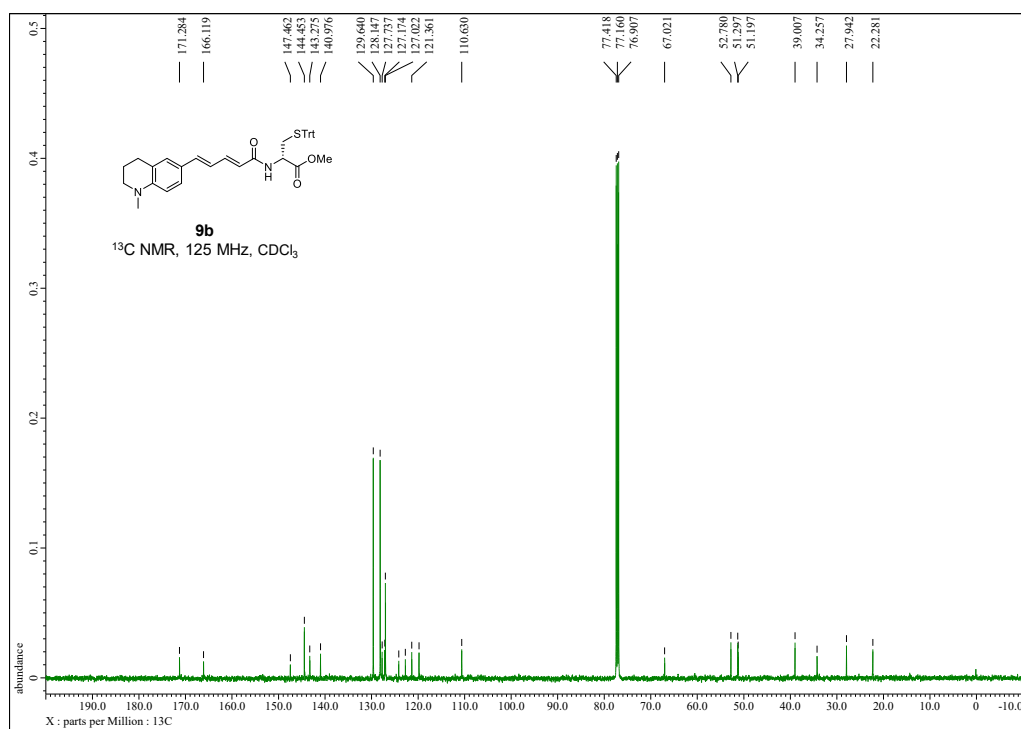
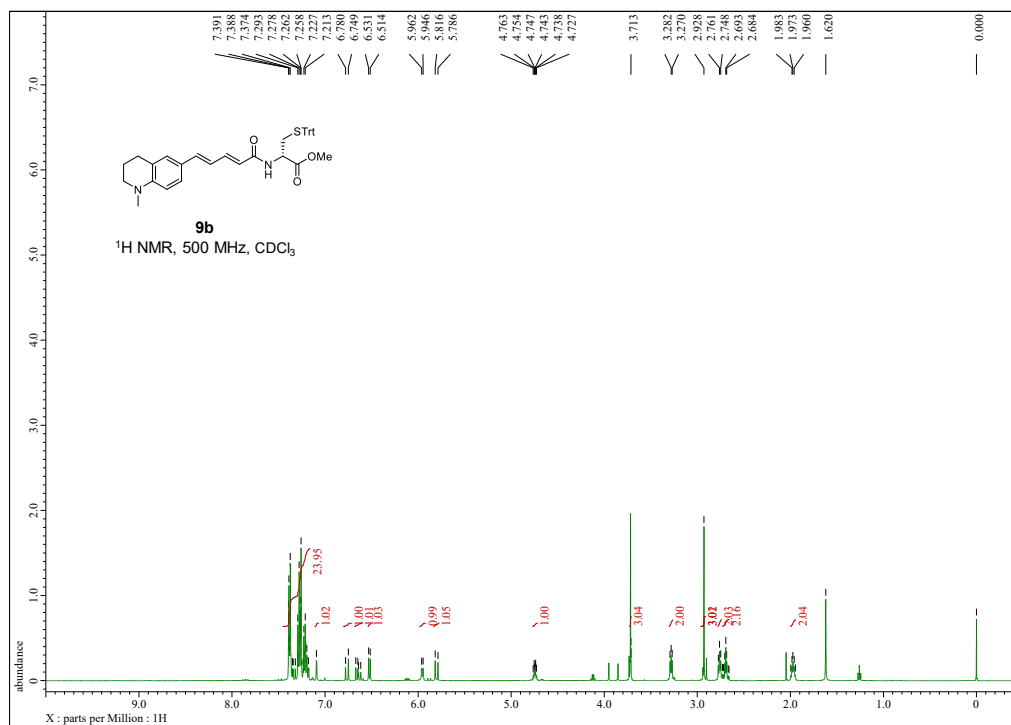
## Compound 8f



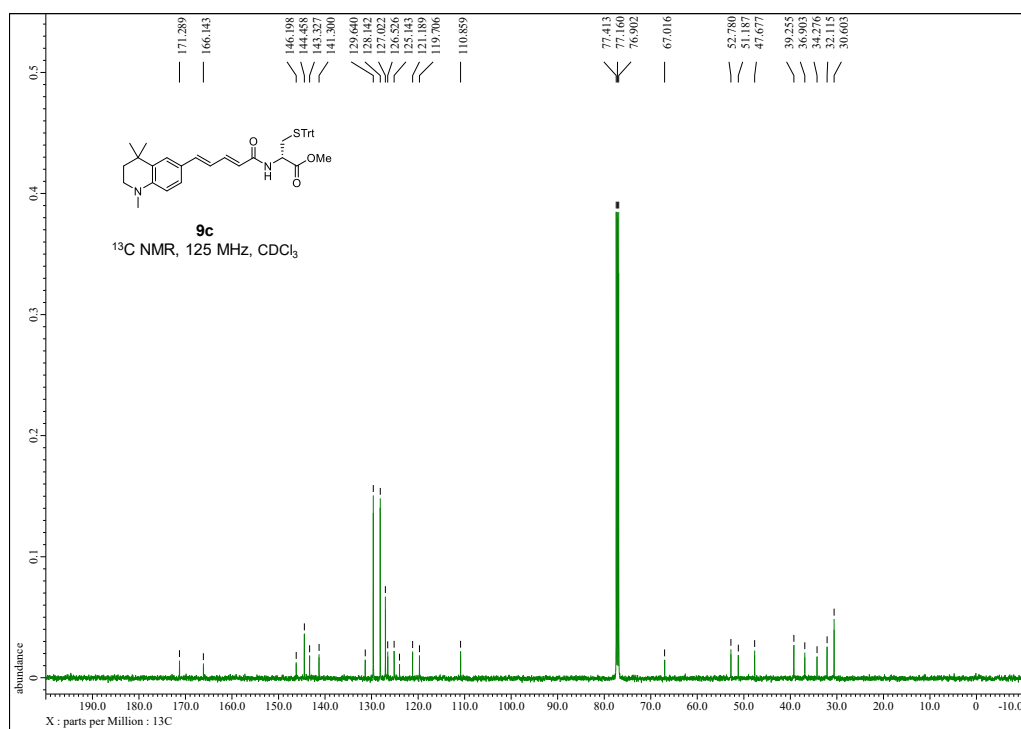
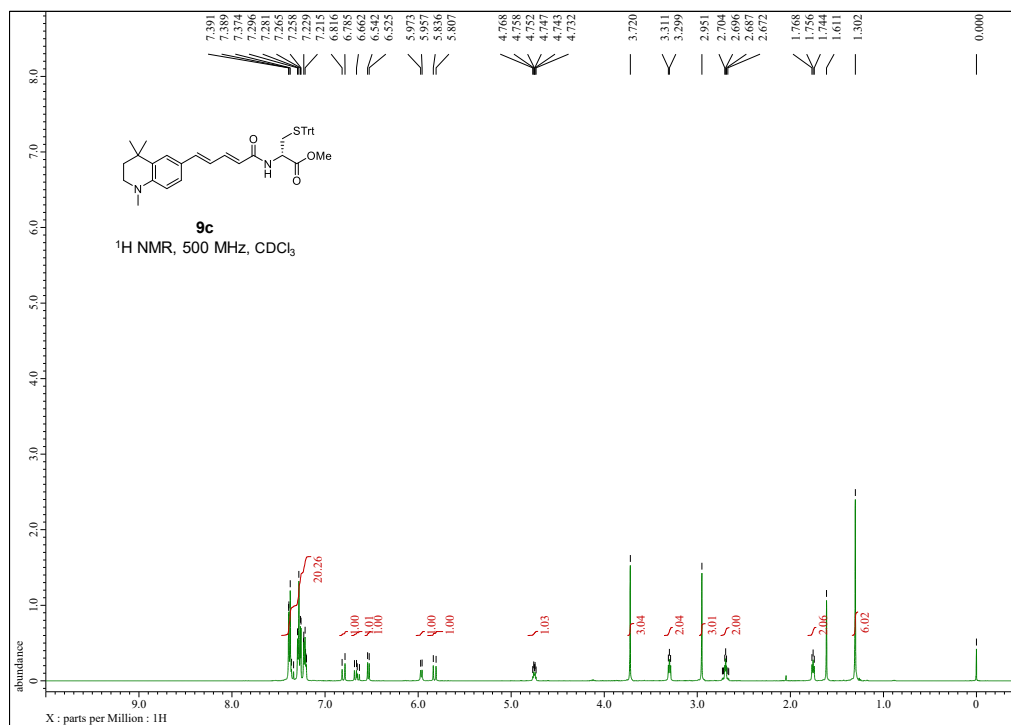
## Compound 9a



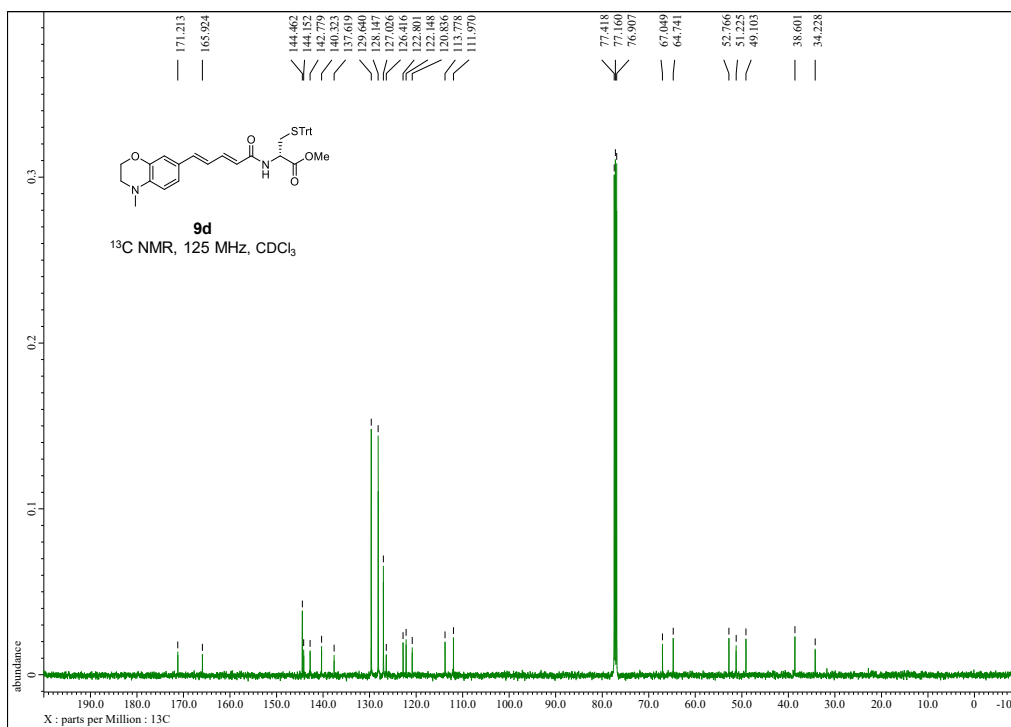
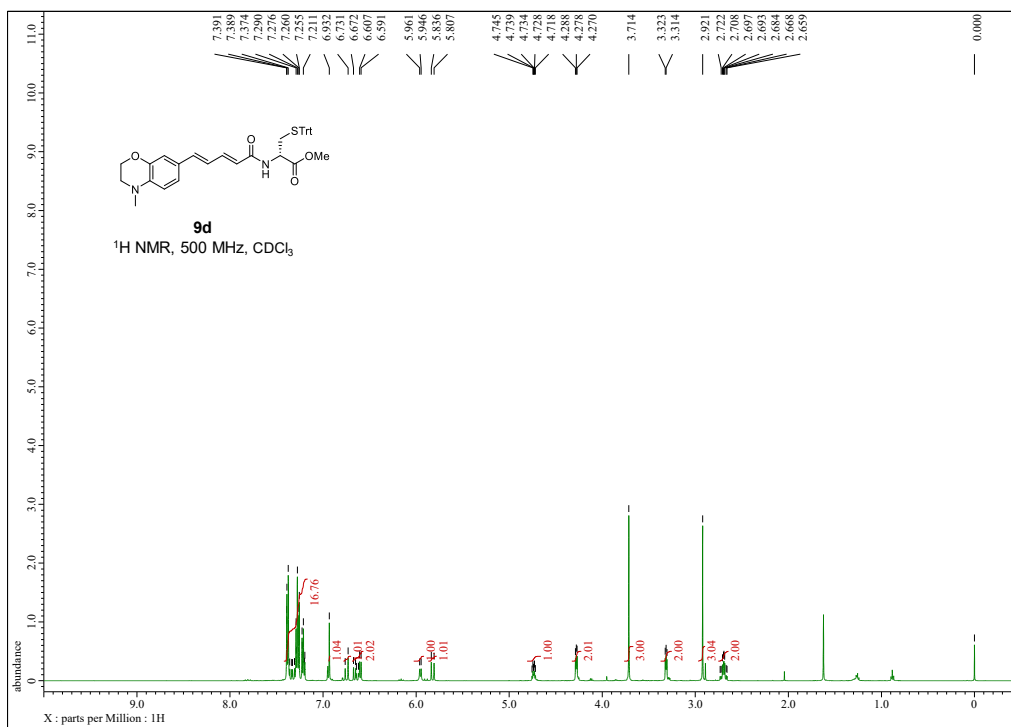
## Compound 9b



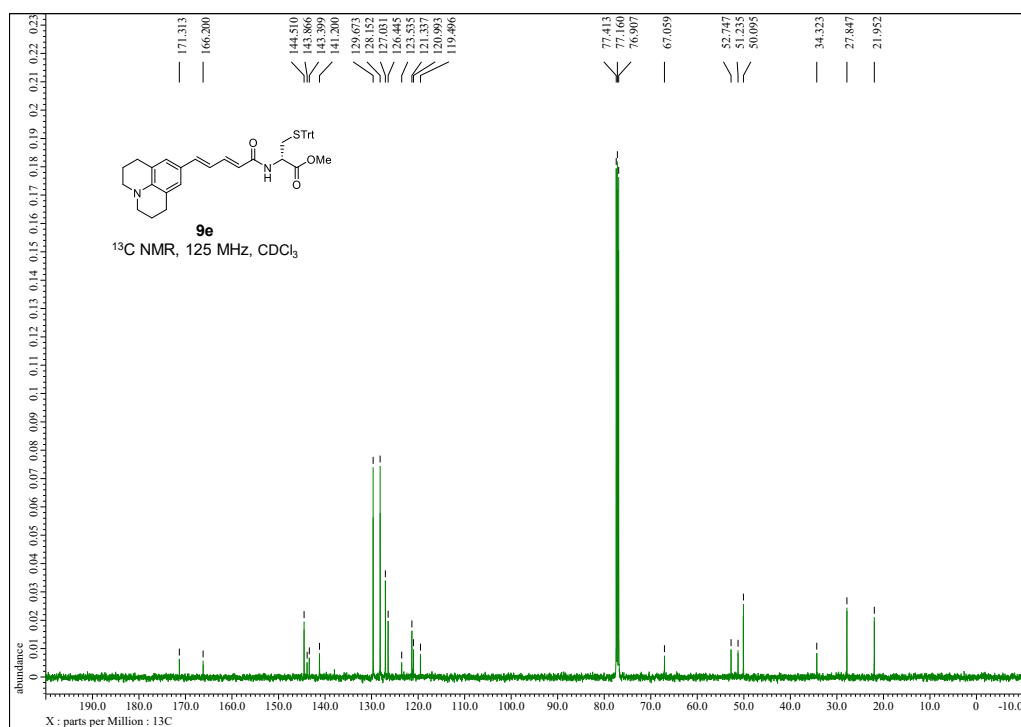
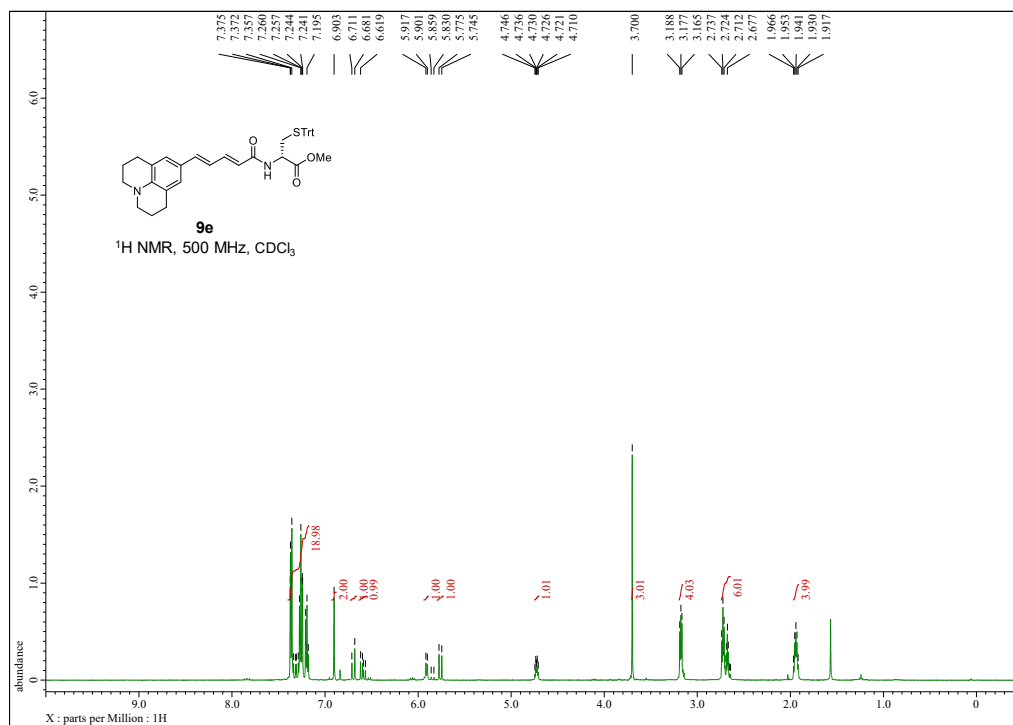
## Compound 9c



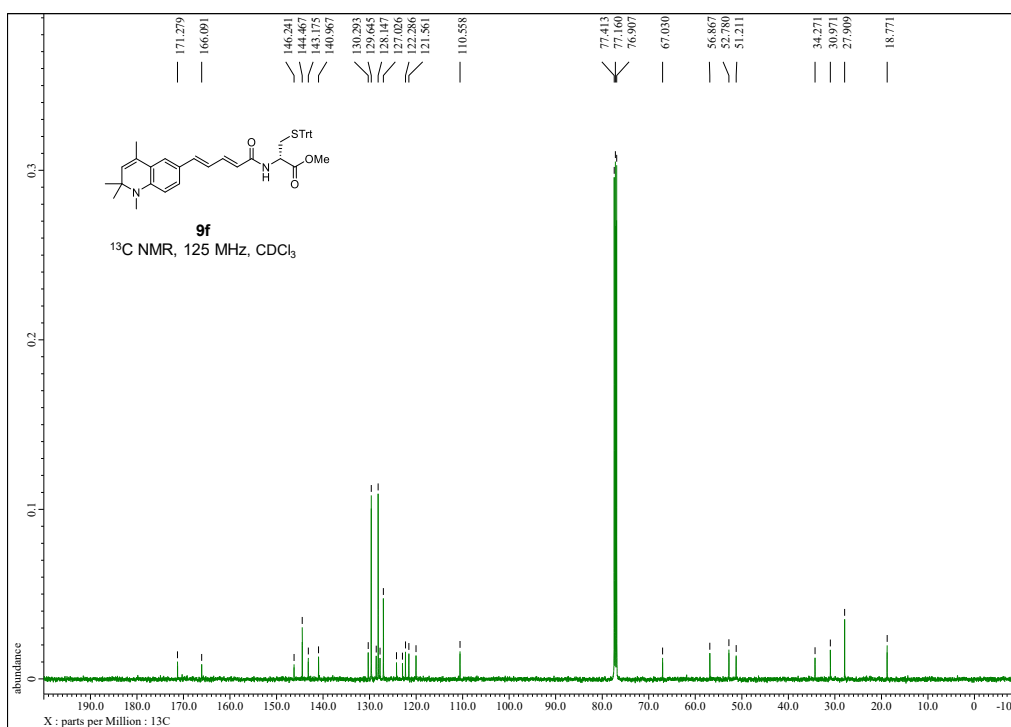
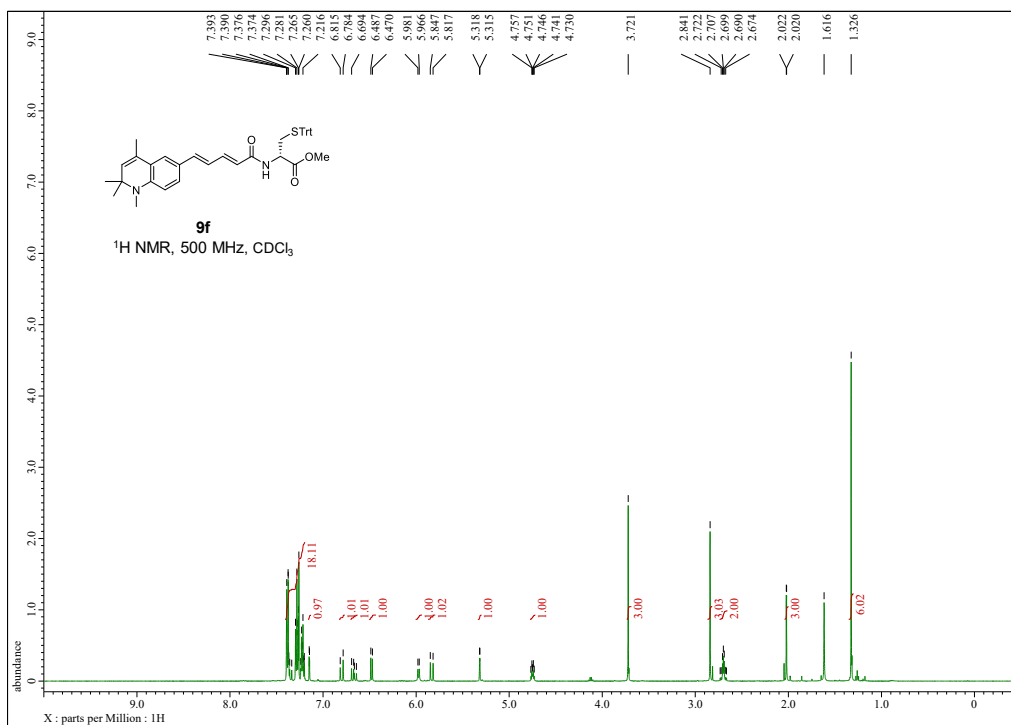
## Compound 9d



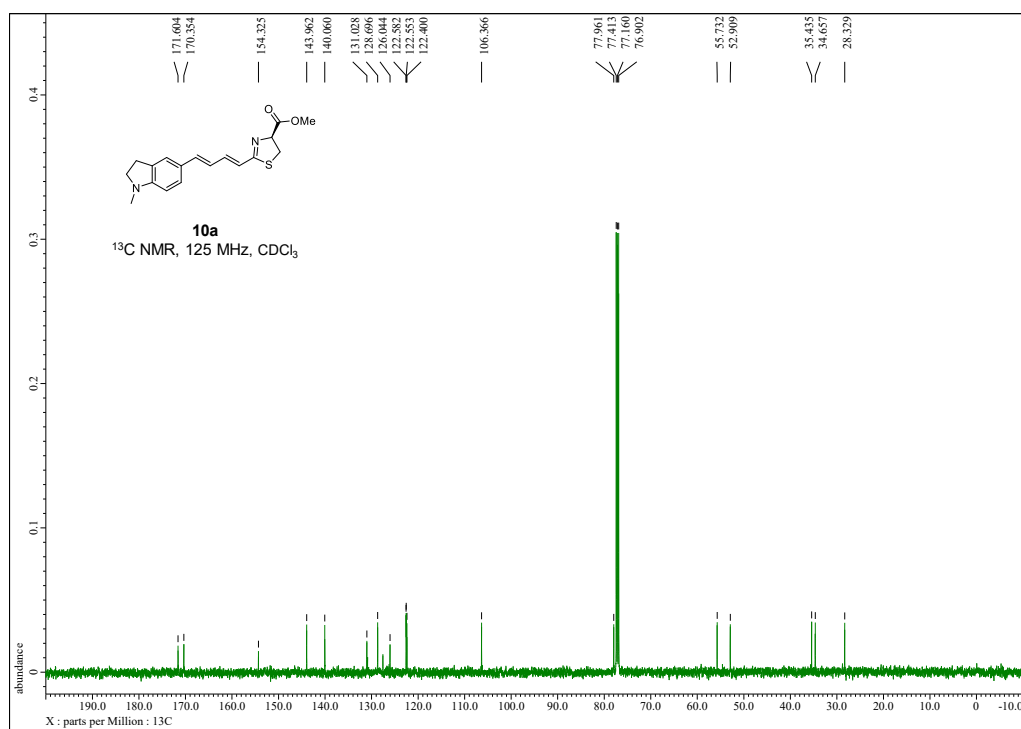
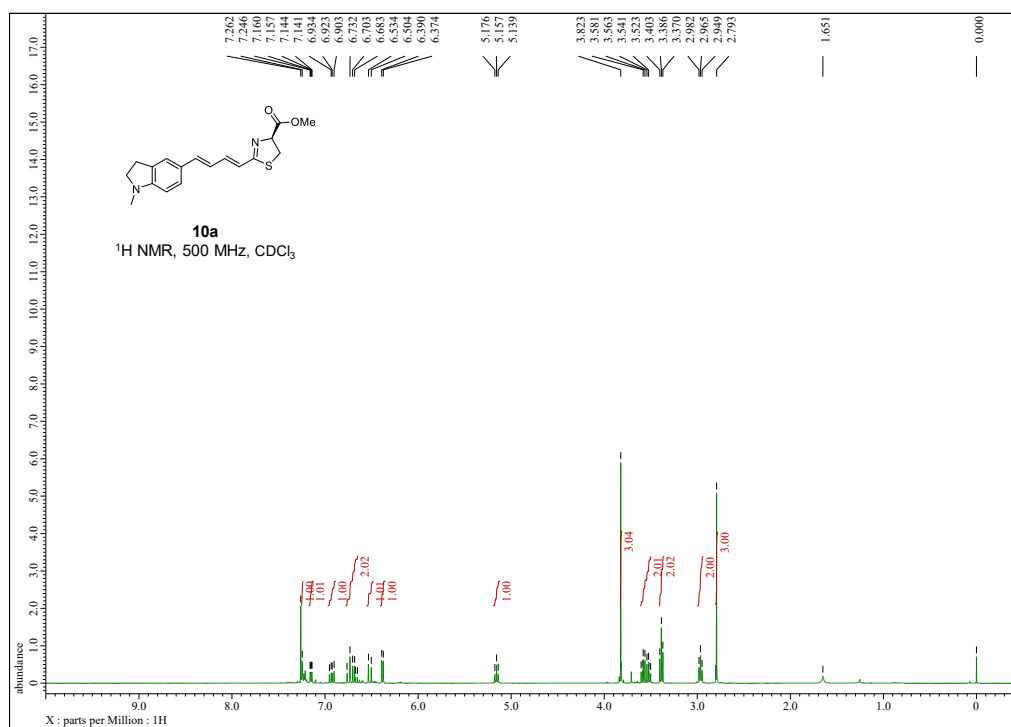
## Compound 9e



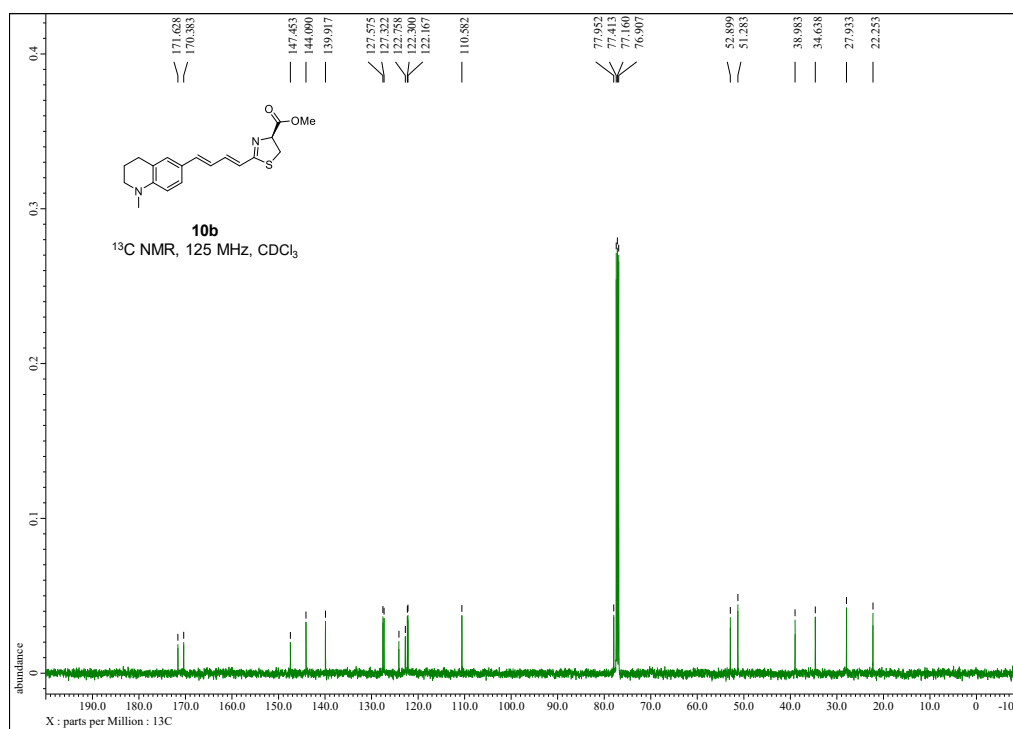
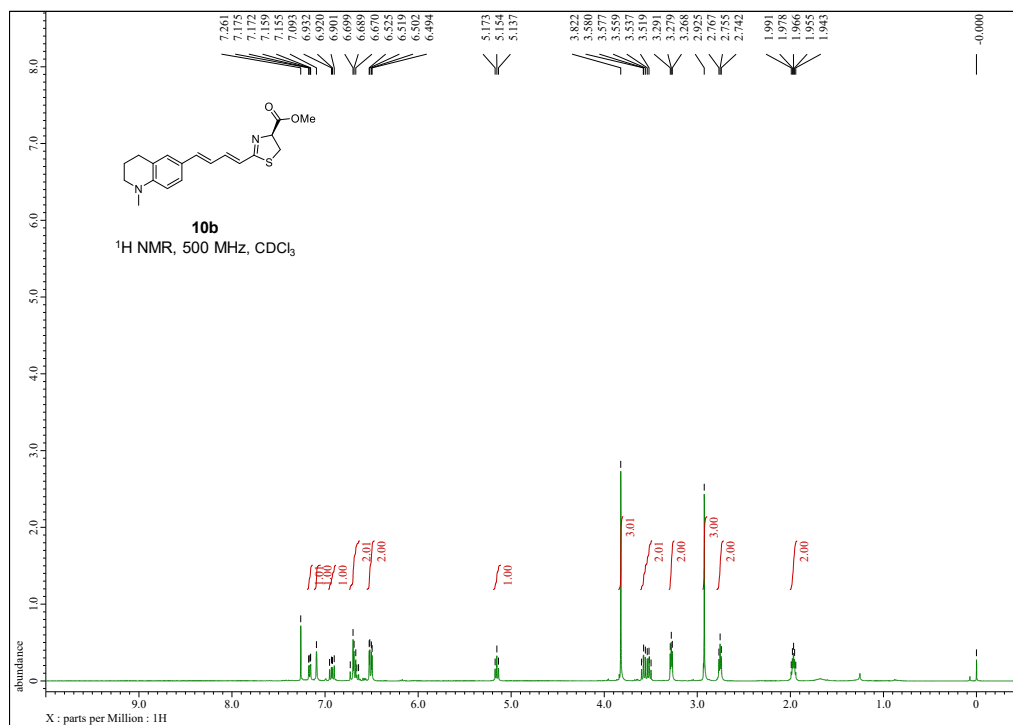
## Compound 9f



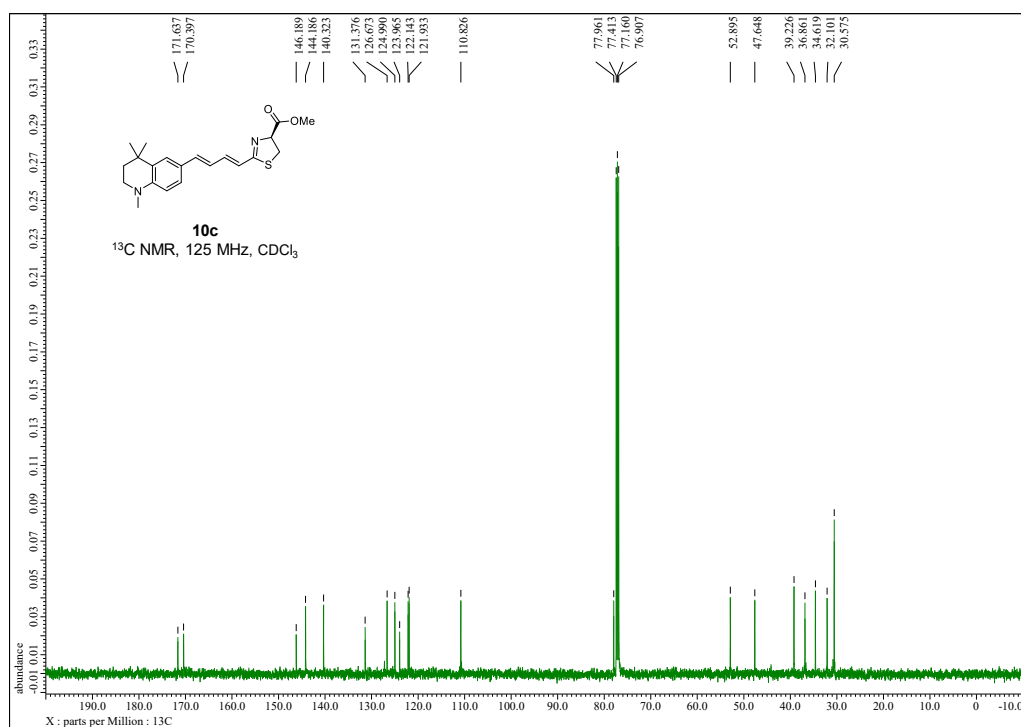
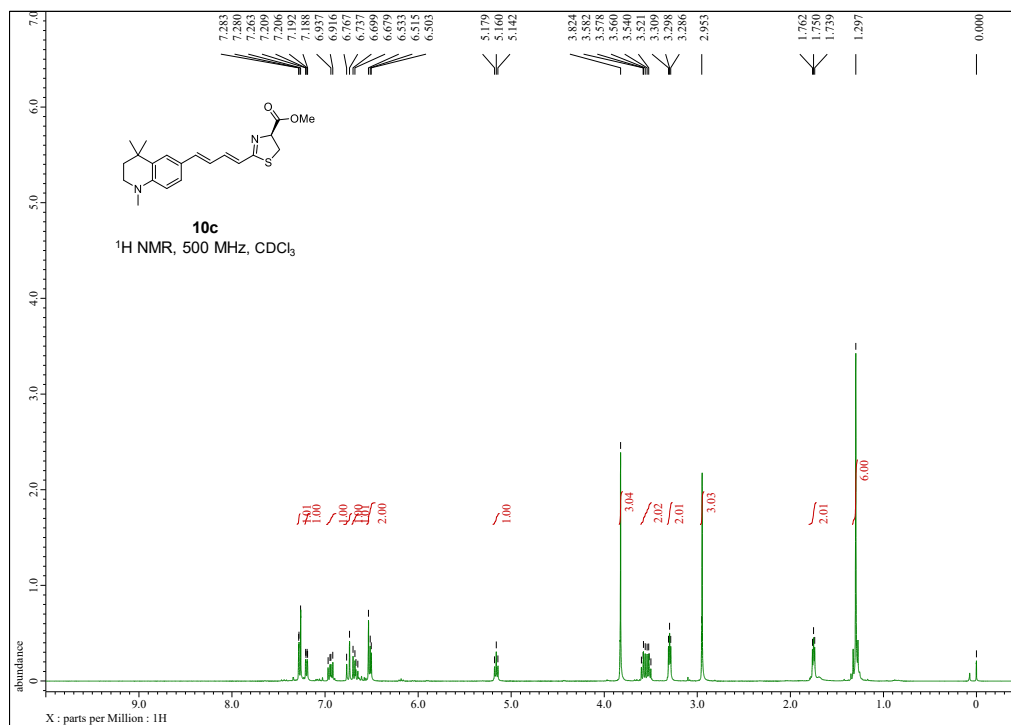
## Compound 10a



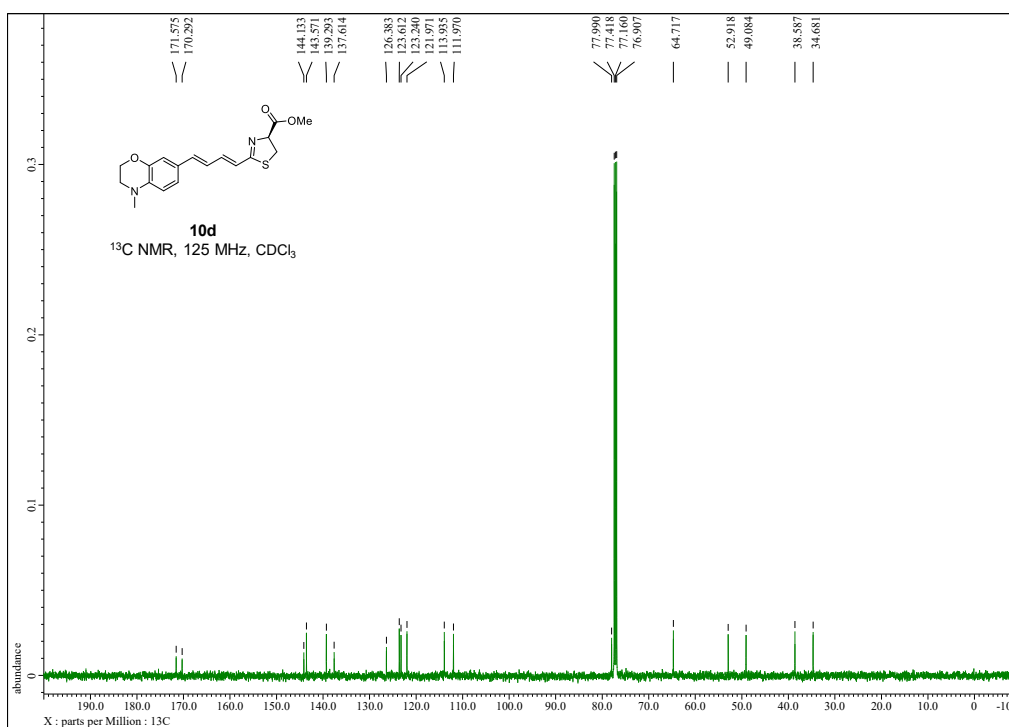
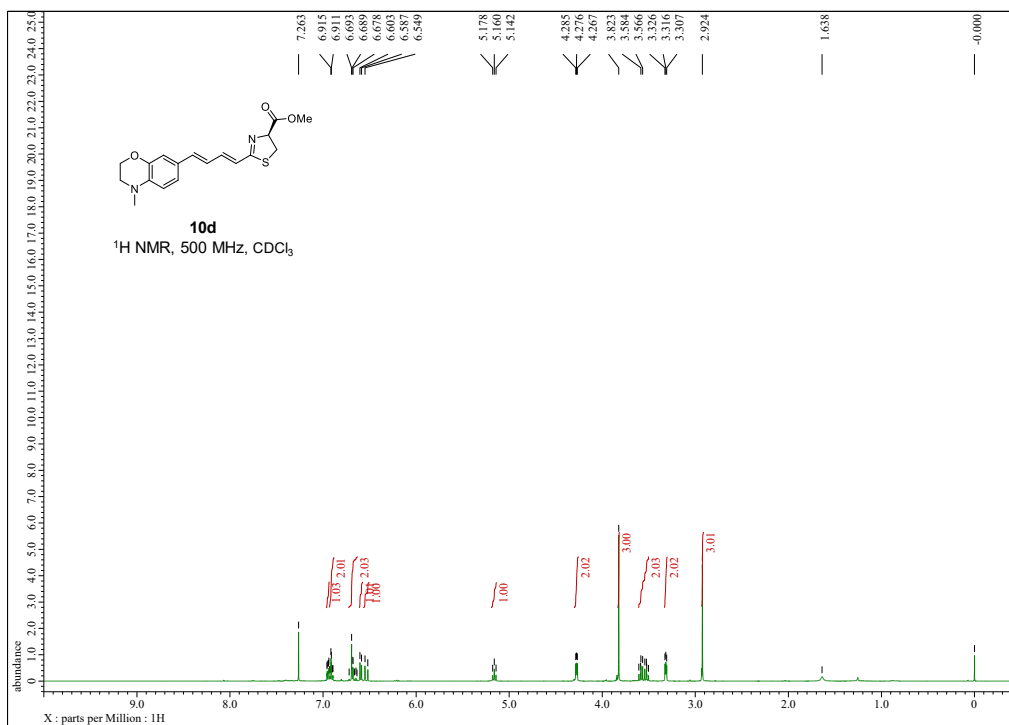
## Compound 10b



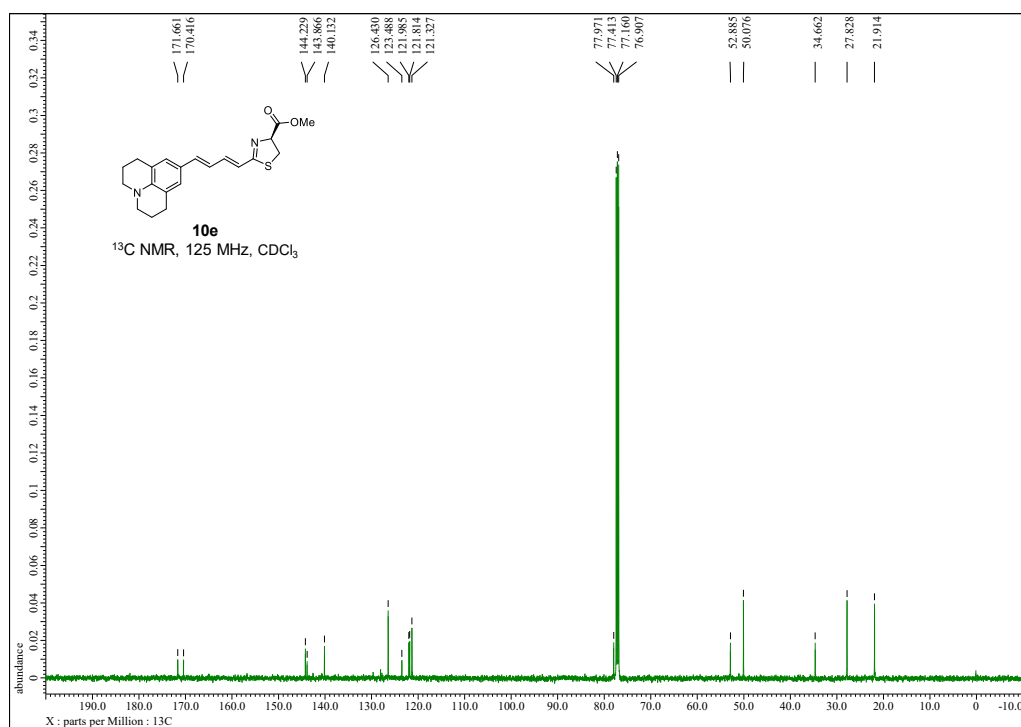
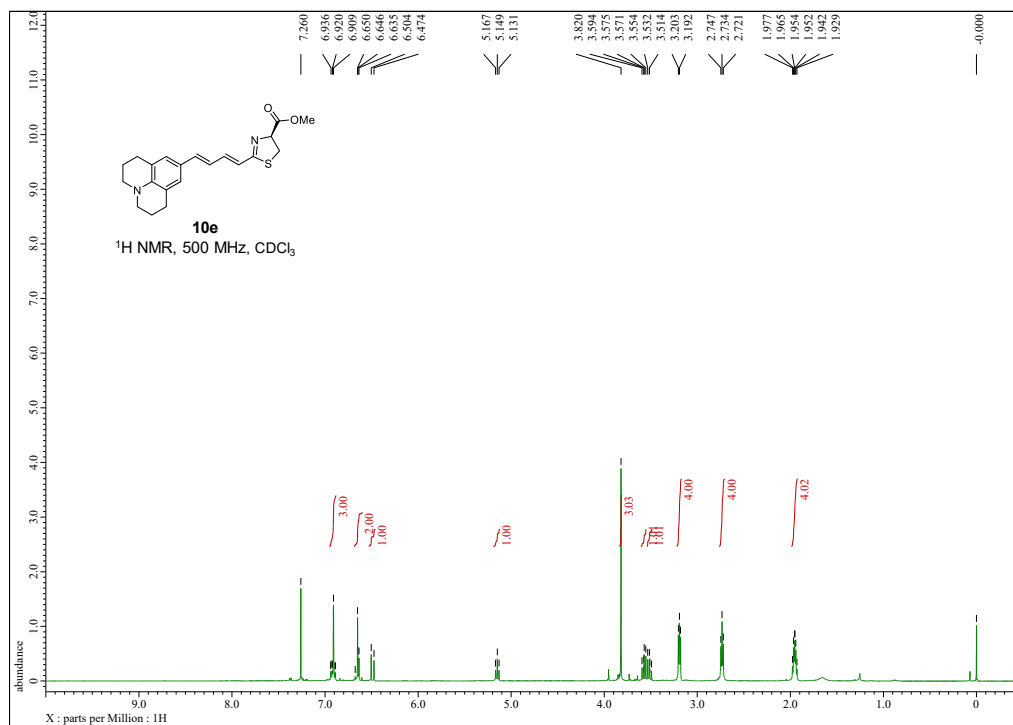
## Compound 10c



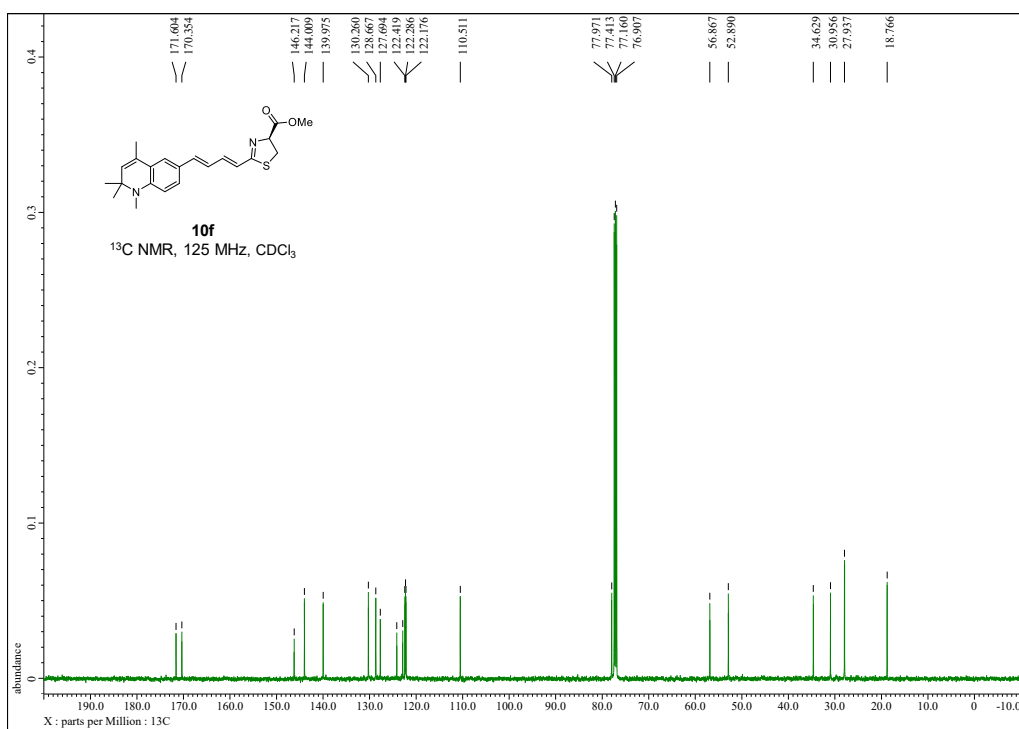
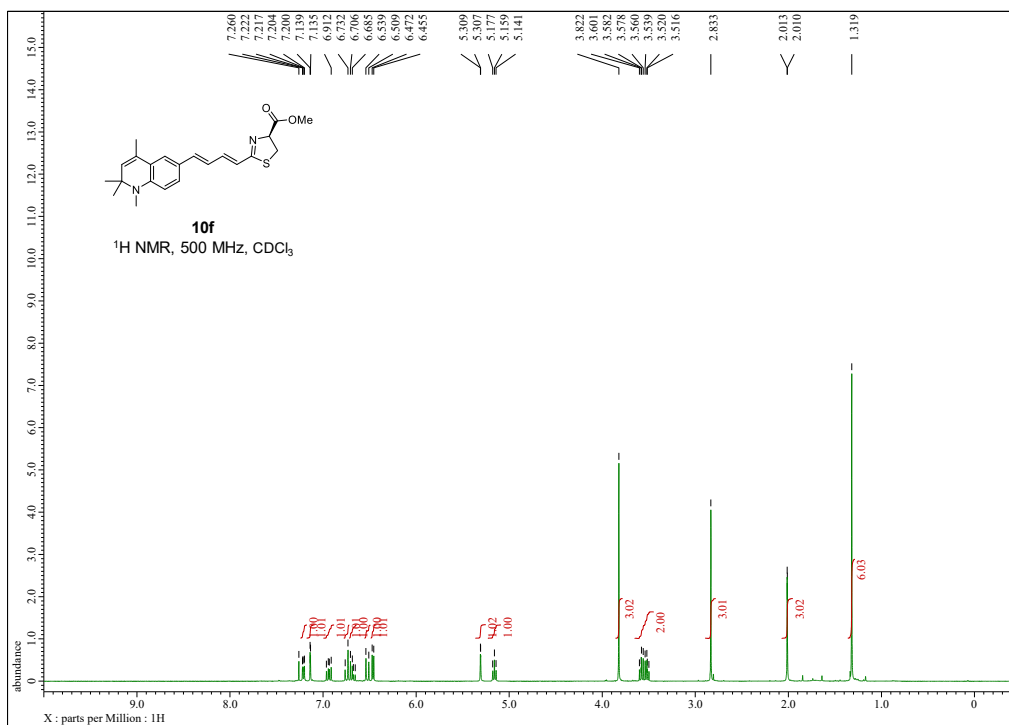
## Compound 10d



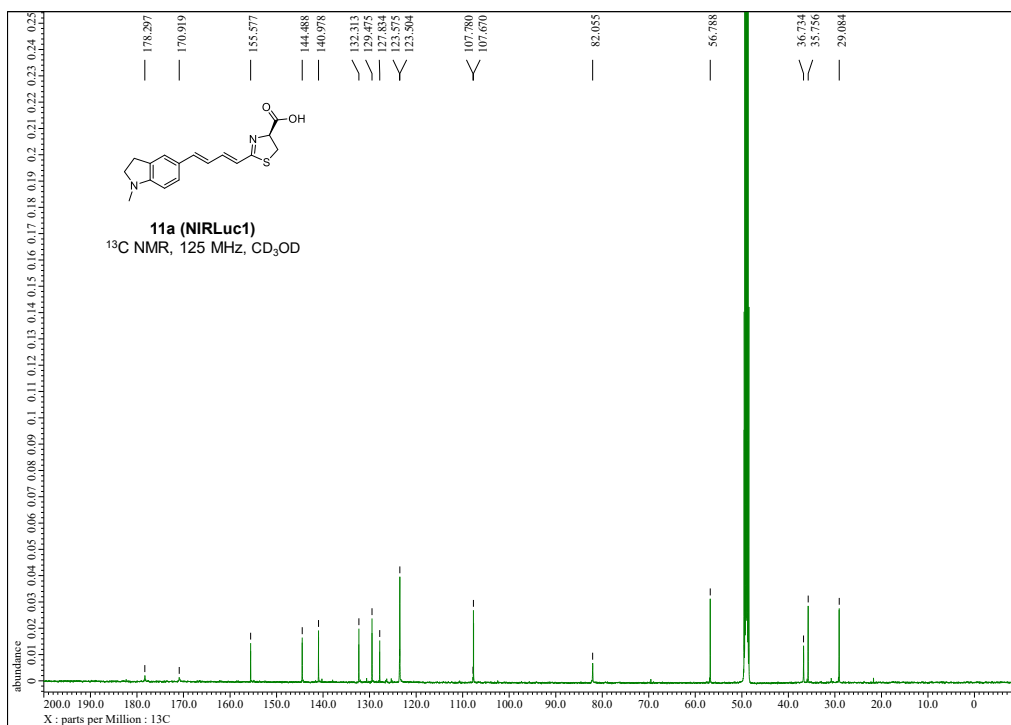
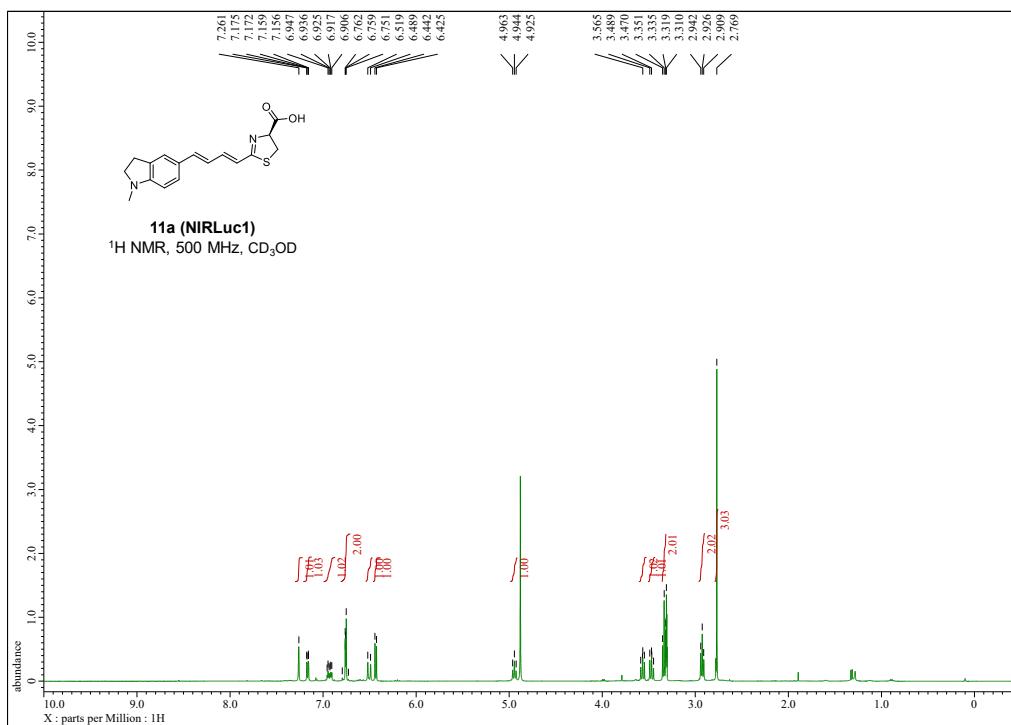
## Compound 10e



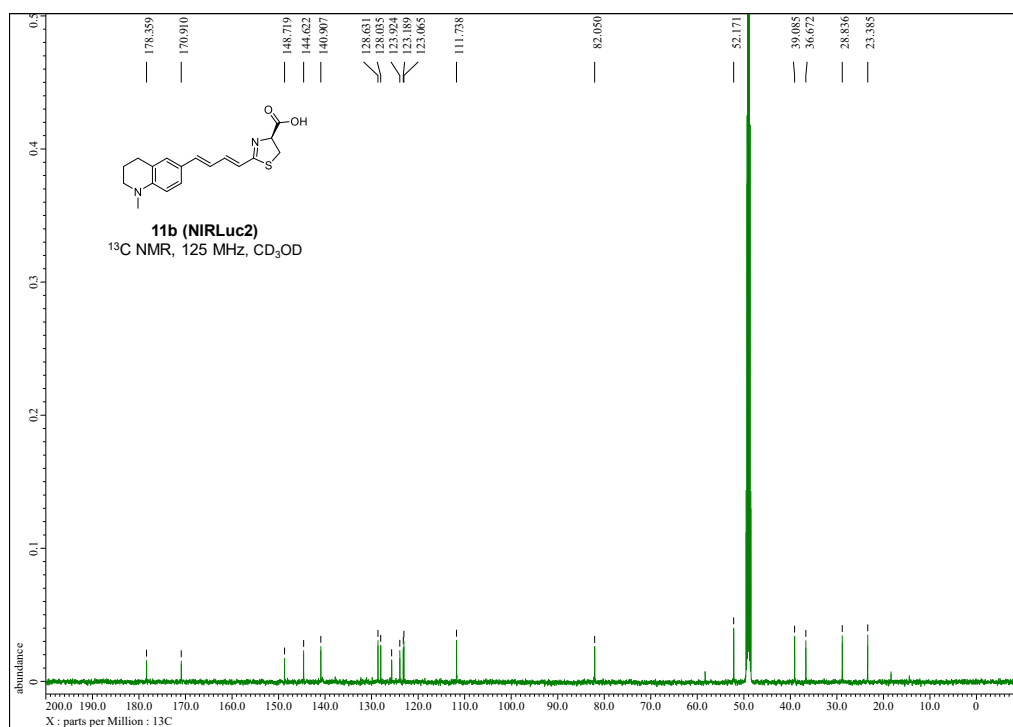
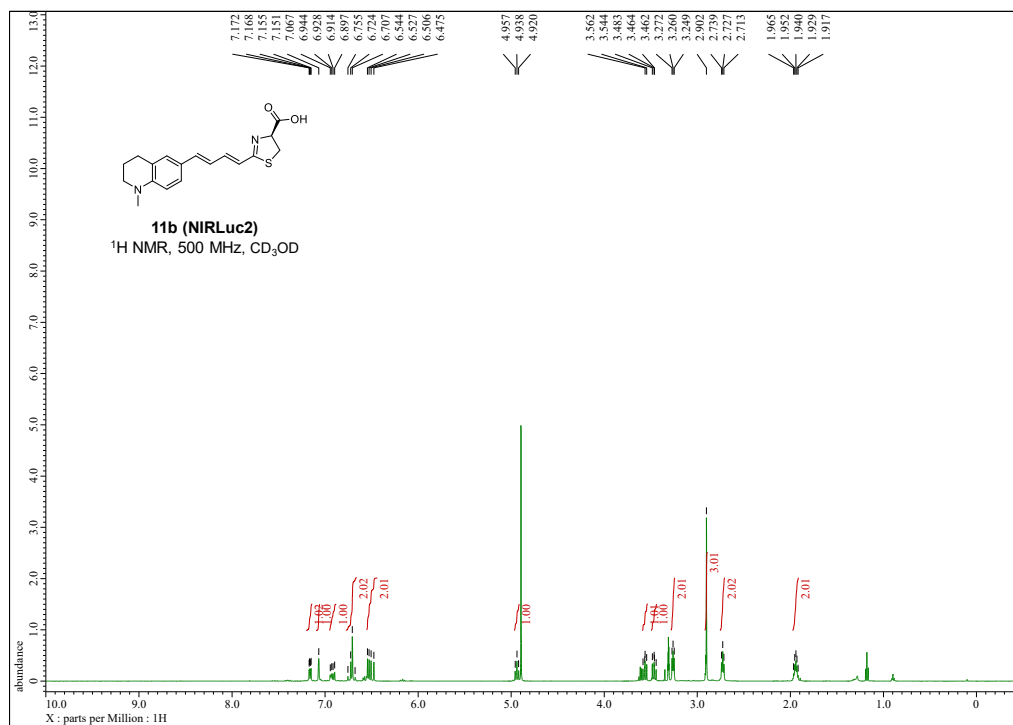
## Compound 10f



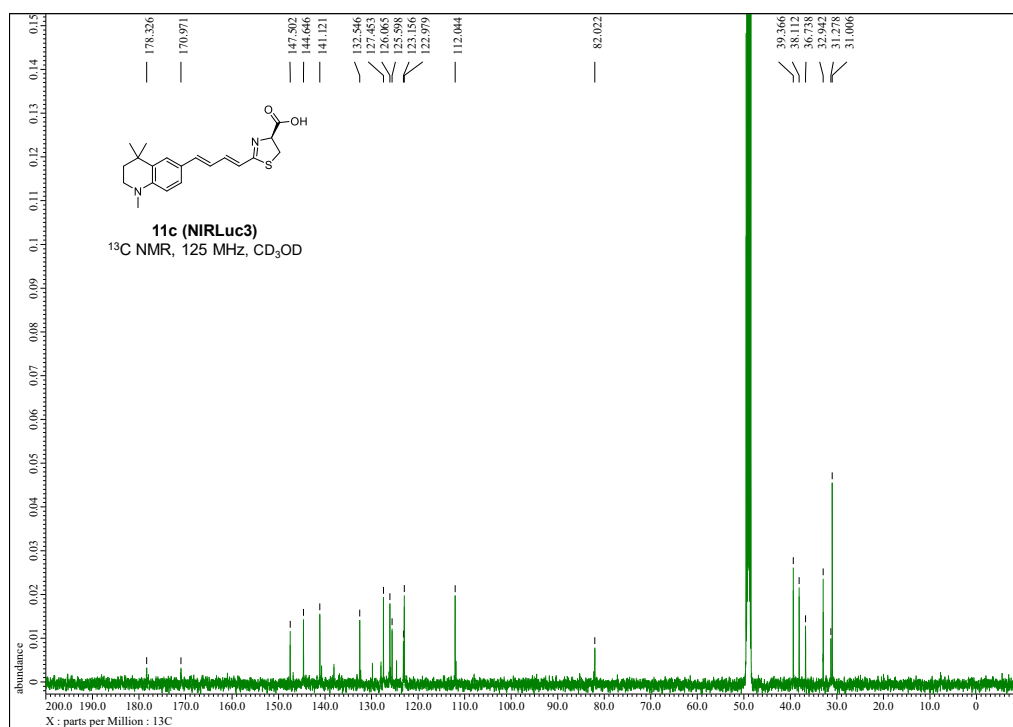
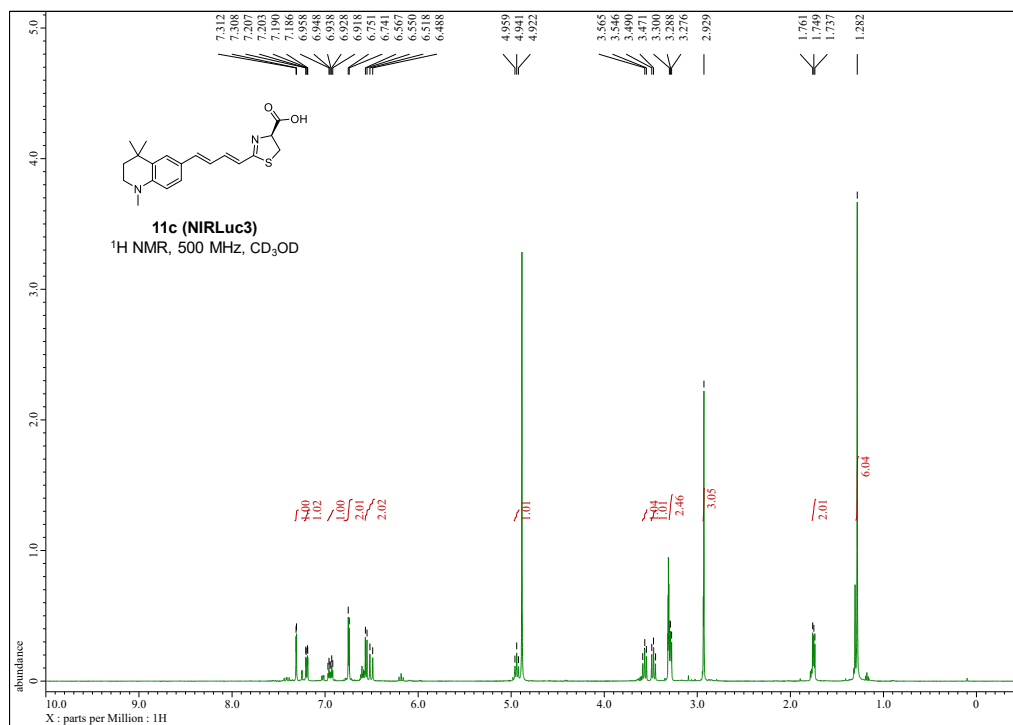
## Compound 11a (NIRLuc1)

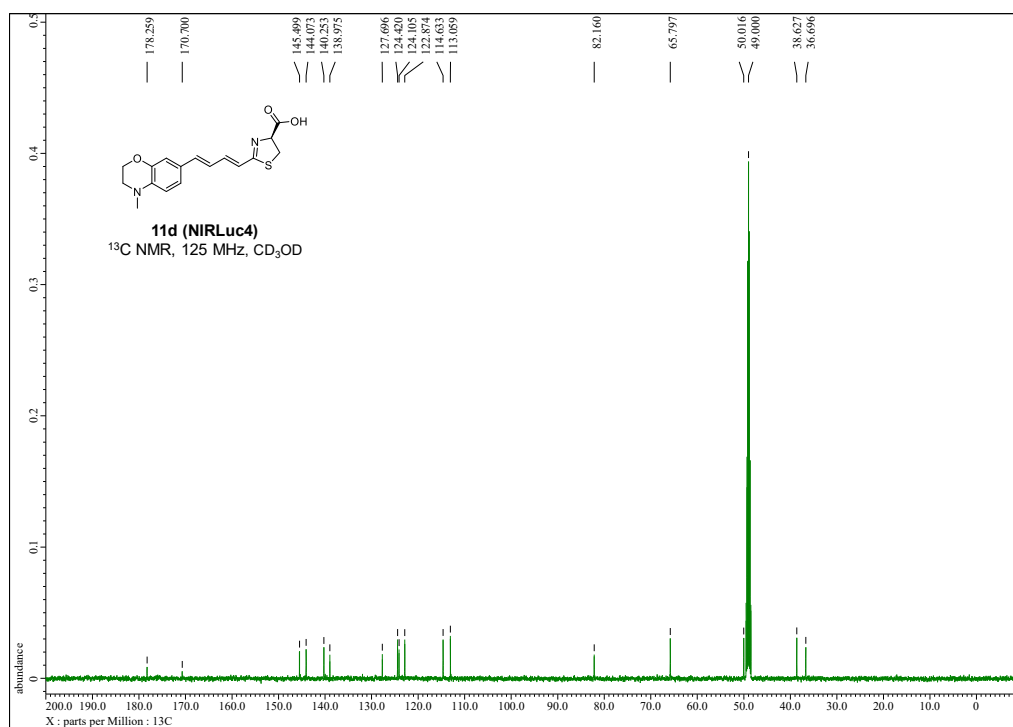
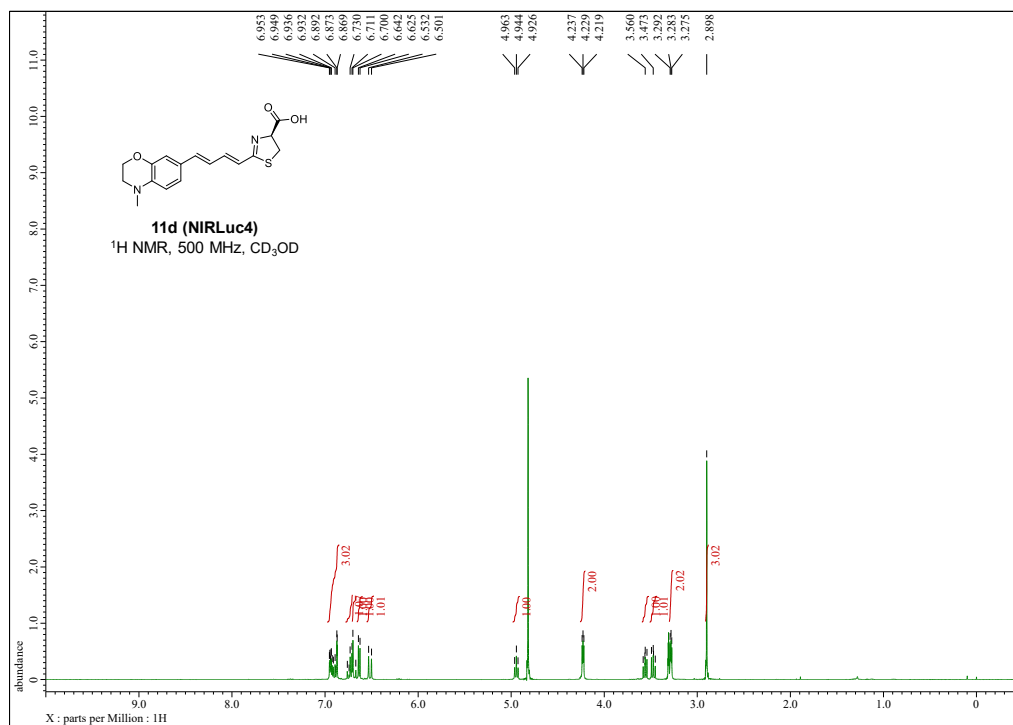


## Compound 11b (NIRLuc2)

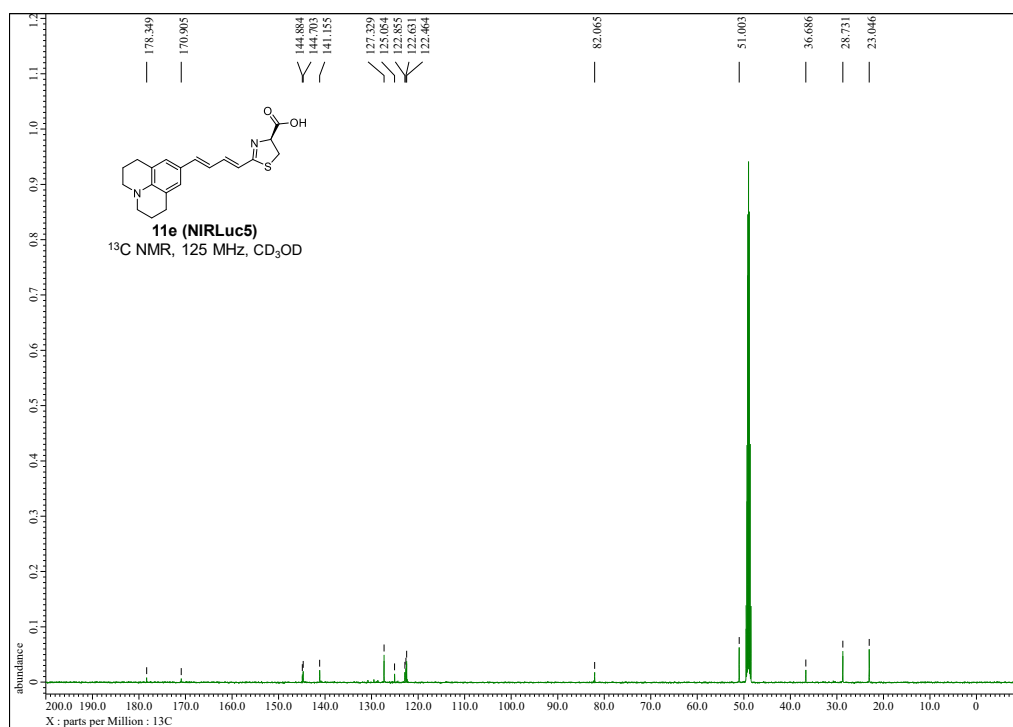
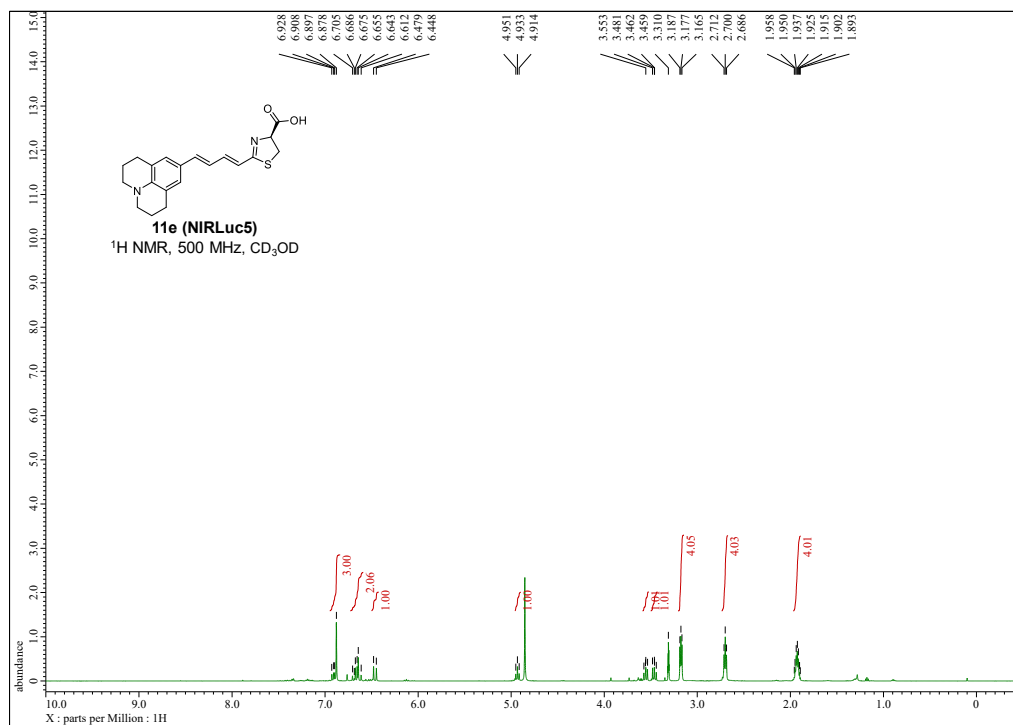


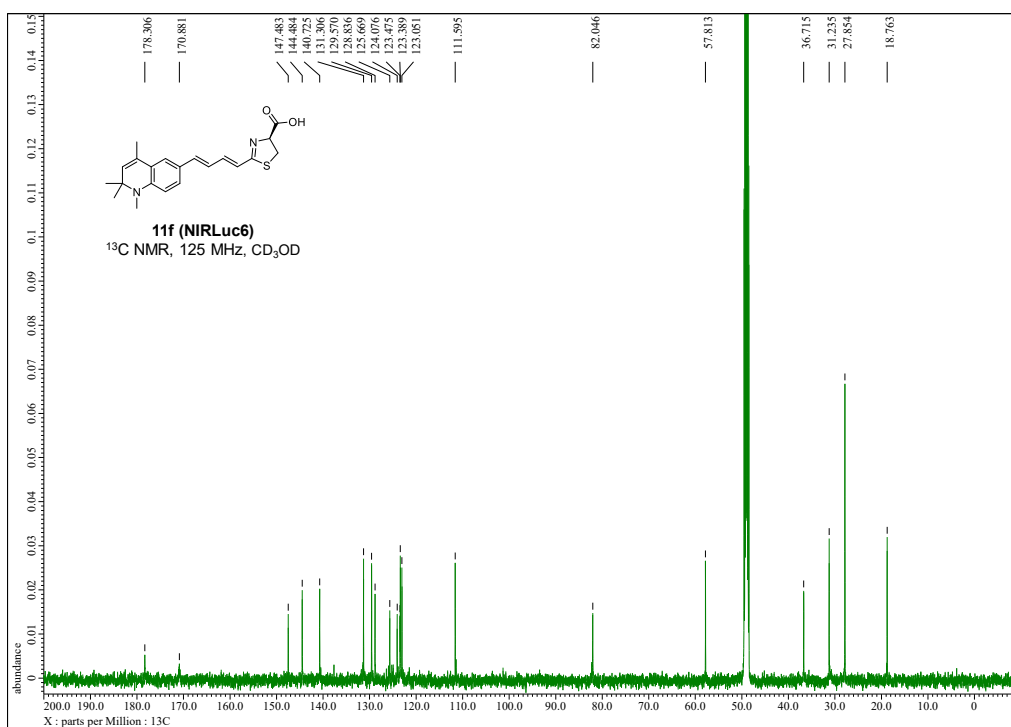
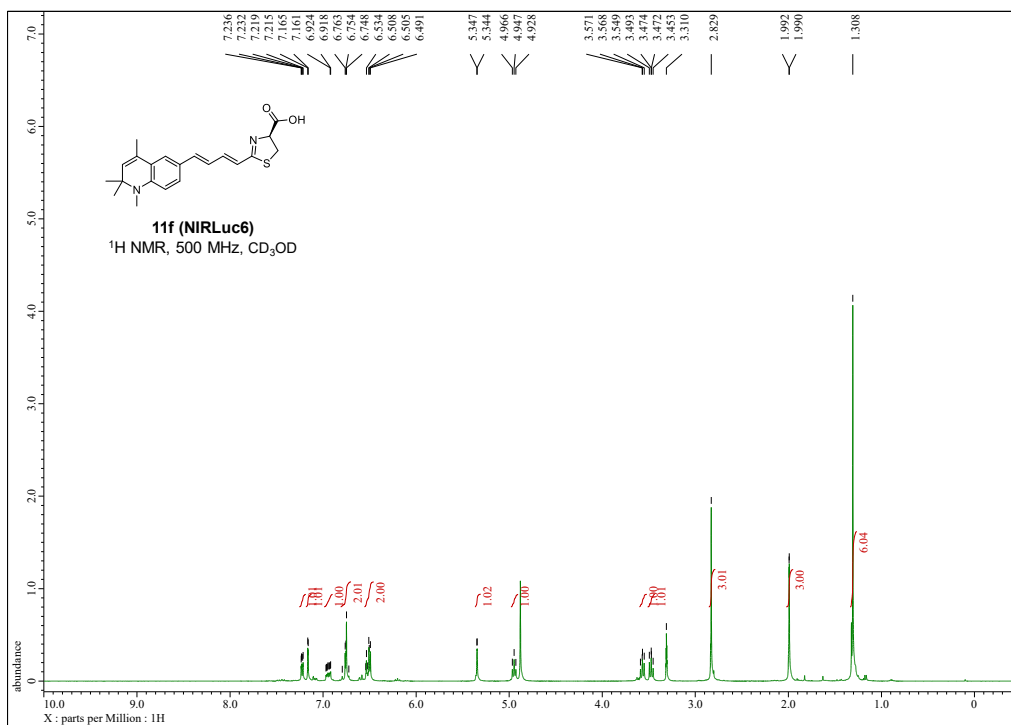
## Compound 11c (NIRLuc3)



**Compound 11d (NIRLuc4)**

## Compound 11e (NIRLuc5)



**Compound 11f (NIRLuc6)**

## References

1. Yao, Z., Zhang, B. S. and Prescher, J. A., "Advances in bioluminescence imaging: new probes from old recipes", *Curr. Opin. Chem. Biol.*, **2018**, *45*, 148-156.
2. Mezzanotte, L., van 't Root, M., Karatas, H., Goun, E. A. and Lowik, C., "In Vivo Molecular Bioluminescence Imaging: New Tools and Applications", *Trends Biotechnol.*, **2017**, *35*, 640-652.
3. Vieira, J., da Silva, L. P. and da Silva, J. C. E., "Advances in the knowledge of light emission by firefly luciferin and oxyluciferin", *J. Photochem. Photobiol. B.*, **2012**, *117*, 33-39.
4. Negrin, R. S. and Contag, C. H., "In vivo imaging using bioluminescence: a tool for probing graft-versus-host disease", *Nat. Rev. Immunol.*, **2006**, *6*, 484-490.
5. Weissleder, R., "A clearer vision for *in vivo* imaging", *Nat. Biotech.*, **2001**, *19*, 316-317.
6. Naumov, P., Ozawa, Y., Ohkubo, K. and Fukuzumi, S., "Structure and Spectroscopy of Oxyluciferin, the Light Emitter of the Firefly Bioluminescence", *J. Am. Chem. Soc.*, **2009**, *131*, 11590-11605.
7. Miller, S. C., Mofford, D. M. and Adams, S. T., Jr., "Lessons Learned from Luminous Luciferins and Latent Luciferases", *ACS Chem. Biol.*, **2018**, *13*, 1734-1740.
8. Steinhardt, R. C., Rathbun, C. M., Krull, B. T., Yu, J. M., Yang, Y., Nguyen, B. D., Kwon, J., McCutcheon, D. C., Jones, K. A., Furche, F. and Prescher, J. A., "Brominated Luciferins Are Versatile Bioluminescent Probes", *ChemBioChem*, **2017**, *18*, 96-100.
9. Jathoul, A. P., Grounds, H., Anderson, J. C. and Pule, M. A., "A dual-color far-red to near-infrared firefly luciferin analogue designed for multiparametric bioluminescence imaging", *Angew. Chem. Int. Ed.*, **2014**, *53*, 13059-13063.
10. Hall, M. P., Woodroffe, C. C., Wood, M. G., Que, I., Van't Root, M., Ridwan, Y., Shi, C., Kirkland, T. A., Encell, L. P., Wood, K. V., Lowik, C. and Mezzanotte, L., "Click beetle luciferase mutant and near infrared naphthyl-luciferins for improved bioluminescence imaging", *Nat. Commun.*, **2018**, *9*, 132-143.
11. Kuchimaru, T., Iwano, S., Kiyama, M., Mitsumata, S., Kadonosono, T., Niwa, H., Maki, S. and Kizaka-Kondoh, S., "A luciferin analogue generating near-infrared bioluminescence achieves highly sensitive deep-tissue imaging", *Nat. Commun.*, **2016**, *7*, 11856-11863.
12. Iwano, S., Obata, R., Miura, C., Kiyama, M., Hama, K., Nakamura, M., Amano, Y., Kojima, S., Hirano, T., Maki, S. and Niwa, H., "Development of simple firefly luciferin analogs emitting blue, green, red, and near-infrared biological window light", *Tetrahedron*, **2013**, *69*, 3847-3856.
13. Iwano, S., Sugiyama, M., Hama, H., Watakabe, A., Hasegawa, N., Kuchimaru, T., Tanaka, K. Z., Takahashi, M., Ishida, Y., Hata, J., Shimozono, S., Namiki, K., Fukano, T., Kiyama, M., Okano, H., Kizaka-Kondoh, S., McHugh, T. J., Yamamori, T., Hioki, H., Maki, S. and Miyawaki, A., "Single-cell bioluminescence imaging of deep tissue in freely moving animals", *Science*, **2018**, *359*, 935-939.

14. Kitada, N., Saitoh, T., Ikeda, Y., Iwano, S., Obata, R., Niwa, H., Hirano, T., Miyawaki, A., Suzuki, K., Nishiyama, S. and Maki, S. A., "Toward bioluminescence in the near-infrared region: Tuning the emission wavelength of firefly luciferin analogues by allyl substitution", *Tetrahedron Lett.*, **2018**, *59*, 1087-1090.
15. Kiyama, M., Iwano, S., Otsuka, S., Lu, S. W., Obata, R., Miyawaki, A., Hirano, T. and Maki, S. A., "Quantum yield improvement of red-light-emitting firefly luciferin analogues for *in vivo* bioluminescence imaging", *Tetrahedron*, **2018**, *74*, 652-660.
16. Saito, R., Kuchimaru, T., Higashi, S., Lu, S. W., Kiyama, M., Iwano, S., Obata, R., Hirano, T., Kizaka-Kondoh, S. and Maki, S. A., "Synthesis and Luminescence Properties of Near-Infrared *N*-Heterocyclic Luciferin Analogues for *In Vivo* Optical Imaging", *Bull. Chem. Soc. Jpn.*, **2019**, *92*, 608-618.
17. Ioka, S., Saitoh, T., Iwano, S., Suzuki, K., Maki, S. A., Miyawaki, A., Imoto, M. and Nishiyama, S., "Synthesis of Firefly Luciferin Analogues and Evaluation of the Luminescent Properties", *Chem. Eur. J.*, **2016**, *22*, 9330-9337.
18. Jones, K. A., Porterfield, W. B., Rathbun, C. M., McCutcheon, D. C., Paley, M. A. and Prescher, J. A., "Orthogonal Luciferase-Luciferin Pairs for Bioluminescence Imaging", *J. Am. Chem. Soc.*, **2017**, *139*, 2351-2358.
19. McCutcheon, D. C., Paley, M. A., Steinhardt, R. C. and Prescher, J. A., "Expedient synthesis of electronically modified luciferins for bioluminescence imaging", *J. Am. Chem. Soc.*, **2012**, *134*, 7604-7607.
20. Ikeda, Y., Saitoh, T., Niwa, K., Nakajima, T., Kitada, N., Maki, S. A., Sato, M., Citterio, D., Nishiyama, S. and Suzuki, K., "An allylated firefly luciferin analogue with luciferase specific response in living cells", *Chem. Commun.*, **2018**, *54*, 1774-1777.
21. Koide, Y., Urano, Y., Hanaoka, K., Piao, W., Kusakabe, M., Saito, N., Terai, T., Okabe, T. and Nagano, T., "Development of NIR fluorescent dyes based on Si-rhodamine for *in vivo* imaging", *J. Am. Chem. Soc.*, **2012**, *134*, 5029-5031.
22. Mofford, D. M., Reddy, G. R. and Miller, S. C., "Aminoluciferins extend firefly luciferase bioluminescence into the near-infrared and can be preferred substrates over D-luciferin", *J. Am. Chem. Soc.*, **2014**, *136*, 13277-13282.
23. Reddy, G. R., Thompson, W. C. and Miller, S. C., "Robust light emission from cyclic alkylaminoluciferin substrates for firefly luciferase", *J. Am. Chem. Soc.*, **2010**, *132*, 13586-13587.
24. Kato, D., Shirakawa, D., Polz, R., Maenaka, M., Takeo, M., Negoro, S. and Niwa, K., "A firefly inspired one-pot chemiluminescence system using *n*-propylphosphonic anhydride (T3P)", *Photochem. Photobiol. Sci.*, **2014**, *13*, 1640-1645.
25. Kakiuchi, M., Ito, S., Yamaji, M., Viviani, V. R., Maki, S. and Hirano, T., "Spectroscopic Properties of Amine-substituted Analogues of Firefly Luciferin and Oxyluciferin", *Photochem. Photobiol.*, **2017**, *93*, 486-494.
26. White, E. H., Rapaport, E., Seliger, H. H. and Hopkins, T. A., "The chemi- and bioluminescence of firefly luciferin: an efficient chemical production of electronically excited states", *Bioorg. Chem.*, **1971**, *1*, 92-122.
27. Woodroffe, C. C., Meisenheimer, P. L., Klaubert, D. H., Kovic, Y., Rosenberg, J. C., Behney, C. E., Southworth, T. L. and Branchini, B. R., "Novel heterocyclic analogues of firefly luciferin", *Biochemistry*, **2012**, *51*, 9807-9813.

28. Woodroffe, C. C., Shultz, J. W., Wood, M. G., Osterman, J., Cali, J. J., Daily, W. J., Meisenheimer, P. L. and Klaubert, D. H., "*N*-Alkylated 6'-aminoluciferins are bioluminescent substrates for Ultra-Glo and QuantiLum luciferase: new potential scaffolds for bioluminescent assays", *Biochemistry*, **2008**, *47*, 10383-10393.
29. Ando, Y., Niwa, K., Yamada, N., Enomoto, T., Irie, T., Kubota, H., Ohmiya, Y. and Akiyama, H., "Firefly bioluminescence quantum yield and colour change by pH-sensitive green emission", *Nat. Photo.*, **2007**, *2*, 44-47.
30. Hiyama, M., Akiyama, H., Yamada, K. and Koga, N., "Theoretical study of firefly luciferin pKa values-relative absorption intensity in aqueous solutions", *Photochem. Photobiol.*, **2013**, *89*, 571-578.
31. Mayer, R. J., Hampel, N., Mayer, P., Ofial, A. R. and Mayr, H., "Synthesis, Structure, and Properties of Amino-Substituted Benzhydrylium Ions – A Link between Ordinary Carbocations and Neutral Electrophiles", *Eur. J. Org. Chem.*, **2019**, 2-3, 412-421.
32. Orchard, A., Schamerhorn, G. A., Calitree, B. D., Sawada, G. A., Loo, T. W., Claire Bartlett, M., Clarke, D. M. and Detty, M. R., "Thiorhodamines containing amide and thioamide functionality as inhibitors of the ATP-binding cassette drug transporter P-glycoprotein (ABCB1)", *Bioorg. Med. Chem.*, **2012**, *20*, 4290-4302.
33. Kotha, S. and Kuki, A., "A new synthetic approach to unusually electron rich  $\alpha$ -amino acids", *Chem. Commun.*, **1992**, *5*, 404-406.
34. Tian, K., Hu, D., Hu, R., Wang, S., Li, S., Li, Y. and Yang, G., "Multiple fluorescence  $\Delta$ CIE and  $\Delta$ RGB codes for sensing volatile organic compounds with a wide range of responses", *Chem. Commun.*, **2011**, *47*, 10052-10054.

## Chapter 5

# General Conclusions

## 5.1. Summary of the results

Bioluminescence-based assays are now broadly applied as a highly sensitive and non-invasive imaging modality to trace biological functions without having to sacrifice animals. The most commonly used luciferin-luciferase pairs in these assays originate from insects, such as firefly. These bioluminescence systems consist of D-luciferin and the corresponding luciferases. Compared to research activities on new luciferases, the variety of available luciferins is poor. Therefore, the development of synthetic luciferins is indispensable to expand the application of the firefly bioluminescence system. This work aims at the development of elemental strategies for next-generation bioluminescence imaging through synthetic luciferins. The current work mainly focuses on the three elements: 1) orthogonal imaging, 2) brightness of analogues and 3) NIR emission (**Figure 5.1**).

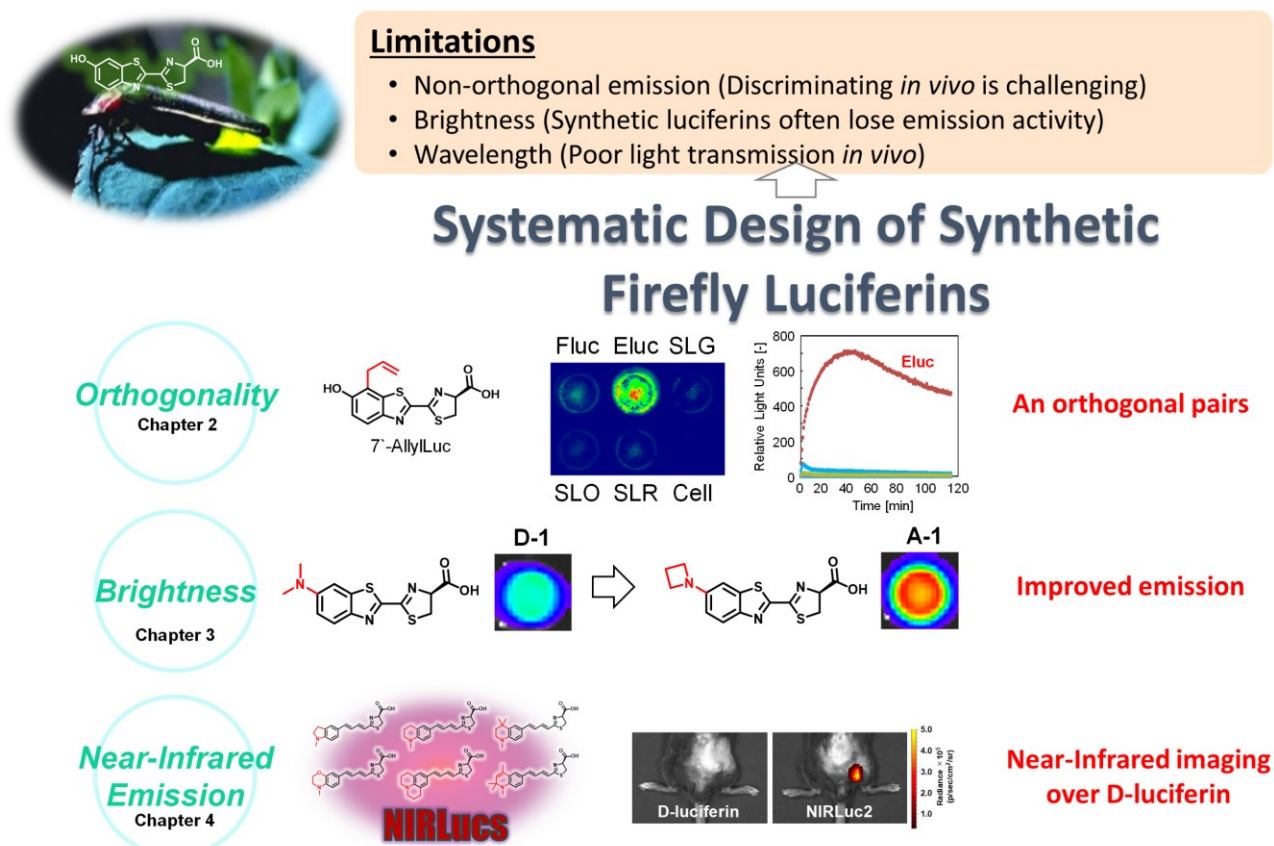


Figure 5.1. Summary of the synthetic luciferins developed in thesis.

The second chapter described an orthogonal luciferin analogue, **7'-AllylLuc**, modified with an allyl group at the C-7' position of benzothiazole core. One important result is that this simply modified analogue exhibit bioluminescence in combination with a commercially available luciferase, Eluc. Moreover, the emission from the **7'-AllylLuc**/Eluc pairs lasted over 100 min.

The third chapter described a strategy to improve bioluminescence photon production through a simple replacement of electron donor on firefly luciferins. Significantly reduced photon flux from synthetic luciferins is a major issue in luciferin developments. However, no logical approach to improve photon production has been reported so far. Replacing the *N,N*-dimethylamino group in classical fluorophores with a four membered azetidine ring provides improved luminescence quantum yields. In my thesis, this strategy was extended to bioluminescent firefly luciferin analogues and its general applicability was demonstrated. For this purpose, five-types of luciferin cores were employed, and a total of 10 analogues were evaluated. Among them, only the benzothiazole core analogue benefited from azetidine substitution and improved the fluorescence and bioluminescence emission.

The fourth chapter described a panel of structure-inherent near-infrared emitting luciferin analogues. One limitation in firefly bioluminescence imaging is the limited variety of luciferins emitting in the near-infrared (NIR) region (650-900 nm), where tissue penetration is high. I newly synthesized **NIRLucs** based on the NIR emitting firefly luciferin AkaLumine through a ring fusion strategy. This simple, but effective strategy resulted in pH-independent structure-inherent NIR emission (680-690 nm) with a native firefly luciferase. When applied to cells, **NIRLucs** displayed dose-independent improved NIR emission even at low substrate concentrations where the native D-luciferin does not emit. Furthermore, excellent blood retention and brighter photon flux (7-fold overall, 16-fold in the NIR spectral range) than in the case of D-luciferin have been observed with **NIRLuc2** in mice bearing subcutaneous tumors. My approach offered a solution to the longstanding limitation in *in vivo* firefly bioluminescence imaging.

In summary, this thesis provided a several synthetic luciferins through precise molecular designs, focusing on 1) orthogonal imaging, 2) brightness of analogues and 3) NIR emission. Notably, developed analogues have further potential to improve performance by combined engineered mutant luciferases. These new synthetic luciferins contribute to the expansion of bioluminescence imaging applications both *in vitro* and *in vivo*.

## 5.2. Future outlook

Discovery of the green fluorescent protein (GFP) has definitely brought a paradigm shift to life science. I believe that bioluminescence imaging will also bring a paradigm shift. Recent numerous efforts on luciferin/luciferase development have evolved bioluminescence imaging as a promising imaging modality. Nowadays, a few all-engineered luciferin/luciferase pairs are beyond native D-luciferin/luciferase pairs. One strong points of bioluminescence imaging is translation from single cells to a whole body, *sometimes called "trans-scale imaging"*. Expanded bioluminescent tool box would also enable real-time imaging in larger animals such as minipigs. Although the promising luciferin/luciferase pairs have been developed, further studies must be required to realize a "paradigm shift".

### 1. Brightness

One of a major problem in luciferin development is that the brightness of synthetic luciferin is significantly lower than that of D-luciferin. In chapter 3, I introduced a method for improving quantum yield through azetidione-substituent strategy, however, this strategy would be not enough to a sufficient improvement. To solve this problem, I focus on intermediates in firefly bioluminescence reactions. The luminescence reaction proceeds in two stages: 1) adenylation and 2) oxidation, and it has been suggested that the rate-limiting step is adenylation. In fact, it has been reported that using the luciferyl adenylate, which is the reaction intermediate, as a substrate and making the reaction only an oxidation reaction can improve the emission luminance by about 1000 times. However, the luciferyl adenylate is extremely unstable and is not suitable for practical applications. It may be possible to improve the brightness of firefly bioluminescence systems through development of a stable synthetic luciferyl adenylate analogue (**Figure 5.2**).

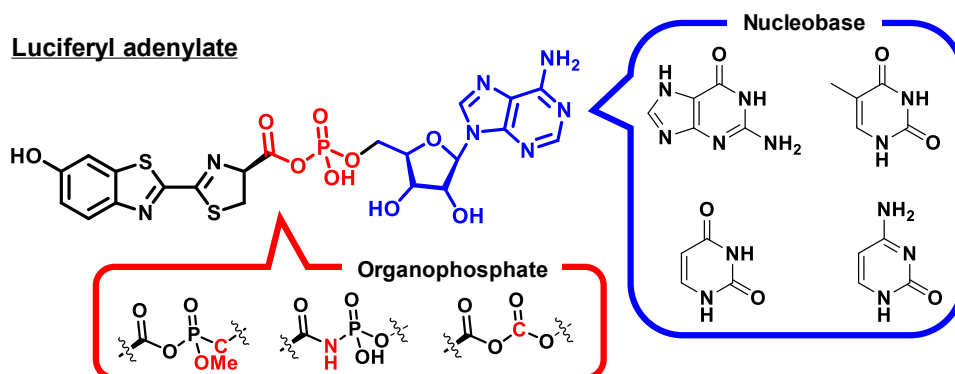


**Figure 5.2. Chemical structure of luciferyl adenylate and research strategy.**

## 2. Emission wavelength

In chapter 4, I successfully developed a family of NIR emitting firefly luciferin analogues and applied one of them to subcutaneous tumor *in vivo*. Although recent efforts have achieved NIR emission up to 758 nm, further longer emission are still desired to image deeper tissues. In addition, sharper emission spectra are required to realize multi-component bioluminescence assay. One effective strategy to achieve NIR emissions and sharper spectra is bioluminescence resonance energy transfer (BRET) to NIR fluorescent dyes. However, this strategy requires external modifications of luciferase. Recently, I have designed and synthesized NIR fluorescent dye (cyanine 5) fusion luciferins as new conceptual luciferins (**Figure 5.3**). Although these synthetic luciferins have dramatically reduced emissions, they are expected to exhibit emission wavelengths attributed to fluorescent dyes.

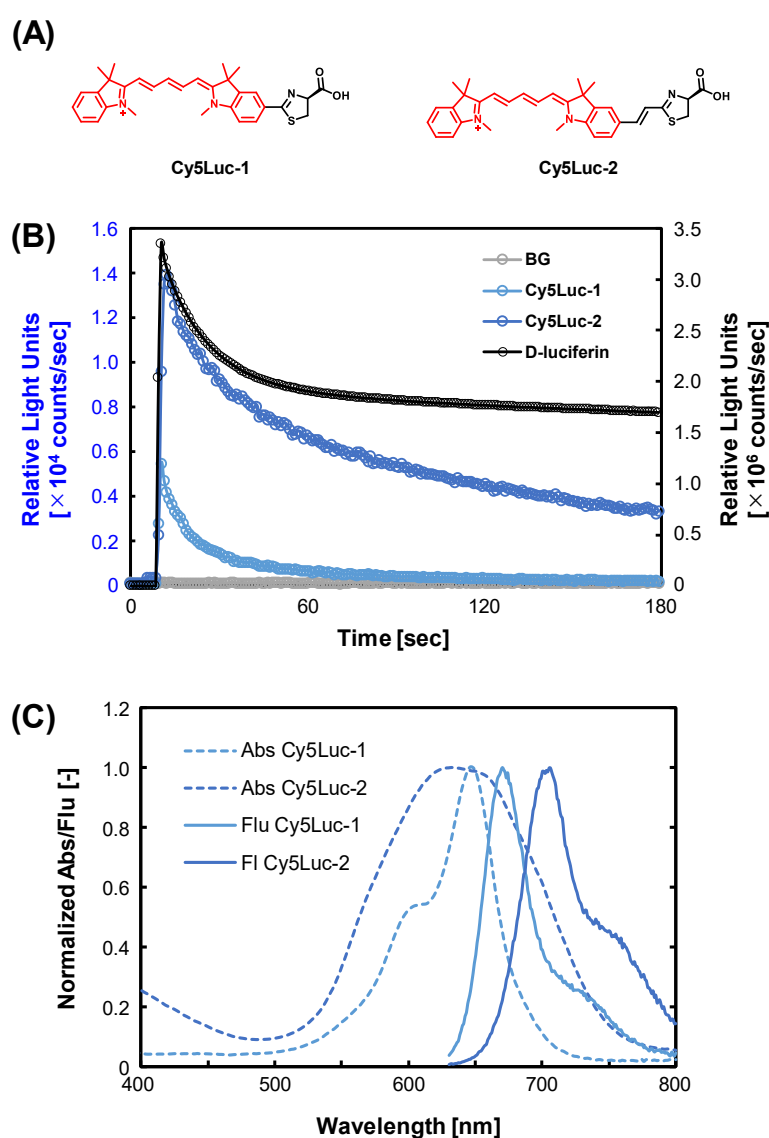


**Figure 5.3. Cyanine fusion luciferins.** (A) Chemical structures. (B) Bioluminescence of Cy5Luc with Fluc. (C) Absorbance and fluorescence spectra of Cy5Luc.  $\lambda_{\text{exc}} = 590$  nm.

In addition, spatial and temporal resolution should be solved to spy actual functions of target molecules (or cells). It is also necessary to perform a quantitative analysis of photons from the bioluminescence reaction. To overcome these issues, for example, three-dimensional highly traceable detector is necessary. Moreover, methodological efforts to expand the potential of bioluminescence imaging, such as development of new luciferases and genetic engineering techniques, generation of highly catalytically active luciferases and optimizing an imaging systems and algorithms, are essential (**Figure 5.4**). Therefore, collaborative action of academic researcher including chemists, biologists and industry is indispensable. Imaging modalities usually does not cover all types of imaging targets, "molecules-cells-organs". Therefore, trans-scale imaging can be realized only when the respective imaging modalities complement each other. One big advantage of bioluminescence imaging is that it can image the dynamics of a small number of cells with high sensitivity. Taking this advantage, for example, by developing a bimodal imaging tool with the fluorescent method, it may be possible to develop an imaging technology that seamlessly connects micro to macro.

Finally, I really hope that bioluminescence "*lights*" our future brightly.

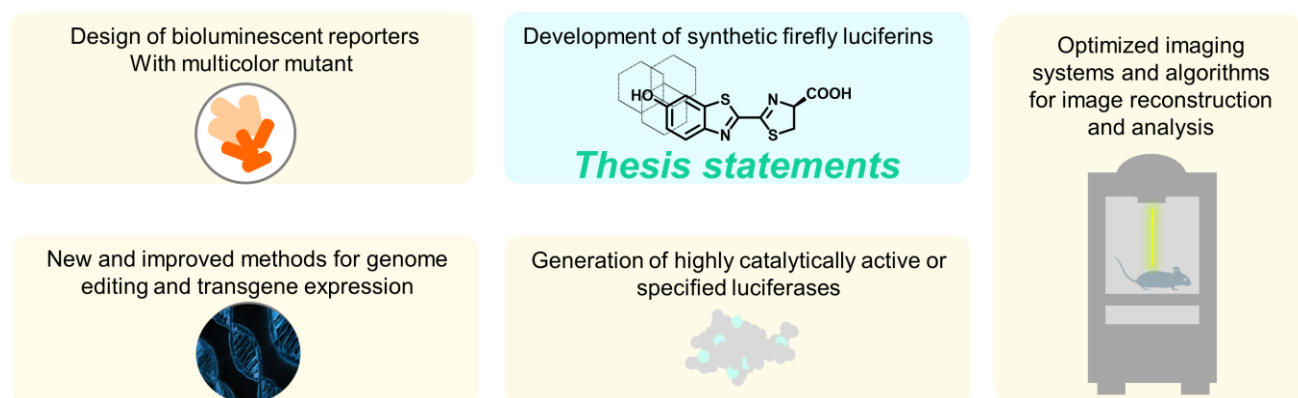


**Figure 5.4. Key technologies for future bioluminescence imaging.**

# Achievement list

## Original papers related to this thesis

- (1) **Yuma Ikeda**; Tsuyoshi Saitoh; Kazuki Niwa; Takahiro Nakajima; Nobuo Kitada; Shojiro A. Maki; Moritoshi Sato; Daniel Citterio; Shigeru Nishiyama; Koji Suzuki  
"An Allylated Firefly Luciferin Analogue with Luciferase Specific Response in Living Cells",  
*Chemical Communications*, **2018**, *54*, 1774-1777.
- (2) **Yuma Ikeda**; Takahiro Nomoto; Yuki Hiruta; Nobuhiro Nishiyama; Daniel Citterio  
"Ring-Fused Firefly Luciferins: Expanded Palette of Near-Infrared Emitting Bioluminescent Substrates",  
*Analytical Chemistry*, **2019**, *accepted* (DOI: 10.1021/acs.analchem.9b04562).

## Other original papers

- (1) Mayu Hemmi; **Yuma Ikeda**; Yutaka Shindo; Takahiro Nakajima; Shigeru Nishiyama; Kotaro Oka; Moritoshi Sato; Yuki Hiruta; Daniel Citterio; Koji Suzuki  
"Highly Sensitive Bioluminescent Probe for Thiol Detection in Living Cells", *Chemistry an Asian Journal*,  
**2018**, *13*, 648–655.
- (2) Nobuo Kitada; Tsuyoshi Saitoh; **Yuma Ikeda**; Satoshi Iwano; Rika Obata; Haruki Niwa; Takashi Hirano; Atsushi Miyawaki; Koji Suzuki; Shigeru Nishiyama; Shojiro A. Maki  
"Toward Bioluminescence in the Near-Infrared Region: Tuning the Emission Wavelength of Firefly Luciferin Analogues by Allyl Substitution", *Tetrahedron Letter*, **2018**, *59*, 1087-1090.
- (3) Masahiro Abe; Ryo Nishihara; **Yuma Ikeda**; Takahiro Nakajima; Moritoshi Sato; Naoko Iwasawa; Shigeru Nishiyama; Ramasamy Paulmurugan; Daniel Citterio; Sung Bae Kim; Koji Suzuki  
"Near-Infrared Bioluminescence Imaging with a Through-Bond Energy Transfer Cassette", *ChemBioChem*,  
**2019**, *20*, 1919-1923.
- (4) Hiroyuki Shibata; **Yuma Ikeda**; Yuki Hiruta; Daniel Citterio  
"Inkjet-Printed pH-Independent Paper-Based Calcium Sensor with Fluorescence Signal Readout Relying on a Solvatochromic Dye", *Analytical and Bioanalytical Chemistry*, **2019**, *accepted*.
- (5) Osamu Murata; Yutaka Shindo; **Yuma Ikeda**; Naoko Iwasawa; Daniel Citterio; Kotaro Oka; Yuki Hiruta  
"Near-Infrared Fluorescent Probes for Imaging of Intracellular Mg<sup>2+</sup> and Application to Multi-Color Imaging of Mg<sup>2+</sup>, ATP and Mitochondrial Membrane Potential", *Analytical Chemistry*, **2020**, *92*, 966-974.

## International conference presentations

### Oral presentations

- (1) "Structural Modified Firefly Luciferin Analogues for Bioluminescence Assays",  
OYuma Ikeda; Daniel Citterio; Shigeru Nishiyama; Koji Suzuki  
Pittsburgh Conference 2017, Chicago (USA), March 7, 2017.
- (2) "Structural Modified Firefly Luciferin Analogues for Bioluminescence Imaging",  
OYuma Ikeda; Naoko Iwasawa; Shigeru Nishiyama; Koji Suzuki; Daniel Citterio  
4<sup>th</sup> International Workshop on Quantitative Biology 2017, Kanagawa (Japan), April 14, 2017.
- (3) "Luciferin Analogues Extend Firefly Bioluminescence into Near-InfraRed for Deep Bioluminescence Imaging",  
OYuma Ikeda; Shigeru Nishiyama; Daniel Citterio; Koji Suzuki  
2017 World Molecular Imaging Congress, Philadelphia (USA), September 14, 2017.
- (4) "Azacyclic Analogues of Firefly Luciferin: Effective Luminescent Substrates for Bioimaging",  
OYuma Ikeda; Yuki Hiruta; Daniel Citterio  
20<sup>th</sup> International Symposium on Bioluminescence & Chemiluminescence, Nantes (France),  
May 29, 2018.
- (5) "Synthetic Firefly Luciferins for Bioluminescence Applications",  
OYuma Ikeda; Yuki Hiruta; Daniel Citterio  
6<sup>th</sup> National Tsing Hua University/Keio University Bilateral Symposium of Advanced Chemistry, Kanagawa  
(Japan), July 10, 2018.
- (6) "Structure-Luminescence Relationship of Near-Infrared Firefly Luciferin Analogues",  
OYuma Ikeda; Yuki Hiruta; Daniel Citterio  
The ACS Fall 2019 National Meeting & Exposition, San Diego (USA), August 26, 2019.

### Poster presentations

- (1) "Development of Red-Shifted Luciferin Analogues"  
OYuma Ikeda; Tomohisa Toyama; Naoko Iwasawa; Daniel Citterio; Shigeru Nishiyama; Koji Suzuki  
RSC Tokyo International Conference 2015, Chiba (Japan), September 4, 2015.
- (2) "Design and Synthesis of Novel Red-Shifted Firefly Luciferin Analogues"  
OYuma Ikeda; Tomohisa Toyama; Yuki Adachi; Naoko Iwasawa; Daniel Citterio; Shigeru Nishiyama; Koji Suzuki  
Pacifichem 2015, Honolulu (USA), December 16, 2015.
- (3) "Development of Red-Shifted Firefly Luciferin Analogues Modified with Allyl Group"  
OYuma Ikeda; Naoko Iwasawa; Daniel Citterio; Shigeru Nishiyama; Koji Suzuki  
19<sup>th</sup> International Symposium on Bioluminescence & Chemiluminescence, Ibaraki (Japan),  
May 31, 2016.
- (4) "Structural Modified Firefly Luciferin Analogues for Bioluminescence Imaging"  
OYuma Ikeda; Naoko Iwasawa; Daniel Citterio; Shigeru Nishiyama; Koji Suzuki  
RSC Tokyo International Conference 2016, Chiba (Japan), September 8, 2016.

- (5) "Azacyclic Analogues of Firefly Luciferin: Effective Luminescent Substrates for Deep Bioluminescence Imaging"  
 ○Yuma Ikeda; Yuki Hiruta; Shigeru Nishiyama; Koji Suzuki; Daniel Citterio  
 RSC Tokyo International Conference 2017, Chiba (Japan), September 7, 2017.
- (6) "Azacyclic Analogues of Firefly Luciferin: Effective Luminescent Substrates for Bioimaging"  
 ○Yuma Ikeda; Yuki Hiruta; Shigeru Nishiyama; Koji Suzuki; Daniel Citterio  
 Europt(r)ode 2018, Naples (Italy), March 26-27, 2018.

## Domestic conference presentations

### Oral presentations

- (1) "Design and Synthesis of Firefly Luciferin Analogues Emitting in Near-Infrared Wavelength"  
 ○Yuma Ikeda; Tsuyoshi Saitoh; Kazuki Niwa; Naoko Iwasawa; Daniel Citterio; Shigeru Nishiyama; Koji Suzuki  
 日本化学会 第 97 春季年会, 慶應義塾大学 日吉キャンパス, 横浜, 2017 年 3 月 16 日.
- (2) 「バイオ分析に向けたホタル生物発光基質アナログの設計と合成」  
 ○池田 裕真, 蛭田 勇樹, 西山 繁, チッテリオ ダニエル, 鈴木 孝治  
 第 27 会インテリジェント材料・システムシンポジウム, 東京女子医科大学, 東京, 2018 年 1 月 10 日.
- (3) 「生体分析応用に向けた合成ホタル生物発光基質誘導体」  
 ○池田 裕真  
 令和元年度日本分析化学会関東支部若手交流会、マホロバ・マインズ三浦, 神奈川, 2019 年 7 月 6 日.

### Poster presentation

- (1) 「バイオ分析を指向した近赤外ホタル生物発光基質アナログの設計と合成」  
 ○池田 裕真, 岩澤 尚子, Citterio Daniel, 西山 繁, 鈴木 孝治  
 日本分析化学会第 65 年会, 北海道大学, 北海道, 2016 年 9 月 15 日.
- (2) 「バイオ分析に向けたホタル生物発光基質アナログの設計と合成」  
 ○池田 裕真, 西山 繁, 鈴木 孝治, Citterio Daniel  
 平成 29 年度日本分析化学会関東支部若手交流会, ホテルニュー塩原, 栃木, 2017 年 3 月 16 日.
- (3) 「バイオ分析に向けたホタル生物発光基質アナログの設計と合成」  
 ○池田 裕真, 斎藤 毅, 丹羽 一樹, 中嶋 隆浩, 佐藤 守俊, Citterio Daniel, 西山 繁, 鈴木 孝治  
 生物発光化学発光研究会第 33 回学術講演会, 東邦大学, 千葉, 2017 年 10 月 21 日.
- (4) 「アリル基導入型ホタルルシフェリン誘導体の開発」  
 ○池田 裕真, 牧 昌次郎, 蛭田 勇樹, 西山 繁, 鈴木 孝治, Citterio Daniel  
 平成 30 年度日本分析化学会関東支部若手交流会, 新富亭, 宮城, 2018 年 7 月 7 日.
- (5) 「生物発光イメージングに向けた合成ホタル生物発光基質の開発」  
 ○池田 裕真, 牧 昌次郎, 蛭田 勇樹, 西山 繁, 鈴木 孝治, Citterio Daniel  
 In vivo イメージングフォーラム 2018, グランドホール品川, 東京, 2018 年 10 月 19 日.
- (6) 「環融合戦略を基盤とした近赤外発光ホタルルシフェリン誘導体群の創製」  
 ○池田 裕真, 野本 貴大, 蛭田 勇樹, 西山 伸宏, チッテリオ ダニエル

生物発光化学発光研究会第 35 回学術講演会, 国立開発法人 産業技術総合研究所 臨界副都心センター, 東京, 2019 年 10 月 5 日.

## Other conference activities

### International conferences

- (1) "Quantum Yield Measurement of Coelenterazine-Luciferase Emission System"  
OMasanobu Tanaka; Ryo Nishihara; Kazuki Niwa; Sung Bae Kim; Masahiro Abe; Yuma Ikeda; Naoko Iwasawa; Shigeru Nishiyama; Daniel Citterio; Koji Suzuki  
RSC Tokyo International Conference 2016, Chiba (Japan), September 9, 2016.
- (2) "Structure Activity Relationship Study on Substituent Modified Firefly Luciferin Analogues"  
OOsamu Murata; Yuma Ikeda; Shuji Ioka; Tsuyoshi Saito; Kazuki Niwa; Naoko Iwasawa; Daniel Citterio; Shigeru Nishiyama; Koji Suzuki  
4<sup>th</sup> International Workshop on Quantitative Biology 2017, Kanagawa (Japan), April 14, 2017.
- (3) "Firefly Luciferin Analogues for Hypoxia Detection"  
OYumi Kamiya; Yuma Ikeda; Yutaka Shindo; Naoko Iwasawa; Kotaro Oka; Shigeru Nishiyama; Koji Suzuki; Daniel Citterio  
RSC Tokyo International Conference 2017, Chiba (Japan), September 7, 2017.
- (4) "A Thiol Sensing Probe Based on a Caged Luciferin"  
OMayu Hemmi; Yuma Ikeda; Yutaka Shindo; Shigeru Nishiyama; Kotaro Oka; Daniel Citterio; Koji Suzuki  
RSC Tokyo International Conference 2017, Chiba (Japan), September 7, 2017.
- (5) "Quantum yield measurement of coelenterazine-luciferase emission system"  
OMasanobu Tanaka; Ryo Nishihara; Kazuki Niwa; Sung Bae Kim; Yuma Ikeda; Shigeru Nishiyama; Koji Suzuki; Daniel Citterio  
RSC Tokyo International Conference 2017, Chiba (Japan), September 8, 2017.
- (6) "A Thiol Sensing Probe Based on Caged Luciferin"  
OMayu Hemmi; Yuma Ikeda; Naoko Iwasawa; Shigeru Nishiyama; Daniel Citterio; Koji Suzuki  
2017 World Molecular Imaging Congress, Philadelphia (USA), September 15, 2017.
- (7) "Paper-Based pH-Independent Optical Calcium Sensor with Lipophilic Solvatochromic Dye"  
OHiroyuki Shibata; Yuma Ikeda; Yuki hiruta; Daniel Citterio  
RSC Tokyo International Conference 2018, Chiba (Japan), September 7, 2018.

### Domestic conferences

- (1) 「細胞内チオール検出用蛍光・生物発光プローブの開発」  
O逸見 茉由, 池田 裕真, 新藤 豊, 中嶋 隆浩, 佐藤 守俊, 岡 浩太郎, チッテリオ ダニエル, 鈴木 孝治  
第 27 会インテリジェント材料・システムシンポジウム, 東京女子医科大学, 東京, 2018 年 1 月 10 日.
- (2) "A bioluminescent probe for thiol detection"  
OMayu Hemmi; Yuma Ikeda; Naoko Iwasawa; Daniel Citterio; Shigeru Nishiyama; Koji Suzuki  
日本化学会 第 97 春季年会, 慶應義塾大学 日吉キャンパス, 横浜, 2017 年 3 月 16 日.

- (3) "Structure Activity Relationship Study on Substituent Modified Firefly Luciferin Analogues"  
 OOsamu Murata; Yuma Ikeda; Shuji Ioka; Tsuyoshi Saitoh; Kazuki Niwa; Naoko Iwasawa; Daniel Citterio;  
 Shigeru Nishiyama; Koji Suzuki  
 日本化学会 第 97 春季年会, 慶應義塾大学 日吉キャンパス, 横浜, 2017 年 3 月 16 日.
- (4) 「バイオイメーキングのための高 S/N 比・長時間発光基質フリマジン誘導体の開発」  
 O水井 侑希, 池田 裕真, 蛭田 勇樹, チッテリオ ダニエル  
 日本分析化学会第 68 年会, 千葉大学, 千葉, 2019 年 9 月 11 日.
- (5) 「近赤外蛍光マグネシウムイオンプローブの開発とマルチカラー細胞イメージングへの応用」  
 O蛭田 勇樹, 村田 理, 新藤 豊, 池田 裕真, 岩澤 尚子, 岡 浩太郎, チッテリオ ダニエル  
 日本分析化学会第 68 年会, 千葉大学, 千葉, 2019 年 9 月 13 日.
- (6) 「ソルバトクロミック蛍光色素を用いた pH に依存しない紙基盤オプトードセンサー」  
 O柴田 寛之, 池田 裕真, 蛭田 勇樹, チッテリオ ダニエル  
 日本分析化学会第 68 年会, 千葉大学, 千葉, 2019 年 9 月 13 日.
- (7) 「長時間バイオイメーキングのための安定生物発光基質フリマジン誘導体の開発」  
 O水井 侑希, 池田 裕真, 江口 正敏, 吉村 英哲, 小澤 岳昌, チッテリオ ダニエル, 蛭田 勇樹  
 生物発光化学発光研究会第 35 回学術講演会, 国立開発法人 産業技術総合研究所 臨界副都心センタ  
 ー, 東京, 2019 年 10 月 5 日.

## Other publications

- (1) Hiroyuki Shibata; Yuma Ikeda; Daniel Citterio,  
 "Inkjet-Printed Colorimetric Paper-Based Gas Sensor Arrays for the Discrimination of Volatile Primary Amines with Amine-Responsive Dye-Encapsulating Polymer Nanoparticles",  
*Biomimetic Sensing: Methods and Protocols*, Springer Protocols, pp. 101-114, USA, **2018**.

## Awards

- (1) "Marlene DeLuca Award", 19<sup>th</sup> International Symposium on Bioluminescence and Chemiluminescence, June 2, 2016.
- (2) "Poster Presentation Award", RSC Tokyo International Conference 2016, September 8, 2016.
- (3) "CSJ Student Presentation Award 2017", 日本化学会第 97 春季年会、2017 年 4 月 18 日
- (4) "Student Travel Stipend Award", 2017 World Molecular Imaging Congress, September 14, 2017.
- (5) 「奨励賞」、第 27 回インテリジェント材料・システムシンポジウム、2018 年 1 月 10 日
- (6) 「優秀ポスター賞」、平成 30 年度東日本分析化学若手交流会、2018 年 7 月 7 日
- (7) 「優秀賞」、In vivo イメージングフォーラム 2018、2018 年 10 月 19 日
- (8) 「ルミカ賞」、第 35 回生物発光化学発光研究会、2019 年 10 月 5 日
- (9) "Very Important Paper", *ChemBioChem*, **2019**, 20, 1919-1923.
- (10) "Cover Feature", *ChemBioChem*, **2019**, 20, 1919-1923.

# Acknowledgement

Firstly, I would like to express my heartfelt thanks to my academic supervisor, Prof. Daniel Citterio, for his enormous efforts in guidance and encouragement throughout the progress of my research activity. This thesis would not have been possible without his persistent help and extensive knowledge as a scientist.

I would also like to express my sincere appreciation to my former academic supervisor, Prof. Koji Suzuki, who provided these various encounters and opportunities. I wish to express my great gratitude to Prof. Kotaro Oka, Prof. Yasuaki Einaga and Prof. Yukari Fujimoto for their efforts as the member of the thesis committee to provide me with variable and constructive suggestions. I am deeply grateful to Assistant Prof. Yuki Hiruta for his great guidance, helpful discussion and constructive comments. Prof. Shigeru Nishiyama and Dr. Naoko Iwasawa are acknowledged for her helpful support and comments. I would like to thank my research collaborators: Dr. Kazuki Niwa and Dr. Sung Bae Kim at National Institute of Advanced Industrial Science and Technology, Prof. Moritoshi Sato and Dr. Takahiro Nakajima at Tokyo University. My deepest appreciation goes to them for their helpful discussion regarding the applications of synthetic luciferins. Prof. Nobuhiro Nishiyama and Dr. Takahiro Nomoto made enormous contribution to cellular and animal applications of synthetic luciferins.

This work was financially supported by a Grant-in Aid for Scientific Research (A); Grant-in-Aid for JSPS Fellows for Young Scientist from the Japan Society for the Promotion of Science (JSPS); a Grant-in-Aid for Scientific Research on Innovative Areas "Singularity Biology (No. 8007)" from The Ministry of Education, Culture, Sports, Science, and Technology, Japan.

I am grateful for the assistance and encouragement given by laboratory members. I would like to express my special thanks to Dr. Ryo Nishihara for his guidance and generous support. I gratefully acknowledge Dr. Hiroyuki Shibata for his support as my friend. Although it is impossible to list all names, I would like to thank to all of my lab mates both past and present for their kind support and fruitful discussions.

Finally, I wish to show my greatest appreciation to my family for their understanding and continued support during my research life.

February, 2020



*Integrated Design Engineering*

*Graduate School of Science and Technology, Keio University*